

1W-34
55503
239P

TRANSITIONAL BOUNDARY LAYERS UNDER THE INFLUENCE OF HIGH FREE
STREAM TURBULENCE, INTENSIVE WALL COOLING AND HIGH PRESSURE GRADIENTS
IN HOT GAS CIRCULATION

Klaus Rued

Translation of: "Transitionale Grenzschichten unter dem Einfluss
hoher Freistromturbulenz, intensiver Wandkuehlung und starken
Druckgradienten in Heissgasstroemungen;" thesis submitted at
University Karlsruhe, 1985, pp. 1-191

TRANSITIONAL BOUNDARY LAYERS UNDER THE INFLUENCE
OF HIGH FREE STREAM TURBULENCE, INTENSIVE WALL COOLING AND
HIGH PRESSURE GRADIENTS IN HOT GAS CIRCULATION

Approved Dissertation for a Doctorate in
Engineering
Faculty for Mechanical Engineering
University of Karlsruhe (Technical College)

By

Klaus Rued, Engineer
Waldshut

Oral Examination: 26 June 1985

Principle Reviewer: Prof. Dr. Sigmar Wittig, Engineer

1st Co-Reviewer: Prof. Dietmar Hennecke, Ph.D.

2nd Co-Reviewer: Prof. Darryl Metzger, Ph.D.

Karlsruhe 1985

PREFIX

This dissertation was written during my employment at the Institute for Thermal Dynamics, University of Karlsruhe, and was financially supported by the Research Association for Internal Combustion Engines (FVV) within the framework of project Nr. 241 "gas turbine blade cooling".

I would like to express my appreciation to the director of the institute, Professor Dr. Sigmar Wittig, for his constant support of this paper and for lecturing on this dissertation.

I would further like to thank Professor Dr. D. Hennecke from the Institute for Jet Propulsion Drives of the University of Darmstadt, and Professor Dr. D. Metzger from the Department of Mechanical Engineering, Arizona State University, Phoenix, USA, for co-lecturing.

During his time as visiting professor at the University of Karlsruhe, Professor Dr. D. Metzger, in numerous discussions, contributed significantly to my understanding of the physical aspects of this matter. For this, I am very grateful.

My special thanks to engineer Dr. K.H. Sill for his valuable advice during the design of the test unit and for the many discussion which aided considerably in the successful completion of this paper.

I would also like to thank all members of the Institute for Thermal Dynamics for always providing help and a creative atmosphere. My special appreciation goes to engineers S. Eriksen, R. Kutz and A. Schulz. I also wish to thank Mr. W. Rabold, Mr. W. Zwirner and, specially, Mrs. L. Foedisch for their support in writing this dissertation and with the the graphic illustration of the many design drawings. Additionally, I want to thank the shop supervisors of the institute, Mr. E. Link and Mr. E. Neuerer, and their employees for their helpfulness and for manufacturing the test and measuring equipment.

Karlsruhe, July 1985

CONTENT

	Page
List of Symbols	v
1. Introduction	1
1.1 Problem	1
1.2 Focal Points	5
2. Present State of Research	6
2.1 Appearances of Transitional Boundary Layers	6
2.1.1 Laminar Boundary Layers	6
2.1.2 The Laminar-Turbulent Boundary Layer Reversal	7
2.1.3 Turbulent Boundary Layers	10
2.2 Overview of Available Literature	15
2.2.1 Boundary Layers under the Influence of Free Stream Turbulence	15
2.2.1.1 Laminar Boundary Layers and Reversal with Varying Free Stream Turbulence	15
2.2.1.2 Turbulent Boundary Layers with Free Flow Turbulence	18
2.2.2 Boundary Layers under the Influence of Varying Material Values	22
2.2.2.1 Laminar Boundary Layers and Reversal during Wall Cooling	22
2.2.2.2 Turbulent Boundary Layers with Varying Wall and Free Stream Temperatures	24
2.2.3 Boundary Layers under the Influence of Pressure Gradients	26
3. Experimental Goals	30
4. Test Design and Experimental Methods	32
4.1 Test Unit	32
4.2 Measuring Section	34
4.2.1 Design Description	34
4.2.2 Expanded Design to Generate Pressure Gradients	36
4.2.3 Additions to Generate Turbulence	38
4.2.4 Cooling the Measuring Plate	39

	PAGE
4.3 Test Methods	41
4.3.1 Determining Free Stream Conditions	41
4.3.2 Determining Heat Transfer Coefficients	44
4.3.3 Boundary Layer Tests and Evaluation	48
4.3.4 Test Value: Pressures and Temperatures	54
4.3.5 Determining Free Stream Turbulence with Laser-Doppler-Anemometry (LDA)	55
4.3.5.1 Describing the LDA Procedure	56
4.3.5.2 Evaluation of the Measuring Signals	56
4.3.5.3 Particle Preparation and Particle Feed	58
4.4 Test and Calibration Measurements	59
4.4.1 Calibration of the Measurement Plate Thermal Elements	59
4.4.2 Test Measurements at the Boundary Layer Tunnel	61
5. Description and Discussion of Measured Results	
5.1 Test Program	
5.2 Free Stream Turbulence	65
5.3 Boundary Layers on Adiabatic Walls	72
5.3.1 Transitional Boundary Layers with Varying Free Stream Turbulence	73
5.3.2 Turbulent Boundary Layers with Changeable Free Stream Turbulence	80
5.4 Boundary Layer Flows with Wall Cooling	85
5.4.1 Boundary Layer Development and Heat Transfer with Varying Wall Cooling and Free Stream Turbulence	86
5.5 Analysis of the Influencing Parameters	99
5.5.1 Material Value Influences due to Wall Cooling	99
5.5.1.1 Laminar Boundary Layer	99
5.5.1.2 Turbulent Boundary Layers	104
5.5.1.3 Integral Boundary Layer Characteristic Values for Wall Cooling	
5.5.2 Influences of the Free Stream Turbulence	

5.5.2.1	The Laminar-Turbulent Boundary Layer Reversal	116
5.5.2.2	Turbulent Boundary Layers	125
5.5.3	Influences of Negative Pressure Gradients	134
5.5.3.1	Basic Influences of Free Stream Acceleration	135
5.5.3.2	Reynolds Number and Turbulence Intensity Influences	140
5.5.3.3	Correlation Equations for Calculating Turbulent Heat Transfer in Accelerated Flow	147
6.	Development of an Integral Procedure to Compute Two- Dimensional Boundary Layers with Reversal, Heat Transfer, Pressure Gradients and Free Stream Turbulence	152
6.1	Procedure Selection	152
6.2	Basic Equations	153
6.3	Profile Formulations	157
6.3.1	Boundary Layer Profiles in Flows with Constant Material Values	157
6.3.1.1	Laminar Profiles	159
6.3.1.2	Turbulent Boundary Layer Profiles	161
6.3.2	Boundary Layer Profiles in Flows with Changing Density	163
6.4	The Turbulence Model	166
6.5	Modelling the Boundary Layer Reversal	171
6.5.1	Determination of the Boundary Layer Intermittency	171
6.5.2	The Turbulence Model during Reversal	175
6.5.3	Boundary Layer Profiles during Reversal	176
6.6	Solution Procedures	178
6.6.1	Evaluation of the Profile Equations	178
6.6.2	Integrating the Differential Equation	180
6.7	Testing the Calculation Program with the Aid of Experimental Results	180

6.7.1	Boundary Layers without Pressure Gradient	181
6.7.1.1	The Laminar-Turbulent Boundary Layer Reversal with Low Free Stream Turbulence Intermittency	181
6.7.1.2	Boundary Layers with Varying Free Flow Turbulence	184
6.7.1.3	Transitional Boundary Layers with Wall Cooling	191
6.7.2	Flows with Pressure Gradients	199
6.7.2.1	Comparative Calculations for Constant Free Stream Acceleration	199
6.7.2.2	Comparative Calculations for Flows Accelerated on the Vacuum Side	204
7.	Summary	211
8.	References	215

LIST OF SYMBOLS

<u>Symbol</u>	<u>Unit</u>	<u>Physical Entity</u>
A, a, a_0, a_1, a_2, a_3	-	coefficients or structural parameters (eq. 6.48)
b	m	tunnel width
C, C_T, C^*, C_T^*	-	constants of the logarithmic wall theory (eq. 5.7)
c_p	J/(kgK)	specific heat capacity
$c_f = \frac{2 \cdot \tau_w}{\rho_\infty u_\infty^2}$	-	tangential stress coefficient
c_{f0}, c_{f0}	-	tangential stress coefficient for $Tu = 0$
c_{fi}	-	transformed c_f -value (eq. 6.40; eq. 6.41)
C_D, C_{DH}	-	dissipation integral (eq. 6.4; eq. 6.8)
D	-	van Driest attenuation constant (eq. 6.52)
E	-	entrainment eq. 6.47
F_T, F_k	-	correction factor (eq. 5.12)
$H_{12} = \frac{\delta_1}{\delta_2}, H_{32} = \frac{\delta_3}{\delta_2}$	-	shape factor (eq. 6.6; 6.9)
$H_{43} = \frac{\delta_4}{\delta_3}, H_{65} = \frac{\delta_6}{\delta_5}$	-	
$H_{12}^u = \frac{\delta_1 u}{\delta_2 u}$	-	kinematic shape factor
h	J/kg	static enthalpy
$h_0 = h + \frac{u^2}{2}$	J/kg	total enthalpy
k	-	acceleration parameter
k_2^*	-	profile parameter (eq. 6.22)
	-	turb. mixing method
L	-	turb. dissipation length (eq 6.50)

l, l', s, S'	-	segment dimension (Ill. 4.7)
L_u	m	linear measurement of the turbulence
m	-	Polhausen parameter (eq. 6.60)
Ma	-	Mach number
Pr	-	Prandtl group
Pr_t	-	turbulent Prandtl group
p	Pa	pressure
\dot{Q}	W	heat flow
\dot{q}	W/m ²	spec. heat flow
q	(m/s) ²	turb.kin. energy (eq. 6.46)
$Re_2 = \frac{u_\infty \delta_2}{\nu_\infty}$	-	Reynolds number, impulse loss thickness
Re_E	-	Reynold number, enthalpy loss thickness
$Re_x = \frac{u_\infty x}{\nu_\infty}$	-	Reynolds number, running length
Re_L	-	Reynolds number formed with plate length and plate flow-off conditions
Re_{L0} or $Re_{L,0}$	-	Reynolds number formed with plate length and plate oncoming flow conditions
$Re_{xS}, Re_{xE}, Re_{2S}, Re_{2E}$	-	Reynolds number at the beginning and end of reversal
r	-	recovery factor
$St = \frac{\dot{q}_w}{\rho_\infty u_\infty c_p (T_w - T_{t_\infty})}$	-	Stanton coefficient
T	K	temperature
T_{ei}	K	intrinsic temperature
T_o, T_u	K	measuring temperatures in the plate segment
T^+	-	log. temperature (eq. 4.14)

ORIGINAL PAGE IS
OF POOR QUALITY

Tu	-	degree of turbulence of the free stream (eq. 4.14)
\overline{Tu}	-	average degree of turbulence
Tu_0	-	degree of turbulence at the beginning of the plate
$-\overline{T'v'}$	mK/s	turbulent temperature fluctuation
u	m/s	speed
$u^+ = \frac{u}{u_\tau}$	-	- log. speed rate (eq. 4.11)
$-\overline{u'v'}$	(m/s) ²	turbulent shear stress
$u_\tau = \sqrt{\tau_w/\rho_w}$	m/s	tangential stress velocity
u', v', w'	m/s	speed fluctuation components in the direction of and vertical to the main flow direction
$w(y/\delta)$	-	Wake function
x	m	running length
x_0	m	beginning of the equation
y	m	wall distance coordinate
$y^+ = \frac{y u_\tau}{\nu_w}$	-	log. wall distance coordinate
$y_s^+; y_{st}^+$	-	profile parameters (Ill. 6.1)
z	m	diagonal coordinate
Z	-	standardized Reynolds number in the reversal (eq. 6.61)
α_g	W(m ² K)	heat transfer coefficient (eq. 4.4)
β	-	influence parameter of the Reynolds number (Ill.5.42)
γ	-	boundary layer intermittance (eq. 6.57)

γ_e			balance intermittance (eq. 6.61)
δ		m	boundary layer thickness
δ_t		m	temperature boundary layer thickness
δ_1	$= \int_0^{\delta} \left(1 - \frac{\rho u}{\rho_{\infty} u_{\infty}}\right) dy$	m	displacement thickness
δ_2	$= \int_0^{\delta} \frac{\rho u}{\rho_{\infty} u_{\infty}} \left(1 - \frac{u}{u_{\infty}}\right) dy$	m	impulse loss thickness
δ_h	$= \int_0^{\delta} \frac{\rho u}{\rho_{\infty} u_{\infty}} \left(\frac{h_{\infty} - h}{h_{\infty}}\right) dy$	m	enthalpy loss thickness
δ_1^u	$= \int_0^{\delta} \left(1 - \frac{u}{u_{\infty}}\right) dy$	m	kinematic displacement thickness (eq. 4.14)
δ_2^u	$= \int_0^{\delta} \frac{u}{u_{\infty}} \left(1 - \frac{u}{u_{\infty}}\right) dy$	m	kinematic impulse loss thickness
δ_3	$= \int_0^{\delta} \frac{\rho \cdot u}{\rho_{\delta} \cdot u_{\delta}} \left[1 - \left(\frac{u}{u_{\delta}}\right)^2\right] dy$	m	energy loss thickness
δ_4	$= \int_0^{\delta} \frac{\delta \cdot u}{\rho_{\delta} \cdot u_{\delta}} \cdot \left(\frac{\rho_{\delta}}{\rho} - 1\right) dy$	m	energy loss thickness
δ_5	$= \int_0^{\delta t} \frac{\rho \cdot u}{\rho_{\delta} \cdot u_{\delta}} \cdot \left(\frac{h_0 - h_{0\infty}}{h_w - h_{0\infty}}\right) dy$	m	enthalpy loss thickness
δ_6	$= \int_0^{\delta t} \frac{\rho \cdot u}{\rho_{\delta} \cdot u_{\delta}} \cdot \left(\frac{h_0 - h_{0\infty}}{h_w - h_{0\infty}}\right)^2 dy$	m	enthalpy loss thickness

ϵ	m^2/s^3	turbulent dissipation rate (eq. 6.48)
$\kappa, \kappa_T, \kappa^*, \kappa_T^*$	-	constants of the log. wall theory (eq. 5.7)
λ	W/m	heat conductivity
λ_t	W/m	turb. heat conductivity
λ_{Cu}	W/m	heat conductivity in the segment
μ	Ns/m ²	dyn. viscosity
μ_t	Ns/m ²	eddy viscosity
ν	m/s	kin. viscosity
ν_t	m/s ²	kin. eddy viscosity (eq. 6.55)
n	m	standardized wall distance coordinate
Ω	-	heat flow parameter (eq. 5.5)
ρ	kg/m ³	density
τ	Pa	tangential stress
ζ	m	length of the un-cooled leading edge of the plate

Indices

∞	outer flow
w	wall
t	total
δ	at the edge of the flow boundary layer
δ_t	at the edge of the temperature boundary layer
o	at the beginning of the plate
umschl	reversal
lam	laminar
turb	turbulent

1. INTRODUCTION

1.1 Problem

Improving thermal efficiency and the specific performance by increasing a turbine's inlet temperature and by increasing the compression ratio is an important element in the further development of gas turbines. In current engine designs it is possible to control compression ratios of approximately 30:1 and turbine inlet temperatures of almost 1,700 K [1,2]. However, the goal of future developments are turbine inlet temperatures which are as close as possible to the stoichiometric combustion temperature ($\approx 2,400$ K) of the combustion chamber (see [1,2]). Standard values for an increase of the compression ratio are contained in latest thermo-dynamic circulation procedure studies performed by NASA [1]. In accordance with these studies and according to the turbine's inlet temperature, compression ratios of a 64:1 magnitude will be required in order to achieve minimum specific fuel consumption.

Despite further development of available materials, cooling of components which are subjected to high thermal and mechanical stress will remain a necessity in the foreseeable future. Therefore, the main task in achieving these goals is an optimization of the cooling requirement. By removing that portion of the exhaust which is necessary for cooling, the mass flow is reduced from the combustion chamber. This, in connection with further losses, results in a decrease of performance and thermal efficiency. Therefore, an appropriate design of the cooled components will avoid a situation where, with the intended additional temperature and pressure increases, an expected gain is compensated by an additional cooling air requirement.

Components with the highest cooling requirement are the stationary and rotating blades at the initial stages of a turbine. They are exposed to high thermal and mechanical stress. With these components, the cooling requirement and the necessary design of the cooling configuration on the inside of the blade depend on the development of heat transfer along the blade surface. To predict this heat transfer in a reliable manner is presently the main difficulty in the design and the further development of cooled gas turbine blades. Available calculation procedures are still very limited with respect to their efficiency. According to latest studies [1], available calculation methods can only be used for advance computation of blade surface temperatures with an exactness of ± 100 K. This uncertainty in the theoretical determination of the outer heat transfer and the resulting blade temperatures would require an unacceptable overcooling of the blade to guarantee the required strength and life expectancy. In order to avoid this inefficiency, the calculation is, in a comprehensive design process, always supplemented by an experimental test on a model blade. This, however, requires considerable additional effort with respect to cost and time [1]. As a result, the strategy of modern gas turbine construction strives to reduce additional efforts for experiments by constant improvement of calculation methods.

The causes for the above problems with blade design can be found in the complex and partially inexplicable heat transfer and flow procedures along the blade surface [1,2]. In addition, a number of parameters and flow phenomena have a decisive influence on the boundary layer behavior and the heat transfer to the blade. The following parameters are of great significance:

- the laminar-turbulent reversal behavior of the boundary layer
- the blade's longitudinal surface curvature
- the highly negative pressure gradients in the flow
- superimposed free stream turbulence
- material value influences generated by the cooling of the blade, and
- separation in the boundary layer.

Another significant factor in blade flow of gas turbines is that the magnitude of the influence of these effects are always superimposed in a non-linear manner. Even when each parameter is studied on an individual basis, we presently have no full appreciation of respect its effect [1,2]. Therefore, ignorance of basic knowledge and available data are the reasons for incomplete modelling of numeric boundary layer calculation procedures and the resulting uncertainties for blade design when the outer heat transfer is calculated. This was recently demonstrated in parallel studies for the development of differential equations to describe heat transfer on cooled gas turbine blades [4].

For the development of calculation procedures, there is a basic lack of experimental studies, which provide information on the significance of the most important quantities:

- free stream turbulence
- free stream acceleration
- and wall cooling

and which take into consideration the mutual interaction of these parameters.

This dissertation will meet the requirements for fundamental experimental studies of the influence of free stream turbulence, pressure gradients and wall cooling. Under turbine-like free stream conditions, comprehensive tests of transitional boundary layers with laminar, reversing and turbulent flow increments were performed to decouple the effects of the parameters and to determine the effects during mutual interaction.

In light of further development of calculation procedures, a high degree of general expressiveness was required of the tests. Although blade configuration tests are the real purpose of this dissertation, their results are always influenced by individual blade geometry. Therefore, a genuine reproduction of basic effects cannot be achieved. Because of this, I did not select this type of flow but the more general, flat plate boundary layer which is not influenced by geometry. In addition, numerous test procedures which were developed with the this type of boundary layer provided the advantage that, in addition to heat transfer measurements, more complex boundary layer measurements could be accomplished.

The above requirement for more exact ways to calculate heat transfer at the surface of gas turbine blades has resulted more and more in the use of so-called field methods whereby the differential equations are solved numerically in connection with a turbulence model [4-9]. Only this method was recognized as having the flexibility necessary to describe the complex blade boundary layer flow conditions with sufficient accuracy.

In contrast, integral procedures - despite a certain amount of success ([10-13], see [3], [14]) - did not seem suitable for the calculation of heat transfer on cooled gas turbine blades. This is supported by the fact that, to date, no method has been developed to describe the long transfer zones, which are characteristic for blade conditions, with integral procedures. In addition, the calculation methods for heat transfer, which are decisive in blade cooling, and their main analogy equations were only partially developed and encouraging proposals for improvement did not evolve. The obvious disadvantages of integral procedures are mainly attributable to the fact that, with the introduction of field methods, the development of integral calculation methods was neglected, although their use is still relatively common in industry.

With integral procedures, the basic equations, which describe the boundary layer, are integrated in a normal manner to the main flow direction by adopting known profile equations. This results in a system of common differential equations which can be solved in a quick and easy manner. This method is widely used because of its economy and simple application. In order to utilize these advantages in the future it seemed practical to use integral procedures and examine them with respect to their actual efficiency. In order to accomplish this, the development of a universal integral procedure was introduced which, as an alternative to field methods, demonstrates the usefulness of these methods for calculating heat transfer coefficients for gas turbine blades and which, at the same time, maintains the advantages of economy and simple application. My immediate goal was to provide a calculation model based on the integral method which calculates the influences of free stream turbulence, continuous reversal processes and heat transfer coefficients in cooled boundary layers with high pressure gradients without using analogy equations or purely empiric additive functions.

1.2 Focal Points

This dissertation contains theoretical and experimental aspects. Experimental work consists of heat transfer and boundary layer tests on the flat transitional plate boundary layer which separates the influences of free stream turbulence, wall cooling and negative pressure gradients as well as describing them during mutual superimposition. The experimental portion is the main component of this dissertation. It is the basis for the chapter "Present State of Research" and the reference list.

Chapter 6 discusses the above integral procedure and makes a comparison with tests of other authors and those made by me.

2. PRESENT STATE OF RESEARCH

2.1 Appearance of Transitional Boundary Layers

Before discussing the analysis of the influencing parameters, I consider it practical to describe the basic components and properties of transitional boundary layers. This will explain the basic conditions and the surroundings which causes the interaction of boundary layer and influencing parameters.

2.1.1 Laminar Boundary Layers

A transitional boundary layer, which is formed along a fixed surface, begins in a laminar manner and becomes turbulent in its further development. The laminar-turbulent transition occurs within a defined intermediate area, which is referred to as the reversal area, and in which the boundary layer undergoes a continuous change of significant consequences.

The boundary layer, whose beginning is laminar, describes a shear flow in which turbulence flows are steamed out. This flow is controlled exclusively by viscous impulse and energy exchange phenomena. This causes typical boundary layer profiles which, in the vicinity of the wall, distinguish themselves by large areas of linear velocity and temperature distribution.

Because there is no exchange process, the calculation of laminar boundary layers is relatively simple. With certain conditions for the distribution of the free stream velocity $u_{\infty}(x)$, analytically exact solutions of the boundary layer differential equations are possible. This applies especially to the flat un-accelerated plate boundary layer and, generally, to the wedge flow with $u_{\infty}(x) = \text{const} \times x^m$. These cases have "similar solutions" with the characteristic property that boundary layers are not dependent on the running length in the similarity description:

$$\frac{T - T_w}{T_{\infty} - T_w} \text{ resp. } \frac{u}{u_{\infty}} = f(\eta = y \cdot \sqrt{\frac{u_{\infty}}{\nu \cdot x}}) \quad (2.1)$$

In boundary layers with arbitrary velocity distribution, which includes the flow around gas turbine blades in the vicinity of the wall, similar approximations cannot be used. Solutions to describe laminar heat transfer and tangential stress conditions can only be obtained via the numeric integration of the boundary layer differential equations.

2.1.2. The Laminar-Turbulent Boundary Layer Reversal

After a long running time, laminar flows with total pressure gradients become unstable even with very small disturbances. This generally occurs after a characteristic value of the Reynolds number Re_2 , which is formed with the impulse loss thickness, is exceeded. The laminar boundary layer remains stable below this "neutral Reynolds number" ($Re_2 \approx 160$). If the boundary layer has higher impulse loss thickness Reynolds numbers, flows are generated which cause turbulence further along in the flow, thus generating the laminar-turbulent reversal process. Arnal [13] demonstrates this process with comprehensive hot wire tests. He shows how, with increasing running length, low long-wave flows are transferred into high-frequency turbulence which results in pronounced, turbulent shear stresses and profile deformations. The key phenomenon of the reversal is a process of generation, excitation and propagation of eddy systems which occurs in several phases (see [3]):

1. In the first phase - after the neutral Reynold number has been exceeded - unstable interference waves are generated and excited in the boundary layer. The interference waves are two-dimensional and bear the names of their discoverers, i.e. Tollmien-Schlichting waves. They can be generated by irregularities in the external flow (turbulence, acoustic vibrations, etc.) and by irregularities of the surface. Tollmien-Schlichting waves move with approximately 30% of the outside velocity in the direction of the main stream; their wave lengths can have a thickness of several boundary layers.

2. Further along the path, slight irregularities in the boundary layer or in the free stream may cause three-dimensional waves and the formation of a three-dimensional wave system which alternates with the main stream ('peak-valley development'). This results in initial eddy systems whose axes are in the direction of the flow and which rotate in pairs in an opposed manner. In a diagonal direction, this secondary flow generates zones with varying interference wave intensity thereby causing a slight three-dimensionality of the basic flow. The planes of the maximum interference wave amplitudes are called "peak profiles", the planes of minimum amplitudes are referred to as "valley profiles".

3. Further down-stream, the formation of a high shear layer with a high eddy concentration occurs in the peak/valley profiles. In the breakdown process, the longitudinal eddies disintegrate at this location, thus generating higher-frequency eddies with the center of rotation in the diagonal direction (hairpin eddies).

4. These hairpin eddies form wedge-shaped turbulence spots which, during their up-stream movement, move in and diagonal to the flow direction. In experiments, the occurrence of turbulence spots resulted in boundary layer intermittance along with a chronological alternation of laminar and turbulent form of flow.

5. When the turbulence spots grow together, the boundary layer become increasingly turbulent.

The above processes are, for the most part, extracted from reports by Schubauer and Skramstadt [16], Schubauer and Klebanoff [17] and Klebanoff et al [18]. Overviews are provided by Tani [19], Morkovin [20], Reshotko [21], Schlichting [22], Eppler and Fasel [23] and in the dissertation by Ghon [24]. Reshotko [21] and Eppler & Fasel [23] describe current research, while Scheurer [4] and Ghon [24] include parameter influences and the theoretical accessibility (calculation procedures) into their studies.

The process of individual reversal phases can be influenced by different parameters (e.g. free stream turbulence, surface roughness, surface curvature, pressure gradients, etc.). Under certain conditions there may even be situations where one or more reversal phases are bypassed. An important example is the presence of high external turbulence ($Tu > 1\%$). When such conditions exist, the presence of Tollmien-Schlichting waves was, at times, not observed (Morkovin [20]).

In the above, the process of boundary layer turbulence generation was emphasized without an evaluation of the resulting deformation of the boundary profiles, or the alteration (increase) of the heat transfer, and wall tangential stress. Available tests (e.g. [15, 16, 17]) show that there is a distinct difference between the turbulence process and a noticeable profile deformation. The boundary layer profiles, which are determined in a chronological manner, and their friction and heat transfer coefficients begin shedding laminar behavior and their laminar values only after the turbulent spots are formed. According to Schubauer and Skramstad (see [25, 26]), a minimum intermittance of approximately 16% is necessary during turbulent external flow, before a deformation of the velocity profiles is noted. The external occurrence of the reversal is thus concentrated on the last phase (phase 5) of the reversal process. This is important for the evaluation and assignment of quantitative statements for the beginning of the reversal, if reversal Reynolds coefficients were not determined by the turbulence but with the aid of measured velocity profile deformations or heat transfer distributions.

2.1.3 Turbulent Boundary Layers

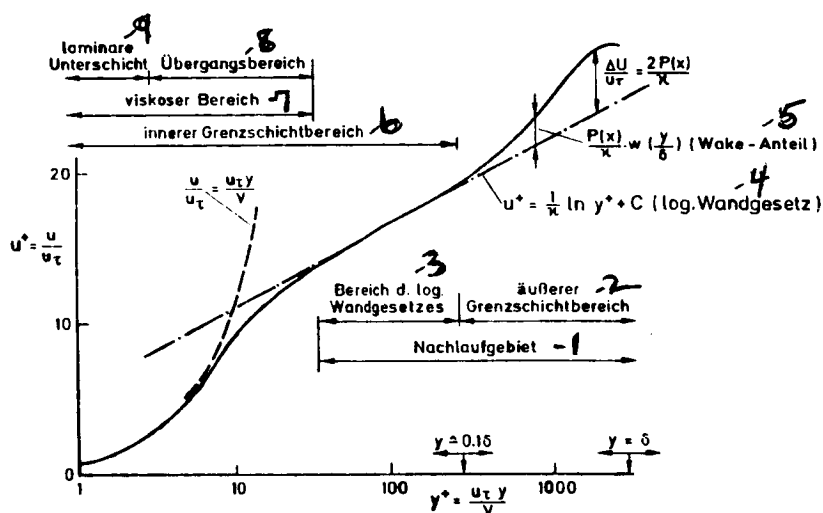
In turbulent boundary layers, flow types occur which are mainly generated by a regularly recurring 'burst' process. The burst process occurs in a given pattern. Slower moving flow sections are torn out of the zone near the wall and, during down-stream movement, are pushed toward the edge of the boundary layer while creating turbulence (see [27-29]). The turbulence of this rotational flow is similar to a conglomerate of eddy structures with varying sizes, the largest of which has the same thickness as the boundary layer. The smallest eddies are dissipated by the flow and are transferred into heat. In an energy cascade, the large eddies withdraw energy from the main stream; this energy is transferred in stages to smaller eddies and to the dissipating eddies. This turbulence mechanism depends very little on the viscosity. Higher viscosity will not result in higher dissipation. Its only effect is that the dissipation starts with large eddy systems (see [30]).

Turbulent boundary layers have distinct velocity, turbulence and tangential stress distribution structures which provide this type of flow with a similar character in most areas. Based on dimensional analyses and numerous experiments, the velocity profiles and turbulent shear stress profiles can be described by a universal interrelationship.

$$\begin{aligned} u^+ = \frac{u}{u_\tau} &= f_1 \left(y^+ = \frac{y \cdot u_\tau}{\nu} \right) \\ - \frac{u^+ v^+}{u_\tau} &= f_2 \left(y^+ = \frac{y \cdot u_\tau}{\nu} \right) ; u_\tau = \sqrt{\tau_w / \rho} \end{aligned} \quad (2.2)$$

The wall distance y is also a linear measure for the largest eddies with the most energy and u_τ can be assigned to them as the applicable measure of speed. Because of this, the standardized wall distance coordinate y^+ is compared to a turbulence Reynolds number which represents the energy carrying eddy systems of the turbulent boundary layer.

Illustration 2.1 is a schematic of the velocity distribution described with equation (2.2). The behavior of this velocity profile extends through several phases which are marked by characteristic differences in the relative influence of viscous and turbulent tangential forces. It is practical to break down the entire profile into an internal and external area. The internal area is comprised of the areas near the wall ($y/\delta < 0.1-0.2$), consisting of the laminar bottom layer, the intermediate layer and the logarithmic area. This boundary layer section distinguishes itself by almost constant tangential stress $\tau = \tau_w$. In the external section of the boundary layer, the transition from the highly turbulent flow to the almost eddy-free external flow occurs near the wall.



1 - wake area; 2 - external boundary layer section; 3 - area of the log. wall theory; 4 - log. wall theory; 5 - wake portion; 6 - internal boundary layer section; 7 - viscous area; 8 - transition area; 9 - laminar bottom layer

Illustration 2.1: Approximation of a Turbulent Velocity Profile (according to Bradshaw [30])

Depending on the Reynolds number, the laminar bottom layer $y^+ \leq 5$ is extraordinarily thin. It is dominated by viscous forces, although in the chronological disintegration of the flow, a structure occurs which is already disturbed by continuous small scale velocity fluctuations and fluid elements, which penetrate this layer from the outside. In the buffer layer ($5 < y^+ < 30$), a continuous transition occurs from the laminar bottom layer to the fully turbulent flow form which, in the subsequent layer, is characterized by the validity of the logarithmic wall theory. In the buffer area, the turbulent shear stress portion increases by the same amount as the decrease of the viscous tangential stress portion.

Only the turbulent impulse exchange events and tangential stress portions are important in the subsequent area ($y^+ > 30$). The logarithmic wall theory applies:

$$\frac{u}{u_\tau} = \frac{1}{\kappa} \cdot \ln \left(\frac{y \cdot u_\tau}{\nu} \right) + C \quad (2.3)$$

The condition $\tau = -\rho \overline{u'v'} = \tau_w = \text{const.}$ is the theoretical basis of this relationship. However, according to test results, turbulent boundary layer flows are possible (e.g. when free stream turbulence is present) where, because of special turbulence structure, the logarithmic wall theory satisfactorily describes the velocity path, even for large wall distances with a clearly reduced tangential stress (Bradshaw [30]).

In the external section of the boundary layer (Illustration 2.1), the velocity profile is dominated by the statutes of free or wake turbulence. Because of the intermittent ejection of turbulence to the edge of the boundary layer, turbulent boundary layer flows alternate with rotation-free shear flows with viscous properties.

The velocity in the external portion of the boundary layer is described by the wake function $w(y/\delta)$. This function is assigned an additional weighting factor $P(x)/k$ and is then added to the logarithmic wall theory (see Illustration 2.1). There are a number of empirical approximations for this wake function (see [22, 35]). Coles, for examples, proposed:

$$w(y/\delta) = 2 \cdot \sin^2\left(\frac{\pi}{2} \cdot \frac{y}{\delta}\right) \quad (2.4)$$

In the variable wake force $P(x)$, consideration is given to the fact that turbulent boundary layers often depend on their history. The longer life of large eddies is the reason for this memory effect. It requires that stored information be carried down-stream; changes of external conditions like pressure gradients, roughness, etc. are only realized at the boundary layer with a certain amount of delay (relaxation). Because relaxation effects decrease from the outer edge to the wall, the wake area is mainly affected by this. The logarithmic wall theory and the flow along the wall remain unchanged during semi-logarithmic application (as in Illustration 2.1). After the relaxation effects have subsided, the boundary layer is in a total equilibrium condition ('equilibrium boundary layer'). This condition, like other similar solutions in laminar cases, distinguishes itself by totally similar velocity profiles with unchanging wake areas and similar turbulence structures. Therefore, the convective terms (see [30]) become negligible in the maintenance equation which describes turbulent energy exchange events.

The turbulent boundary layer with low impulse loss thickness reynolds numbers ($Re_2 < 5,000$), which is characteristic for blade flows, also belongs to relaxation flows. In transitional boundary layers it can always be found immediately after the laminar-turbulent boundary layer reversal.

**ORIGINAL PAGE IS
OF POOR QUALITY**

Turbulent boundary layers with small impulse loss thickness Reynolds numbers are highly affected by viscosity influences. They are present near the wall and are caused by thickened laminar bottom layers; they can also be found at the outer edge of the boundary layer where they are caused by decreased wake portions. According to White [31], additional changes can be observed in the constants of the logarithmic wall theory (C and K) when impulse loss thickness Reynolds numbers Re_2 are < 600 . Because of this, events in turbulent boundary layers with low Reynolds numbers have a higher Reynolds number dependency on the characteristic boundary layer quantities like friction coefficient c_f and profile shape parameter H_{12} . In addition there is a Reynolds number dependency on the production, dissipation, convection and diffusion of turbulent kinetic energy. Murlis [33] and Murlis et al [32] quantify these basic phenomena in comprehensive analyses with the aid of measured velocity profiles and turbulence distribution at the boundary layer.

Photographs taken by Head et al [34] (visualization with smoke) (Illustration 2.2) show the differences of the global turbulence structure for impulse loss thickness Reynolds numbers of 500 to 10,000. With lower Reynolds numbers (Illustration 2.2a), vortex loops with highly viscous portions occur at the edge of the boundary layer. When the Reynolds number is increased, they are replaced by hairpin eddies (Illustration 2.2b), thus making the transition to the equilibrium boundary layer.

← Strömungsrichtung →



(a) $Re_2 = 5000$



(b) $Re_2 = 10000$

1 - flow direction

Illustrations 2.2a and b: Turbulence Structures in the Boundary Layer with $Re_2 = 5,000$ (a) and $Re_2 = 10,000$ (b) (according to Head [32])

2.2 Overview of Available Literature

2.2.1 Boundary Layers under the Influence of Free Flow Turbulence

The influence of free stream turbulence extends to all areas of a transitional boundary layer. In addition to the influence of the reversal process, effects occur mainly in turbulent boundary layers. In laminar boundary layer zones, events caused by the degree of turbulence occur predominantly when pressure gradients are present.

2.2.1.1 Laminar Boundary Layers and Reversal with Varying Free Stream Turbulence

The generation of heat transfer on cooled gas turbine blades is determined by the laminar-turbulent boundary layer reversal. Beginning and length of the reversal process are subjected to a multitude of influencing parameters, with the most important being free stream turbulence. Several publications demonstrate their significance under flat plate conditions with a mostly adiabatic flow [35-46]; this was proven with comprehensive quantitative information [37-39, 42, 43, 44]. Because pressure gradients also change the reversal process, many studies determined both parameters together [35, 37, 38, 41-45]. All authors recognized that, with increasing turbulence, an upstream shift of the reversal and a shortening of the reversal length occurred. In flows with pressure gradients it was determined that with a superimposition of both parameters the prefix of the pressure gradient has a decisive significance: positive pressure gradients excite turbulence movements in the boundary layer and cause, similar to free stream turbulence, an early reversal. In accelerated flows, a stabilization of the laminar boundary layer and a delay of the reversal start taking place. Negative pressure gradients thus counter-act the external turbulence, and the relative strength of both components becomes a decisive factor for the final formation of the reversal.

Experimental test results are based on observations of the heat transfer coefficient path or on scanning of the boundary layer with hot wire and Pitot tubes. Hall and Gibbings [43] (1972) provide a comprehensive summary and evaluation of all experiments made up to that time and of models - developed on a semi-empirical basis - for the prediction of the impulse loss thickness Reynolds number at the initiation of the reversal. In an analysis of their tests and previous studies they express the opinion that, with increasing turbulence, the reversal Reynolds number approaches a lower threshold which is considered a stability limit and which must not be exceeded even by the highest degree of turbulence. The Reynolds number at the neutral point ($Re_2 \approx 160$), which is used in the stability theory, is named as the limit. This theory is supported in recent studies by Abu-Ghannam and Shaw [45]. As of this date, however, a clear explanation of this fact which is based on experimental data, has not been possible because of instabilities and the spread of measured reversal Reynolds numbers (see [45]). In addition, little data is available which deal with the high turbulence area in a satisfactory manner.

The significance of pressure gradients in flows with external turbulence was expressed by correlations in several publications. Abu-Ghannam and Shaw [45] provide an overview of these relationships. The impulse loss thickness Reynolds number is predominant for the global characterization of the reversal initiation.

In accordance with experimental findings, the boundary layer stabilization, which occurs with accelerated flows, results in an additional down-stream relocation of the reversal initiation and in an increase of the reversal length. With lower degrees of turbulence, this event is coupled with an increase of the impulse loss thickness Reynolds number at the beginning of the reversal. In accordance with recent studies by Abu-Ghannam and Shaw [45] and Blair [39], the latter event no longer applies to accelerated boundary layers with more than 1% of free stream turbulence:

In contrast to earlier explanations by Hall and Gibbings [43], with turbulence in excess of 1% the same impulse loss thickness Reynolds number is present at the beginning of the reversal as with identical external turbulence in the case without acceleration. Therefore, the smaller boundary layer or impulse loss thickness increase is the sole reason for the down-stream relocation of the reversal.

Abu-Ghannam and Shaw [45] deal with the significance of the boundary layer's history. They describe the difficulties of a correlation, which is based on reversal prediction, if the reversal occurs in flows with non-constant acceleration.

An estimation of the reversal length has only been made in few studies (see [45]) and only for boundary layers without pressure gradients. So far, measurements in flows with applied pressure gradients have not shown any noticeable correlation possibilities for reversal length.

Büyüktür et al [41] and Hislop (see [43]) pointed out the significance of free stream turbulence structure as an additional parameter which influences the reversal process. In experiments, various turbulence structures with the same degree of turbulence were generated by various types of turbulence nozzles. While Büyüktür et al [41] did not realize any effects caused by changed linear measures of the free stream turbulence, Hislop (see [43]) recognized these tendencies. Hall and Gibbings [43] believe that the great differences and spreads of the reversal Reynolds numbers, which were measured by various authors, are caused by linear measurement influences.

The laminar boundary behavior under the influence of free stream turbulence was mostly evaluated with the aid of measured heat transfer distributions [35-41, 44]. It was mutually determined that laminar boundary layers without pressure gradients are not subject to any influences, but that laminar boundary layers in an accelerated flow experience a slight increase of the heat transfer. This effect in accelerated flows was verified by Junkhan and Serovy [35] in boundary layer measurements. In these experiments, fuller velocity profiles were observed under the influence of external turbulence; however, they continue to show the typical laminar boundary layer shape.

2.2.1.2 Turbulent Boundary Layers with Free Stream Turbulence

The influence of free stream turbulence on turbulent boundary layers has been the subject of many experimental, analytical and numeric studies [see 35-41, 46-63]. With adiabatic boundary layer flows, all authors agreed that free stream turbulence results in an increase of the friction coefficient c_f and in a higher boundary layer growth. Higher tangential stress coefficients and boundary layer growth are in agreement with fuller boundary layer profiles which can generally be identified by greater displacement thicknesses δ_1 , impulse loss thicknesses δ_2 and, especially, by the decreased form parameters H_{12} . However, despite a restructuring of the boundary layer profiles, the validity of the logarithmic wall theory has proven to be unchanged so that the deformation of the profiles with semi-logarithmic application (see Illustration 2.1) extends exclusively to the external area of the boundary layer (wake portion). The wake portion decreases with increasing turbulence.

Kline et al [46] and Junkhan et al [35] were the first to demonstrate such effects. Their theory was mostly based on the analysis of velocity profiles. With additional registration of turbulence structures, Charney et al [47], Huffman et al [48] and Evans [50] were able to show an increased turbulence level, stronger turbulent exchange events and increased turbulent shear stresses within the boundary layers as a result of free stream turbulence. Huffman [48] balanced the turbulent energy exchange within the boundary layer. By doing so, he was able to demonstrate that production and dissipation of turbulent kinetic energy are increased and, compared to the convective portions, dominate in the same manner as in boundary layers without external turbulence. In addition, he provides a comprehensive analysis about the change of the turbulent mixing path and the turbulent dissipation length as a result of free stream turbulence. Evans [50] describes the increase of individual turbulent fluctuation components in and vertical to the main flow direction caused by external turbulence. In his tests he further determines that an increase of the impulse loss thickness does not necessarily have to occur with increased free stream turbulence. The deformation of the profiles near the wall and at the edge of the boundary layer can adopt shapes which compensate each other in the impulse loss thickness determination. These effects were also discovered by Raghunathan et al [60] in more recent studies.

Green [51] and Robertson & Holt [52] also perform analytical and theoretical studies of boundary layer phenomena during free stream turbulence. They were taken up by Bradshaw [53] who summarizes them in an overview which includes additional experimental results. It provides a theoretical reason for the linear increase of the tangential stress coefficient with increasing external turbulence which was demonstrated by numerous experimental studies (e.g. [47, 49, 52, 54]). Experiments have shown that, compared to boundary layers with identical impulse loss thickness Reynolds number, a 2-4 percent increase of the tangential stress must be expected for each percentile of external turbulence. The reasons for this increase of

c_f are, in addition to technical difficulties with measuring equipment, instabilities which are a result of additional Reynolds number effects and varying free stream turbulence structures [49, 53].

The significance of turbulence structure was realized in recent studies (Simonich and Bradshaw [54], Bradshaw [54], Hancock [56], Hancock et al [59], Meier and Kreplin [58], Blair [36, 39]. In order to characterize the structure, a turbulent linear measure was created with the attenuation behaviour or with the energy spectrum of the local free stream turbulence. This measure is also referred to as dissipation length. The studies show that the strongest influence of external influence occurs in those cases where these linear measures have almost the same magnitude as the boundary layer thickness. According to Hancock et al [59], in turbulent eddy structures with large linear measures turbulence motions at the edge of the boundary layer are impaired by the vicinity of the wall. This causes their interaction with the boundary layer to attenuate. With these considerations, Bradshaw and Hancock [55, 56] also studied the measurements by Meier and Kreplin [58] where, for low degrees of turbulence below 1%, only very minor increases of the tangential stress coefficient c_f were noted. There was, however, a square-law dependency on the turbulence intensity. At the same time, linear measure influences were cited as possible reasons for findings in recent studies [52, 57] (see [53, 55, 59]) whereby, for high turbulence intensities above 8%, the increase of the tangential stress coefficient c_f asymptotically strives toward a limit of approximately 20-30%.

In another study, which provides a detailed introduction of boundary layer measurements and heat transfer measurements, Blair ([36, 38]) discusses and correlates the mutual importance of linear measure and Reynolds number influences. He states that Reynolds number influences have the same effect as linear measures, which are too large, and thus contribute to a decrease of the turbulence intensity influence.

Raghunathan [58] expands the studies about the influence of free stream turbulence in turbulent boundary layers to flows with high velocities ($Ma = 0.8$). While circumventing the above Reynolds number and linear measure influences he quantitatively demonstrates that, even under these conditions, the same turbulence intensity effects exist as in previous studies with low free stream velocity.

Numerous experiments with the adiabatic boundary layer provide consistent information about the behavior of the flow boundary layer. However, distinct differences of opinion are noted in the evaluation of the turbulent heat transfer under the influence of free stream turbulence. In the publications of Edwards and Furber [61], Reynolds et al [63], Kestin and Maeder [41], Büyüktür and Kestin [40], Junkhan and Serovy [35] and Cosigny et al [44] it is stated that the influence of the turbulence on the turbulent heat transfer is negligible. Tests by Sugawara and Sato [62] and recent studies by Blair [36, 39], Simonich and Bradshaw [54] and Pedisius et al [57] show that increased rates of heat transfer were observed which are comparable with increases of the tangential stress. The discrepancy in this evaluation can be explained by the fact that, in many cases, the heat transfer coefficients were compared at locations with identical running length or identical running length Reynolds numbers. This procedure does not consider that boundary layers with increased external turbulence increase at a higher rate. Therefore, thicker boundary layers with increased heat transfer resistance occur at the same location x or Re_x . This process counteracts the actual increase of the heat transfer; consequently, no net effect may be visible when the heat transfer coefficients are locally applied. The heat transfer changes caused by free stream turbulence will only occur when boundary layers with identical local characteristics (e.g. impulse loss thickness) are used for the evaluation. In comprehensive comparisons of boundary layers with identical impulse loss thickness Reynolds numbers, Simonich et al [54], Blair [36, 39] and Pedisius [57] demonstrate that there is a close interrelation between the behavior of the heat

/17

transfer and the wall tangential stress. The increase of the heat transfer with increasing turbulence as well as the significance of linear measures and Reynolds number effects, which we know from the tangential stress coefficients, were thus discovered.

Detailed boundary layer measurements which show the reaction of velocity and temperature profiles to increased free stream turbulence are described by Simonich et al [54], Blair [36-39] and Pedisius et al [57]. All authors demonstrate that, even in the temperature profile, the influence of the turbulence is mainly in the wake area.

2.2.2 Boundary Layers under the Influence of Varying Material Values

Boundary layers with heat transfer and constant material properties, which were used as a basis for the above analyses of the influence of free stream turbulence on the heat transfer, are an exception in practical engineering. They are often generated in tests to demonstrate basic heat transfer phenomena. In contrast, boundary layer flows, which are generated around gas turbine blades with wall cooling, contain high temperature gradients which result in pronounced material value variations within the boundary layer. This has a major effect on air and comparable combustible gases with respect to density ρ , viscosity μ , and heat conductivity λ . The specific heat c_p and the Prandtl number Pr experience only minor alterations.

2.2.2.1 Laminar Boundary Layers and Reversal during Wall Cooling

Statements about the influence of variable material values for laminar boundary layers are almost exclusively based on theoretical or numerical boundary layer analyses [64-67]. An examination of available literature revealed no representative or conclusive test results which provide a detailed description of the laminar heat transfer and the laminar wall tangential stress or which demonstrate

conclusive boundary layer profile measurements. According to theoretical calculations, only minor increases of heat transfer and wall tangential stress occur with wall cooling, despite a distinct deformation of the velocity and temperature profiles. The reason for these insignificant effects is that the velocity and temperature gradients near the wall, which have been increased by the cooling, are almost totally offset by a simultaneous heat conductivity and viscosity decrease.

Eckert (see [64, 68]) developed the concept of considering the influence of material values in such a manner that they are established for a suitable, empirically determined reference temperature; they are then used for the relations obtained in the case of constant fluid properties. Eckert proposes the arithmetic average between free stream temperature and wall temperature as the reference temperature for incompressible laminar boundary layers.

A second possibility of registering material value influences is to expand correlations determined for constant fluid properties by temperature correction functions. Proposals on this subject are made by Kays [64] and Brand & Wehle [65].

Schlichting [22] discusses the influence of material value changes in the boundary layer on the laminar-turbulent boundary layer reversal for flow cases without external turbulence. Based on the linear stability theory, a profile theory referred to as reversing point criteria, calculations by Cebeci and Smith (see [22]), and measurements by Liepmann (see [22]) the opinion is expressed that wall cooling increases the stability of the laminar boundary layer, thus delaying the reversal of the boundary layer. Ghon [22] summarizes this theory in a general study on the subject of laminar-turbulent boundary layer reversal and provides additional background information.

More recent experiments with supersonic flows made by Watson [69] and Fischer [70], however, contradict the idea of boundary layer stabilization by wall cooling. According to their measurement results, no altered reversal occurs in flows with wall cooling if the same free stream Reynolds number is maintained in a varying temperature ratio T_w/T_∞ .

2.2.2.2 Turbulent Boundary Layers with Varying Wall and Free Stream Temperatures

The influence of changeable material values originally became a dominant part of boundary layer research with the study of compressible boundary layers. The friction heating, which develops within these boundary layers, causes temperature increases which - even without heat transfer at the wall - are related to fluid property changes of such magnitudes that they can no longer be neglected. In addition to experimental gathering of information about specific events, it was the goal of studies performed on this subject to find those conditions with which the boundary layer differential equations could be transformed to a simpler incompressible form. Another focal point was to convert these transformations to turbulent boundary layer profiles, friction coefficients and, at a later time, to heat transfer coefficients. The relationships and correlations obtained for constant fluid properties would then be used for further research (see [71]). In studies about the influence of compressibility, Spalding and Chi [72] included the aspects of additional heat transfer; Gran et al [73], Watson [69] and Lee et al [74] included the specific aspects of wall cooling. In contrast to the influence of compressibility, wall cooling affects a slight increase of heat transfer and wall tangential stress. Together with other research about compressible turbulent boundary layers, White [70] summarized these effects in an overview.

Parallel to research with compressible boundary layers, interest increased on the significance of variable material values in incompressible boundary layers in subsonic flows. This has a special significance for the flow conditions in gas turbines. Because the exhaust Mach numbers of current turbine nozzles are only in the area of

$$0.6 < Ma < 1.2$$

and local values in excess of $Ma = 1.8$ rarely occur, no pronounced compressibility influences are expected (see [4]).

Tests were made for boundary layers with wall cooling [75-80] as well as for flows with high wall heating [81-84]. Comparisons with compressible boundary layers were frequently made and the relationships and transformation equations obtained for them were assumed and further developed. For example, Spalding and Chi [75] used equations, which were obtained with the description of compressible boundary layers, for the analytical computation of heat transfer and wall tangential stress and expanded them for the calculation of incompressible boundary layers. I performed the test for incompressible flows in the preparation of this dissertation with highly cooled flat plates. With increased wall cooling, these measurements show an increase of the heat transfer which, with a running length Reynolds number of $Re_x = 10^6$ and a decrease of the temperature ratio to $T_w/T_\infty = 0.4$, is between 15 and 20 %. Similar local increase rates were observed by Back and colleagues [67].

The effects are more distinct if, instead of wall cooling, the surface is heated. Instead of a heat transfer increase, there is a decrease in the local heat transfer coefficients which, according to the measurement results achieved by Rotta [83] and the analyses by Kays [64] can be approximated with the factor

$$(T_w/T_\infty)^{-0.4}$$

In further studies of the influence of wall cooling, Back, Cuffel and Massier [76] and Sill [78] made detailed analyses of turbulent boundary layer profiles and friction coefficients. The illustration of velocity and temperature profiles in a semi-logarithmic plot demonstrates differences to the isothermal flow; these differences are especially pronounced with respect to the logarithmic wall theory. To describe these events, Rotta [86] developed expanded analytical equations for the logarithmic wall theories of flow and temperature boundary layers.

The development of optical measuring methods (Laser-Bi-Focus and Laser-Doppler measuring procedure) provided the opportunity for studying the transport events within the boundary layer, which are responsible for profile deformations and tangential stress alterations, even under high cooling or wall heat conditions. With optical measurement procedures Eriksen, Wittig et al [79, 80] performed tests in highly cooled boundary layers, while Cheng and Ng [84] made their tests in highly heated subsonic boundary layers. Independent of the type of heat transfer (heat, cooling), it was demonstrated that material value variations have no influence on the turbulence structure. The turbulent shear stress distribution $-\rho \overline{u'v'}$ followed the influence of the distinct temperature field only because of its immediate relationship with the density ρ . A great number of details are contained in the test results by Eriksen et al [79, 80]. In addition to turbulence and shear stress distribution, the authors determined turbulent energy balances, triple products of the turbulent fluctuation quantity, and linear dissipation measures in the boundary layer.

2.2.3 Boundary Layers under the Influence of Pressure Gradients

The pressure gradient is the parameter with the most extensive consequences for the boundary layer of the gas turbine blade under flow conditions. It can result in flow separation or relaminization and plays a major part in the formation of the laminar-turbulent

boundary layer reversal. The reasons for this are the destabilizing effects of positive pressure gradients and the stabilizing effects of negative pressure gradients (acceleration). Back [66] demonstrates this with the aid of numeric calculations for accelerated laminar boundary layers. Stabilization occurs because the profile gradients near the wall increase thereby generating fuller boundary layer profiles which distinguish themselves by increased heat transfer and increased wall tangential stress, but also by decreased boundary layer thickness growth.

The above effects are also present in turbulent boundary layers. In addition to the stabilization of the boundary layer, an attenuation of the boundary layer turbulence occurs which, in extreme cases, may result in relaminization. According to Kays and Moffat [86], relaminization occurs in flows without free stream turbulence when the local acceleration parameter $k(x)$ exceeds the value

$$k = \frac{v_{\infty}}{u_{\infty}^2} \cdot \frac{du_{\infty}}{dx} \sim 3 \cdot 10^{-6}$$

For comparison, the real flow in the initial stages of gas turbine blades frequently has much higher acceleration intensities. There are, at times, k -values with a magnitude of 10^{-5} .

For the most part, the analysis of pressure gradient influences is determined by the observation of turbulent boundary layers and laminar-turbulent reversal events. The interest in purely laminar boundary layers without free stream turbulence has, for the most part, been exhausted. Due to a lack of turbulence events, this type of flow has theoretically been revealed and can be mastered in a relatively simple manner with available computers.

Turbulent boundary layers were experimentally studied for delayed as well as for accelerated flows [86-92]. Clauser [93], Rotta [94] and Cebeci [91] published overviews on this subject. Their experiments were mainly concentrated on the representation of the boundary layer profile [86-92] and the analysis of heat transfer distributions [86, 89, 90]. In these tests it was discovered that the logarithmic wall theory which applies to unaccelerated boundary layers can, without any changes, be applied to boundary layers with pressure gradients even for compressible flows, if there is no danger of flow separation or relaminization tendencies. Therefore, the effects of pressure gradients occur only in the wake area and near the wall. The deformations near the wall can be explained by the wall bond of the boundary layer differential equations (see chapter 6). Events in the external area can be identified by the fact that the wake portion decreases with acceleration. The wake portion increases when a delay occurs. Analytical possibilities of describing these transformations were developed by Townsend [95], Szablewsky [96], Coles [97] and McDonald [98].

Tests performed by Kays and Moffat [86] and Back et al (see [91]) are particularly interesting, because they deal with basic properties of turbulent boundary layer development in flows with pressure gradients and because they demonstrate the differences between flow and temperature boundary layers. Measurements by Kays and Moffat [86] show that, for constant accelerated flows with $k(x) = \text{const.}$, the boundary layer strives toward a condition of equilibrium which distinguishes itself by constant impulse loss thickness Reynolds numbers, shape parameters, tangential stress coefficients and 'similar' velocity profile shapes. This, however, does not apply to the temperature boundary layer; consequently, the Stanton coefficients continue to fall with the running length. Additionally, this report [86] notes that the turbulent Stanton coefficients decrease with acceleration; because of this, special consideration must be given to the starting conditions of the boundary layer before entering the acceleration phase. The enthalpy loss thickness/impulse

loss thickness relationship at the beginning of the pressure gradient is named as the characteristic parameter of the boundary layer's history.

Back et al (see Cebeci [91]) performed tests in a nozzle with the greatest acceleration ($k \leq 8 \times 10^{-6}$). The report makes a direct comparison between the different reactions of temperature and velocity profiles when a staggered acceleration increase, which culminates in relaminization, occurs. In the velocity profile, relaminization occurs earlier than indicated in the distribution of the heat transfer coefficients or in the temperature profile. A similar divergence of flow and temperature boundary layers was discovered by Blair [37, 39] in the laminar-turbulent reversal behavior. In spite of a relatively low acceleration ($k < 1 \times 10^{-6}$), the reversal in the flow boundary layer was terminated noticeably faster than in the heat transfer distribution along the plate. The reason for the sluggish behavior of the temperature boundary layer is that the temperature profile is affected only indirectly by the pressure gradient via convective events in the boundary layer, which depend on the deformation of the velocity profile (see boundary layer differential equations in chapter 6.2).

The importance of pressure gradients for the laminar-turbulent reversal process was discussed in the previous chapter on the influence of free stream turbulence. Because of this, I will not deal with it a second time. Additionally, I will not provide information about positive pressure gradients. As explained before, I am mainly concerned with accelerated flows.

3. EXPERIMENTAL GOALS

A reading of the aforementioned literature revealed a number of reports which deal with the influences of free stream turbulence, variable material values and pressure gradients. These reports show the significant effects of these parameters and are supported by quantitative statements.

Well-known experimental tests were preferred for tests of turbulent boundary layers. Therefore, the number of those experiments which expand the knowledge of the reversal process to laminar boundary layer section is comparatively small. Laminar boundary layers are almost exclusively discussed on a theoretical basis; this applies especially to the influence of variable material values on wall cooling.

The measurements themselves are based on flow parameters which are rarely found in a turbine. For example, in the examination and further development of calculation procedures there are no boundary layer studies which determine the range of low Reynolds numbers, which is characteristic for blade flow. Therefore, an accurate description of the additional effect caused by low Reynolds numbers does not exist. Additionally, there is no basic data on boundary layers with free stream turbulence which are characterized by acceleration intensities similar to those in a turbine. In a turbine, the acceleration parameter k (see equation 3.1) achieved values of a 10^{-5} magnitude. In current experiments with transitional boundary layers with free stream turbulence, only acceleration forces below $k = 1 \times 10^{-6}$ (see [39]) were achieved. From the high increase of laminar heat transfer (e.g. Krisnamoorthy [99]), which was observed in blade tests, it was concluded that special effects occur when highly accelerated flows with a strong external turbulence are applied.

Another decisive factor of this study was that, to date, no experiments have been published which describe the influence of external turbulence and pressure gradients under turbine-like cooling conditions. The reversal behavior during wall cooling was as unclear as the effect of the cooling on the local heat transfer rates. Present knowledge on the influence of free stream turbulence was obtained with adiabatic or slightly heated surfaces, i.e. only for flows with almost constant material values. Because of this, it is also unclear whether turbulence intensity effects in turbulent boundary layers experience a change due to strong wall cooling.

Because of the above conditions, further studies were required which, for a direct relationship to the turbine flow, describe transitional boundary layers in the area of low Reynolds numbers and, when under the influence of high free stream turbulence, intensive wall cooling and high free stream accelerations occur.

To develop experimental data, a flat boundary layer tunnel was constructed which allows fundamental studies of transitional boundary layers with external turbulence, free stream acceleration and wall cooling. Characteristic flow conditions realized are:

- free stream temperatures of $T_{\infty} = 300 - 600 \text{ K}$
- temperature conditions of $T_w/T_{\infty} = 1.0 - 0.53$
- free stream turbulence intensities of $T_u = 1.6 - 9.3\%$ and
- free stream acceleration $k = 0 - 6.3 \times 10^{-6}$ values of

The acceleration parameter k is defined as follows:

$$k = \frac{v_{\infty}}{u_{\infty}^2} \frac{du_{\infty}}{dx} \quad (3.1)$$

The running length Reynolds numbers at the end of the plate were between 0.25×10^6 and 1.0×10^6 . This sufficiently met the demands of turbine-relevant Reynolds number conditions.

The experiments were made in individual stages. For reasons of comparison, I began by studying the adiabatic boundary layer with varying free stream turbulence. I then superimposed wall cooling and pressure gradients. In addition to local heat transfer coefficients I also measured boundary layer profiles and wall tangential stress values for unaccelerated flow. This was accomplished with mechanical flow and temperature probes. Due to technical constraints, tests with accelerated flow were limited to the determination of local heat transfer numbers. In this case, practical boundary layer measurements were precluded by testing limitations and boundary layer thicknesses which were estimated to be extremely thin.

Free stream turbulence was determined with the aid of Laser Doppler anemometry. The use of this optical test method enabled a reaction-free determination of individual turbulence intensity components and the registration of the continuous turbulence intensity path over the measuring plate.

4. TEST DESIGN AND EXPERIMENTAL METHODS

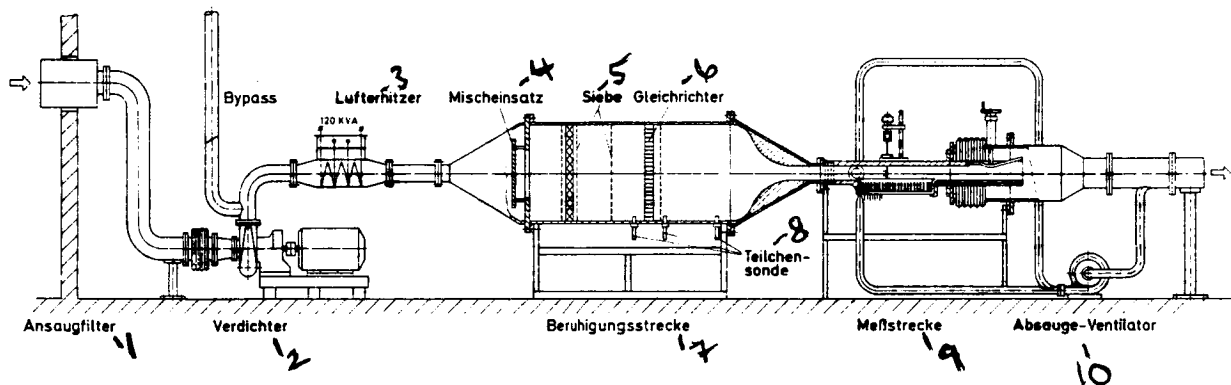
4.1 Test Unit

For the experimental determination of heat transfer coefficients under the ideal conditions of a flat plate, we developed a measuring section which could be incorporated in the available hot gas unit of the Institute for Thermal Dynamics. Illustration 4.1 shows a schematic of the entire test unit which consists of a compressor, an electric air heater, a steadying zone, the measuring section and an exhaust duct.

The air from the compressor is fed into the measuring section via an electric air heater and a steadying zone. The air mass stream, which can be adjusted with a bypass valve, and the adjustable filament power (120 kW max.) enable hot gas temperatures of up to 600 K.

A stabilizing zone is located between the air heater and the test area. This zone contains a mixing unit, a flow straightener and several wire sieves to steady and equalize the flow. The hot gases are fed into the adjacent measuring section via an inlet nozzle (surface contraction ratio 1:25).

The height and, consequently, the profile of the adjoining tunnel outlet are adjustable which enables variation in the pressure level within the measuring section. An additional hot air blower will drain bottom and side wall boundary layers from the test plate.



- 1 - suction filter; 2 - compressor; 3 - air heater; 4 - mixing unit;
 5 - sieves; 6 - straightener; 7 - steadying zone; 8 - particle probe;
 9 - measuring section; 10 - suction fan.

Illustration 4.1: Hot Air Test Unit with Measuring Section to Determine Heat Transfer

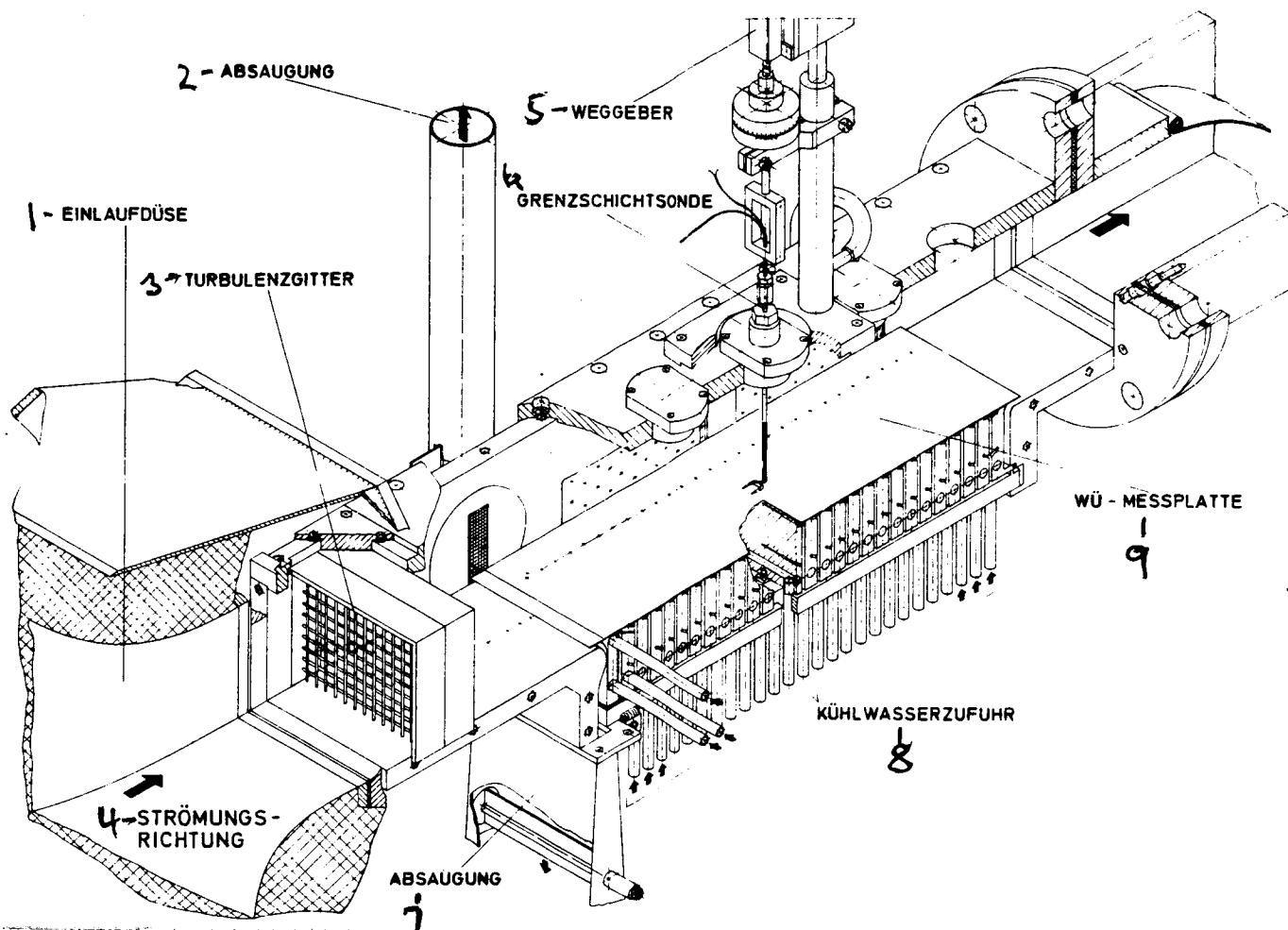
4.2 Measuring Section

My primary goal was the determination of local heat transfer coefficients with varying free stream turbulence, free stream temperatures and free stream acceleration. Additional boundary layer measurements were made for a detailed demonstration of boundary layer events assigned to measure heat transfer. In addition, they provided an opportunity to compare initial studies of the isothermal boundary layer with results available in literature.

4.2.1 Design Description

The design of the measuring section is presented in Illustration 4.2. The measuring section has a rectangular profile of 100 x 125 mm and a total length of 800 mm. The principal part of the tunnel is a copper test plate with a length of 440 mm and a width of 125 mm. The test plate is sub-divided into 28 individual parts which contain one cooling hole each. This allows independent cooling of each individual segment. At the plate surface, the segments are interconnected with a thin bar (1.5 mm), which enables mutual heat exchange to be as low as possible. The length of the bar is 3 mm. In the flow directions, the segments have a length of 12 mm, a width of 115 mm and a height of 68 mm. With the temperature difference in individual segments, which is measured by two 0.5 mm sheathed thermocouples at a distance of 1.5 and 40 mm from the plate surface, we obtain - under the assumption of a one-dimensional heat conduction - the heat flow removed from the hot gas and, consequently, the heat transfer coefficient. (Required measures for the consideration of the influence of the connecting bars are described in following chapters). In our tests, the cooling of the segments was adjusted in such a manner that the temperature along the plate surface was constant. Thermal insulation mats protected the segments from heat from the sides (see Illustration 4.5). The measuring plate is supported by a base plate. An equalization of thermal expansion between the cooled plate and warmer tunnel walls is possible.

(26



1 - inlet nozzle; 2 - suction; 3 - turbulence grid; 4 - flow direction; 5 - position pickup; 6 - boundary layer probe; 7 - suction; 8 - cooling water supply; 9 - measuring plate.

Illustration 4.2: Boundary Layer Tunnel with Measuring Plate

The generation of varying free stream turbulence intensities is achieved by round bar grids with varying grid diameters (see Illustration 4.4). The grids may be inserted in the tunnel 150 - 200 mm in front of the leading edge of the plate. Because free stream turbulence is determined with optical methods (Laser-Doppler-Anemometry), the side walls of the measuring tunnel were equipped with large windows.

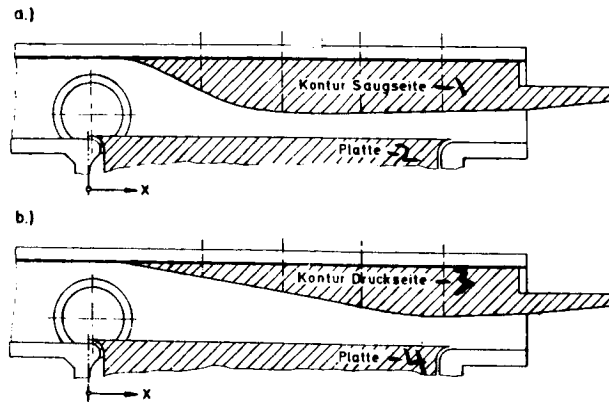
The tunnel lid has four openings for the insertion of the flow probes. This enabled the registration of boundary layer profiles at a distance of 120, 220, 320 and 420 mm from the leading edge of the plate.

In order to achieve an initial laminar boundary layer, it was necessary to expand the test plate with an uncooled, 15 mm long brass plate with an elliptic leading edge profile. In addition, the tunnel inlet flow on the bottom had to be drawn off at the leading edge of the plate to obtain a well defined boundary layer beginning. The boundary layer draw-off was adjusted in such a manner that the static pressure path over the leading edge of the plate remained almost constant. This guaranteed an isokinetic suction. Consequently, there were no flow disturbances at the leading edge of the plate which could have caused a premature laminar-turbulent boundary layer reversal on the plate. We examined a possible dependency of the laminar-turbulent separation reversal on the suction. An up-stream displacement of the reversal was only noticed when the suction was weak, i.e. when the pressure increased at the leading edge of the plate. A high degree of suction had no effect on the reversal or on the measured heat transfer coefficient.

To avoid an influence on the heat transfer measurement by side wall boundary layers, they were drained in the immediate vicinity of the plate's leading edge. This requires a replacement of the round side windows by appropriate suction devices. The required suction strength was determined by measuring the side wall boundary layer thicknesses and with the aid of heat transfer test measurements.

4.2.2 Expanded Design to Generate Pressure Gradients

The desired pressure gradients in the flow were achieved by placing inserts into the tunnel. The inserts were designed in accordance with given acceleration and retardation paths. The contour inserts used were designed in such a manner that the quality of the pressure gradient paths is analogous to the blade flow on the suction and on the pressure side. The two contours are shown in Illustration 4.3. The contour on the "pressure side" accelerates the flow in an even manner almost throughout the entire length of the plate. With the "suction side" contour, the acceleration becomes, after 170 mm, a light, separation-free retardation.



1 - contour, suction side; 2 - plate; 3 - contour, pressure side; 4 - plate.

Illustration 4.3: Pressure Gradient Contours

- a) Contour 2 ('suction side')
for high acceleration ($k(x) = \text{const.}$)
- b) Contour 1 ('pressure side')
for low acceleration ($k(x) = \text{const.}$)

The geometric design of the 'suction side' contour is a compromise between the technical solution of the heat transfer in the acceleration range (with an established segment width S) and the achieved maximum acceleration. When designing the 'pressure side' contour, I intended an even ($k(x) = \text{const.}$) acceleration of the flow on those velocities, which were expected at the plate end on the 'suction side' contour. With constant acceleration, acceleration values $k(x)$ achieved with the contours were between $k = 1.2 \times 10^{-6}$ and $k = 2.5 \times 10^{-6}$. Depending on temperature and flow velocity, maximum values of up to 6.3×10^{-6} were obtained on the 'suction side' contour.

For clarification of these fundamental velocity and k -parameter paths I would like to refer to illustration 5.45 in chapter 5.6.

4.2.3 Additions to Generate Turbulence

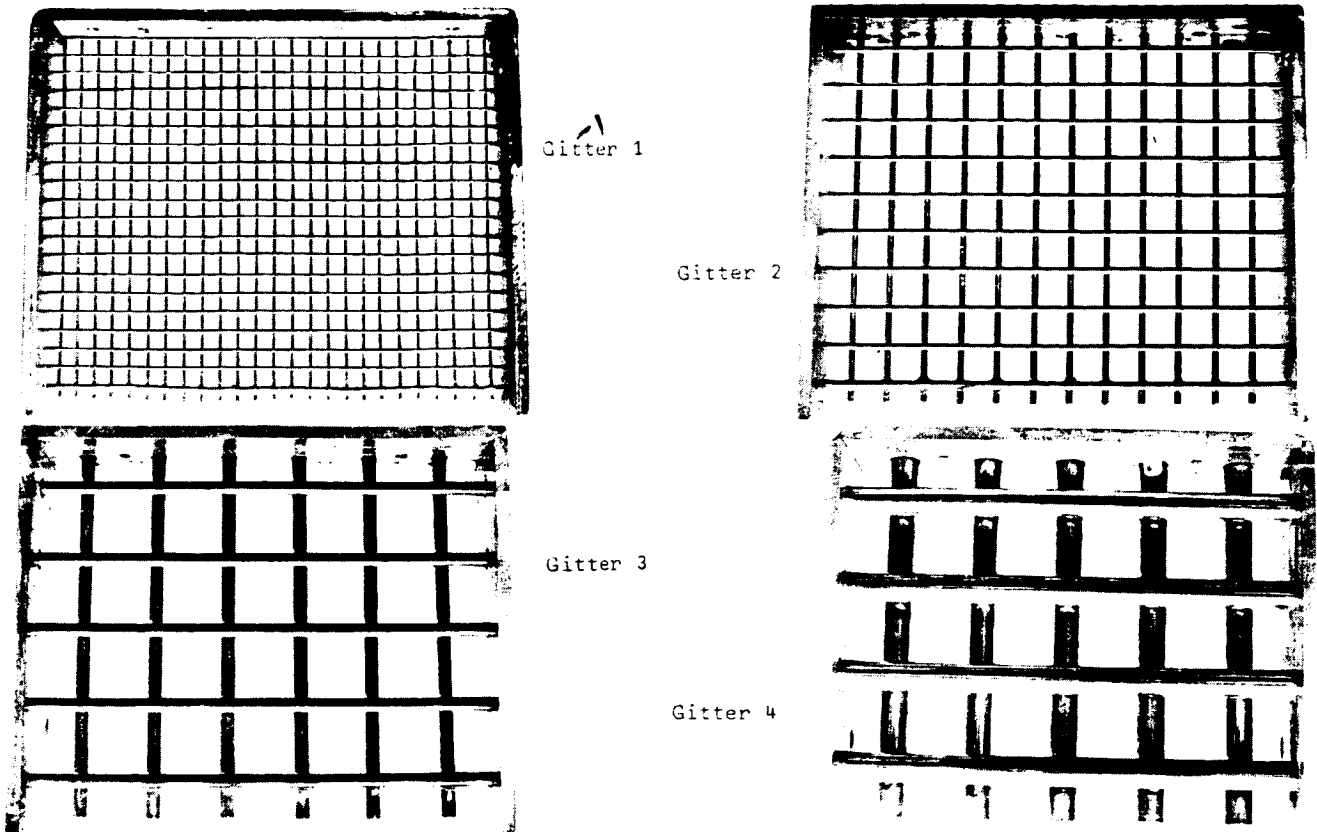
The measurement unit was designed in such a manner that, with the installation of various turbulence grids, a change of the free stream turbulence could be made. In order to correctly simulate conditions in a gas turbine, top turbulence intensities of 8 - 10% and higher were strived for. Known tests by Rosa [100] and Baines & Peterson [101] (see Wittig, Eriksen, et al [110]) were used for the grid design. A turbulence intensity range of approximately 2 - 11 % was achieved with the aid of 4 grids. In order to generate isotropic turbulence, the grids were manufactured from smooth, round wires with square meshes and an obstruction ratio of 0.64. The grids for the boundary layer tunnel are depicted in Illustration 4.4. The geometric data of these grids and an approximation of achieved turbulence intensities are contained in Table 4.1. That portion of the surface, which is occupied by the grid bars, is referred to as the degree of obstruction.

Grid	Mesh Width [mm]	Wire Strength [mm]	Degree of Obstruction	Degree of Turbulence [%]
1	5	1	0.64	2 - 3
2	10	2	0.64	3 - 5
3	20	4	0.64	5 - 7
4	24	8	0.44 *)	8 - 11

*) With given tunnel dimensions a degree of obstruction of 0.64, with a coarse grid 4, proved unfavorable.

Table 4.1: Specifications of the Turbulence Grids Used

ORIGINAL PAGE IS
OF POOR QUALITY



1 - grid

Illustration 4.4: Round Bar Grids for Turbulence Generation
(Grids 1, 2, 3 and 4)

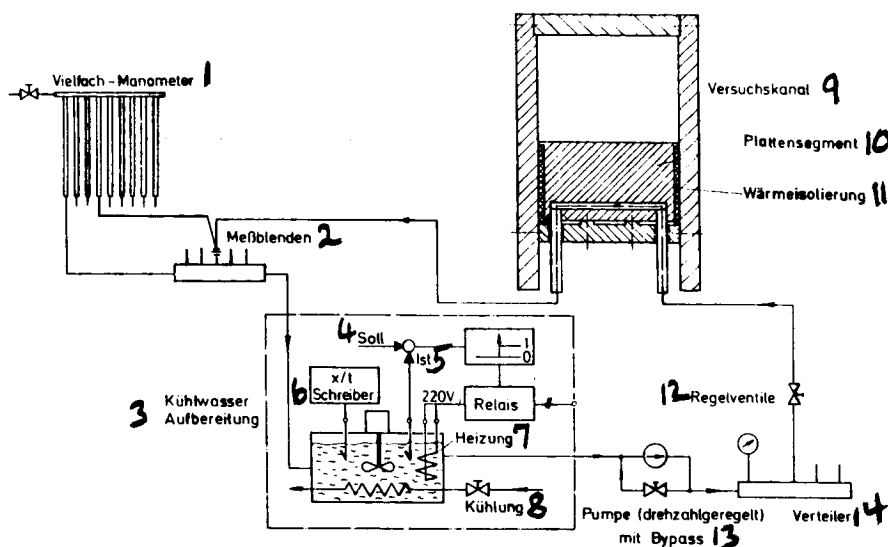
4.2.4 Cooling the Measuring Plate

The measuring plate was cooled with the thermostatic water-cooling cycle, which provided a chronologically constant coolant temperature at the inlets of individual segments.

The cooling design required an estimation of necessary cooling mass flows and coolant temperatures. The ranges of acceptable mass flows and coolant temperatures were determined in such a way that - on the one hand - excessive mechanical stress due to excessive charges and - on the other hand - high coolant heating, which could disturb the one-dimensional heat conductivity process, was avoided. Therefore, the influence of the coolant heating was studied in the segment with the aid of two-dimensional temperature field calculations ('finite elements') and by simulating realistic cooling and gas parameters. The calculations showed that no influence on the measured result is to be expected as long as the coolant heating is not in excess of half of the temperature difference measured in the segment. These parameters for coolant heating, which were constantly monitored during the test, enabled a determination of possible coolant temperatures and cooling mass flows with the aid of simplified heat balance calculations on the segment.

A schematic illustration of the cooling cycle is depicted in Illustration 4.5. A pump, whose speed can be adjusted, transports the thermostabilized cooling water into the 28 cooling segments via a distributor. Because of the varying expansion of tunnel walls and the plate, the cooling water is supplied from the bottom. Each segment is assigned to a control valve which is used to adjust the mass flow to achieve a constant plate surface temperature. Via an accumulator, the heated cooling water is returned to the thermostatic pool. Simple cylinder flow-through restrictors are installed in the cooling water return lines to monitor and reproduce operating conditions. The differential pressures of these restrictors are registered on a multi-tube manometer. The chronological stability of the coolant inlet temperature was monitored with the aid of an x,t-recorder. It was ± 0.2 K during the test. Additional thermo-elements near the feed and outlet of several segments enabled the above mentioned control of the coolant heating.

ORIGINAL PAGE IS
OF POOR QUALITY



1 - multi-tube manometer; 2 - restrictors; 3 - cooling water preparation; 4 - desired; 5 - actual; 6 - recorder; 7 - heating; 8 cooling; 9 - test tunnel; 10 - plate segment; 11 - heat insulation; 12 - control valves; 13 - pump (adjustable speed) with bypass; 14 - distributor.

Illustration 4.5: Cooling Cycle

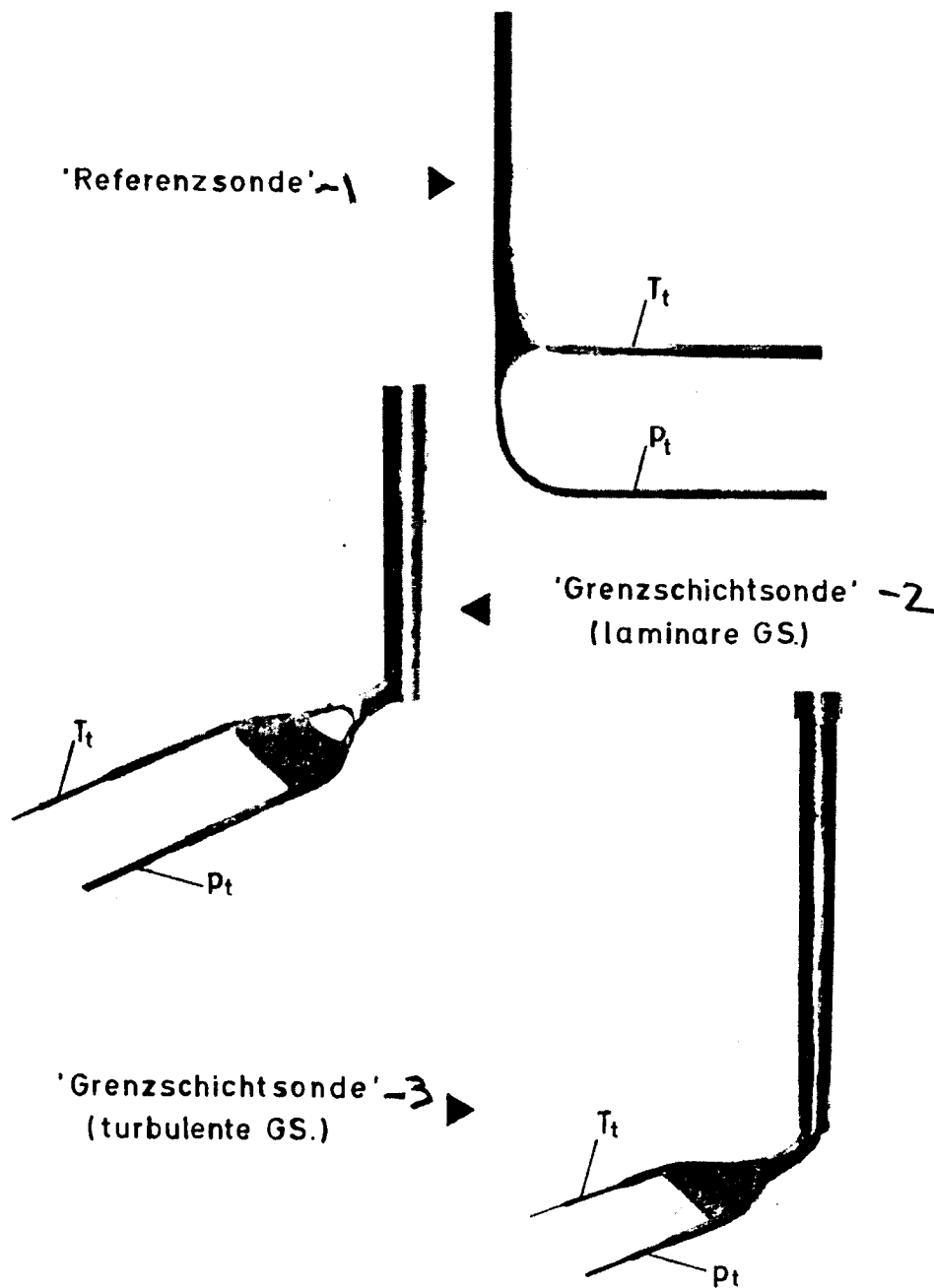
4.3 Test Methods

4.3.1 Determining Free Stream Conditions

Free stream conditions were tested with combined total pressure and total temperature probes. The applicable static pressures were determined with pressure holes in the tunnel walls. The measured values were used to calculate velocity and static temperature with

the known relationship for isentropic condition changes and with the aid of the ideal gas equation for air. When flow parameters and coefficients were determined, the temperature dependency of the material data of the flow medium was considered.

Because, even with acceleration or retardation, total pressure and total temperature in the friction-free free stream flow experienced no change, the velocity distributions along the plate can be determined with applicable static pressure paths. Because of this, the static pressure on each segment was measured with a pressure hole, while total pressure and total temperature were determined in a reference plane. The reference plane was located 100 mm up-stream from the leading edge of the plate. Position and dimensions of the probe (see Illustration 4.6) were selected in such a manner that there was no influence on the boundary layer flow along the test plate.

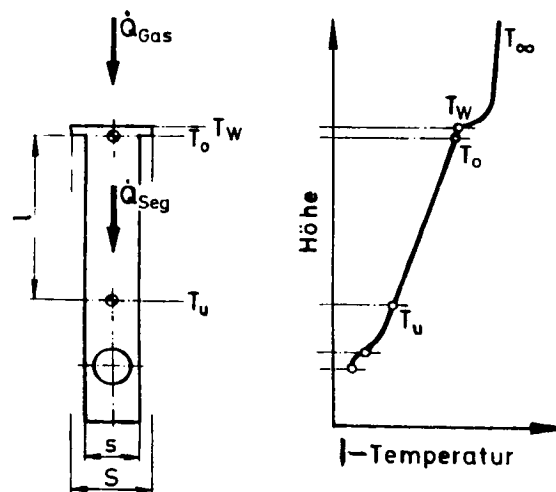


1 - 'reference probe'; 2 - 'boundary layer probe' (laminar boundary layer); 3 - 'boundary layer probe' (turbulent boundary layer)

Illustration 4.6: Flow Probes for Measuring Total Pressure and Total Temperature

4.3.2 Determining Heat Transfer Coefficients

The measurement method for local heat transfer coefficients is based on the supposition of one-dimensional heat conductivity in the cooled segment. Illustration 4.7 is a schematic representation of the temperature path. The linear temperature distribution over the segment, which is assigned to the one-dimensional heat conductivity process, is present up to the immediate vicinity of the cooling hole. The linear temperature path changes near this hole, because the heat flow, which is to be transferred to the coolant, is distributed throughout the entire hole diameter. Two-dimensional temperature field calculations ('finite elements') have proven that this area of influence of the cooling hole does not come in contact with the measurement plane of the lower thermo-element in the segment.



1 - temperature

Illustration 4.7: Schematic Temperature Path in the Segment

Because of the identical heat flows

$$\dot{Q}_{\text{gas}} = \dot{Q}_{\text{seg}} \quad (4.1)$$

the calculation of the heat transfer coefficient with the temperatures measured in the segment can be made by using the following equations (Illustration 4.7):

$$\dot{Q}_{\text{gas}} = \alpha_g \cdot (T_{ei} - T_w) \cdot S \cdot b \quad (4.2)$$

$$\dot{Q}_{\text{seg}} = \frac{\lambda_{Cu}}{l} \cdot (T_o - T_u) \cdot s \cdot b \quad (4.3)$$

\dot{Q}_{gas} is the amount of heat removed from the hot gas by cooling. \dot{Q}_{seg} describes the heat flow in the segment; b is the tunnel width. Both heat flows refer to this width. T_o and T_u are the two measuring temperatures in the segment, T_w is the plate surface temperature, and T_{ei} is the ambient temperature of the wall. The relationship (equation 4.1) provides the following solution for the unknown heat transfer coefficient α_g :

$$\alpha_g = \frac{\lambda_{Cu}}{l} \cdot \frac{T_o - T_u}{T_{ei} - T_w} \cdot \frac{s}{S} \quad (4.4)$$

The wall temperature is derived from the linear extrapolation of the temperature path between the temperature measuring locations:

$$T_w = T_o + \frac{l'}{l} \cdot (T_o - T_u) \quad (4.5)$$

Because of the short distance $l' = 1.5$ mm between plate surface and the top thermo-element, there is little difference between T_o and T_w . The ambient temperature T_{ei} is determined with the recovery factor r :

$$T_{ei} = T_\infty + r \cdot \frac{u_\infty^2}{2 c_p} \sim T_{t_\infty} \quad (4.6)$$

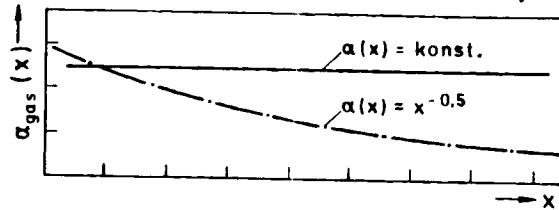
$r = \sqrt{Pr}$ (Pr - Prandtl number = 0.71) applies for laminar flows and $r = \frac{3}{\sqrt{Pr}}$ for turbulent flows. Because, even when pressure gradients are present, available local Mach numbers will not exceed 0.3, inherent and total temperatures are almost identical.

The assumption of one-dimensional heat conduction between the upper and lower thermo-element along the entire width of the segment had to be studied, especially in the area of the upper thermo-element. The reason for this was the presence of a crack in the segment width caused by the bars which connect the segments.

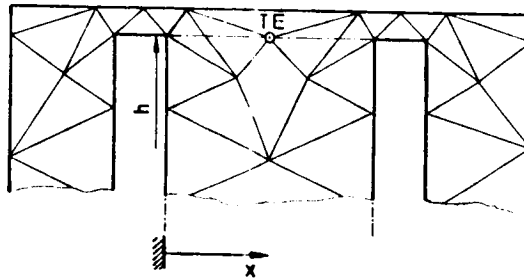
The analysis was made with the aid of two-dimensional temperature field calculations in the finite element method. In order to take into consideration the reciprocal effect of all bars, the calculation was made with three inter-connected segments. The given parameters for the calculation were: the coolant temperature, the heat transfer coefficient on the coolant side, the gas temperature, and the path of the heat transfer coefficient along the three segments on the gas side. In Illustration 4.8 the result of this analysis is shown for two characteristic critical cases for the path of the heat transfer coefficient on the gas side. The illustration depicts the calculated temperature distribution for the center segment area in question, which is marked by the profile crack. T_o and T_u are the temperatures calculated at the thermo-element measuring locations. The example $\alpha_g(x) \approx x^{-5}$ applies to the laminar heat transfer, while $\alpha_g(x) = \text{const.}$ is a good approximation for a turbulent case. Illustration 4.8 shows that the minor deviation (2-4% max. of the temperature difference) at the measuring locations from the temperature distribution during ideal one-dimensional heat conductivity confirms the adoption of the one-dimensional heat conductivity process. The reason for this is the high heat conductivity of copper, which is used as the segment material, which causes a rapid even distribution of the temperature field in this area.

ORIGINAL PAGE IS
OF POOR QUALITY

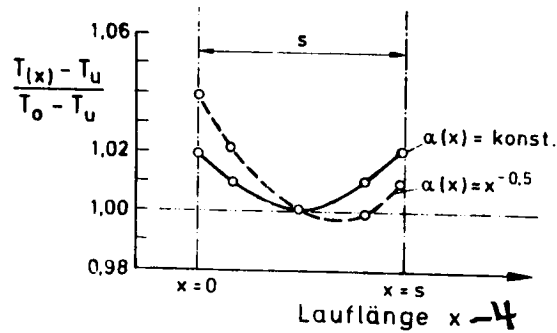
Verteilung der Wärmeübergangszahlen: -1



FEM Gitternetz: -2



Temperaturverteilung in Thermoelementhöhe h: -3



1 - distribution of the heat transfer coefficients; 2 - FEM grid network; 3 - temperature distribution in the height h of the thermo-element; 4 running length x.

Illustration 4.8: Calculated Temperature Losses in the Cooling Segment with a Height h of the Top Thermo-Element for $\alpha(x) = \text{const.}$ (—) and $\alpha_g(x) \approx x^{-0.5}$ (----)

An additional examination of the measuring method was made by calculating the heat transfer coefficients with the aid of the definitive equation (equation 4.4) and the values T_o and T_u , which were obtained with temperature field calculations at the temperature measuring locations. The resulting α_g -numbers were almost identical with the heat transfer coefficients in the segment center for the field calculation.

Because of their significance for an exact determination of the heat transfer coefficients, the heat conductivity of the segment material was also measured. This was accomplished at the Nuclear Research Center Karlsruhe (Institut für Material und Solid State Body Research) with the Laser-Flash method whose principle is discussed in detail in [102]. The value for the temperature range of 290–320 K is $\lambda_{Cu} = 355 \text{ W/mK}$. This result is within the specifications which apply to commercial copper (see [103]).

4.3.3 Boundary Layer Tests and Evaluations

In order to determine the boundary layer profile, total pressure and total temperature profiles in the boundary layer plus the static pressure were measured in a wall hole within the respective test plane. The boundary layer probes used (Illustration 4.6) have two separate, parallel probe arms. One arm serves as a Pitot tube for total pressure measurement, the other contains a sheathed thermocouple ($\phi = 0.25 \text{ mm}$) and is used for total temperature measurement.

For laminar and transitional boundary layers with mostly very thin boundary layer thicknesses of 1.3 mm or less we used a Pitot tube which was reduced from an outer diameter of 0.6 mm to a height of 0.24 mm (see Illustration 4.6). A probe with a circular opening proved to be more practical for fully turbulent boundary layers, because it permits the use of known calibration curves to determine tangential stress.

The probe is moved with a micrometer gauge. It was inserted into a slotted, fixed probe shaft, which has a thickness of 4 mm and which extends to the immediate vicinity of the plate surface (see Illustration 4.2). A fixed shaft arrangement ensured that the effective flow cross-section in the measurement tunnel and, consequently, the flow conditions, would not be altered by probe displacement. The distance of the probe to the wall was electrically registered by a calibrated Ohmic displacement sensor; it was then compared to the reading of a precision dial gauge. The distance of the two probe arms from the plate surface was observed under a microscope against the light.

The evaluation of the measured rough data consisted of the following:

- correcting the total pressure profiles by considering the influence of the shear flow and the wall.
- converting pressures and temperatures to velocities (see paragraph 4.3.1).
- determining tangential stress coefficients and Stanton coefficients.
- calculating integral boundary layer quantities.

Shear flow and wall influences occur because of the velocity gradients and the streamline displacement near the wall caused by the probe. These influences are corrected by assigning to the measuring area a location, which is displaced in the direction of the greater pressure, versus the geometric center of the Pitot tube. McMillan's corrective functions [104] were used for the round Pitot opening, the corrections of Quarmbly et al [105] were applied to flattened probes.

Depending on the type of flow, different procedures were used to determine the wall tangential stress. For laminar boundary layer flows it was calculated with the analytically integrated form of the theorem of momentum, whose derivation is described in detail in [22]:

$$c_f = \frac{\delta_2}{x} \quad (4.7)$$

c_f is the tangential stress coefficient and is obtained with the measured impulse loss thickness δ_2 and the boundary layer running length x . This calculation method applies to incompressible and compressible boundary layers.

A determination of the tangential stress with the linear velocity gradients at the wall was not made in the laminar case. Because of the low boundary layer thickness, the wall gradient could not be obtained with sufficient accuracy.

The following two procedures were used for the determination of turbulent wall tangential stress:

- the Preston method [105] (measurement with applied probe)
- using the general logarithmic wall theory for boundary layers without pressure gradient as an implicit definitive equation for τ_w :

$$\frac{u}{u_\tau} = \frac{1}{k} \cdot \ln \left(\frac{y \cdot u_\tau}{\nu} \right) + C ; \quad u_\tau = \sqrt{\tau_w / \rho} \quad (4.8)$$

with $C = 5.1$; $k = 0.41$

Because of the non-isothermal boundary layers with both test methods, the temperature dependency of the material values (density, viscosity) had to be considered when determining the tangential wall stress with a cooled plate. When using the Preston method, the material values were formed with the Eckert reference temperature which was proven adequate by Holmes and Luxton [107]. This reference

temperature was, in our case, almost identical with the arithmetic mean values of free stream and wall temperatures.

When the wall theory is used to determine tangential stress, the material values were based on a temperature which was determined as an integral throughout the area near the wall ($y \leq 0.2 \times \delta$). This is analogous to a transformation of the velocity profile of a boundary layer with variable density into a velocity profile of a turbulent boundary layer with constant density (see [76, 108]).

Both tangential stress determination procedures provided results with a maximum deviation of 5%. The tangential stress values, which were obtained as the average of both procedures, were used as the actual result.

The measured boundary layer profiles were used to define the (42) integral boundary layer characteristics such as displacement thickness, impulse loss thickness, enthalpy loss thickness, etc. (see list of symbols). Due to the finite dimensions of the boundary layer probes, however, the boundary profiles can only be recorded beginning with a wall distance which is equal to one half the probe diameter. Along the direction of the wall, the measured profiles must be extrapolated with suitable equations to enable a correct integration of the profiles for the determination of integral boundary layer characteristics. As with the determination of wall tangential stress, a differentiation had to be made between laminar and turbulent boundary layer flow. The expansion of the laminar boundary layer profiles was accomplished by approximating the actual boundary layer profiles with the following equation by Polhausen [109]:

$$\frac{u}{u_{\infty}} = 1 - (1-n)^3 \cdot (1+a \cdot n) ; \quad n = \frac{y}{\delta} \quad (4.9)$$

For profiles in the reversal area, the exponential equation

$$\frac{u}{u_{\infty}} = A \cdot \left(\frac{y}{\delta}\right)^{1/B} \quad (4.10)$$

was used with the parameters A and B, which were determined by adjustment to the measuring points. In the turbulent case, the expansion was made with the aid of the logarithmic profile illustration. In the area of $0 \leq y^+ < 5$, the laminar bottom layer was supplemented by the formal statement

$$u^+ = y^+ \text{ with } u^+ = \frac{u}{\sqrt{\tau_w/\rho_w}}, \quad y^+ = \frac{y \cdot \sqrt{\tau_w/\rho_w}}{\nu} \quad (4.11)$$

Starting with $y^+ = 30$ and ending with the first profile measuring point, an extrapolation was made with the logarithmic wall theory:

$$u^+ = \frac{1}{\kappa} \cdot \ln y^+ + c; \quad \kappa = 0.41 \text{ (or according to equation 5.7)} \quad (4.12)$$

The constant "C" was determined by adaptation to the measured profile. With wall cooling, the constant κ was, in accordance with the temperature influence, determined with the derived temperature correction of chapter 5.5.1.2 (equation 5.7a). The area between laminar bottom layer and wall theory ($5 \leq y^+ \leq 30$) was bridged with a polynomial of the 3rd order

$$u^+ = a_0 + a_1 \cdot y^+ + a_2 \cdot y^{+2} + a_3 \cdot y^{+3} \quad (4.13)$$

whose coefficients a_i were determined from equations (4.11) and (4.12) and derivatives of the validity boundaries with $y^+ = 5$ and $y^+ = 30$.

The same method was selected for expanding temperature profiles and (43) analogous equations. $(T-T_w)/(T_\infty-T_w)$ was used instead of u/u_∞ , and u^+ was replaced by the dimensionless temperature

$$T^+ = \frac{(T-T_w) \cdot \rho_w \cdot c_{p,w} \cdot \sqrt{\tau_w / \rho_w}}{\dot{q}_w}, \quad (4.14)$$

which defines the wall heat flow \dot{q}_w , the wall tangential stress τ_w , and the material values $c_{p,w}$ and ρ_w at the wall.

Based on the analogy between enthalpy and impulse exchange, the analytical equation for the temperature profile in the bottom laminar layer is

$$T^+ = Pr \times y^+ \quad (4.15)$$

The following applies to the logarithmic wall theory (see [36]):

$$T^+ = \frac{1}{\kappa_T} \cdot \ln y^+ + C_T \quad (4.16)$$

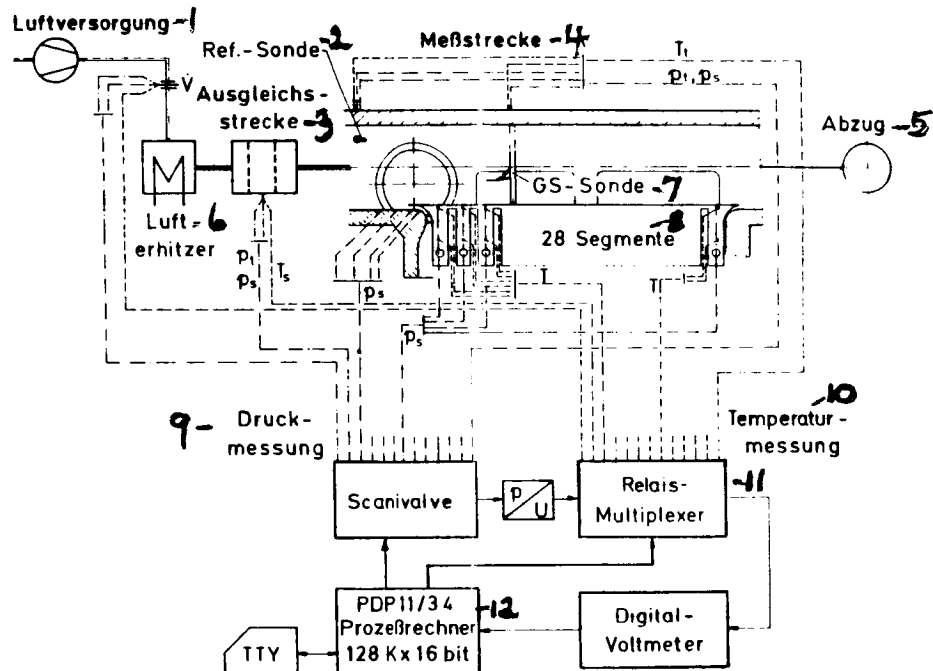
with

$$Pr_t = 0,9$$

$$\kappa_T = \kappa / Pr_t;$$

C_T was determined with the aid of measured profiles.

A summary of all pressure and temperature measurement locations is provided in Illustration 4.9. It is a schematic of the measuring plate equipped with thermal elements and static pressure holes, the positioning of the reference probe to determine free stream data, the static pressure holes in front of the leading edge of the plate to adjust boundary layer suction, and the measurement connections at the boundary layer probe. A PDP 11-34 by 'Digital Equipment Corporation' with a 128 K core memory was used to register pressures and temperatures. With a "Scanivalve" alteration switch, the computer can monitor 48 pressure locations; with a relay multiplexer, it is able to monitor a total of 66 stress and temperature measuring locations.



(44)

- 1 - air supply; 2 - ref. probe; 3 - equalizing distance; 4 - measuring section; 5 - outlet; 6 - air heater; 7 - boundary layer probe; 8 - segments; 9 - pressure measurement; 10 - temperature measurement; 11 - relay multiplexer; 12 - computer.

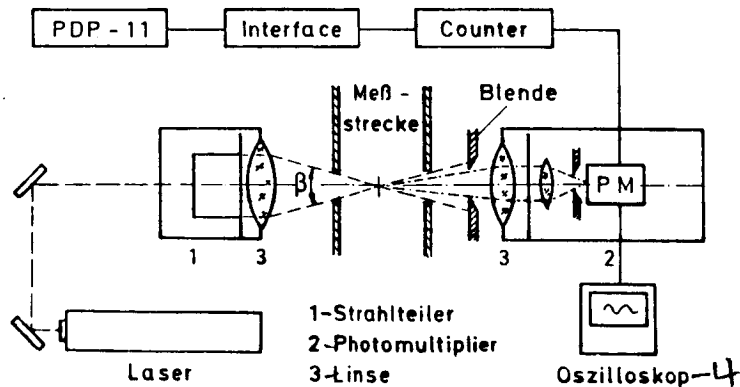
Illustration 4.9: Schematic of the Test Unit with Measuring Value Registration

4.3.5 Determining Free Stream Turbulence with Laser-Doppler

Anemometry

The Institute for Thermal Dynamics at Karlsruhe University has been using and developing optical methods for flow measurements for a long time. This applies specifically to the Laser-Doppler anemometry (LDA) technique for determining turbulence intensity paths throughout the measuring plate. The measuring system used is based on comprehensive development work by S. Eriksen and S. Wittig. They have introduced this system in a number of publications [79, 80, 110, 111]; it is therefore described only in a general way in this dissertation.

(45



1 - beam separator; 2 - photo multiplier; 3 - lens; 4 - oscilloscope

Illustration 4.10: Laser Doppler Anemometer (LDA)

4.3.5.1 Description of the LDA Procedure

A schematic of the Laser-Doppler anemometer is shown in Illustration 4.10. The unit consists of a 4 W argon/ion laser whose beam is directed on the transmitter's optical system after a deflection of 180°. The optical system consists of a beam separator module which splits the beam into two parallel beams of equal intensity with a distance of 30 mm. A lens with a focal length of 500 mm is used to cross and focus the two beams. At this location, the measured volume has a length of 4 mm and a diameter of 0.22 mm.

As shown in Illustration 4.10, the stray light signals are registered in a forward scattered direction. The stray light is focused by a lens, which also has a focal length of 500 mm, on a shutter. A photo multiplier is located behind the shutter to record the signals. The shutter will reduce the effective measured volume diameter to 0.1 mm.

4.3.5.2 Evaluation of the Measuring Signals

For the recording and evaluation of measured signals, a system consisting of counter, interface and computer was used (see illustration 4.10). With aid of the fast counter (500 MHz, TSI [112]) the Doppler frequency (see [110, 111]), which forms the measuring signal, was determined. The statistical evaluation was made on-line with a 128 K PDP-11/34 16 Bit computer. The interface adjusts the counter to the computer; it also serves as an intermediate storage and control unit for the transmission of digitized measured values to the computer. The transmission speed determined by the computer is 1 kHz.

(46

For statistical evaluation, individual measurements were made for each position of the measured volume 7,500. These measurements were then used to calculate values, which were determined chronologically, i.e, average variation and average variation.

The velocity determined chronologically was calculated in accordance with the following formula:

$$\bar{c} = \frac{\sum_1^N c_i \cdot t_{Bi}}{\sum_1^N t_{Bi}}, \quad (4.17)$$

whereby t_{Bi} represents the real measuring time. It could accurately be determined by the evaluation system. In this procedure, the average value of the turbulent variation quantities is equal to the standard deviation of the measured velocities c_i , which is derived from the following equation:

$$\overline{c'^2} = \frac{\sum_1^N (c_i - \bar{c})^2 \cdot t_{Bi}}{\sum_1^N t_{Bi}} \quad (4.18)$$

The turbulence intensity of a flow was defined as the average value of the velocity vector for the three variation components

$$Tu = \sqrt{\frac{1}{3} (\overline{u'^2} + \overline{v'^2} + \overline{w'^2})} / u_{\infty} \quad (4.19)$$

$\overline{u'^2}$, $\overline{v'^2}$ were determined in accordance with equation (4.18); based on a symmetrical tunnel inlet flow, $\overline{w'^2} = \overline{v'^2}$ was used.

The LDA optic is a single component structure. Nevertheless, the velocity component in the main flow direction as well as its vertical component can be determined in two-dimensional flows. The following equations [113] apply to average velocity and standard deviation with an angle ϕ to the main flow direction:

$$\bar{c}_\phi = \bar{u} \cdot \cos\phi + \bar{v} \cdot \sin\phi \quad (4.21) \quad (47)$$

$$\overline{c_\phi^2} = \overline{u^2} \cdot \cos^2\phi + 2 \overline{u'v'} \cdot \cos\phi \cdot \sin\phi + \overline{v^2} \cdot \sin^2\phi \quad (4.20)$$

By measuring \bar{c}_ϕ and $\overline{c_\phi^2}$ in three different directions in the flow field, these two equations can be used to calculate the five unknown values on the right side of the equation. In order to determine the turbulence values $\overline{u'^2}$, $\overline{-u'v'}$ and $\overline{v'^2}$, I therefore used angles of $\phi = -45^\circ, 0^\circ$ and $+45^\circ$ to the main flow direction in my study.

4.3.5.3 Particle Preparation and Particle Feed

The LDA procedure evaluates scattered light signals of particles contained in the flow. In order to achieve reliable data, it was necessary to add particles (SiO_2 solid particles, AEROSIL R972, SiO_2 portion = 99.8% [114]) to the flow.

The particles, which are supplied as a powder, are round and have a diameter of approximately 20 nm. To prevent these primary particles from agglomerating, which would cause them to no longer follow the flow motion in a free-flowing manner, Eriksen et al [110, 111] developed a comprehensive particle preparation system where, with the aid of a fluid bed storage container, the particles are constantly agitated and disagglomerated. The particle distribution volume achieved in this manner showed particle diameters between 0.1 and 2 μm and their maximum frequency was between 0.3 and 0.5 μm . This fulfilled the required conditions for a free-flowing determination of the turbulence volume. The volume distribution of the particles was examined with several procedures (cascade impactor (Anderson sampler), Whisker particle collector, multi ratio individual particle counter) (see [110, 111]).

Detailed information on this particle preparation and the measuring system used can be read in the publications by Eriksen and Wittig [110, 111].

Comprehensive studies were also made to determine the best location for particle insertion into the flow. The pipe used for particle insertion was placed immediately behind the last stabilizing grid of the delay path (Illustration 4.1). With this arrangement, no interference of the flow in the test tunnel was caused by the particle insertion.

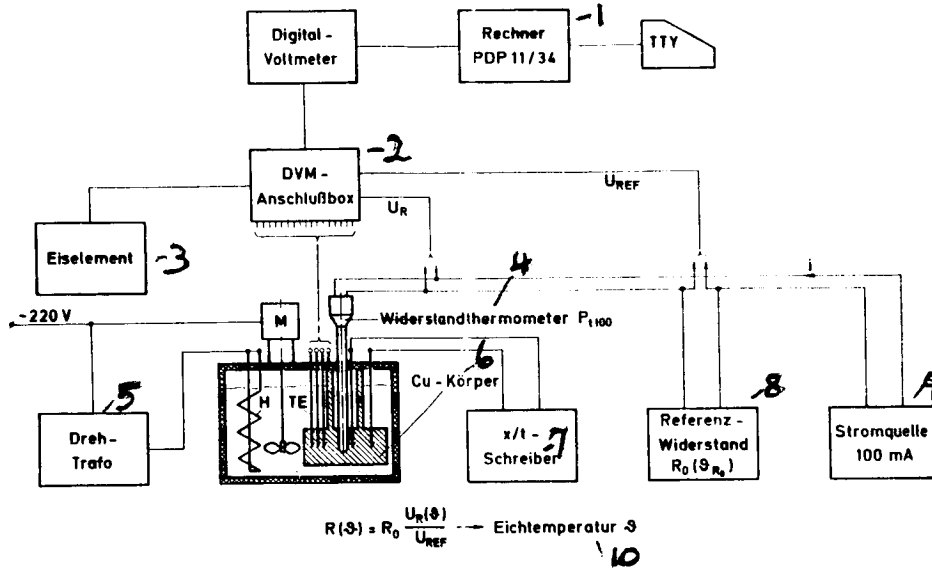
4.4 Test and Calibration Measurements

(48

4.4.1 Calibration of the Measuring Plate Thermal Elements

An important prerequisite for accurate determination of local heat transfer coefficients was the exact calibration of the thermal elements on the measuring plate. This was especially important in my case because, due to the high heat conductivity of the copper used for the measuring plate, temperature differences of less than 1 K had to be anticipated with the low gas temperatures in the segment.

Illustration 4.11 is a schematic of the arrangement used for the calibration of the thermal elements. Together with a resistance thermometer as a standard, the thermal elements were imbedded in a copper body which, in turn, was placed in a closed-off thermostat tank. With this arrangement, the thermal elements and the resistance thermometer have the same temperature; possible temperature variations in the thermostat tank are balanced. The calibration temperature was determined with the voltage decrease at the resistance thermometer and with an additional reference resistance which was connected in series (see Illustration 4.11).



- 1 - computer; 2 - DVM connection box; 3 - ice element; 4 - resistance thermometer; 5 - rotary transformer; 6 - Cu-body; 7 - recorder; 8 - reference resistance; 9 - voltage source; 10 - calibration temperature.

Illustration 4.11: Calibration of Thermal Elements

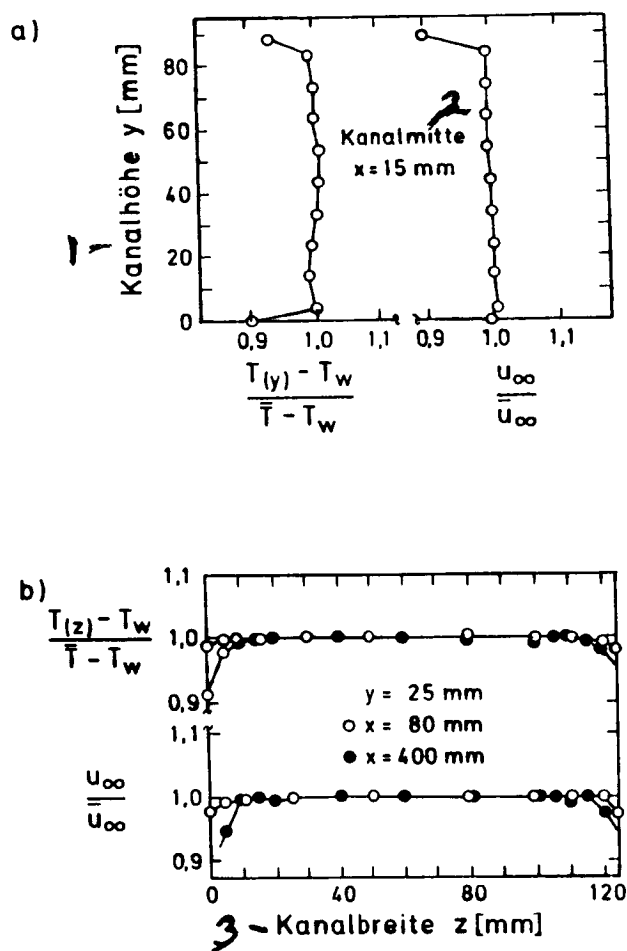
Calibration was made with the aid of a computer controlled measurement value recording unit. Four sets of 16 each Ni-Cr-Ni thermal elements were calibrated for the 0-160° range. The calibration curve (polynomial of the 3rd order) was then calculated for each thermal element. All calibration curves were very similar; therefore, the thermal elements, after separating several extreme cases, could be summarized into four groups with one calibration curve each. In order to examine the calibration accuracy, test measurements on 32 of the 64 thermal elements were performed. With the calibration curves obtained, temperatures of the thermal elements deviated by less than 0.04 K at a temperature of approximately 20°C; the deviated factor doubled to 0.08 K with approximately 130°C.

4.4.2 Test Measurements at the Boundary Layer Tunnel

Test and calibration measurements serve for the determination of the flow properties of the measuring tunnel. The homogeneity of the free flow and the achieved two-dimensionality of the plate boundary layer is of special interest to us. Additionally, the laminar boundary layer development at the leading edge of the plate must be confirmed and the measured heat transfer coefficients must be examined.

The distribution of free stream temperature and velocity throughout the height and width of the tunnel can be seen in Illustration 4.12a and b. These results, which were achieved with a traversing probe, were applied in a dimensionless manner, whereby the temperature paths are referred to the temperature difference between free stream and wall. The paths shown were measured with a free stream temperature of 370 K, a wall temperature of approximately 300 K, and an average free stream velocity of 47 m/s. Illustration 4.12a shows the profiles, which were measured in the center of the tunnel, downstream of the leading edge of the plate through the vertical dimension of the tunnel. Illustration 4.12b shows the temperature and velocity distribution through the width of the tunnel at two distances from the leading edge of the plate. This was done to demonstrate the development of the side wall boundary layers. The low variations of less than 1% and the small portions of the side wall boundaries indicate a free flow which is very smooth.

With the shaped leading edge of the plate, a laminar boundary layer clearly existed at the beginning of the plate. This was determined by boundary layer measurements with low free stream turbulence in the first measuring plane ($x = 120$ mm). With isothermal boundary layer flow, the profile paths measured are in good agreement with Blasius' [109] analytical solution. Examples, which support this solution, are shown in the following evaluation of measured laminar profiles, chapter 5.5.1.1 (e.g. illustration 5.26a).



1 - tunnel height; 2 - tunnel center; 3 - tunnel width.

Illustration 4.12: Temperature and Velocity Distribution through Tunnel Height (a) and Tunnel Width (b) in Different Measuring Planes ($x=15, 80, 400$ mm)

Indications of the two-dimensionality of the laminar and turbulent boundary layers were obtained when determining the tangential stress distribution diagonal to the flow direction; these determinations were made of varying distances from the leading edge of the plate. The measurements were made with a Preston tube ($\phi = 0.6$ mm), which was introduced to the tunnel from the side and which was moved in a traverse direction on the plate. Results, which were obtained with two temperature ratios and flow velocities at 100 and 400 mm of plate running length, are shown in Illustration 4.13a and 4.13b. Illustration 4.13a shows measurements for a plate flow with a completely laminar boundary layer, 100 mm running length and a fully turbulent boundary layer at the plate end with 400 mm. Because the Preston method cannot always be used for laminar and reversing boundary layers, the velocities u_{y0} , which are calculated from the dynamic pressure on the probe, are applied to the free stream value and are illustrated as such. Illustration 4.13b shows the results for the fully turbulent boundary layer, which were achieved at the same distances from the leading edge of the plate. The advanced reversal, which occurs with the same flow, is a result of increased free stream turbulence. Maximum variations in the laminar and in the turbulent boundary layer were below 5% (Illustration 5.13a and b), which sufficiently fulfilled the requirements for two-dimensionality.

In order to evaluate measured heat transfer coefficients, enthalpy balances were made which compare the heat transferred to the plate with increased thickness in the boundary layer due to enthalpy loss. As these balances are suitable for the examination, analysis and interpretation of the results, they will be discussed in the following chapters (chapter 5.4).

TR.Note: German pages 52-53 missing

Nr.	dp/dx	$T_{\infty,0}$ [K]	$T_w / T_{\infty,0}$ [-]	$u_{\infty,0}$ [m/s]	$Re_{L,0} = \left(\frac{u_{\infty,0} \cdot L}{\nu} \right)_{x=0}$ [-]
1.	$k = 0,0$	330	1,0	41	1,0
1.1	0,0	350	1,0	40	0,8
2.	0,0	378	0,8	47	0,9
2.1	0,0	375	0,8	41	0,76
3.	0,0	478	0,64	55	0,65
4.	0,0	570	0,53	38	0,36
1 - KONTUR 1 $k(x) = \text{const.}$					
5.	$k = 1,2 \cdot 10^{-6}$	381	0,8	35	0,64
6.	$1,2 \cdot 10^{-6}$	466	0,64	49	0,64
7.	$2,3 \cdot 10^{-6}$	480	0,64	27	0,33
8.	$2,5 \cdot 10^{-6}$	571	0,53	33	0,32
1 - KONTUR 2 $k(x) = \text{const.}$					
9.	$k_{\max} = 2,9 \cdot 10^{-6}$	376	0,8	39	0,73
10.	$3,2 \cdot 10^{-6}$	463	0,64	48	0,65
11.	$5,65 \cdot 10^{-6}$	385	0,8	20	0,35
12.	$5,7 \cdot 10^{-6}$	467	0,64	27	0,35
13.	$6,3 \cdot 10^{-6}$	570	0,53	34	0,33

1 - contour

Table 5.1: Test Parameters (applicable velocity paths are shown in Illustrations 5.45, 6.15 and 6.19)

The discussion of results for heat transfer and boundary layer measurements is divided into individual paragraphs, which are in accord with normal experimental procedures.

The first paragraph (Chapter 5.3) shows the results of boundary layer measurements without pressure gradients or wall cooling for varying free stream turbulence intensities. These test measurements are used to compare results, which are obtained from literature, and provide a starting point for an analysis of additional measurements with wall cooling and pressure gradients.

The following chapters will introduce the new heat transfer and boundary layer measurements with varying wall cooling ($T_w/T_\infty = 0.8; 0.64; 0.53$) for unaccelerated flow (chapter 5.4) and for accelerated flow (chapter 5.5). Free stream turbulence was a variable in these tests.

Measurement data obtained under hot gas conditions provides new information, which expands the present state of knowledge, of the significance of the individual influencing parameters of free stream turbulence, wall cooling and pressure gradients, and about their effects when these parameters are superimposed. Analyses on this subject are summarized in chapter 5.5. They describe fundamental influences on reversal events, heat transfer rates, tangential stress coefficients, boundary layer characteristics, and profile deformation in the boundary layer.

(55

5.2 Free Stream Turbulence

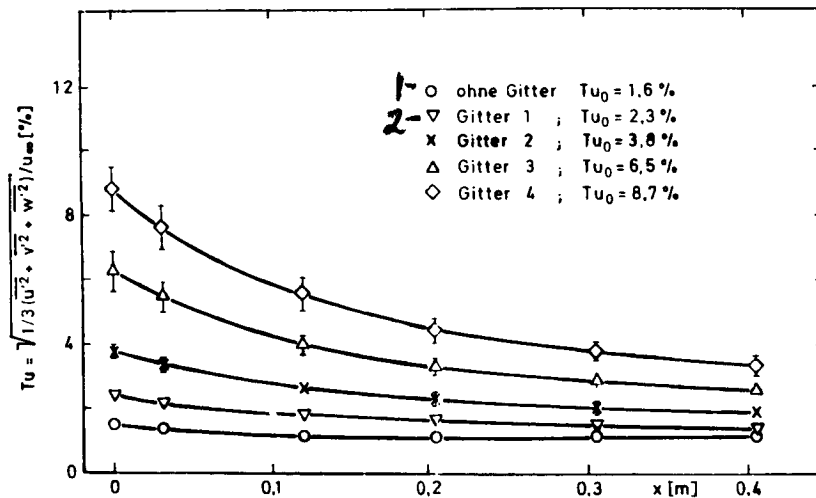
Free stream turbulence is one of the most important parameters of boundary layer flows. Knowing its exact dimensions and path over the measuring plate is an important prerequisite for an accurate evaluation of the boundary layer and heat transfer data obtained from the experiment. In order to meet these requirements, comprehensive turbulence intensity measurements were performed with the aid of the optical Laser-Doppler measurement technique. Other tests made under the same flow conditions are heat transfer and boundary layer measurements with unaccelerated and accelerated flows.

In order to determine the turbulence intensity, the u' and v' components were measured in and perpendicular to the main flow direction, whereby $w'^2 = v'^2$. Because the tunnel inlet flow was symmetrical in the transverse direction, it was assumed that the development of both transverse components of free stream turbulence occurs in the same manner and, therefore, their values are almost identical.

Illustration 5.1 shows - for the situation without pressure gradients - turbulence intensity as a function of the plate's running length, measured without the four installed turbulence grids. The zero point is defined as the leading edge of the plate. The measurement values were determined for 5 wall distances ($\Delta y = 5$ mm) within the flow area with a width of 25 mm which is in contact with the outer edge of the boundary layer. The entire temperature range up to 300° is included in the results. The free stream velocity varies between 39 and 55 m/s, and the Reynolds number, which is a function of the plate length, is between 0.36×10^6 and 1.0×10^6 .

The measurement values describe turbulence intensities at the beginning of the plate. Without a grid, they are 1.6% and with grids 1 through 4 they are 2.3%, 3.8%, 6.5% and 8.7%. As expected, the turbulence intensities showed no influence of the free stream temperature. This is confirmed by comparative tests, which were conducted with the grids installed and with an identical velocity but with different free stream temperatures.

(56)

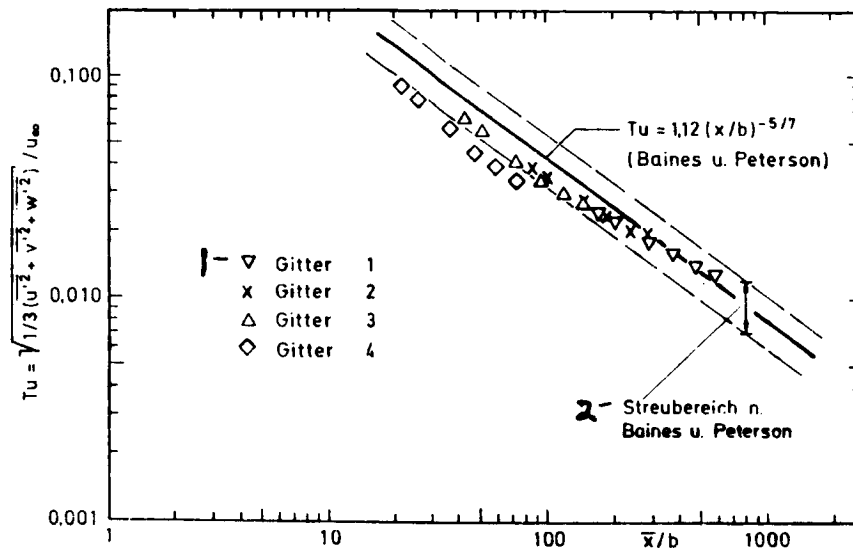


1 - without a grid; 2 - grid

Illustration 5.1: Turbulence Intensity Matrix in an Unaccelerated Flow (Temperature Range $T_{\infty} = 70-300^{\circ}\text{C}$, Leading Edge of the Plate: $x = 0$)

The attenuation behavior, which is typical for grid turbulence, is present in these measurements. A characterization of this event is demonstrated in Illustration 5.2. In this illustration, the data are applied as a function of the dimensionless distance to the turbulence grid \bar{x}/b . The parameter b is the wire strength of the grid. As a comparison, the curve with its applicable spread according to Baines and Peterson [101] was added to the illustration. It serves as an indication for typical grid turbulence and is confirmed by my own measurements.

The spread of the measured turbulence intensity shown in Illustration 5.1 is based on the higher variations of the transverse component v' . This becomes obvious in Illustration 5.3 by the application of individual turbulence intensity components. It applies especially to grid 4, which is the coarsest grid. This effect is supplemented by imbalances in the turbulence intensity distribution over the wall distance. Due to the small distance from the grid, these imbalances can be up to 1% with the high turbulence intensities of grids 3 and 4 (in the u' and in the v' component). Additionally, there is no distinct main flow component in the transverse direction under the given flow situation. This makes a test solution of the turbulence component v' more difficult and results in additional inaccuracies of the measurement result.



1 - grid; 2 - Baines and Patterson spread.

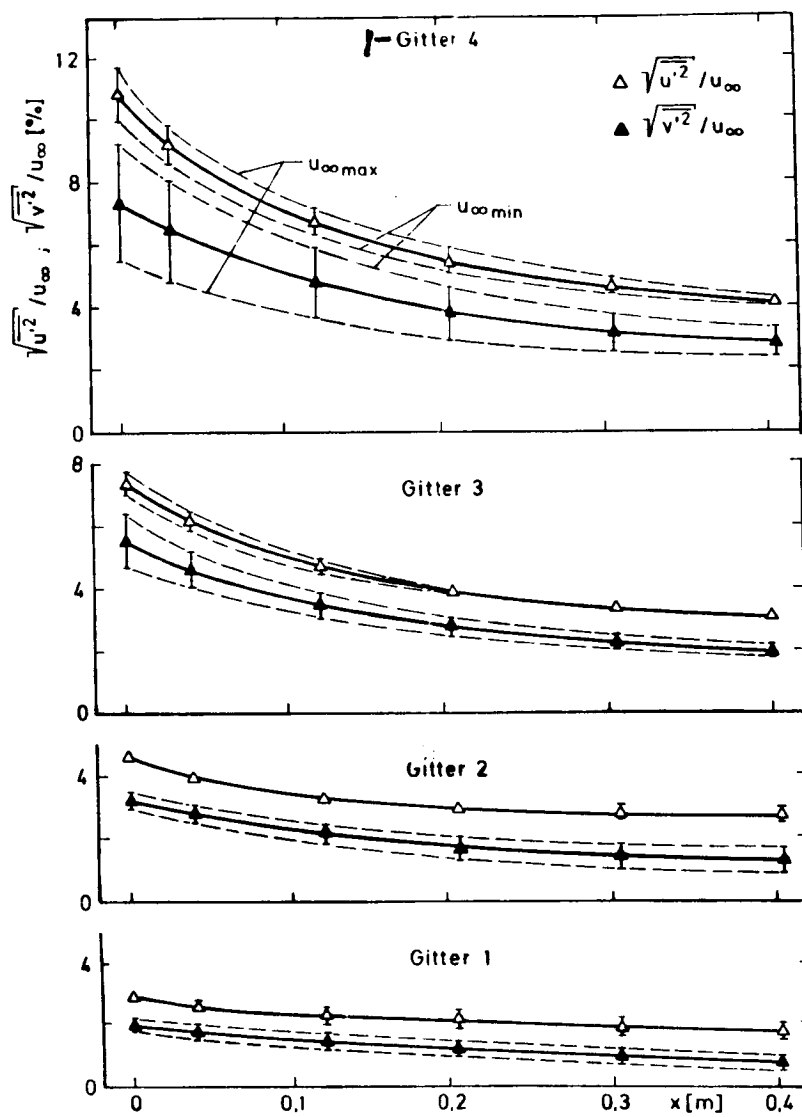
Illustration 5.2: Logarithmic Application of the Turbulence Dependency Matrix Independent of the Dimensionless Distance \bar{x}/b to the Turbulence Grid

In the case of grid 4 it must be noted that, compared to the other grids, this very coarse grid has a different obstruction factor (0.44 versus 0.64). Because of this, it is assumed that it generates turbulences, which are increasingly dependent on the inlet conditions. The basis for this presumption is that a variation of the turbulence intensity component was observed to be dependent on the free stream velocity for this grid only. The greatest influence was observed at high velocity. The turbulence became almost isotropic with decreasing velocity (Illustration 5.3).

All turbulence measurements with pressure gradients were made with a free stream temperature of $T_{\infty} = 100^{\circ}\text{C}$. However, in order to characterize the spread of the values, measurements were performed for all relevant operational Reynolds numbers and, consequently, for all acceleration intensities. This was sufficient, because, after the measurements with pressure gradients, dependency on the free stream temperature was not given.

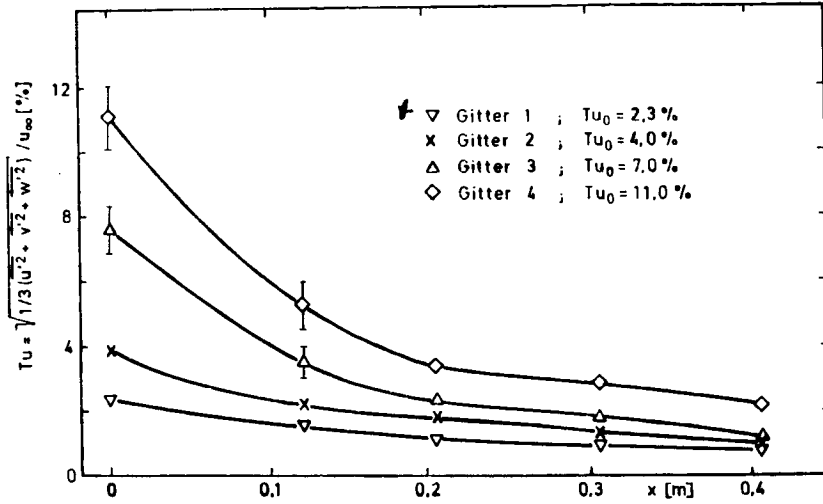
Illustration 5.4 shows the turbulence intensity matrices for accelerated flow ('contour on the 'pressure side' or contour 1) with an almost constant acceleration values. In spite of varying acceleration intensities, identical results were achieved for $k = 1.2 \times 10^{-6}$ and $k = 2.5 \times 10^{-6}$ (varying acceleration intensities were generated by an inlet Reynolds number variation). However, when compared to the results, differences exist in unaccelerated free flows (see Illustration 5.1): a distinctly more rapid decrease of free stream turbulence is caused by accelerations.

The results for the case of the contour on the 'vacuum side' (contour 2) with higher tunnel profile constriction in the forward portion of the plate are shown in Illustration 5.5. It also contains a summary of all measurements with $k_{\text{max}} = 2.9-6.3 \times 10^{-6}$. Compared to Illustration 5.4, an even more rapid decrease of free stream turbulence is noted in the forward portion of the plate. At the end of the highly accelerated zone ($x = 250 \text{ mm}$) the turbulence decrease is again in accordance with the unaccelerated flow (see Illustration 5.1).



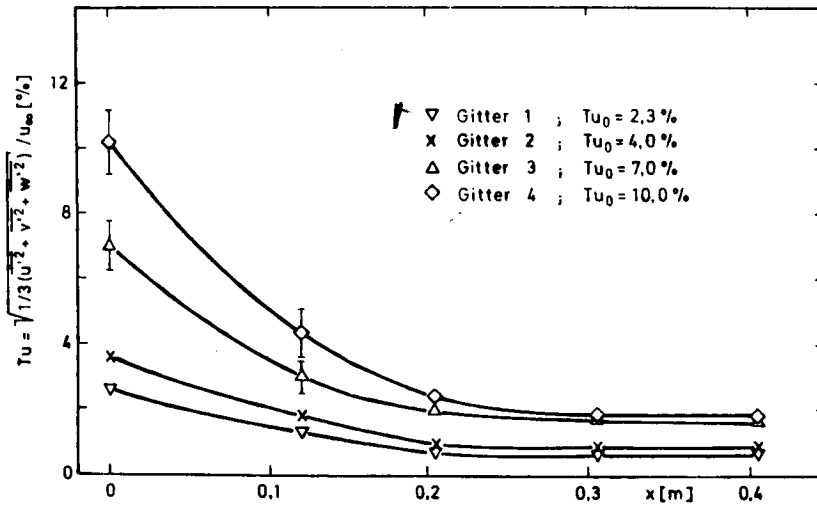
1 - grid.

Illustration 5.3: Turbulence Component Distribution in Unaccelerated Flow



1 - grid.

Illustration 5.4: Turbulence Intensity Matrices in the Boundary Layer Tunnel; Acceleration with Contour 1 (Contour on the 'Pressure Side')

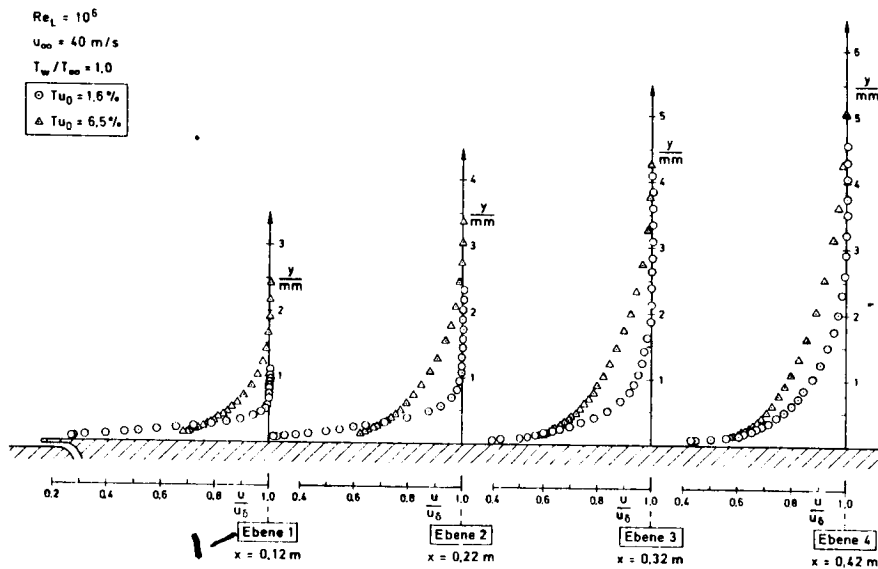


1 - grid.

Illustration 5.5: Turbulence Intensity Matrices in the Boundary Layer Tunnel; Acceleration with Contour 2 (Contour on the 'Vacuum Side')

In accordance with experimental procedures, this paragraph will introduce the measured results on a flat, uncooled plate. They will be used for a basic characterization of available boundary layer types and for the demonstration of the significance of free stream turbulence independent of wall cooling. The measurements refer to free stream velocities of 40-41 m/s and to Reynolds numbers of $Re_{L,0} = 0.8-1.0 \times 10^6$, which were achieved along the entire running length of the plate (see Table 5.1, flow conditions 1 and 2). With low Reynold numbers, the respective boundary layers are already showing characteristics which are relevant for a turbine. In addition to reversal events, which can be found on turbine blades, there are typical relaxation effects (low Reynolds number effects) in turbulent boundary layers. The measurements will characterize these effects by considering the additional influences of free stream turbulence, which is typical in a turbine.

(61



1 - surface.

Illustration 5.6: Velocity Profiles and Boundary Layer Development along a Flat, Adiabatic Wall

5.3.1 Transitional Boundary Layers with Varying Free Stream Turbulence

All boundary layers, which were observed in the measuring section, were transitional. Their appearance at the measurement surfaces, which were detected with probes or heat transfer measurements, was predominantly defined by their Reynolds number and the respective free stream turbulence. Illustration 5.6 shows two critical cases of boundary layer forms and boundary layer development caused by low and high free stream turbulence ($Tu_0 = 1.6\%$ and 6.5%). The measurements of the lowest possible free stream turbulence in the measuring tunnel ($Tu_0 = 1.6\%$) describe events above the laminar-turbulent boundary layer reversal. The profile in surface 1 ($x = 0.11$ m) is a pronounced laminar profile. The matrices in surfaces 1 and 3 ($x = 0.21$ m and 0.22 m) illustrate reversal profiles. A fully-turbulent boundary layer profile is present in surface 4. In contrast, all profiles measured with grid 3 ($Tu_0 = 6.5\%$) are turbulent.

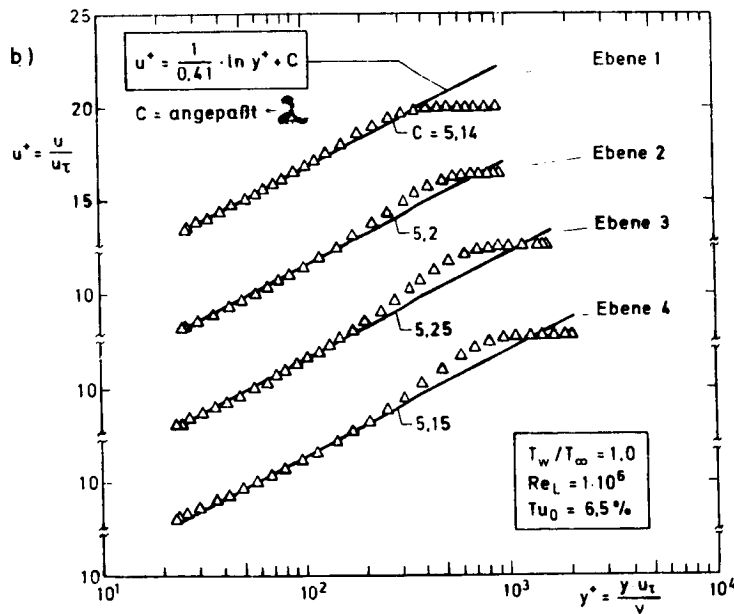
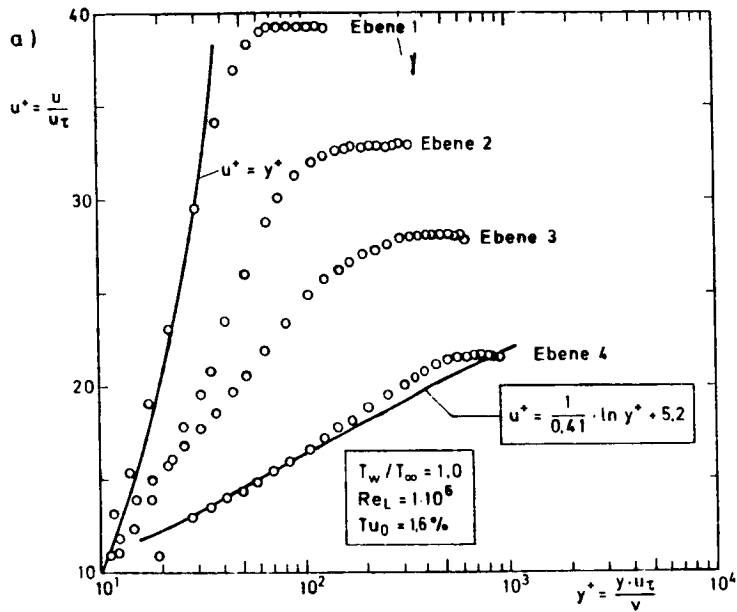
The development of both boundary layers with different external turbulence is accompanied by a varying boundary layer thickness increase and changes in the profile shape. These changes not only exist in the transitional case ($Tu_0 = 1.6\%$) - because of the reversal - but also in the turbulent flow with grid 3 ($Tu_0 = 6.5\%$). A comparison of both profile developments in Illustration 5.7a and b clearly shows these events. The velocity profiles, which are identified with the wall tangential stress velocity u_p , are applied in a semi-logarithmic illustration. As a comparison, the dimensionless linear velocity theory $u^+ = y^+$ (Illustration 5.7a) is shown for the laminar profile in surface 1 and the respective logarithmic wall theory is shown for turbulent profiles. In a diagram, Illustration 5.7 summarizes the turbulent boundary layer profiles of the 3 measured surfaces by displacing the u^+ coordinate.

(62

In Illustration 5.7a, a step-by-step description is provided of the transition from the laminar (surface 1) to the fully-turbulent boundary layer profile form (surface 4). In surface 1, the measurement confirms the linear velocity distribution $u^+ = y^+$ near the wall for the laminar case. In surface 4, achievement of the turbulent boundary layer condition is documented by the good agreement of the measured data with the logarithmic wall theory in the area near the wall ($y^+ < 200$).

In comparison to the fundamental profile deformation of the boundary layer during reversal (Illustration 5.7a), only an increase of the wake portion can be recognized with progressive running length in the laminar case (Illustration 5.7b). The wake increase illustrates a basic property of turbulent boundary layer profiles with relaxation. This condition can also be observed in turbine flows. It describes fundamental deformations of the profile path in the outer portion of the boundary layer, which are not completed until sufficiently high Reynolds numbers have been achieved. In boundary layers without external turbulence, the relaxation behavior which occurs with the increase of the wake component is a sole consequence of the Reynolds number effects. In this case, similar to blade boundary layers, turbulence intensity influences are an additional factor. This additional effect will be discussed in detail in paragraph 5.3.2. In addition, it will be demonstrated (para. 5.5) that these relaxation effects, which are superimposed by external turbulence, will also have an effect on heat transfer and the wall tangential stress.

The profile deformations of two boundary layers with high and low free stream turbulence described in Illustrations 5.6 and 5.7 are based on characteristic differences of the boundary layer value δ_2 (impulse loss thickness), H_{12} (form parameter), and the coefficient of friction c_f . These parameters are not addressed in this chapter.



1 - surface; 2 - adjusted.

Illustration 5.7: Comparison of Transitional and Turbulent Boundary Layer Development

Illustrations 5.8 and 5.9 show the boundary layer characteristics for available measurements. The tangential stress coefficients of the reversal profile for $Y_{u_0} = 1.6\%$ on measurement surfaces 2 and 3 were approximated for that velocity gradient which was formed with the measurement point closest to the wall.

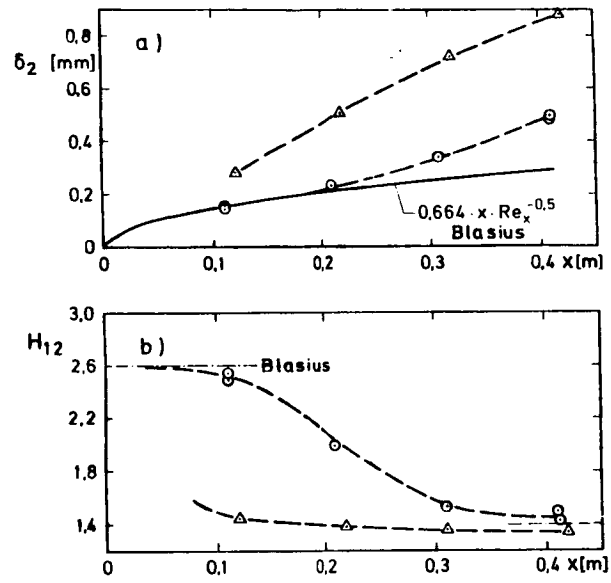


Illustration 5.8: Comparison of Transition and Turbulent Boundary Layer Characteristics (see Illustration 5.7 for Symbols)

Compared to the laminar comparison curve by Blasius [109], the reversal process ($Tu_0 = 1,6\%$) is characterized by an impulse loss thickness increase, the decrease of the form parameter $H_{12} = 2.6$ for laminar profiles to values around 1.4 (Illustration 5.8) which are typical for turbulent boundary layers, and an increase of the local tangential stress coefficients to magnitudes which are above the values of the laminar boundary layer by a factor of 3-4 (Illustration 5.9). The higher turbulence of grid 3 ($Tu_0 = 6.5\%$) will move these reversal events up-stream, to the vicinity of the leading edge of the plate. Therefore, the respective measurement values in Illustration 5.8 describe only turbulent paths which, compared to laminar boundary layers, are characterized by a higher increase of the impulse loss thickness and form parameters with values around 1.4.

(65)

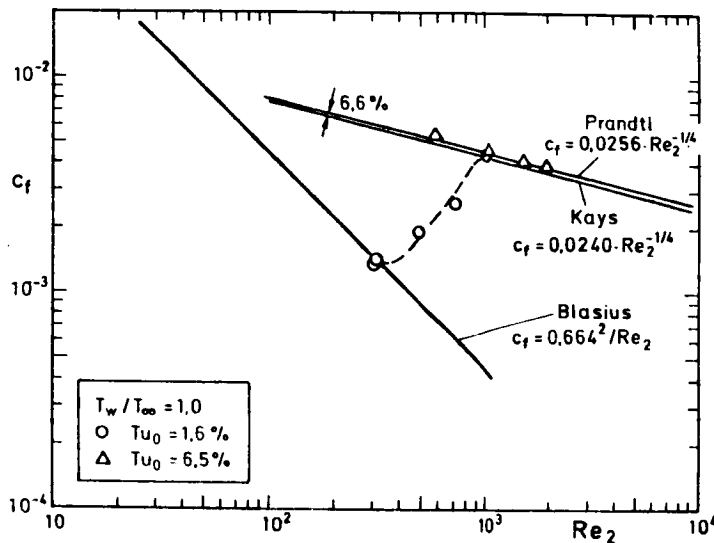
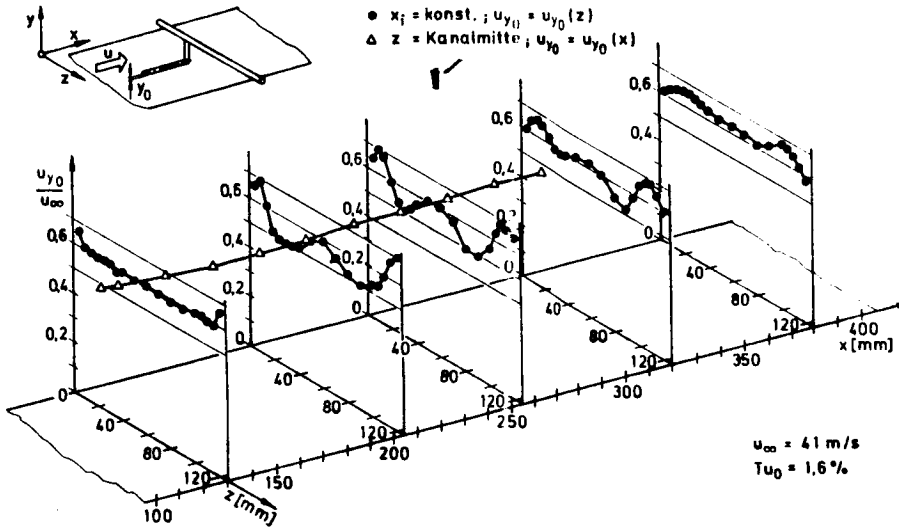


Illustration 5.9: Coefficients of Friction

In Illustration 5.9, the coefficients of friction c_f are applied depending upon the impulse loss thickness Reynolds number. For a general evaluation, they are compared with known, semi-empirical correlations by Blasius [109], Prandtl [22] and Kays [86] for laminar and turbulent boundary layers with a constant-density flow. My own measurements were in good agreement with these correlations. Average results for grid 3 ($Tu_o = 6.5\%$) are about 6-10% above the value which, according to Kays, applies specifically for turbulence free external flow. These increase of the c_f -values can already be attributed to the influence of free stream turbulence.

Reversal events always represent flow processes which were formed three-dimensionally. However, current results relate to measurements which only describe boundary layer events in the center of the tunnel. In order to have an understanding of the three-dimensional formation of the reversal area, transverse measurements were performed; they are contained in Illustration 5.10. In this illustration, velocity distributions $u_y(z)$, which were obtained when low free stream turbulences ($Tu_o = 1.6\%$) were applied. They were measured diagonal to the flow direction with a Pitot tube, (66 which had a thickness of 0.6 mm and which was in contact with the plate surface. Measurements were taken at varying distances from the leading edge of the plate ($x = 130, 205, 255, 320, \text{ and } 380 \text{ mm}$). A laminar boundary layer, which is predominantly two-dimensional, occurs when $x = 130 \text{ mm}$. The subsequent measurement surfaces indicate a three-dimensional, symmetrical reversal development whereby, in the tunnel center and on the sides, zones develop where the beginning of the reversal occurs at various running lengths. The area of highest velocity (tunnel center) can be compared to increased tangential stress values, thus representing a stage of advanced reversal process. When $x = 380 \text{ mm}$, the end of the reversal process is indicated. In accordance with Illustration 5.10, the boundary layer regains its two-dimensional character. In the plate center, no noticeable increase of the velocities can be noted in comparison to the values of the previous measuring surface.

ORIGINAL REVISION
OF POOR QUALITY



1 - tunnel center

Illustration 5.10: 3-Dimensional Reversal Development
($Tu_0 = 1.6\%$)

Because, in the tunnel center, the reversal with the given velocity distribution is visibly separated from the fringe areas, a guarantee is provided that the reversal events in the plate center, which are critical to the results, are not determined by the corner boundary layers at the contact points between tunnel side wall and measuring plate, but by the free stream turbulence itself. (67)

In addition to the diagonal measurements, Illustration 5.10 shows the measurements $u_{y_0}(x)$, which were detected by a probe displacement mechanism specially designed for this procedure. The measurements were taken in the tunnel center by continuously moving the probe in a longitudinal direction between $x = 80$ mm and $x = 300$ mm. The reversal process in the tunnel center is sketched by the longitudinal movement of the probe. With the minimum registered velocity values ($u_{y_0}/u_{\infty} = \min!$) it was possible to approximate the location of the reversal initiation with the respective reversal

Reynolds number and to make a comparison with available results from previous measurements. The reversal Reynolds number for the free stream turbulence of 1.6% is $Re_x = 3.5 \times 10^5$, which is in good agreement with the compiled values from literature by Abu-Ghannam.

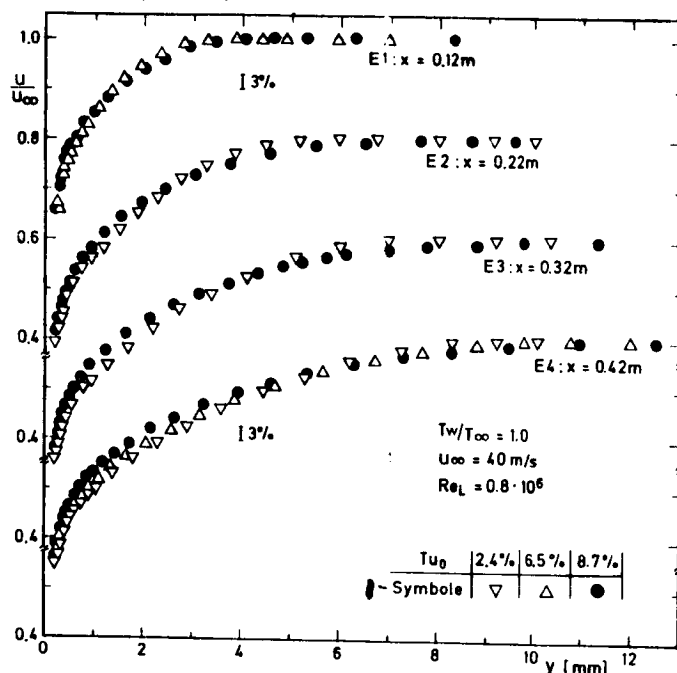
5.3.2 Turbulent Boundary Layers with Changeable Free Stream Turbulence

Due to the low acceleration intensities in the rear blade section on the vacuum side of gas turbine blades, there frequently are expanded areas with turbulent boundary layer flows. It is therefore necessary to know the influence of the free stream turbulence on turbulent boundary layers in these areas of the blade. Illustrations 5.11 and 5.13 show how this turbulence influences the form of turbulent velocity profiles, as it was determined under ideal conditions of a flat, uncooled and unaccelerated flow boundary layer (flow condition 2, Table 5.1). The velocity profiles were recorded in the 4 boundary layer measurement surfaces for three different turbulence intensities ($Tu_0 = 2.3\%$; 6.5% ; 8.7%). In the case of low free stream turbulence ($Tu_0 = 2.3\%$), the illustration of the measurement results starts with surface 2 ($x = 220$ mm), because surface 1 ($x = 120$ mm) still contained distinct reversal profiles.

Illustration 5.11 shows the velocity paths u/u_0 , which were measured with varying free stream turbulence, dependent on the wall distance y . In order to clarify this point, the measurements for all 3 turbulence intensities were only entered for surface 4.

Illustration 5.11 show that, with increasing free stream turbulence, the boundary layer thickness increases and the profile form fills out. However, these effects are relatively small. The velocity gradients at the wall increase at the same time, which results in an increase of the wall tangential stress. Under the given conditions, the higher free stream turbulence causes an overlap of the profile. This does not change the impulse loss thickness, but it decreases the displacement thickness and thus the form parameter H_{12} . Illustration 5.12a confirms these events with the aid of the matrices of the boundary layer values δ_2 and H_{12} , which are measured over the plate, and the friction coefficients.

(68



1 - symbols.

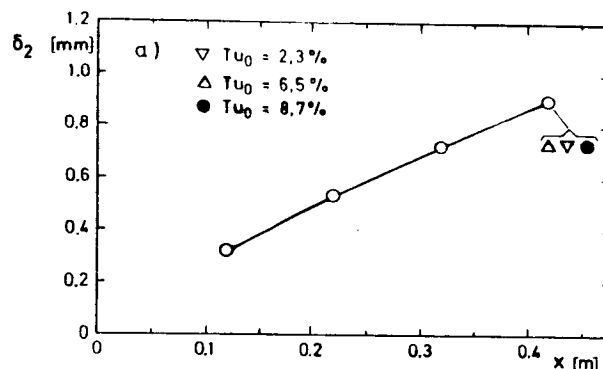
Illustration 5.11: Turbulent Velocity Profiles with Varying Free Stream Turbulence

For a general evaluation of existing tangential stress increases, Illustration 5.12d again applies the measured tangential stress coefficients as a factor of the impulse loss thickness Reynolds number Re_2 . A comparison with a correlation

$$c_f = 0.024 \times Re_2^{-0.25} \quad (5.1)$$

is made. Because of its good agreement with the measurement results by Murlis, Wieghard (see [31]) and Coles [115] (max. deviation 2%), this correlation is especially suitable to describe the conditions without external turbulence.

(69



ORIGINAL PAGE IS
 OF POOR QUALITY

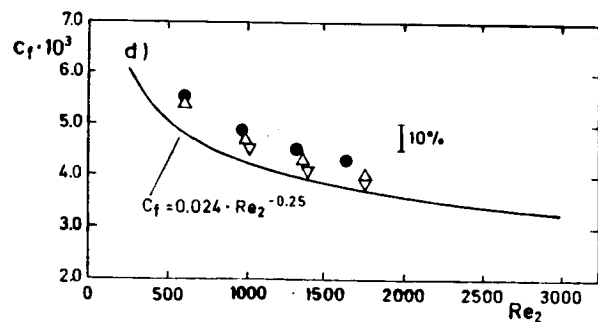
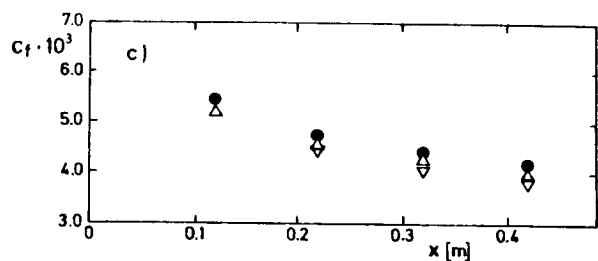
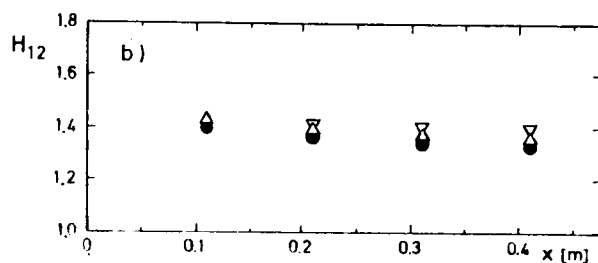
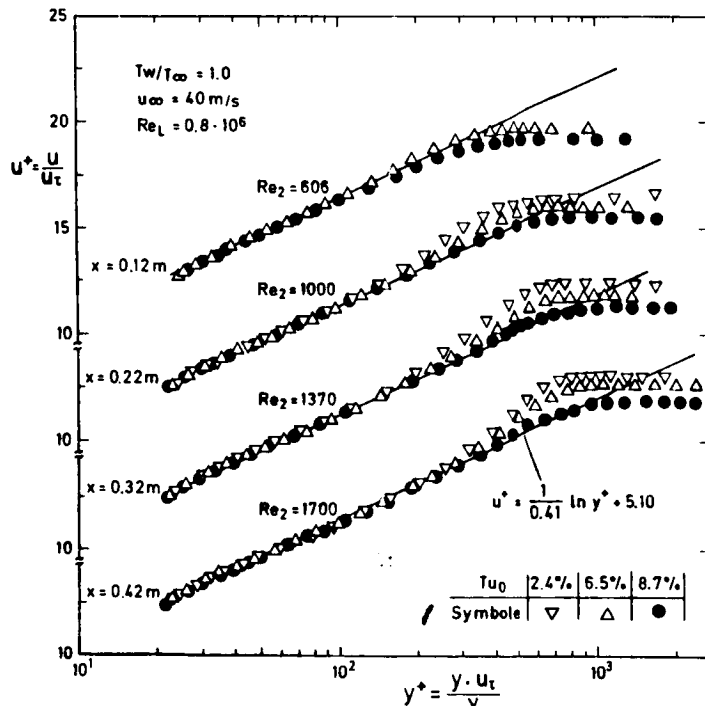


Illustration 5.12: Characteristic Quantities in Turbulent Boundary Layers without Heat Transfer with Varying Free Stream Turbulence (see Ill. 5.11 for Symbols)

In this generally similar illustration, increases of the wall tangential stress of up to 10% can be observed with increasing free stream turbulence.

With semi-logarithmic application of the dimensionless velocity profiles - Illustration 5.13 - an excellent agreement exists for all turbulence intensities near the wall with the known, universal wall theory for turbulent boundary layers with constant material values. Free stream turbulence thus does not change the validity of the logarithmic wall theory (even with low Reynolds numbers; $Re_2 < 2,000$). However, in the external area of the boundary layer the increased free stream turbulence causes a distinct decrease of the wake component. With our flow, this process overlaps with the Reynolds number effects mentioned in the previous paragraph. As shown by Illustration 5.13, free stream turbulence decreases the increase of the wake force $\Delta U/u_f$, which is connected with an increasing Reynolds number (or running length). With sufficiently high turbulence intensities ($Tu_0 = 8.7\%$), the wake portion is completely suppressed.



1 - symbols

Illustration 5.13: Logarithmic Velocity Profiles with Varying Free Stream Turbulence

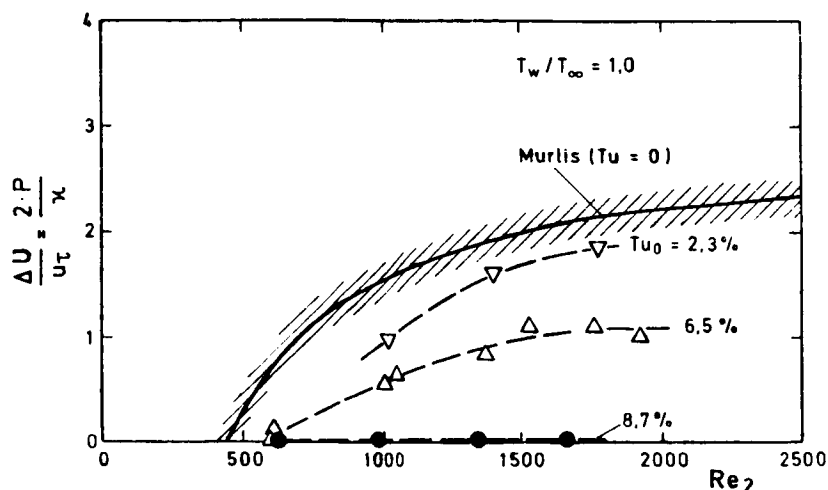


Illustration 5.14: Reynolds Number and Turbulence Intensity Dependencies of the Wake Portion ($\Delta U/u_T =$ Wake Force at the Boundary Layer Edge

Illustration 5.14 quantifies this Reynold number dependency of the wake component with and without free stream turbulence. With the aid of my own measurements and the measuring data for turbulence-free external flows by Murlis [33] it was determined that Reynolds number dependencies below $Re_2 = 2,000$ are especially pronounced. They are thus increasingly connected to profile deformations, if the wake portion is not completely eliminated by very high external turbulence (as in this case, with $Tu_0 = 8.7\%$). Additional profile deformations in the wake area in excess of $Re_2 = 2,000$, which - with turbulence-free external flow - cease when Reynolds numbers Re_2 are around 5,000 (see [33]), seem comparatively small. Reynolds number effects are thus concentrated in the area of the impulse loss thickness Reynolds numbers below 2,000. The additional fact in Illustration 5.14 is that, with very high free stream turbulence ($Tu_0 = 8.7\%$) there is no increase of the wake component increase as a factor of the Reynolds number; this leads to the conclusion that, under these conditions, free stream turbulence dominates over Reynolds number effects in the external area of the boundary layer.

The studies with adiabatic boundary layers created a basis of comparison, which confirms known results from literature (see Chapter 2) about the influences of free stream turbulence on transitional and turbulent boundary layers. These results, together with additional knowledge, are applied to three-dimensional reversal behavior and Reynolds number effects with free stream turbulence, which is also relevant to turbines. Based on this, I would now like to introduce and analyze the tests with wall cooling and pressure gradients, which are the subject of this dissertation.

Special significance is assigned to a comprehensive documentation of measured data. Without them, a verification of the calculation program (and an examination of the developed integral procedure) would not have been possible.

5.4 Boundary Layer Flows with Wall Cooling

To date, only very few detailed measurements on the influence of high wall cooling in sub-sonic flows have been performed. In addition, such measurements were only made for turbulent boundary layers. This includes the studies by Back et al [75], and the measurements made by Sill [77]. In contrast, the significance of wall cooling in transitional boundary layers has not yet been experimentally studied.

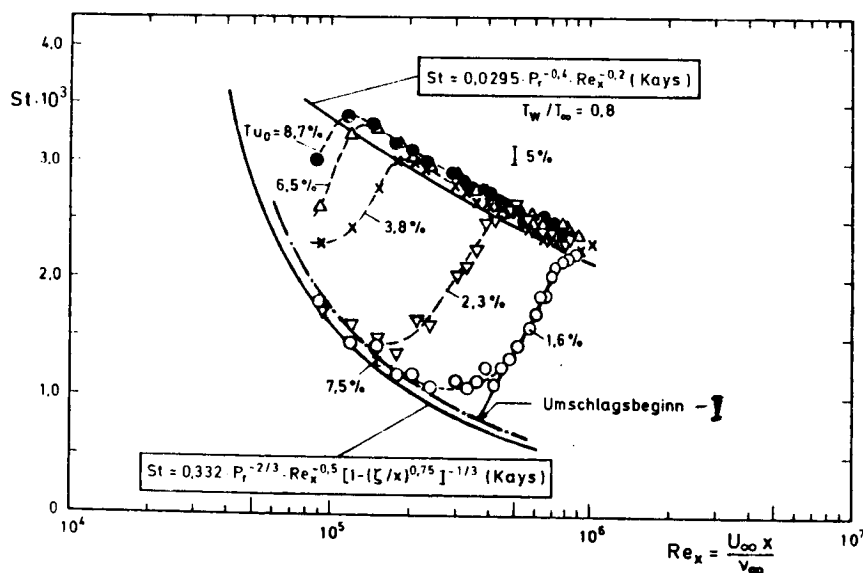
Because of this, I conducted comprehensive basic experiments on the subject of heat transfer on cooled surfaces with transitional boundary layers.

In order to achieve realistic cooling conditions as they are found in cooled gas turbine blades, the free stream temperature was increased step-by-step to 100, 200 and 300°C (flow conditions 2 - 4, Table 5.1) with almost unchanged wall temperature ($T_w = 25 - 30^\circ\text{C}$). Heat transfer distributions with and without all available turbulence grids were measured for each free stream temperature. Characteristic cases with high and low free stream turbulence were supplemented by boundary layer measurements in the 4 measuring surfaces.

5.4.1 Boundary Layer Development and Heat Transfer with Varying Wall Cooling and Free Stream Turbulence

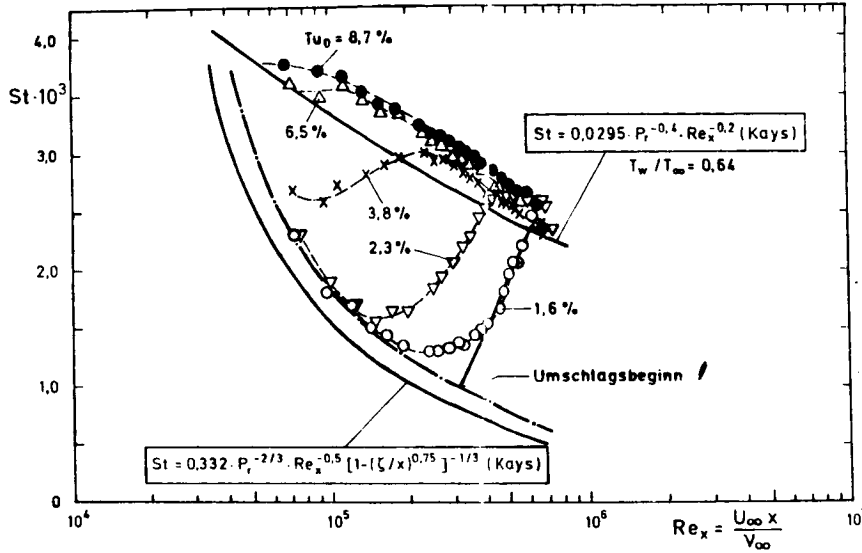
(73)

Heat transfer measurements on a flat plate provide the best information on the influence of varied free stream turbulence and wall cooling on the boundary layer reversal and on the heat transfer itself. Illustration 5.15 shows Stanton numbers for various turbulence intensities with moderate wall cooling ($T_w/T_\infty = 0.8$) and constant free stream velocity as a function of local running length Reynolds numbers ($Re_{L,0} = 0.8 \times 10^6$). Illustrations 5.16 and 5.17 show comparable measurements with more intense cooling conditions with $T_w/T_\infty = 0.64$ and $T_w/T_\infty = 0.53$. Because these flows register lower Reynolds number ranges ($Re_{L,0} = 0.64 \times 10^6$ and 0.36×10^6), the reference measuring points are increasingly shifted into the area of laminar boundary layer sections.

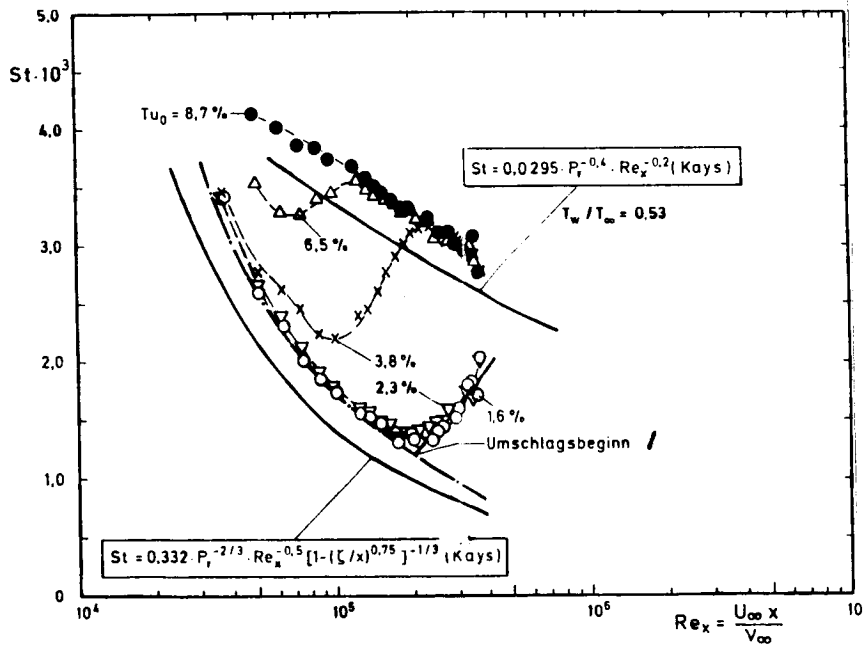


1 - start of reversal

Illustration 5.15: Heat Transfer and Boundary Layer Development during Moderate Wall Cooling ($T_w/T_\infty = 0.8$)



Ill. 5.16



Ill. 5.17

1 - start of reversal

Illustrations 5.16 and 5.17: Heat Transfer and Boundary Layer Development with Intensive Wall Cooling with $T_w/T_\infty = 0.64$ and 0.53

As a comparison, all three illustrations (Illustrations 5.15, 5.16, 5.17) show the matrices of the Stanton numbers according to two relationships by Kays [64], which describe the laminar and turbulent heat transfer in plate boundary layers with constant material values and negligible free stream turbulence. The relationship of the laminar boundary layer takes into consideration the uncooled leading edge of the plate, which has a length of 15 mm. The dotted lines are the measuring points of the laminar boundary layer with lowest free stream turbulence ($Tu_{\infty} = 1.6\%$). Their purpose is a general evaluation of the laminar heat transfer and a determination of the Reynolds numbers at the beginning of the reversal (see equation 5.2, chapter 5.5.1).

(75)

Measurements taken during the three temperature conditions basically show identical characteristics of the boundary layer behavior. As expected, with increasing free stream turbulence Tu_{∞} , an advancing of the laminar-turbulent reversal initiation and a shorter reversal length were observed. In the case of greater turbulence intensity ($Tu_{\infty} \geq 6.5\%$), the reversal range is already in the vicinity of the uncooled leading edge of the plate.

A special case occurs in the tests with highest wall cooling (Illustration 5.17): the reversal matrix is the same for $Tu_{\infty} = 1.6\%$ and $Tu_{\infty} = 2.3\%$. This phenomenon must not be construed as a contradiction to fundamental up-stream movement of the reversal with increasing free stream turbulence. It occurs because secondary influences of corner and side wall boundary layers generate an early reversal process, which - with $Tu_{\infty} = 1.6\%$ - is located far downstream, almost at the end of the plate. In this case, the reversal is co-induced by the side walls. Because the applied measuring method integrates the heat transfer over larger areas diagonal to the flow direction, the Stanton numbers are registered earlier than the boundary layer in the center of the plate. This is confirmed by the reference boundary layer measurements in measuring surface 3 ($x = 310 \text{ mm}$, $Re_x = 2.6 \times 10^5$). Contrary to heat transfer, which is already reversing at this location (see Illustration 5.17), the

boundary layer measurements in the center of the tunnel still show distinctly laminar profile forms and boundary layer characteristics (see Illustration 5.23 a and b).

The point of intersection of the laminar fitting curve, which represents the case of smallest free stream turbulence, is the criteria for the reversal initiation. Its straight line is adjusted to the steeply increasing path of the Stanton number in the reversal area. The reversal Reynolds numbers, which are summarized in Table 5.2, were thus determined for the turbulence intensities $Tu_0 = 1.6\%$, 2.3% and 3.8% . A determination of the reversal initiation with higher turbulence intensities was not possible, because it occurs in the area of the uncooled leading edge of the plate which is outside the measuring area. The Reynolds numbers at the end of the reversal were taken from the matrix of the Stanton numbers. The results are contained in Table 5.2.

The analysis of this reversal data, which was determined under cooling conditions similar to those found in gas turbines, is discussed in Chapter 5.5.2. This analysis requires comprehensive comparisons with reversal measurements performed for adiabatic boundary layers and the inclusion of boundary layer characteristics, which are present in the reversal (impulse loss thickness Reynolds numbers).

(76

		Umschlagsbeginn ¹			Umschlagsende ²		
		$Re_{x_S} \cdot 10^{-5}$			$Re_{x_E} \cdot 10^{-5}$		
Tu_0	T_w/T_∞	0,8	0,64	0,53	0,8	0,64	0,53
1,6 %		3,7	3,1	2,1	8,2	6,7	-
2,3 %		1,8	1,8	1,9	4,7	4,75	-
3,8 %		0,87	0,67	0,88	1,9	2,25	2,15
6,5 %		-	-	-	1,3	1,15	1,25
8,7 %		-	-	-	1,2	-	-

1 - reversal initiation; 2 - reversal end

Table 5.2: Reversal Reynolds Numbers

The measured heat transfer distributions (Illustrations 5.15 - 5.17) showed that, in agreement with previous measurements (see Chapter 2.2), free stream turbulence in unaccelerated flows has no significant influence on laminar heat transfer. I would like to point out that this applies only in the unaccelerated case. With accelerated flow there is a significant influence of free stream turbulence in laminar boundary layers (see Chapter 5.5.3).

In the areas of turbulent flow there is an indication of heat transfer coefficient increases as a function of turbulence intensity. However, a distinctly even increase with increasing turbulence is not noted with the given spread of the measuring values (@ 3%). In the case of highest wall cooling ($T_w/T_\infty = 0.53$; Illustration 5.17) the local turbulent heat transfer coefficients of varying free stream turbulence are completely identical in their path. No influence of free stream turbulence whatsoever is thus noted.

This ambiguous behavior was observed in previous studies (see Chapter 2.2) and resulted in different evaluations of the influence of free stream turbulence on turbulent boundary layers. It was frequently not considered that, with the increase of free stream turbulence, the laminar-turbulent boundary layer reversal takes place further up-stream. This results in additional consequences for the subsequent turbulent boundary layer. Because the reversal occurs earlier, there are greater boundary layer thicknesses with increased heat transfer resistance, although the running length is the same. Because of this, no or only a minor net effect becomes obvious when the heat transfer coefficients are observed locally. Other reasons are the Reynolds number effects, whose importance for the formation of turbulent boundary layer profiles has already been discussed, and characteristic dependencies of turbulent boundary layers on free stream turbulence structure (influences of longitudinal measurements) (see Chapter 5.5.2). (77

During local observation, turbulence intensity influences in turbulent boundary layers can thus only be recorded in a less than desirable manner. Therefore, a complete analysis of turbulent boundary layers requires a technique which is directly related to boundary layer characteristics. For example, such action could compare boundary layers with identical impulse loss thicknesses with and without free stream turbulence. Such measurements are made in Chapter 5.5.2.

The comparisons of measured heat transfer coefficients with laminar and turbulent correlations according to Kays [64] for flows with constant material values ($T_w/T_\infty = 1.0$) (Illustrations 5.15 - 5.17) provide a concept for the influence of wall cooling on local heat transfer. A distinct increase of the Stanton numbers with increasing wall cooling can be observed in laminar flow areas. With a minor temperature decrease at the wall ($T_w/T_\infty = 0.8$; Illustration 5.15), the dotted curve through the data points of the laminar boundary layer confirms a heat transfer which is approximately 7.5% higher than the correlation. A further decrease of the temperature conditions to $T_w/T_\infty = 0.53$ (Illustration 5.17) results in an increase of this amount to almost 20% due to increased material value influences. So far, in theoretical studies the significance of wall cooling for the laminar heat transfer was considered minor or negligible (see [64, 65, 67]). However, the increased rates observed in these new tests show very distinct effects.

In contrast, the temperature dependencies of the local turbulent heat transfer are visibly reduced. In the case of highest free stream turbulence ($Tu_\infty = 8.7\%$) the increase of the Stanton coefficient is only about 6% during the transition from $T_w/T_\infty = 0.8$ to $T_w/T_\infty = 0.53$.

These heat transfer tests, which were conducted under ideal (78 conditions with a smooth, unaccelerated boundary layer, provided quantitative information and pointed out significant influences of free stream turbulence and wall cooling on boundary layer development and heat transfer. However, the study of heat transfer coefficients, which are computed with reference to the boundary layer's running length, is not sufficient to demonstrate the total importance of these influence parameters. As pointed out at several locations in this chapter, more in-depth boundary layer analyses and data, which pertain directly to the boundary layers, are necessary.

Because of this, the previously determined heat transfer distributions for high and low free stream turbulence intensities were supplemented with boundary layer tests for all temperature conditions.

Illustrations 5.18 - 5.23 introduce the boundary layer characteristics obtained in these tests. In order to enable re-calculations of the test results, a plotting method was selected which refers to the boundary layer's running length, as was accomplished with reference to heat transfer distributions. Illustrations 5.18 and 5.19 supplement the heat transfer measurements when $T_w/T_\infty = 0.8$ (flow conditions 2 and 2.1 of Table 5.1). It must be considered that, with maximum free stream turbulence ($Tu_\infty = 8.7\%$), the free stream velocity is somewhat lower than with tests where $Tu_\infty = 1.6, 3.8$ and 6.5% (41 m/s versus 47 m/s). Illustrations 5.20 through 5.23 characterize the respective boundary layer data with intensive wall cooling with $T_w/T_\infty = 0.64$ and 0.53 .

The applied tangential stress coefficients c_f , the kinematic impulse loss thickness matrices $\delta_2(x)$, and the distribution of the form parameter $H_{12}(x)$ show identical characteristics to those in uncooled boundary layers (see Chapter 5.3) in all temperature conditions. For example, with increasing outer turbulence, impulse loss thicknesses increase due to the advanced location of the boundary layer reversal; at the same time, the kinematic form parameters decrease. In the transition from $Tu_0 = 6.5\%$ to $Tu_0 = 8.7\%$, the differences are only minor because, in both cases, the reversal occurs in the immediate vicinity of the plate's leading edge. In comparison to the indication of an increase of local turbulent heat transfer (Illustration 5.15 - 5.17), there are, with high turbulence intensities, relatively minor turbulence-dependent changes of the local turbulent tangential stress coefficients c_f (see specifically Illustrations 5.20 and 5.22). This corresponding behavior of slow speed and temperature boundary layers can be attributed to the Reynolds analogy, which applies to unaccelerated boundary layers. The enthalpy loss thickness δ_h (see Illustration 5.19d, 5.21d, 5.23d) is an additional boundary layer quantity which characterizes the temperature boundary layer. Its significance is on the same level as the impulse loss thickness δ_2 . Because of the analogy, which applies to impulse exchange and heat exchange (Reynolds analogy) in unaccelerated flow, the development of both quantities along the plate is identical. (79

Before I make a general analysis of the influencing parameters of boundary layer and heat transfer data introduced in this chapter, a more accurate description of the quality of these values is required. An expert application of this data for the examination and further development of two-dimensional calculation procedures requires proof that maximum two-dimensionality existed in individual boundary layer flows. Because of this, data obtained with heat transfer and boundary layer tests are subjected to a mutual examination in Illustration 5.24. The results of two-dimensional enthalpy balance calculations, which are summarized in Illustration

5.24, compare the increase of the enthalpy loss thickness between two measuring surfaces to the amount of heat transferred to the plate surface by cooling. With a maximum deviation of 8-10%, the average values fluctuate around the ideal value of 1. If consideration is given to the sensitivity of such integral balances, the results can be regarded as an excellent confirmation of the results achieved with heat transfer and boundary layer measurements. Additionally, these results can be considered as a guarantee of a two-dimensional boundary layer. An exception to this is the case with the lowest free stream turbulence, which shows average deviations of up to 30%. The reason for this is the three-dimensional (no longer two-dimensional) formation of the boundary layer reversal which, in this case, occurs throughout a wide range of plate sections. The non-ideal balance values for $Tu_o = 1.6\%$ thus emphasizes again the three-dimensional character of the reversal process, as was shown in Illustration 5.13 (see Chapter 5.3) with the aid of traverse measurements.

In Illustration 5.24c ($T_w/T_o = 0.53$), the outstanding average values for $Tu_o = 1.6\%$ with $x = 0.21\text{m}$ can also be used as a confirmation of the laminar measurement result (specifically the increase of laminar heat transfer caused by wall cooling). With this flow, the respective reversal occurs after a greater length of plate running length.

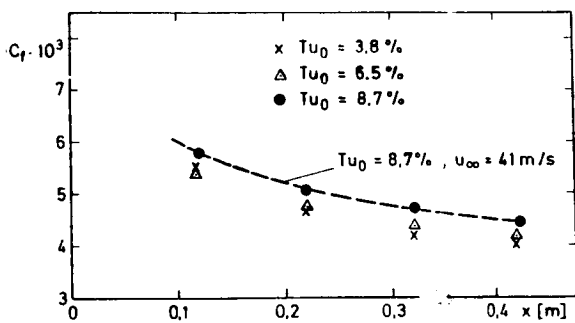


Illustration 5.18:
Turbulent Tangential
Stress Coefficients
($T_w/T_\infty = 0.8$)

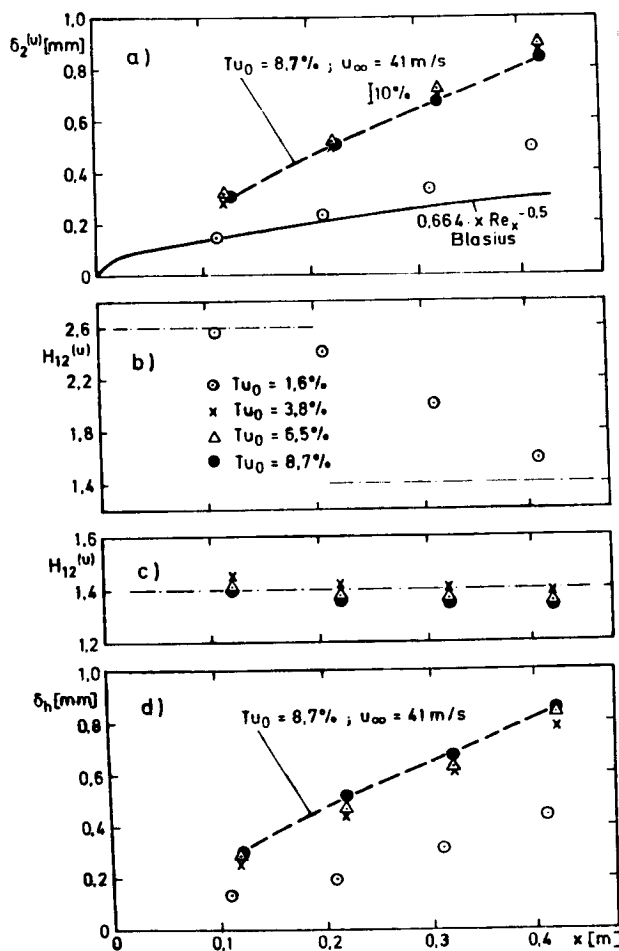


Illustration 5.19:
Boundary Layer
Quantities ($T_w/T_\infty = 0.8$)
(See Ill. b for Symbols)

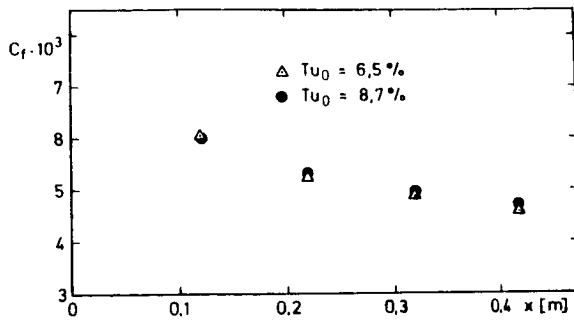


Illustration 5.20:
Turbulent Tangential
Stress Coefficients
($T_w/T_\infty = 0.64$)

(81)

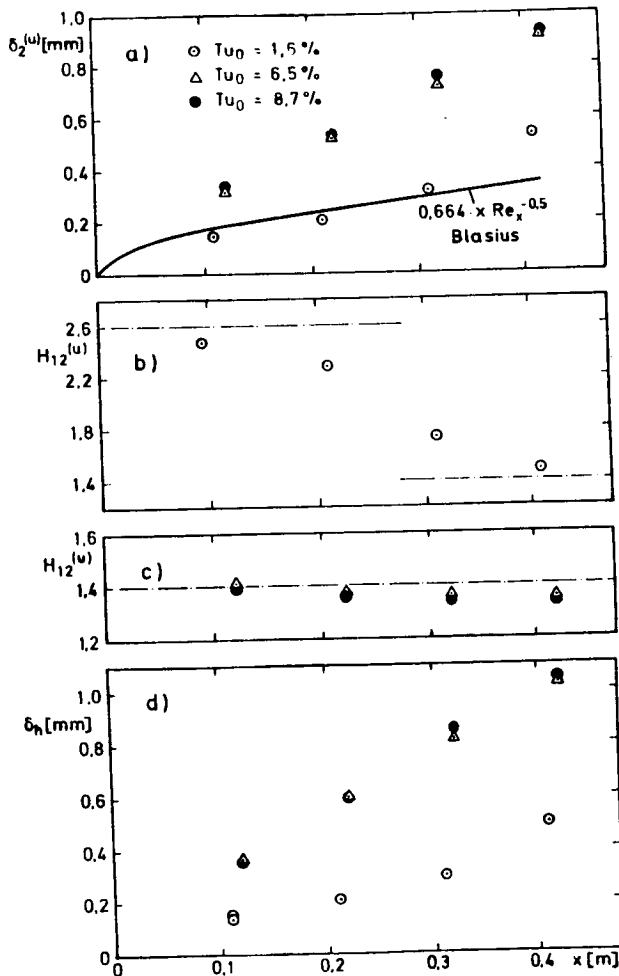


Illustration 5.21:
Boundary Layer
Quantities ($T_w/T_\infty = 0.64$)

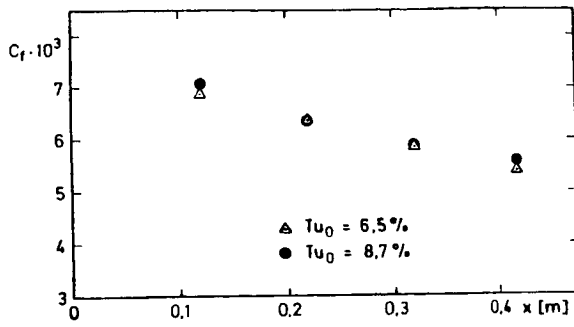


Illustration 5.22:
Turbulent Tangential
Stress Coefficients
($T_w/T_\infty = 0.53$)

ORIGINAL PAGE IS
OF POOR QUALITY

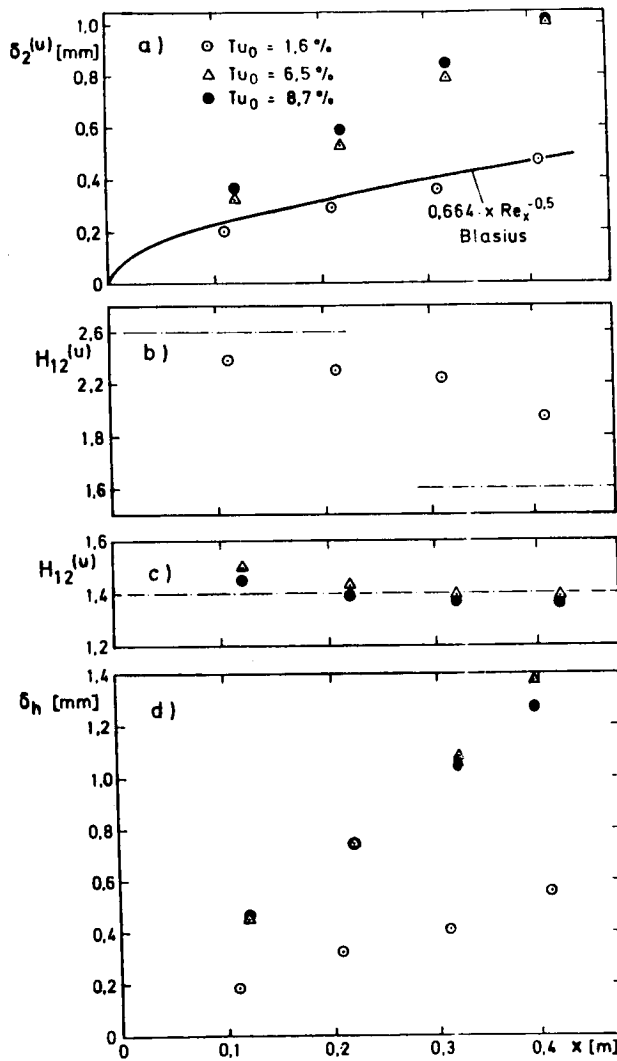


Illustration 5.23:
Boundary Layer Quantities
($T_w/T_\infty = 0.53$)

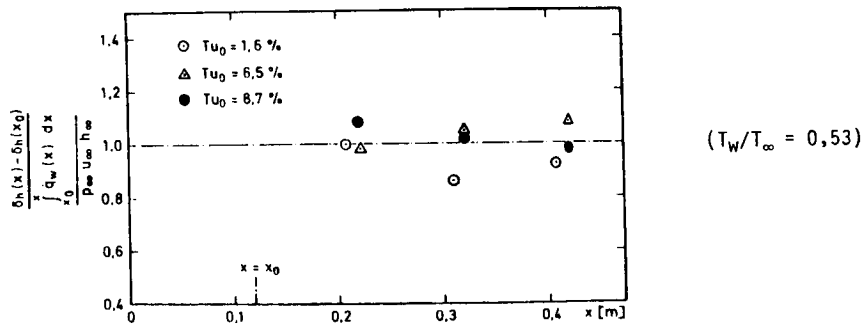
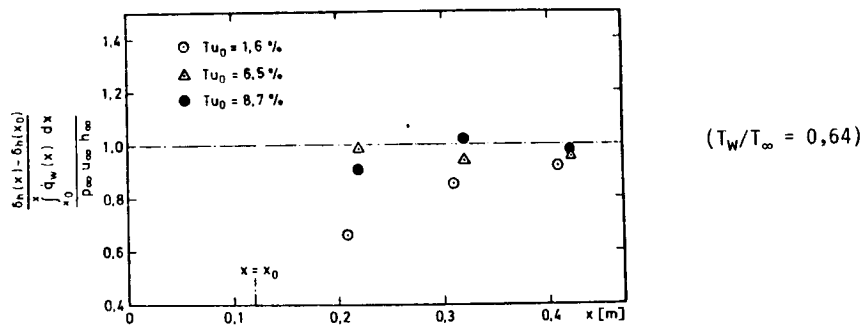
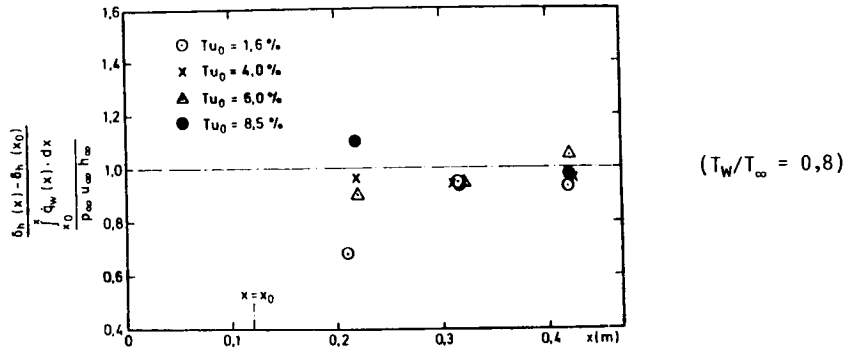


Illustration 5.24: Enthalpy Balance Calculation

The following chapters provide a detailed evaluation of the measurements. An additional component of this evaluation is the measurement results with pressure gradients.

A fundamental description of the influences of free stream turbulence, wall cooling and pressure gradients is provided and a quantitative analysis is made. This includes a mutual superimposition of the parameters. The experimental results will be separated from their respective situations and will be generalized with dimensional analyses. The main focus of my analysis is the influence of heat transfer, wall tangential stress, boundary layer profile and reversal process.

5.5.1 Material Value Influence due to Wall Cooling

5.5.1.1 Laminar Boundary Layers

The laminar heat transfer:

The heat transfer tests described in chapter 5.4 clearly showed that increased wall cooling results in a distinct increase of the laminar heat transfer. This was visually demonstrated by a comparison of the resulting Stanton coefficients with a relationship proposed by Kays [64] for the laminar heat transfer in flows with constant material values (Illustrations 5.15 - 5.17). The following paragraphs will make a quantitative evaluation of this observation. The laminar curves (see Illustrations 5.15 - 5.17), which are assigned to the measurements for all temperature ratios T_w/T_∞ are used as a basis. These laminar curves were determined in conjunction with the relationships by Kays [64]:

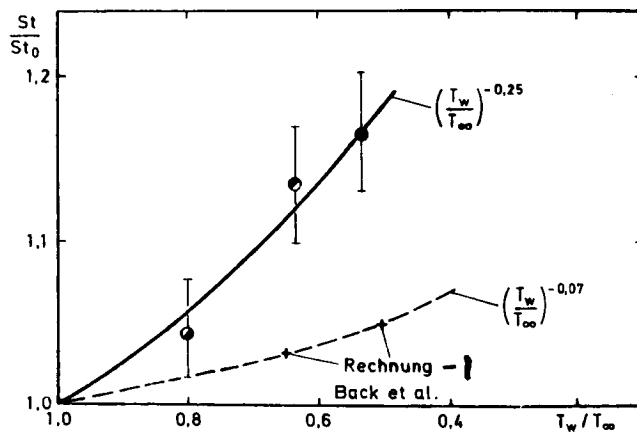
$$St = A \cdot Re_x^{-0.5} \cdot Pr^{-2/3} \cdot \left(1 - \left(\frac{\xi}{x}\right)^{0.75}\right)^{-1/3} \quad (5.2)$$

ζ refers to the uncooled take-off distance of the boundary layer. The factor "A" was determined with lowest free stream turbulence ($Tu_\infty = 1.6\%$). It was then summarized to a general relationship, which is dependent on the temperature ratio T_w/T_∞ and which describes the influence of wall cooling:

$$A = 0,342 \cdot (T_w/T_\infty)^{-0,25} \quad (5.3)$$

Illustration 5.25 shows the temperature dependence of the laminar heat transfer, which is given with equation 5.3, in a standard application as a factor of the temperature ratio T_w/T_∞ . The laminar measurement values with their respective fluctuations are illustrated as confirmation of these results.

(85)



1 - calculation

Illustration 5.25: Influence of Wall Cooling on Local Laminar Heat Transfer (St_0 describes the isothermal, critical case in accordance with equation 5.2)

According to the test results, the local heat transfer increases up to 18% as a result of the decrease of the temperature ratio $T_w/T_\infty = 0.5$. In contrast, available information from literature [64, 65, 67] shows values which are considerably lower. According to the theoretical boundary studies by Back et al [67], cooling influences can be expected (Illustration 5.25) which, with identical temperature decrease at the wall, are approximately 10% lower. The increases of laminar heat transfer, which were calculated in accordance with the reference temperature schematic by Eckert (see [67, 64]) with incompressible laminar heat transfer correlations (Illustrations 5.15 - 5.17), are also lower by the same percentages. (Eckert proposes the average value between free stream and wall temperatures as a reference temperature) The results according to the reference temperature procedure - as the calculations by Back et al - can be described by the potency law $(T_w/T_\infty)^{-0.07}$ with sufficient accuracy. According to new tests, however, there is a higher proportional dependency - $(T_w/T_\infty)^{-0.25}$ - on the wall cooling (Illustration 5.25). The biggest contrast to my tests are the proposals by Kays [64], which are based on estimated material value analyses, where cooling influences in boundary layers with constant free stream velocity can be completely neglected. To date, the low or negligible effects of the cooling were based on the following: the effect of the boundary layer profiles, which became fuller as a result of cooling, and the steeper wall gradients are almost completely compensated by the decreased heat conductivity and viscosity near the wall (see Back et al [67]). However, recent tests have shown that there is an imbalance of the profile deformation, which results in distinctly higher increases of the laminar heat transfer as a function of cooling than was presumed in previous theoretical analyses.

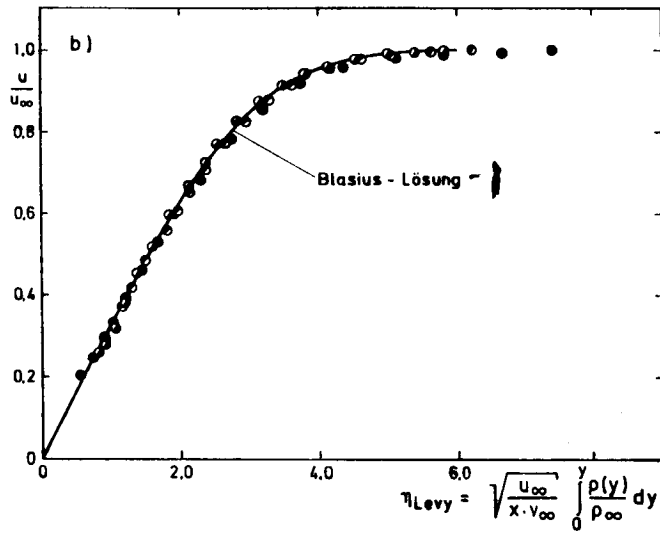
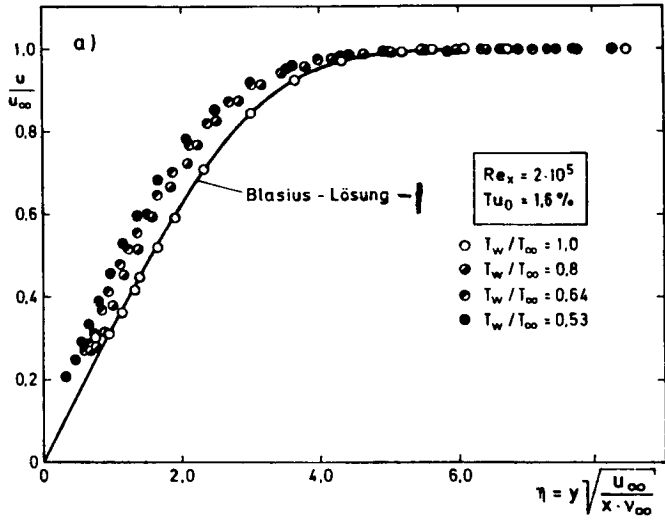
(86

In order to clarify the profile deformations on which the resulting heat transfer increases were based, Illustration 5.26a shows laminar velocity profiles with an identical running length Reynolds number Re_x for different temperature conditions. In this application, which was made with the similarity coordinates of laminar balancing boundary layers, fuller velocity profiles can be observed with increasing wall cooling. These profiles are different from the ideal solution of isothermal boundary layers according to Blasius (see [109]). As a confirmation of this procedure, they experience a decrease of the kinematic form parameter from $H_{12}^u = 2.55$ ($T_w/T_\infty = 1.0$) to $H_{12}^u = 2.39$ ($T_w/T_\infty = 0.53$). The fuller profiles show steeper wall gradients which, despite reduced viscosity and heat conductivity, result in a measured increase in the laminar heat transfer at the wall.

Suitable transformation equations provide the opportunity for applying incompressible laminar profile equations to flows with heat transfer. An example of this is shown in Illustration 5.26b. The Levy transformation [116] shown in Illustration 5.26b supplements the standard wall distance coordinate η with an additional material value weighting, which is directly dependent on the wall distance y :

$$\eta_{\text{Levy}} = \sqrt{\frac{u_\infty}{\nu_\infty \cdot x}} \cdot \int_0^y \frac{\rho(y)}{\rho_\infty} dy$$

Because of this transformation, the profiles which were changed by cooling are converted to the standard condition for adiabatic boundary layer flows, according to Blasius. With the Eckert transformation, which was also studied for this profile evaluation, the influence of wall cooling was compensated considerably less than with the Levy procedure (Illustration 5.26b). This was also confirmed by the inaccuracy of the Eckert transformation, as is shown in Illustration 5.25, where dependency of the laminar heat transfer on the wall cooling was not adequately considered.



1 - Blasius solution

Illustration 5.26: Laminar Velocity Profiles with Wall Cooling.

Heat transfer and wall tangential stress:

Events observed in turbulent boundary layers with respect to running length are always subjected to additional influences, which are caused by the formation of the respective boundary layer reversal. In order to eliminate resulting side effects, Illustrations 5.27a and 5.27b provide an analysis of the turbulent friction coefficients measured by me for the temperature ratios $T_w/T_{\infty} = 1.0; 0.8; 0.64$ and 0.53 as a factor of a similar value, which has a direct relationship to the boundary layer: the impulse loss thickness Reynolds number Re_2 . Both illustrations describe cases with constant free stream turbulence ($Tu_{\infty} = 6.5\%$ and 8.7%). With increased wall cooling, the friction coefficient increases by up to 16% (Illustration 5.27). The increased rates in both cases of varying and, at the same time, high free stream turbulence are almost identical. Also, they are in good agreement with the results by Sill [78], which were determined in previous tests for turbulent boundary layers with very low outer turbulence. The increases of the turbulent heat transfer as a result of wall cooling are thus independent of the amount of free stream turbulence.

In order to quantify the influence of wall cooling, comprehensive analytical studies were made. Illustration 5.17 shows the result of these analyses with the aid of curve systems which, for given temperature conditions, describe the behavior of tangential stress coefficients in turbulent boundary layers with heat transfer. The relationship is as follows:

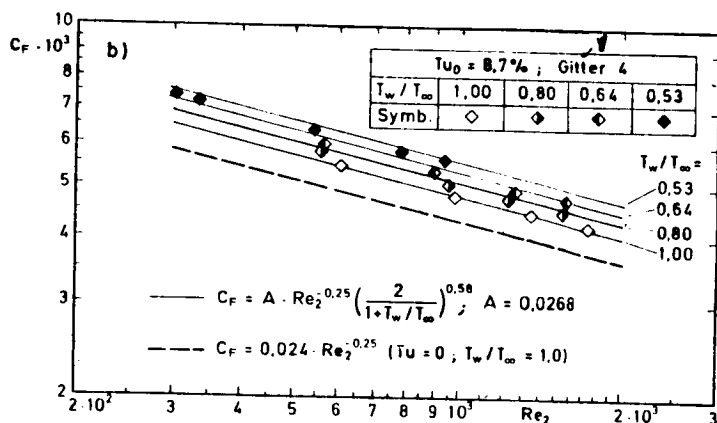
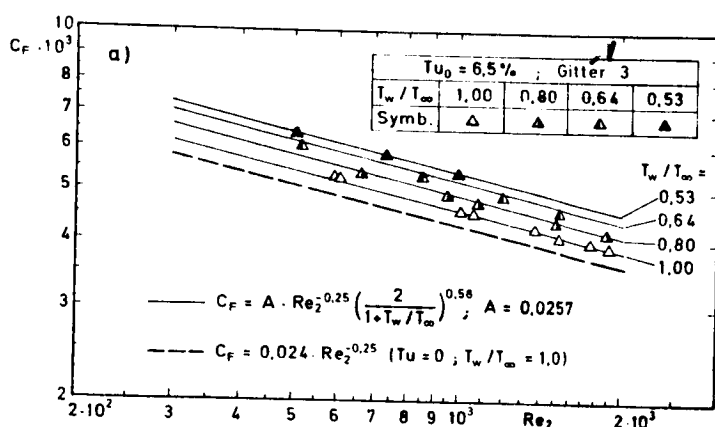
$$c_f = A \cdot Re_2^{-0,25} \left(\frac{2}{1+T_w/T_{\infty}} \right)^{0,58}; \quad Re_2 = \frac{u_{\infty} \cdot \delta_2}{\nu_{\infty}} \quad (5.4)$$

This equation is based on the statement for the friction coefficient in accordance with equation (5.1), as it applies to the flow on adiabatic walls. By introducing a suitable reference temperature

(mean value between wall and free stream temperatures) to determine the material values contained therein, this statement was expanded to flows with variable density. The connection described by equation (5.4) with the values Re_2 and c_f which, in turn, relate to the free stream material values, was then achieved with a formula substitution proposed by Back et al [76] of these newly introduced reference material values.

ORIGINAL PAGES ARE
OF POOR QUALITY

(89



1 - grid

Illustrations 5.27a and b: Turbulent Friction Coefficients
Under the Influence of Wall Cooling

To confirm the theoretical temperature influences of equation 5.4, the empirical constant "A" was determined by approximating this relationship to the respective measurement points of the uncooled boundary layer flow. With this determination for the constant "A", the relationship 5.4 describes the measured influence of wall cooling in both cases of varying free stream turbulence with sufficient accuracy for all temperature conditions (see Illustration 5.27 a and b). Compared to the test, the calculation shows slightly increased tangential stress coefficients. However, the difference is less than 3% in all cases. Equation 5.4 thus provides a practical condition which describes the basic cooling influence in turbulent boundary layers in a simple manner.

Because comparative isothermal tests ($T_w/T_\infty = 1.0$) were not possible for the heat transfer, the above result for tangential stress coefficients was linked to measured analogy factors in order to determine the cooling influence on the heat transfer. The analogy factors determined in my experiments (see Illustration 5.43, Chapter 5.5.2.2) $2 \times St/c_f$ fluctuate around the mean value 1.1. They neither show an identifiable dependency on the wall cooling nor a direct dependency on the free stream turbulence. This proves that the increases, which are a factor of cooling and which exist in the heat transfer, are identical to those in the wall tangential stress. Therefore, the temperature dependency, which was obtained in equation 5.4 for the friction coefficient, is also suitable to describe the increase rates in heat transfer.

(90)

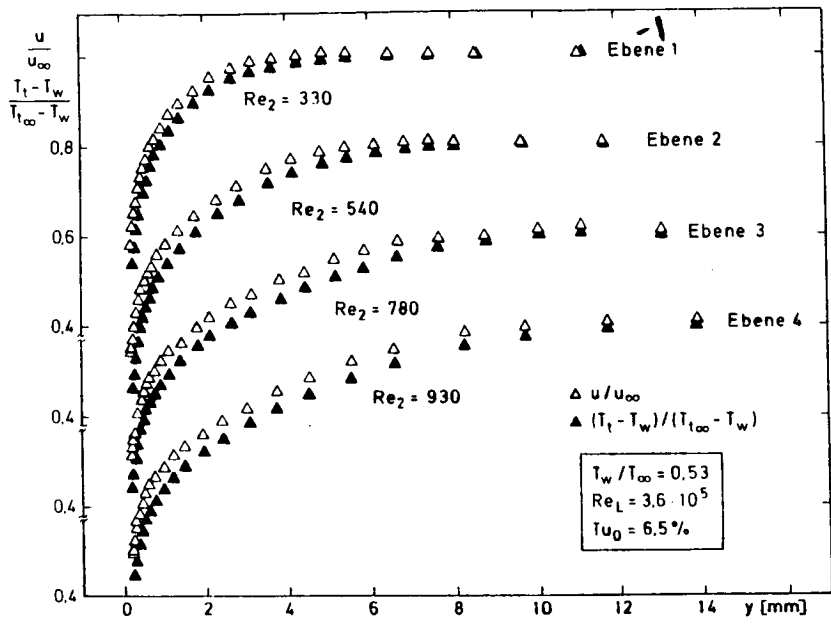
Velocity and Temperature Profiles:

The formation of heat transfer and wall tangential stress in flows with varying density is mainly determined by the properties and the behavior of the boundary layer profiles. Illustration 5.28 shows typical velocity and temperature profiles whose type and development were measured along the plate surface in all temperature conditions and turbulence intensities. The measurement in Illustration 5.18

refers to turbulent boundary layers with high free stream turbulence ($Tu_\infty = 6.5\%$) and the highest wall cooling ($T_w/T_\infty = 0.53$). Measuring surface 1 is located in the immediate vicinity of the end of the laminar-turbulent boundary layer reversal. As can be expected with unaccelerated boundary layers, there are almost identical velocity and temperature profile forms. This can be attributed to a synchronous development of slow speed and temperature boundary layers. With an increasing Reynolds number Re_2 , Reynolds number influences become less significant and the profiles visibly approach a form which is characteristic for equilibrium boundary layers. Due to Prandtl numbers for gases (in our case: air, $Pr = 0.71$), which deviate from 1, the temperature boundary layer thickness δ_t is always greater than the flow boundary layer thickness δ , and the respective value of the temperature profile - with the same wall distance - is always lesser than the value of the velocity profile (see Illustration 6.14b; Chapter 6.7.1.3; and Rüd et al [123]). Drastic difference in the development of velocity and temperature profiles will only occur if the flow has considerable pressure gradients, or if the heat stream parameter

$$\Omega = \frac{\delta_1}{c_f/2} \cdot \frac{1}{\dot{q}_w} \cdot \frac{d\dot{q}_w}{dx} \quad (5.5)$$

which is analogous to the Clauser parameter, has very high values. According to studies by Taylor [121] and Sill [78], pressure gradients and distinct heat stream parameters Ω have a considerable additional influence on the temperature profile.



1 - surface

Illustration 5.28: Velocity and Temperature Profiles in a Highly Cooled Turbulent Boundary Layer

The Logarithmic Wall Theory:

The boundary layer profiles in Illustration 5.28 have the same basic matrices as those measured in adiabatic boundary layers with identical free stream turbulence but without wall cooling (see Illustration 5.6). Therefore, changes which affect cooled boundary layer profiles cannot be recognized with this application. A demonstration of the influences caused by wall cooling requires a similarity analysis of the profiles in the form of the logarithmic wall theory. Because of this, Illustration 5.29 shows dimensionless velocity and temperature profiles with identical free stream turbulence ($Tu_0 = 8.7\%$) for varying cooling intensities. The profiles were measured in surface 4. With falling temperature conditions, the applicable Reynolds number Re_2 has the values:

$Re_2 = 1,640, 1,550, 1,530$ and 940 . As shown in Illustration 5.29, the profile properties which exist when wall cooling is present can now be clearly seen. Even with high wall cooling, the measured profiles show a distinct logarithmic wall section. However, with increased wall cooling, the matrices show higher velocities and temperatures plus a slight profile twist.

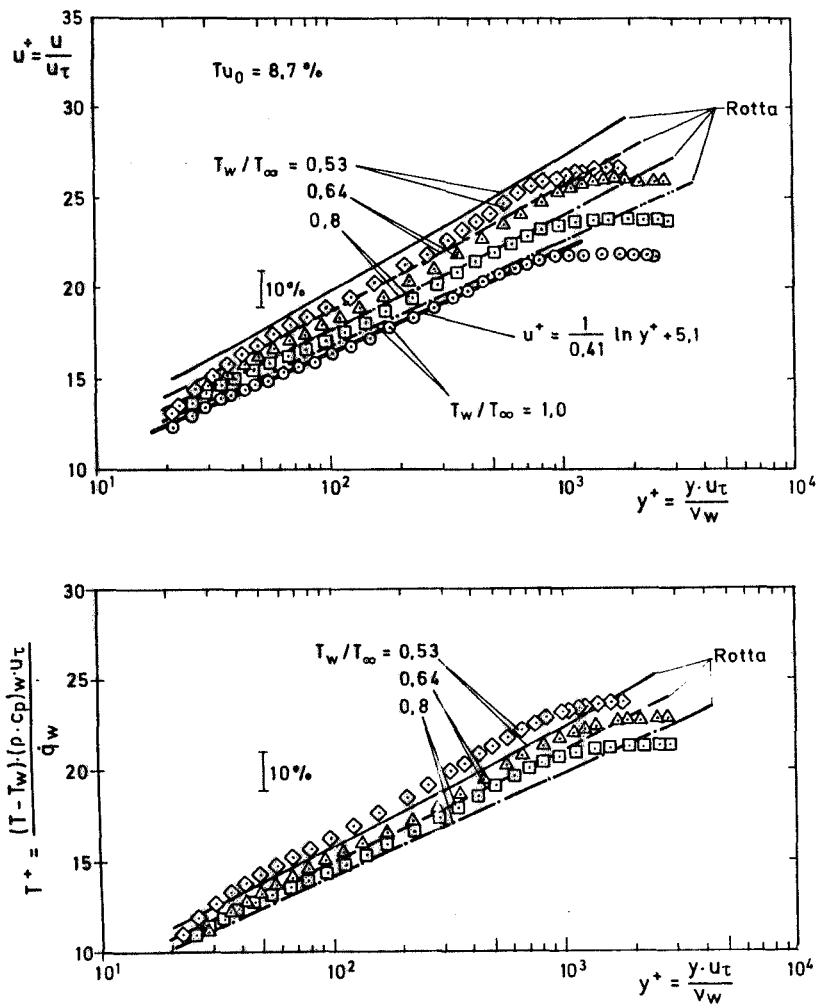


Illustration 5.29: Dimensionless Velocity and Temperature Profiles

Only a very few experimental studies (Sill [78] and Back et al [76]) (93 have been conducted on the effects of highly changeable material values in turbulent sub-sonic boundary layers. These tests showed an increase of velocity and temperature values with semi-logarithmic application. However, the simultaneous rotation of the logarithmic wall theory was, in most cases, not demonstrated. For an evaluation of our test results I will therefore use the theoretical study by Rotta [85] on the influence of Mach number and heat transfer in turbulent flows. By integrating the boundary layer differential equations, Rotta [85] deduced an asymptotic wall theory which addresses the influence of wall cooling. Illustration 5.29 compares this wall theory to the profile measurements. Mach number influences are neglected, as they are not important in this case. If the sensitivity of the semi-logarithmic application method is considered, there is a very good agreement of the theory with the test results. The velocity and temperature value increases as well as the rotation of the wall theory are correctly recorded by Rotta's equations. This also confirmed Rotta's assumption that the cooling effects will not change the basic turbulence structure but are generated exclusively by the material values, which vary throughout the boundary layer.

When revising calculation models, it is often important to have a simple and quick test method for computing profile matrices. To date, no suitable methods have been developed; therefore, an attempt was made to apply, based on the reference temperature principle, the simple logarithmic wall theory for adiabatic flows in highly cooled boundary layers. At the same time, it was to be determined whether reference temperature methods used in integral procedures are suitable to expand the profile matrices, to a situation with wall cooling (see Chapter 6; development of the integral procedure). The mean temperature between free flow and wall, which was used in the tangential stress analysis, was again considered valid.

Illustration 5.30a shows, for the representation of two cases with high wall cooling, the logarithmic velocity and temperature profiles with the coordinates y_{Ref}^+ , u_{Ref}^+ and T_{Ref}^+ , which were formed with material values at reference temperature. The wall theories for (94) adiabatic boundary layers are also illustrated for a direct evaluation with of the useability of this reference temperature. As expected, the material value transformation near the wall again shows agreement of the measurement points with the logarithmic wall theory for adiabatic boundary layers (see Illustration 5.30a).

Based on this determination, the logarithmic wall theory for adiabatic flows can also be applied to boundary layers with high temperature variations, if the coordinates T^+ , u^+ and y^+ are generated from the material values (density, viscosity) at reference temperature. If, with the aid of suitable material value relationships for density and viscosity ($\rho \approx 1/T$; $\nu = \mu/\rho$; $\mu \approx T^{0.7}$), we perform a simple re-transformation of these coordinates into quantities formed with wall material values, the wall theory for adiabatic boundary layers is validated in a general context. This context has a common notation, which is independent of wall coordinates, and, at the same time, describes the influences of wall cooling. The wall theory for velocity and temperature profiles is as follows:

$$u^+ = \frac{1}{\kappa^*} \cdot \ln y^+ + C^* \quad (5.6)$$

$$T^+ = \frac{1}{\kappa_T^*} \cdot \ln y^+ + C_T^*$$

with

$$\kappa^* = \kappa / \left[\frac{1}{2} (1 + T_\infty/T_w) \right]^{0.5} \quad (5.7a)$$

$$C^* = \left[\frac{1}{2} (1 + T_w/T_\infty) \right]^{0.5} \left(\frac{1.2}{\kappa} \cdot \ln \left(\frac{2}{1 + T_\infty/T_w} \right) + C \right) \quad (5.7b)$$

$$\kappa_T^* = \kappa^*/Pr_t \quad (5.7c)$$

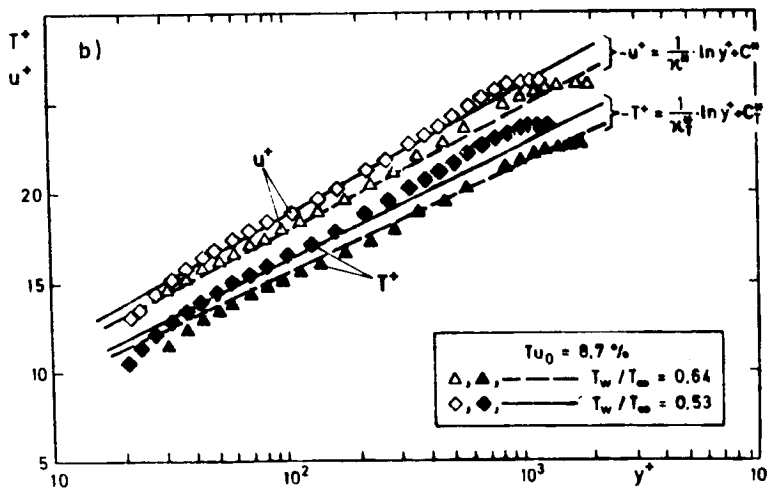
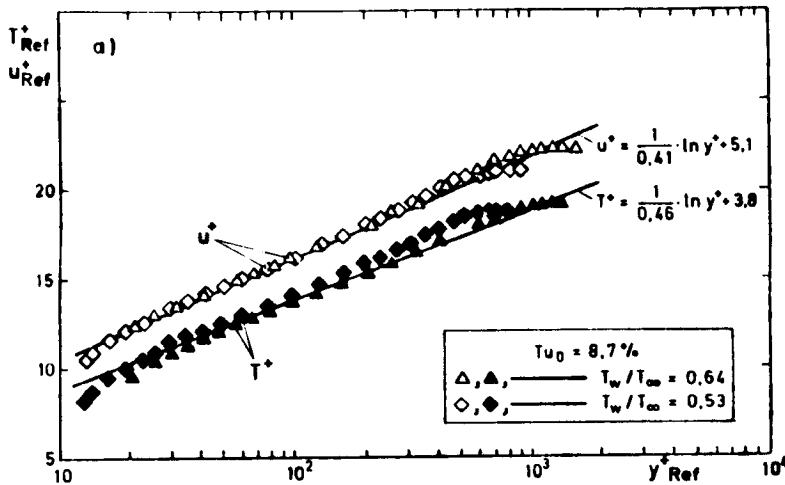
$$C_T^* = \left[\frac{1}{2} \left(1 + \frac{T_w}{T_\infty} \right) \right]^{0,5} \cdot \left(\frac{1,2}{\kappa_T^*} \ln \left(\frac{2}{1 + T_w/T_\infty} \right) + C_T \right) \quad (5.7d)$$

and

$$C = 5,1; \quad \kappa = 0,41; \quad C_T = 3,8; \quad \kappa_T = \kappa/Pr_t; \quad Pr_t = 0,9$$

ORIGINAL PAGE IS
OF POOR QUALITY

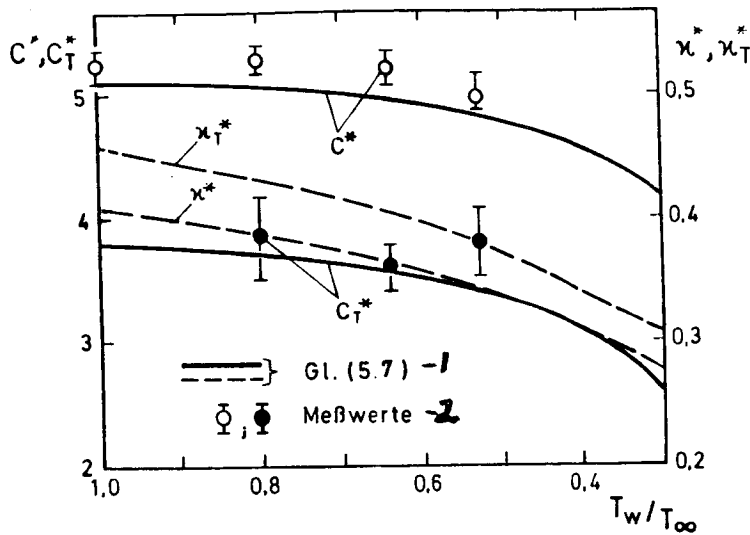
(95)



Illustrations 5.30 a and b: The Logarithmic Wall Theory when Considering Material Value Transformations

The relationships of the logarithmic wall theory with wall cooling gained in this manner are considerably simpler and clearer in comparison to the Rotta equations (see [85]). Their validity is emphasized in Illustration 5.30b by a good agreement with the applicable profile test data. The deduced relationships are a good reproduction of the profile rotation and the increased temperature and velocity values with increasing wall cooling.

With the newly developed wall theories there is a similarly good agreement as in Illustration 5.30b of all other test situations with wall cooling. This is confirmed in Illustration 5.31 in a comparison of all measured profile constants c^* and c_T^* which were calculated in accordance with equation 5.7. The measurement values, which are a factor of the temperature relationship, were determined by adjusting the wall theory in accordance with equation 5.6 to the measured profiles. c^* and c_T^* were assumed as a parameter in accordance with equation 5.7. Additionally, Illustration 5.31 shows that, based on the profile rotation due to wall cooling, there are only minor changes in the profile constants c^* and c_T^* . In addition to the simple method of calculating the wall theory in accordance with equation 5.6, this provides another method of simplification. In accordance with Illustration 5.31, the values c^* and c_T^* with temperature conditions in excess of $T_w/T_\infty = 0.5$, can also be satisfactorily determined with their adiabatic values.



1 - equation (5.7); 2 - test values

Illustration 5.31: The Profile Constants of the Logarithmic Wall Theory in Accordance with Equation 5.7 and Test Values

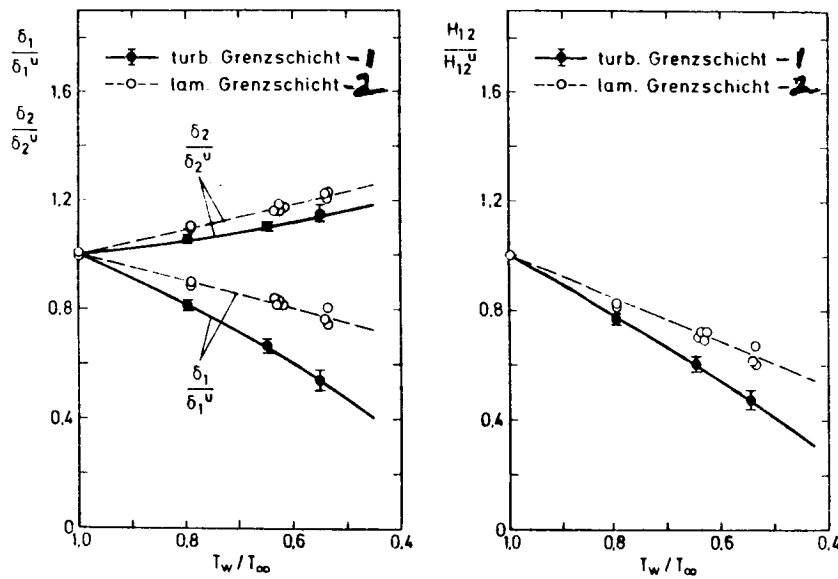
5.5.1.3 Integral Boundary Layer Characteristic Values for Wall Cooling

(97

A favorable comparison of kinematic boundary layer characteristic values to material values in laminar and turbulent boundary layers in Illustration 5.32 is the preliminary conclusion of my comprehensive and detailed analysis of the influences of wall cooling. Material value influence occurs in all characteristic values. When wall coolings are present, they effect an increase of the impulse loss thickness. At the same time, they cause an even greater decrease of the displacement thickness, which results in a decrease of the form parameters $H_{12} H_{12}^u$ in laminar and turbulent boundary layers. In our temperature range, impulse loss thickness ratios increase by up to 20%. Despite very different profile forms,

there are no striking differences between laminar and turbulent boundary layers. In contrast, the differences in the displacement thickness and, consequently, in the form parameters are more distinct.

ORIGINAL PAGE IS
OF POOR QUALITY



- 1 - turbulent boundary layer
- 2 - laminar boundary layer

Illustration 5.32: Laminar and Turbulent Boundary Layer
Characteristic Values under the Influence
of Wall Cooling (Test Values)

This chapter will provide a quantitative analysis of the influences of free stream turbulence. A comparison of test data with and without wall cooling will determine whether turbulence intensity effects are subjected to additional wall cooling influences.

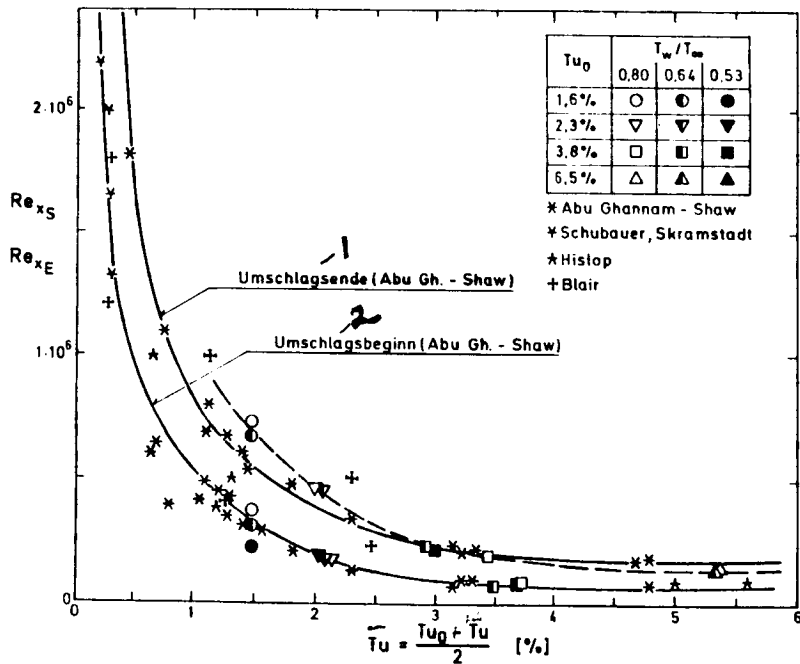
5.5.2.1 The Laminar-Turbulent Boundary Layer Reversal

In the design of cooled gas turbine blades, the question is always raised whether the reversal processes caused by free stream turbulence are also subjected to dramatic influences from wall cooling. The linear stability theory [22] for boundary layers without external turbulence lets us presume that this is the case. The same applies to the measured laminar profiles in Illustration 5.26, because the profile matrices, which have become fuller as a function of cooling, point to a stability increase of the boundary layer. In a careful comparison of reversal events observed in experiments with data of other authors, which have all been determined in adiabatic flows, I would like to identify the actual circumstances.

An evaluation of the laminar-turbulent reversal is made with the aid of the measured heat transfer distributions along the plate. The reversal Reynolds numbers Re_{xS} , which were deduced from heat transfer tests, resulted from the intersection of laminar compensating curves with a straight line, which is adjusted to the matrix of steeply increasing Stanton numbers in the reversal area (see Illustrations 5.15 - 5.17). Reversal locations and matrices, which are comparable to information available in literature, are thus determined. These transform the three-dimensional process into a good approximation of a two-dimensional description, which can identify the reversal initiation point.

The reversal determination in previous studies (see [45]) was obtained with the aid of probes. The reversal initiation in my analysis of the heat transfer is in context with a notable deformation of the boundary layer profiles. As demonstrated by Owen [25] in his own boundary layer tests and with the aid of those conducted by Schubauer and Klebanoff [17], a distinct boundary layer turbulence formation is required (see Chapter 2.2). Because of this, the visible initiation of the reversal in the heat transfer is not equal to the formation of boundary layer turbulence.

(99)



- 1 - reversal completion
- 2 - reversal initiation

Illustration 5.33: Running Length Reynolds Numbers Re_x at Reversal Initiation and Completion

Illustration 5.33 shows the running length Reynolds numbers at reversal initiation and at the end of the reversal (see Table 5.2), which were determined with heat transfer tests, as a factor of free stream turbulence. It also makes a comparison with results achieved by Abu Ghannam and Shaw [45], Schubauer and Skramstad [14], Hislop [118] and Blair [36]. The Reynolds numbers refer to the viscosity of the free flow. In accordance with a proposal by Abu Ghannam and Shaw, average turbulence intensities are used. These are formed with the local free stream turbulence Tu at the reversal location and with the respective inlet turbulence Tu_0 at the beginning of the plate. This takes into consideration the turbulence intensity decrease along the plate and, therefore, the history of the boundary layer up to the point of reversal.

My own determinations of the reversal initiation are in good agreement with the data of other authors. Even the fluctuations with varying wall cooling can be integrated in other test results, which were obtained exclusively under isothermal conditions. This shows that, contrary to information obtained from the stability theory, no influence of wall cooling is noted on the reversal initiation. The only differences to previous tests are noted in the description of the reversal completion. With low turbulence intensities, my tests show a tendency toward higher Reynolds numbers and, consequently, toward greater reversal lengths while, with high turbulence intensities in excess of 5%, the reversal is completed after shorter running lengths.

(100

In order to present a more general picture not dependent on the running length, as is required for the development of general reversal criteria, Illustration 5.34 provides a reversal analysis with the aid of local boundary layer characteristics. Instead of running length Reynolds numbers, impulse loss thickness Reynolds numbers are studied at the initiation and completion of the reversal. The required impulse loss thickness Reynolds numbers were determined with the running length Reynolds numbers at reversal initiation described above.

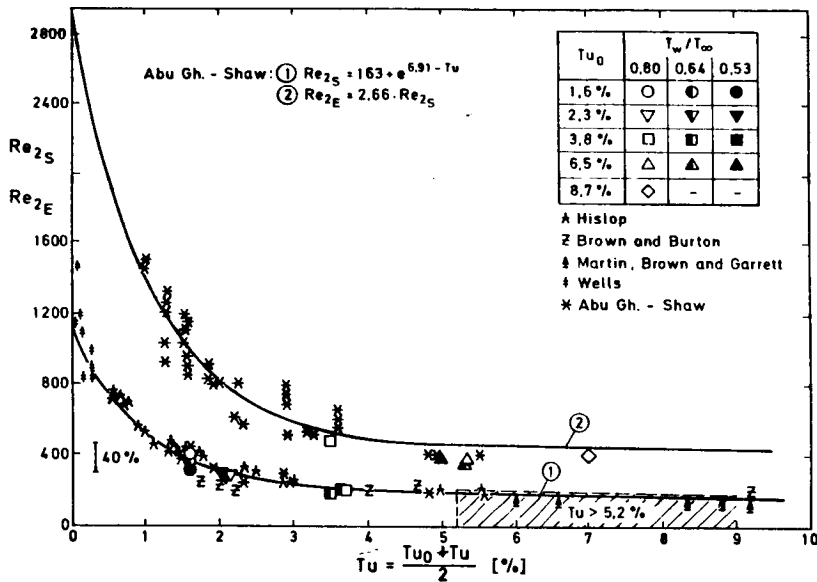


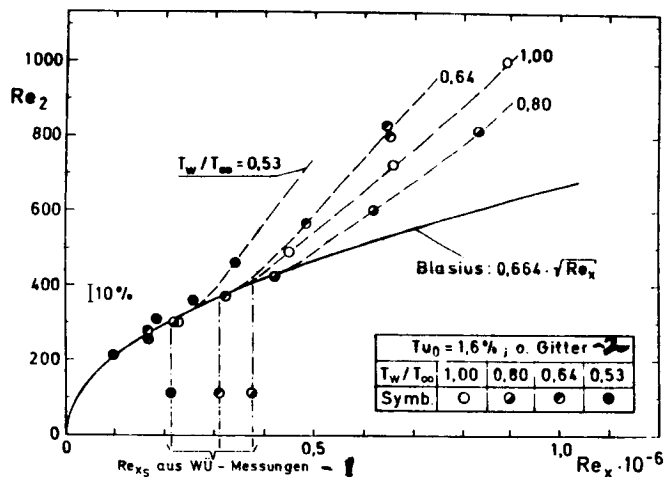
Illustration 5.34: Impulse Loss Thickness Reynolds Numbers at Reversal Initiation and Completion

As shown by Illustration 5.35 with test values for lowest free stream turbulence, the impulse loss thickness Reynolds number at reversal initiation can, for all temperature conditions, be calculated with the simple Blasius relationship (101

$$Re_2 = 0,664 \sqrt{Re_x} \quad (5.8)$$

with the aid of the applicable running length Reynolds number. Because, for higher turbulence intensities, laminar boundary layers could not be accessed with probes, the Blasius relationship (equation 5.8) was also used for these cases to determine the impulse loss thickness Reynolds number at reversal initiation. This procedure, which is also used by other authors, is supported by the experience (see Illustrations 5.16 and 5.17) that laminar boundary layers in unaccelerated flows are not subject to turbulence intensity influences. The impulse loss thickness Reynolds number at

the end of the reversal was determined only for flow conditions obtained with boundary layer measurements. To do this, the measured Re_2 matrices were either interpolated or extrapolated.



1 - Re_{xS} from WU tests; 2 - grid

Illustration 5.35: Determining the Reynolds Number Re_2 at Reversal Initiation

The application of the reversal Reynolds numbers Re_{2S} , Re_{2E} in Illustration 5.35 again compares my tests to the previous results achieved by Hislop [117], Brown and Burton [118], Martin [119], Well [120], and Abu Ghannam and Shaw [45]. The distinct spread of available measurement data in this diagram indicates the difficulty of an exact determination of the reversal. As in Illustration 5.33, my analysis of the impulse loss thickness Reynolds number is also in good agreement with the data of other authors determined exclusively under isothermal conditions. Because the test results show no tendencies which could be attributed to the temperature ratio T_w/T_∞ , they confirm that no boundary layer stabilization exists, which could be attributed to cooling influences.

(102

According to both stability theory and previous tests, there should - for turbulence intensities in excess of 5% - be a minimum asymptotic value for the reversal Reynolds number (with $Re_{2S} \approx 160$) which should not be exceeded, even with maximum free stream turbulence intensities (see Illustration 5.33). My tests do not confirm this reversal behavior. The heat transfer distributions along the measuring plate (see Chapter 5.4) have shown that the reversal with high turbulence intensities ($Tu_0 = 6.5$ and 8.7%) occurs very early; it is almost complete at the first measuring location ($x = 47$ mm). In accordance with calculations from equation 5.8 it can be expected that, upstream in this initial measuring surface, there are impulse loss thickness Reynolds numbers in the reversal initiation which are considerably lower than the asymptotic boundary value (with $Re_{2S} \approx 160$). Tests with free stream acceleration come to the same conclusion. With high turbulence intensities, the reversal always initiates directly at the leading edge of the plate (see Chapter 5.6).

The reasons for the discrepancy between the new and the few previous test results, which confirm the presence of a stability limit, can be found in the varying geometric parameters of boundary layer generation (design of the leading edge of the plate). In distinct contrast to previous tests, our measurements were taken with a very thin, streamlined leading edge of the plate (with a thickness of only 2 mm). With thick leading edges of a plate and a respective stream-lining, acceleration effects occur which provide additional stability to boundary layer development, thus displacing the reversal to higher Reynolds numbers. The boundary layers generated on thin leading edges are not subject to additional stabilization. They can therefore react much more sensitively to a fluctuation in the flow caused by free stream turbulence. They may, as with our boundary layer flows, experience a premature reversal, especially when high turbulence intensities are present. It cannot be discounted that there may be a situation where the increased sensitivity to free stream turbulence completely prevents the formation of an initial laminar boundary layer. As a consequence, a turbulent boundary layer may be generated at boundary layer initiation.

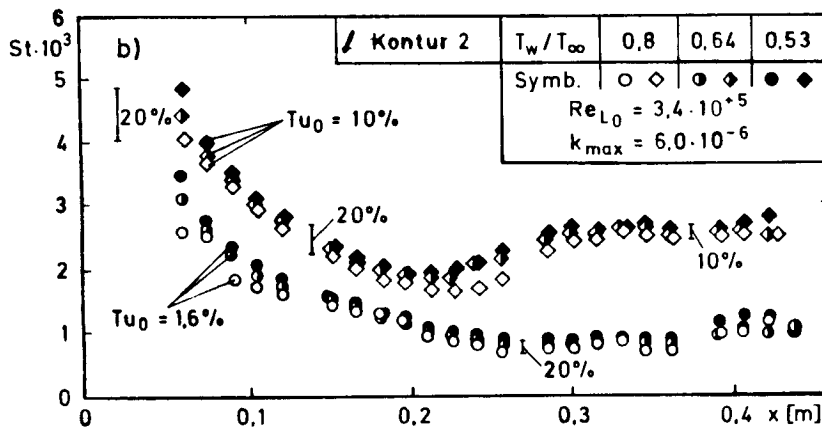
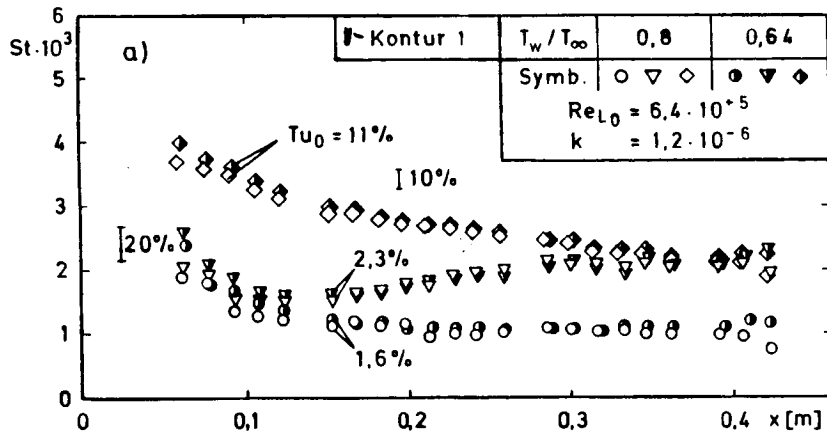
(103

These geometric aspects of reversal behavior and the resulting consequences for heat transfer are especially relevant for modern engine design: Aeronautic engines have, in their initial turbine stages, very thin blade profiles which are constantly exposed to highly turbulent gas circulation.

According to recent determinations, there is, when free stream turbulence is present, no stabilizing influence of wall cooling on the boundary layer which might result in higher reversal Reynolds numbers. With the turbulence and cooling intensities, which have technical relevance in our case, the influence of free stream turbulence dominates over reversal stabilizations which, are normally expected when wall cooling is present and which are predicted by the linear stability theory for flows without external turbulence. This, however, is not a fundamental contradiction to stability theory. The existence of cooling effects, which stabilize the boundary layer, is also demonstrated in our tests. It is clearly described in Illustration 5.26 by the fuller laminar profile forms. However, its significance - in contrast to the importance of free stream turbulence - is negligible.

In addition, the analysis of the reversal events measured with wall cooling and the comparison with results for adiabatic boundary layers (Illustrations 5.33 and 5.34) point out the Reynolds number, which is based on the material data of the free flow, as an appropriate description measure for the reversal - at least for low and medium turbulence intensities. Despite drastic viscosity differences between free flow and wall, the introduction of reversal Reynolds numbers, which were formed with material values at an average reference temperature, has not proven to be practical. This is clearly emphasized by the tests with accelerated flow in Illustration 5.36 and also applies to highest turbulence intensities. By using both pressure gradient contours, slightly accelerated flows with varying wall cooling were generated in Illustration 5.36a. Highly accelerated flows with varying wall cooling were generated in Illustration 5.36b. The plate flow

velocities were adjusted to the selected free stream temperature in such a manner that, in the test cases of Illustrations 5.36a and 5.36b, there are identical plate flow Reynolds numbers $Re_{L,0}$. By maintaining constant plate running length Reynolds numbers, which were formed with the free stream data at the influx, and with varying wall cooling, constant matrices of the acceleration parameter $k(x)$ were achieved (see equation 3.1) along the plate, i.e. events which are comparable with respect to flow (see Illustrations 5.45, 6.15, 6.19). At the same time and in spite of varying free stream temperature, identical local running length Reynolds numbers occur at each location x , if they are also formed with free stream viscosity. Even with maximum turbulence intensities, the Stanton numbers (Illustration 5.36) measured under these conditions show no influence of the wall cooling on the boundary layer development or on the reversal. There are no stabilizing effects on the reversal due to wall cooling. Reversal events show a distinct correlation to the Reynolds numbers which refer to free stream material values. As shown in Illustration 5.36, the influence of the cooling is limited to the fact that the local heat transfer rates can be increased with a decreased temperature ratio. Increase rates are comparable to test results achieved without pressure gradients (see Chapter 5.4).



1 - contour

Illustration 5.36: Influence of Wall Cooling on Reversal Events
in Both Highly and Slightly Accelerated Flow

Chapter 5.3.2 showed the effects of increased free stream turbulence on adiabatic turbulent boundary layers. Based on this, the following chapter will analyze events with wall cooling as a factor of turbulence intensity. Turbulence intensity influences, which are almost completely known for other situations, have not been researched yet for this combination. The complexity of events induced by free stream turbulence, which was shown in previous studies, requires that accompanying longitudinal measurement and Reynolds number influences must be included in this study. In addition to heat transfer and resistance coefficients, the behavior of the boundary layer profiles must also be considered.

Velocity and Temperature Profiles:

Turbulent boundary layers with identical Reynolds numbers Re_2 and a different free stream turbulence are shown in Illustration 5.37 for the case of moderate wall cooling ($T_w/T_\infty = 0.8$) and in Illustration 5.38 for the case of maximum wall cooling ($T_w/T_\infty = 0.53$). The logarithmic wall lines were determined by adjusting the temperature correcting wall theory, developed in the previous chapter, to equation 5.6. As shown by the profile matrices, which were measured for wall cooling for the first time, the influence of increased free stream turbulence is in complete agreement with the events in adiabatic flows. It is, in turn, limited to the decrease of the wake portion with increasing free stream turbulence intensity. In agreement with the measurements by Blair [36, 39] in a slightly heated flow with an almost constant density, this also applies to the temperature profile with high wall cooling (Illustrations 5.37b and 5.38b).

In order to make a quantitative evaluation of the illustrated profile deformations and a possible discovery of cooling influences not shown by Illustrations 5.37 and 5.38, a comprehensive similarity analysis for the kinematic form parameter is conducted in Illustration 5.39. With its respective values for turbulence-free

external flow, the kinematic form parameter H_{12}^U is standardized for all measured profiles with and without wall cooling in Illustration 5.39. It is illustrated as a function of local turbulence intensity.

(106)

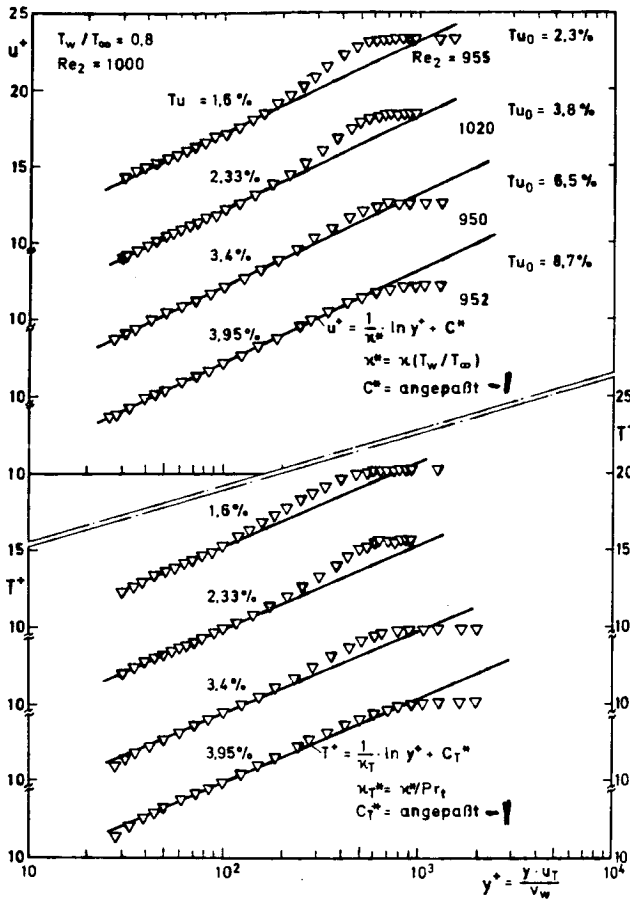


Illustration 5.37

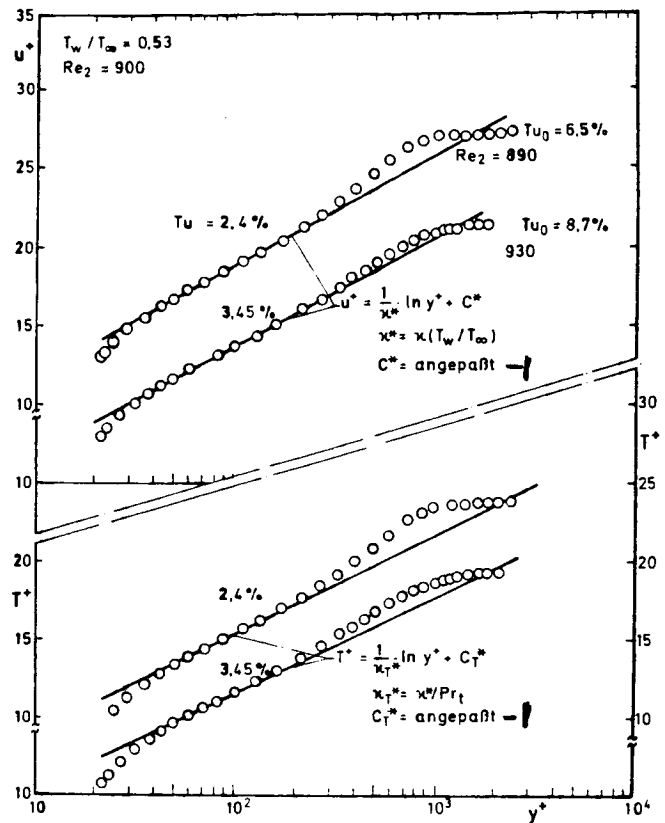


Illustration 5.38

1 - adjusted

Illustrations 5.37 and 5.38: Velocity and Temperature Profiles under the Influence of Free Stream Turbulence ($T_w/T_\infty = 0.8$ and 0.53)

ORIGINAL PAGE IS OF POOR QUALITY

The form parameters for boundary layers of negligible free stream turbulence, which were not available in my tests, were taken from the data by Murlis [33]. Illustration 5.39 confirms a distinct decrease of the form parameter with increasing free stream turbulence, which - for the most part - is in agreement with the matrix determined for isothermal flows by Green [51]. The decrease of the form parameter can be attributed to fuller velocity profiles. Starting with approximately 4%, the form parameters in Illustration 5.39 - similar to the behavior described by Robertson and Holt [50] - strive toward a boundary value. When this phenomenon occurs, the wake portion has achieved its final condition which is marked by complete disappearance (see Illustrations 5.37a and 5.38a). Because the tests show no systematic differences for cases with and without wall cooling, wall cooling generally has no additional influence on the transformation of the boundary layer profiles caused by turbulence intensity in the free flow.

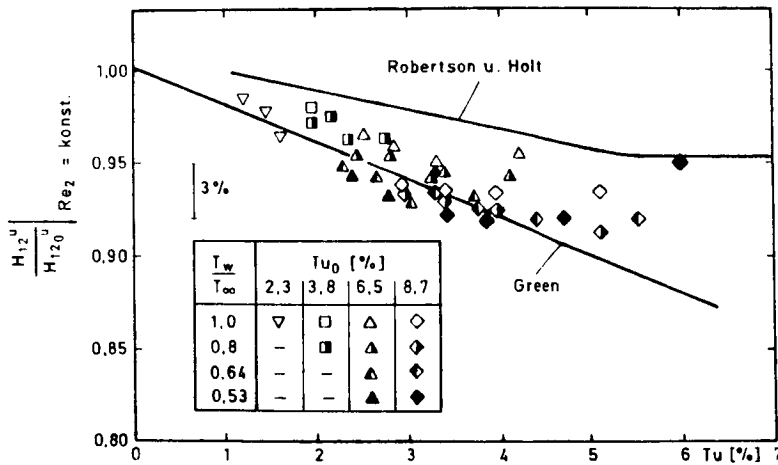


Illustration 5.39: Form Parameter H_{12}^u as a Function of Local Free Stream Turbulence

Tangential Stress Coefficients and Reynolds Analogy:

As already known, free stream turbulence increases the impulse exchange within the boundary layer. This results in higher velocity gradients at the wall and, therefore, higher wall tangential stresses. A quantitative illustration of the measured tangential stress increase is contained in Illustration 5.40a and Illustration 5.40b. For a basic explanation of these circumstances, these illustrations compare the resistance coefficients of boundary layers with identical impulse loss thickness Reynolds numbers with and without external turbulence. The values for turbulence-free external flow, which are required for this comparison, were calculated on the basis of an analytical relationship (equation 5.1 or 5.9) for incompressible boundary layers.

$$c_{f_0} = 0,024 \cdot Re_2^{-0,25} \quad (5.9)$$

Equation (5.9) was used because of its excellent agreement with the test results for turbulence-free external flows by Murlis, Wieghard (see [33]) and Coles [115] (max. deviation 2%).

The influence of the wall cooling, which increases the tangential stress, on the resistance coefficient in turbulence-free flows was considered with the temperature correction function achieved in Chapter 5.5.1.2 (equation 5.4):

$$\frac{c_{f_0}'}{c_{f_0}} = \left(\frac{2}{1 + T_w/T_\infty} \right)^{0,58} \quad (5.10)$$

Illustration 5.40a shows the resulting values c_f/c_{f_0} for all local turbulence intensities and temperature ratios. The illustration shows that an increase of the tangential stress coefficient, which is a function of the turbulence intensity, exists. This increase can satisfactorily be illustrated with a relationship by Simonich and Bradshaw [54], which can be applied to our case of flows with high wall cooling. The relationship states that, when the free stream turbulence is increased by 1%, the wall tangential stress increases by approximately 2%. This statement plus the fact that no

distinct additional influences caused by wall cooling can be observed (see Illustration 5.40) is of great significance to the development of boundary layer calculation procedures and to the practical application for gas turbine blades.

Because our tests were based on turbine-relevant boundary layer flows with low impulse loss thickness Reynolds numbers of $Re_e = 330 - 2,000$ (see Illustration 5.27), there are Reynolds number influences, which superimpose themselves to the effect of external turbulence with an opposing sign. In order to demonstrate this, an application procedure was selected in Illustration 5.40b, as proposed by Blair [36], which considered the Reynolds number as an additional parameter. In this application, the measurements show - as a consequence of the corrected Reynolds number influences and, therefore, a confirmation of the existence of Reynolds number influences - lesser fluctuations and a clear dependency on the turbulence intensity. The balancing line in the illustration describes the combined influence of Reynolds number and free stream turbulence as it was obtained with the tests for the given Reynolds number and turbulence intensity areas. The reference relationship for the balancing curve (Illustration 5.40b) points out that Reynolds number effects counter-act the influence of free stream turbulence below $Re_2 = 1,000$. (109

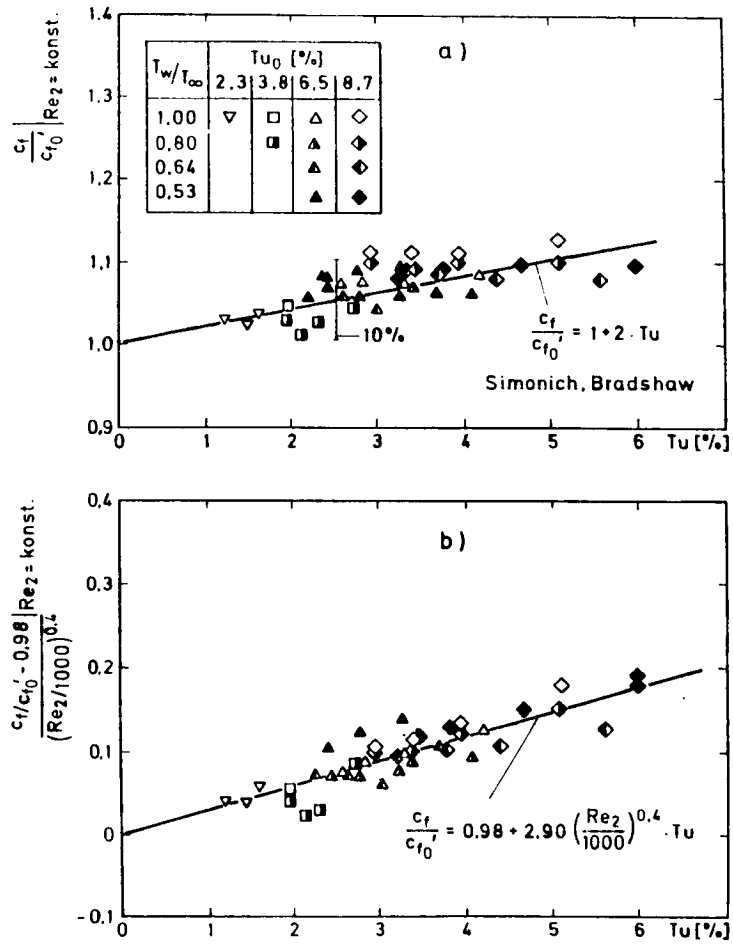


Illustration 5.40: Dependency of Turbulent Tangential Stress Coefficients on Local Free Stream Turbulence Tu when Considering the Impulse Loss Thickness Reynolds Number Re_2 ($Re_2 = 330 - 2,000$)

In accordance with recent findings, increases of the wall tangential stress as a function of turbulence intensity also depend on the eddy structure of the free stream turbulence. According to statements by Bradshaw and Hancock [55, 59], turbulence influences are highest, when the longitudinal measurements

$$L_e^u = - \frac{\overline{u'^2}^{3/2}}{u_\infty \cdot \frac{du'^2}{dx}} \quad (5.11)$$

which are formed by the longitudinal component of the free stream turbulence have the same size as the reference boundary layer thickness. As shown in Illustration 5.41, this applies for a large portion of our tests. In addition, however, there are distinctly greater longitudinal measurements which, due to the smaller boundary layer thicknesses, can always be found in those measuring surfaces which are closest to where the boundary layer is formed.

In order to understand the influence of free stream turbulence longitudinal measurements, Hancock [56] (see [55, 59]) - in comprehensive tests and comparisons with literature - developed a correlation which describes the tangential stress increases as a function of turbulence intensity and the ratio L_e^u/δ . It considered the fact that, with large longitudinal measurement ratios L_e^u/δ , the tangential stress increase is suppressed. It further considered that, with very low turbulence intensities below 1%, the tangential stress - according to tests by Meier and Kreplin [58] - the tangential stress no longer increases in a linear manner but squarely with the free stream turbulence. As an expansion of this study, Blair [39] developed an empirically deduced supplement, with which Hancock's correlation can also be applied to flows with additional Reynolds number influences. Illustration 5.42 compares this modified correlation to my own measurements. The correlation and the surrounding hatched range, which encompasses all test data of other authors (see [39]), represent the parameters for this comparison. In Illustration 5.42, my own test data are in good agreement with the total picture of available results; they also confirm Hancock's correlation.

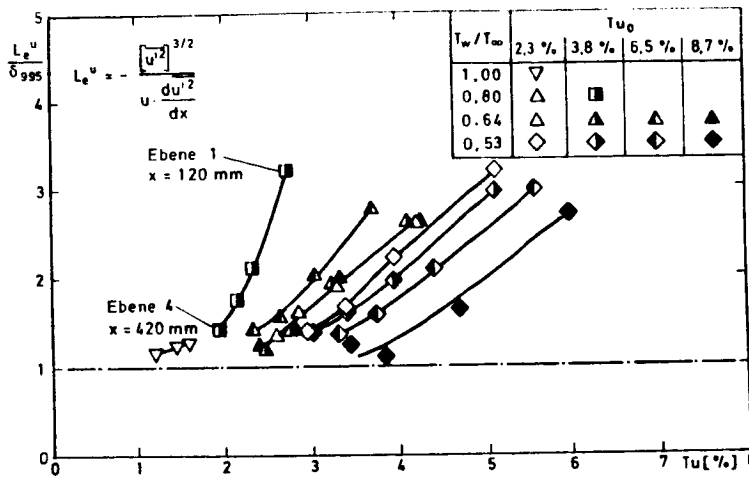
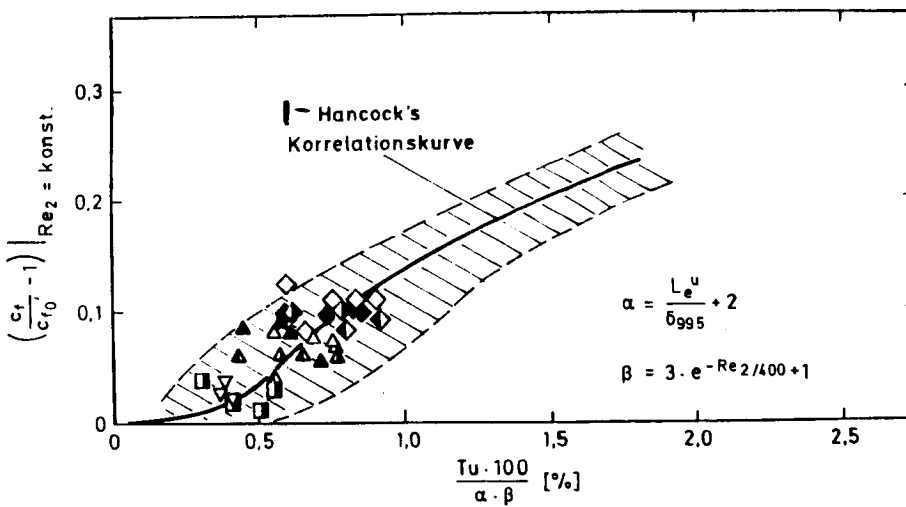


Illustration 5.41: Longitudinal Measurements of the Free Stream Turbulence



1 -

Hancock's Correlation Curve

Illustration 5.42: Tangential Stress Increase with Free Stream Turbulence when Considering Reynolds Number and Longitudinal Measurement Influences (see Illustrations 5.40 and 5.41 for Symbols)

However, the good agreement in this study was achieved by using the Reynolds number correction. Without consideration of the correction (112 term ϵ (see Illustration 5.42), the measuring points had distinctly greater abscissa values which made for a bad agreement. This showed that, when very low Reynolds numbers ($Re_2 = 330-2,000$) were used, the boundary layer related Reynolds number influences outweigh the longitudinal measurement influences ($L_e^4/\delta = 1.1 - 3.0$) of the free stream influence.

A determination had to be made of how turbulence intensities, identified from comprehensive studies of the friction coefficient, can be applied to heat transfer. To do this, the connection between heat and impulse exchanges was examined with the aid of measured analogy factors. The analogy factors $2 \times St/c_f$, which were obtained from the measured Stanton numbers and the tangential stress coefficients, are shown in Illustration 5.42. The results evenly fluctuate around the mean value $2 \times St/c_f = 1.1$. The analogy factor is independent of external turbulence and is not influenced by wall cooling. Consequently, wall tangential stress and heat transfer are increased by free stream turbulence. The Reynolds number and longitudinal measurement influences observed for tangential stress coefficients are also present in the heat transfer.

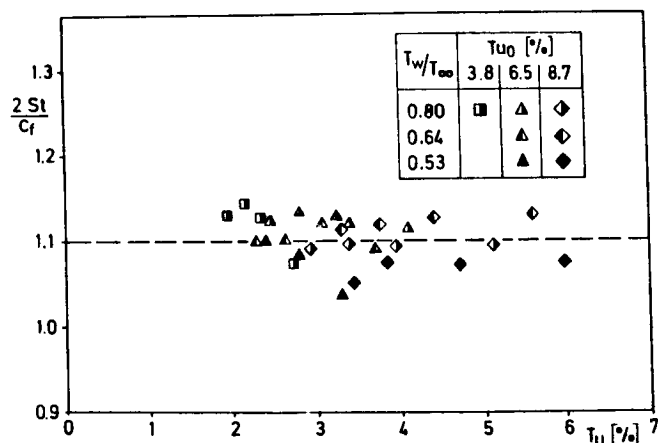


Illustration 5.43: Analogy Factors with Varying Wall Cooling and Free Stream Turbulence

The answer to the original question whether wall cooling alters turbulence intensity influences can be summarized as follows: No additional effects on the wall cooling were observed in analyses on the influence of free stream turbulence on the reversal, wall tangential stress and heat transfer. Turbulence intensity effects and material value influences caused by wall cooling are thus not connected. They can therefore be studied independently or they can be combined by a simple superimposition for a total effect. This is confirmed by Eriksen et al [79, 80] and Cheng et al [84] by direct turbine tests in boundary layers with very low or negligible free stream turbulence. These tests showed that, in turbulent boundary layers with highly varying material values, the turbulence structure is the same as in the isothermal case. Therefore, the influence of wall cooling can be regarded separately.

5.5.3 Influences of Negative Pressure Gradients

In gas turbines, the influences of external turbulence and wall cooling are superimposed by high pressure gradient effects, which play an important role in the development of heat transfer and the boundary layer along the blade surface. Only very few experimental studies on the influence of pressure gradients on transitional boundary layers with external turbulence have been conducted. These studies were only made for low acceleration intensities ($k < 1.0 \times 10^{-6}$) (see reference list, Chapter 2.2). The goal of my studies was to analyze flows with free stream acceleration as close to realistic turbine conditions as possible. The extraordinarily high increases of laminar heat transfer (see e.g. Krisnamoorthy [99]) observed in blade tests led to the conclusion that there are effects, which are yet unclear and which occur, when very highly accelerated boundary layers are admitted.

My analysis is made exclusively as a result of measured heat transfer distributions. Due to the very high accelerations, the boundary layer estimates made in design calculations resulted in very thin boundary layer thicknesses. Therefore, using probes for boundary layer measurements was considered impractical.

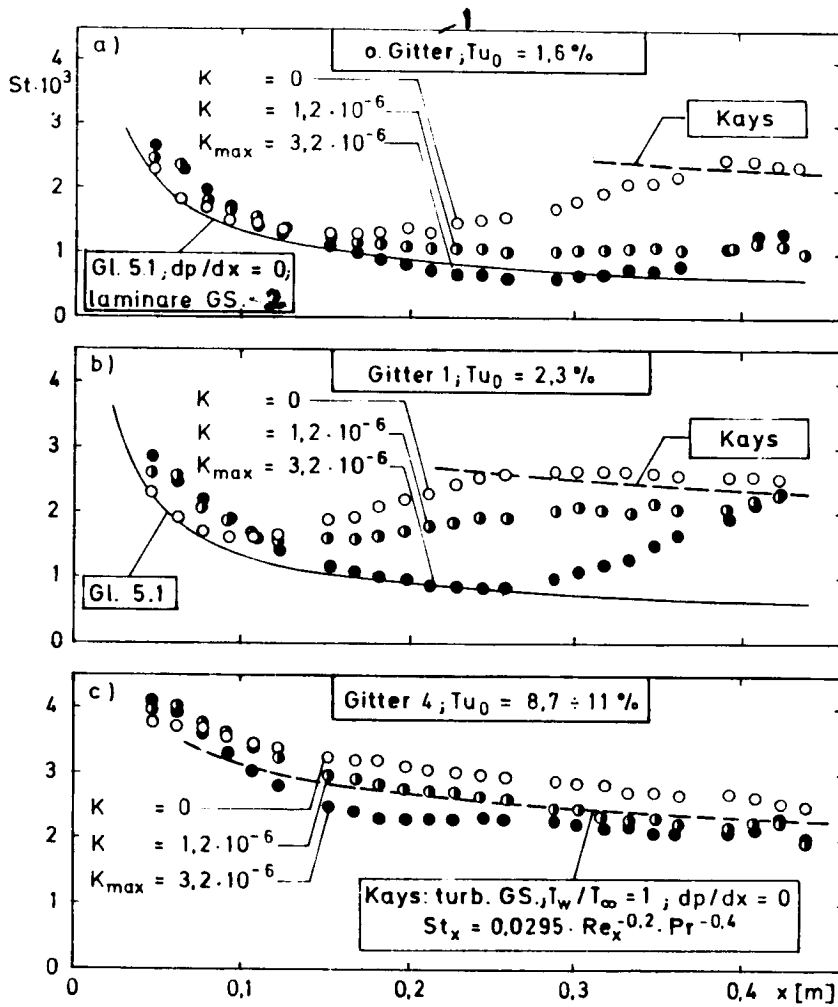
In order to be able to demonstrate the basic influences of highly negative pressure gradients in transitional boundary layers, I conducted comparative tests with and without free stream acceleration. The comparison was made with identical inlet conditions at the leading edge of the plate and acceleration events with varying intensity along the test plate.

Illustration 5.44 shows situations measured with a constant inlet Reynolds number ($Re_{Lo} = 6.4 \times 10^5$) and intensive wall cooling ($T_w/T_\infty = 0.64$). The Stanton numbers applied as a factor of the plate's running length were formed with local free stream velocity and the local free stream material values. The lower acceleration occurred with contour 1 and an acceleration parameter along the plate which was almost constant ($k = 1.2 \times 10^{-6}$). The intensive acceleration with $k_{max} = 3.2 \times 10^{-6}$ was realized by using contour 2 (Illustration 5.45). In contour 2, flow conditions on the vacuum side of gas turbine blades are simulated. The contour generates an alternating velocity matrix; the acceleration in the forward portion of the plate greatly increases and then experiences a slight retardation (Illustration 5.45).

The heat transfer coefficients applied in Illustrations 5.44a and 5.44b represent the test results with very low free stream turbulence ($Tu_o = 1.6\%$ and 2.3%). They describe flow events with a highly transitional character which, under the influence of negative pressure gradients, show varying reversal behavior. As clearly shown in Illustration 5.44b, the low acceleration ($k = 1.2 \times 10^{-6}$) - in contrast to the unaccelerated situation ($k = 0$) - results in an extension of the reversal area with an almost unchanged reversal initiation point. The higher acceleration, with $k_{max} = 3.2 \times 10^{-6}$, shows a later reversal initiation with the minimum Stanton number further down-stream. The reversal delay and the expansion of the reversal area can be attributed to the known effect of negative pressure gradients, which stabilizes the boundary layer. This results in fuller boundary layer profiles and steeper wall gradients (see Chapter 2.2). In accordance with classical reversal theory

(stability theory), the higher velocity gradients at the wall are mainly responsible for the greater stability of the laminar boundary layer (see Schlichting [22]).

(115)



1 - grid; 2 - laminar boundary layer

Illustration 5.44: Pressure Gradient Influences with Identical Plate Flow Reynolds Number ($Re_{L,0} = 6.4 \times 10^5$) and Varying Free Stream Turbulence

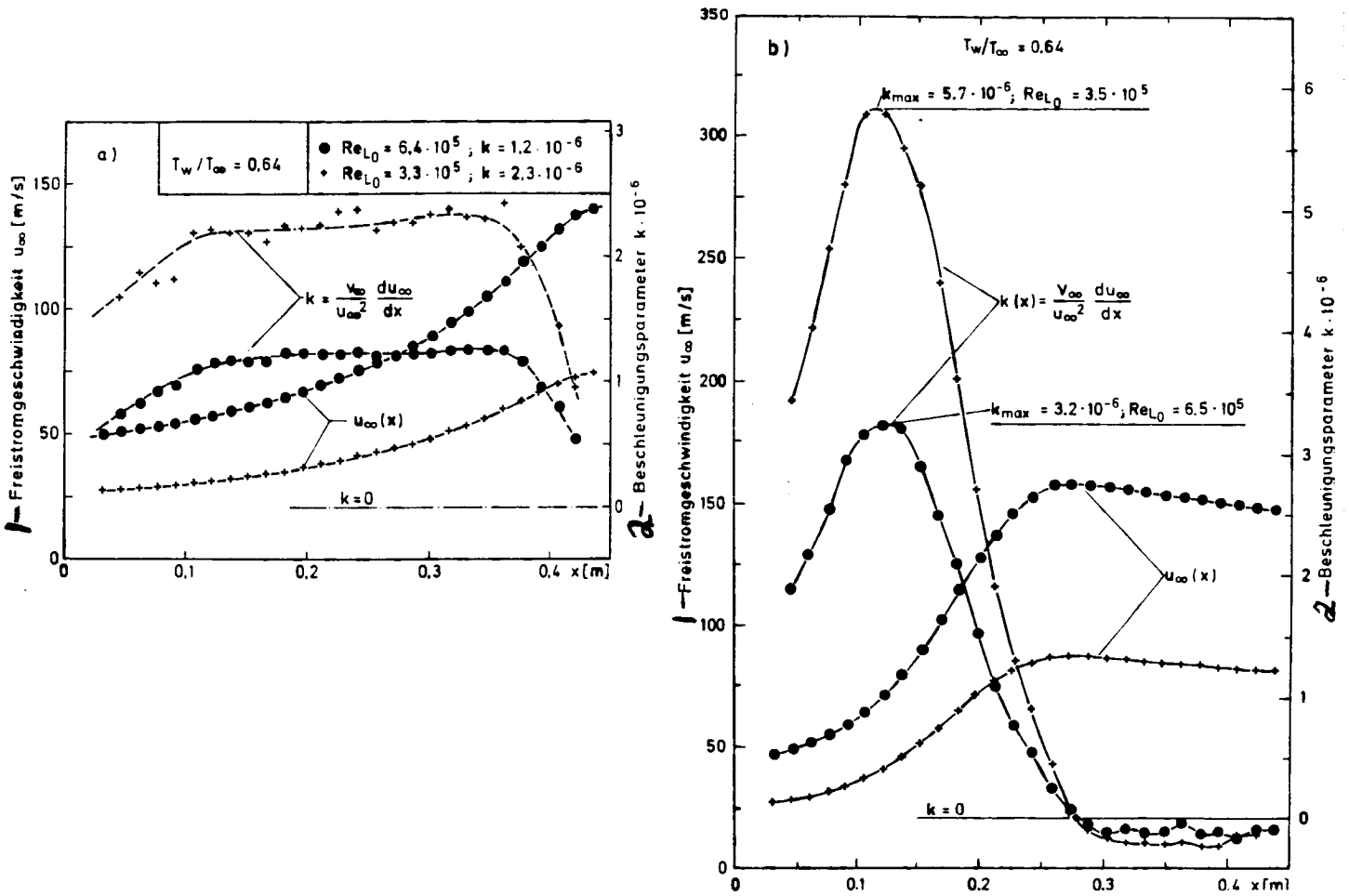
In addition to the changed reversal behavior, there are - in the forward portion of the plate - distinct increases of the laminar heat transfer coefficients (Illustration 5.44a and b), which can also be attributed to the influence of free stream acceleration. Its cause can be explained by steeper profile gradients at the wall which occur in accelerated flows. In comparison to test values without pressure gradients, these increases are approximately 20-30% near the leading edge of the plate in the laminar heat transfer. However, they decrease as the running length increases. The decay behavior of the Stanton number with pressure gradients is slower and more viscous than in unaccelerated situations. The reason for this effect is also due to increased stability of accelerated laminar boundary layers.

Illustration 5.44c rounds out the basic study on the influence of negative pressure gradients. In contrast to the above examples, flows with very high external turbulence are analyzed. The high turbulence intensities generated with grid 4 show no stabilizing effects on the reversal caused by the pressure gradients. In all cases, the reversal occurred immediately behind the leading edge of the plate. Due to intense free stream turbulence, there is no re-laminization tendency, even with high acceleration of $k_{\max} = 3.2 \times 10^{-6}$. Therefore, Illustration 5.44c describes only the turbulent heat transfer. These tests show that, with increasing free stream acceleration, there is a decrease of the local turbulent Stanton number. Similar pressure gradient effects were identified by Kays and Moffat [86] in turbulent boundary layers without external turbulence. Therefore, the results confirm that, even with maximum external turbulence, acceleration causes an attenuation of the turbulent exchange events in the boundary layer (especially near the wall), which results in a decrease of local heat transfer coefficients. If the description of turbulent exchange events in the boundary layer is made with mixing method equations (see integral procedures, Chapter 6), these changes are theoretically recorded in the boundary layer turbulence with increased van Driest wall attenuation constants.

(116

With a detailed comparison of measured heat transfer distributions both with and without pressure gradients it can be demonstrated that pressure gradient influences generate significant changes in the reversal behavior and in laminar and turbulent heat transfer. They are therefore very important for the computation of accelerated blade boundary layers. The causes can be attributed to dampening effects of negative pressure gradients on boundary stability and boundary layer turbulence, as they are described in classic boundary layer theory and as demonstrated in previous experimental studies with low free stream acceleration. Based on this, a study is made in the following chapters on how these effects are dependent on the respective flow conditions (inlet Reynolds number, free stream turbulence). I will also show additional effects if very high acceleration intensities, as they occur in gas turbines, are applied to a boundary layer with high free stream turbulence.

ORIGINAL PAGE IS
OF POOR QUALITY



- 1 - free stream velocity
- 2 - acceleration parameters

Illustration 5.45: Free Stream Velocity and Acceleration Parameters with Varying Inlet Reynolds Number and $T_w/T_\infty = 0.64$

Illustration 5.45a) for contour 1 "contour on the pressure side"

Illustration 5.45b) for contour 2 "contour on the vacuum side"

In gas turbines, Reynolds number effects always occur when operating conditions are changed. They are therefore of great significance to the turbine's operation.

The acceleration parameter k is inversely proportional to the Reynolds number

$$k \approx 1/Re$$

An increased Reynolds number will, therefore, result in increased acceleration values. This is shown by Illustration 5.45a for the tests with contour 1, and by Illustration 5.45b for the tests with contour 2. When the flow Reynolds number decrease from $Re_{Lo} = 6.4 \times 10^5$ to $Re_{Lo} = 3.3$ or 3.5×10^5 , the k -values of contour 1 increase from 1.2×10^{-6} to 2.3×10^{-6} , and the k_{max} -values for contour 2 from 3.2×10^{-6} to 5.7×10^{-6} . The flow with $k_{max} = 5.7 \times 10^{-6}$ shows those acceleration intensities, which are representative for realistic blade flows. Events in the heat transfer and boundary layer behavior caused by Reynolds number changes are shown for the flow with contour 1 in Illustration 5.46 and for the flow with contour 2 in Illustration 5.47.

Tests conducted with contour 1 with varying plate flow Reynolds numbers and varying free stream turbulence are based on low (Illustration 5.46a) and medium (Illustration 5.46b) acceleration intensities with $k = 1.2 \times 10^{-6}$ and $k = 2.3 \times 10^{-6}$. A special characteristic of these flows is that there are acceleration parameters (see Illustration 5.45, sink-flow) which are almost constant in the test section. As expected, the increase of the pressure gradient parameter k , which is caused by the decreased Reynolds number, results in an increasing boundary layer stability. With unchanged flow turbulence, this boundary layer stability results in an additional down-stream re-location of the reversal. It may, as shown in situations with low free stream velocity ($Tu_o = 1.6\%$ and 2.3%), even suppress the reversal completely. The absolute

level of laminar and turbulent Stanton numbers will also be changed. With lower Reynolds numbers (Illustration 5.46b), the heat transfer coefficients - in the laminar case (see $Tu_0 = 1.6\%$) - may be up to 30% higher. In turbulent boundary layer sections, however, there is a comparatively low increase of approximately 5%. We already know about lower Reynolds number dependency of turbulent heat transfer in unaccelerated flow situations: In unaccelerated laminar boundary layers the local Stanton number is proportional to $Re_x^{-0.5}$. In turbulent boundary layers without pressure gradient, there is only a dependency on $Re_x^{-0.2}$ (see my test results in Illustrations 5.15 - 5.17, Chapter 5.4).

(119)

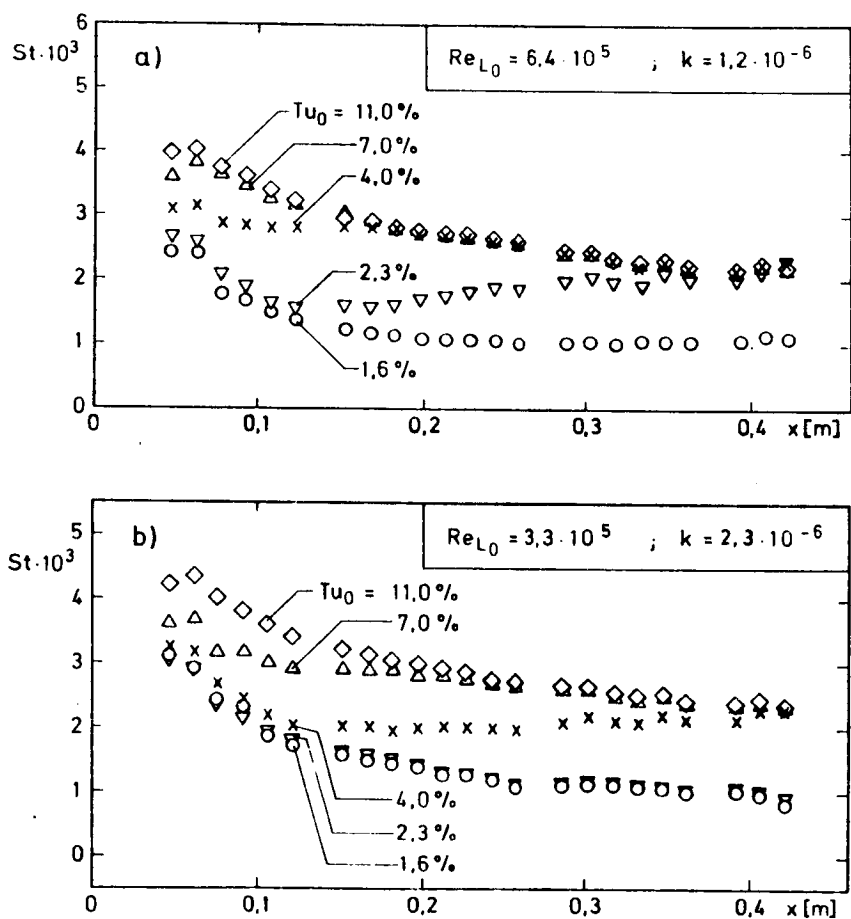


Illustration 5.46: Reynolds Number Influences with Low Acceleration and Varying Free Stream Turbulence (Contour 1)

In flows with pressure gradients (Illustration 5.46), this difference is emphasized by the following: In accordance with Illustration 5.44, the increase of the pressure gradient parameter $k(x)$, which is a function of the decreasing Reynolds number, results - in laminar boundary layers - in an additional increase and - in turbulent boundary layer sections - in an additional decrease of the Stanton numbers. (120

For both Reynolds numbers, the heat transfer distributions shown in Illustration 5.46 give no indication of noticeable dependencies of the turbulent heat transfer on free stream turbulence. Additionally, it was determined that, due to the thin leading edge of the plate and despite acceleration with high flow turbulence, the reversal occurs in the area of the uncooled leading edge (see Chapter 5.5). These observations are in complete agreement with the results obtained in unaccelerated boundary layers with a local application of the Stanton number (see Illustrations 5.15 - 5.17). However, events in the laminar boundary layer sections during acceleration in contrast to the tests without pressure gradients. Illustration 5.46 ($x < 0.12$ m) shows increases of the laminar heat transfer as a factor of turbulence intensity. This was observed in previous studies with lower pressure gradient intensities (see [35, 38] and Chapter 2.2.1). Increase rates are up to 15% if, as shown in Illustration 5.46b, the flow turbulence is increased from 1.6% to 4%. These turbulence intensity influences are greatly dependent on the relative strength of free flow acceleration and, therefore, on the respective flow Reynolds number. As shown by the measurements with $Tu_0 = 2.3\%$ in the forward section of the plate, turbulence intensity dependent increases of the heat transfer (compared to $Tu_0 = 1.6\%$) are almost completely suppressed by higher acceleration (Illustration 5.46b).

The increases of the laminar heat transfer, which are induced by external turbulence, exist only when negative pressure gradients are present. This effect was not observed in tests with constant external velocities. Without free stream acceleration, the required stabilization of the laminar boundary layer does not exist. Therefore, the disturbance caused by external turbulence results directly in a laminar-turbulent boundary layer reversal.

In order to provide a better classification of this new flow situation with free stream acceleration, I would like to refer to the studies by Junkhan and Serovy [35]. Junkhan and Serovy [35] measured similar pressure gradient effects with comparable increases of the laminar heat transfer in less accelerated boundary layers. The boundary layer tests conducted under these conditions show that fuller velocity profiles occur which, despite the influence of outer turbulence, maintain the typical boundary profile form described by Hartree [108]. Due to the comparable heat transfer increase (15%), this result can be applied to our tests. This means that, under the conditions described here, the laminar properties of the boundary layer continue to prevail despite the influence of free stream turbulence. Therefore, the flow can be assigned to laminar boundary layers.

(121

I have presented a detailed discussion of Reynolds number and turbulence intensity influences for simple flow forms with constant acceleration parameters and moderate pressure gradient intensities. The question now arises how the measured effects can be applied to the more complex flow conditions on the vacuum side of gas turbine blades. In contrast to the cases shown in Illustration 5.26, this flow is characterized by pressure gradient matrices with down-stream variations and by maximum acceleration intensities. In order to demonstrate the resulting additional effects, free stream velocity distributions were generated with contour 2 on the vacuum side (Illustration 5.45). In addition, an analysis was made of heat transfer distributions measured in a comparison with varying plate flow Reynolds numbers ($Re_{Lo} = 6.5 \times 10^5$ and $Re_{Lo} = 3.5 \times 10^5$). The

results are summarized and discussed in Illustration 5.47. Illustration 5.47b describes boundary layer flows which, due to their maximum acceleration intensities ($k_{\max} = 5.7 \times 10^{-6}$), are particularly relevant to turbines.

The comparison in Illustration 5.47 shows that, with a high Reynolds number (Illustration 5.47a), an increase of the flow turbulence from $Tu_0 = 2.3\%$ to $Tu_0 = 4\%$ will result in a noticeable relocation of reversal initiation toward the leading edge of the plate. With a lower Reynolds number (Illustration 5.47b), this is completely suppressed by the higher pressure gradient. In the entire acceleration distance ($x \leq 0.25$ m), all measurement points with less than 4% flow turbulence are in accordance with the matrix described in Illustration 5.46 with low turbulence intensity dependent increases and a laminar heat transfer. Only the high turbulence intensities of grids 3 and 4 ($Tu_0 = 7\%$ and 10%) - with the turbine pressure gradient conditions in Illustration 5.47b - result in a higher influence of free stream turbulence. Starting with the beginning of the plate, they effect a drastic increase of the local Stanton numbers (up to 100%). However, in their path along the plate, they continue to be similar to laminar heat transfer. The high turbulence intensities induce distinct disturbances in the boundary layer which cannot be attenuated despite maximum acceleration ($k_{\max} = 5.7 \times 10^{-6}$). In our tests, a balance was observed as result of the destabilizing effect of external turbulence and the stabilizing influence of acceleration. This balance causes large portions of the boundary layers to be in a stable, laminar-turbulent intermediate condition; it therefore has the typical properties for boundary layer reversal. The distribution of the Stanton numbers measured in Illustration 5.46a for 4% flow turbulence can also be regarded as confirmation of the potential occurrence of stable, laminar-turbulent intermediate conditions. In this flow situation, the measurement points are evenly distributed throughout the entire forward section of the plate ($x < 0.12$ m) in the center between laminar ($Tu_0 = 1.6\%$) and turbulent ($Tu_0 = 10\%$) heat transfer.

(122

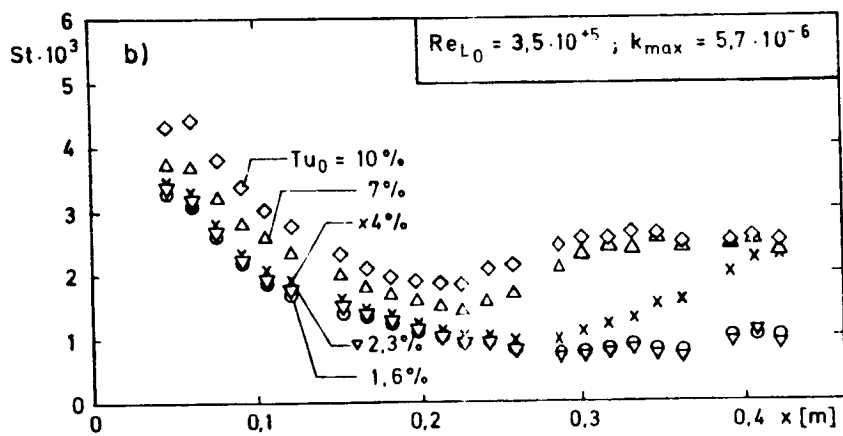
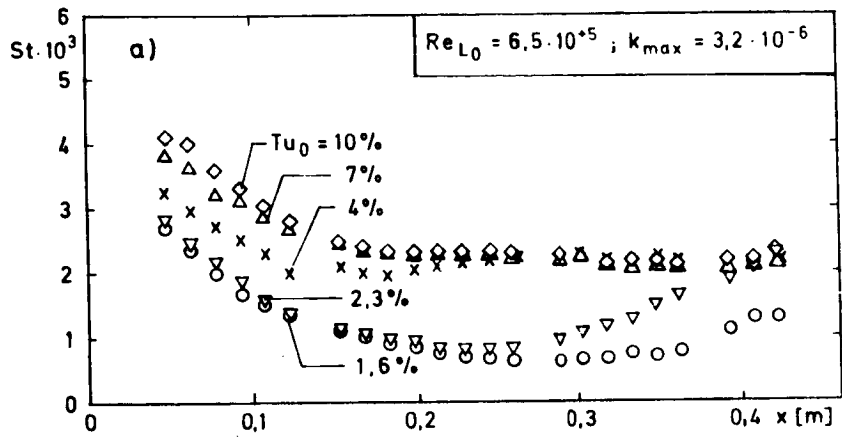


Illustration 5.47: Reynolds Number Influences with High Acceleration and Varying Free Stream Turbulence (Contour 2)

According to our experiences, this special behavior of the boundary layer, which was not observed in tests with constant acceleration (see Illustration 5.45), occurs when high turbulence intensities exist simultaneously with intensive acceleration. However, another

(123

factor for these stable, reversal-like boundary layer conditions is that, as with flows modelled on the vacuum side, the acceleration intensity increases with increasing running length (see Illustration 4.45b). This is the main reason why further excitation of the boundary layer turbulence is suppressed. This excitation, in an unaccelerated or constantly accelerated situation (Illustration 5.46), will result in a continuation of the reversal process.

A systematic comparison of tests with varying free stream temperature conditions has thus shown that, for the initiation of heat transfer on gas turbine blades, absolute turbulence and pressure gradient intensities are not the only factors to be considered. A significant role is also played by the acceleration matrix along the blade surface. Certain combinations of these influencing parameters may result in flow situations which will have to be re-classified. In these situations, the heat transfer can neither be identified as laminar nor as turbulent. In large sections, it will obtain a laminar-turbulent intermediate condition. This knowledge can be used to explain the extraordinarily high increases of local heat transfer, which were observed in blade tests with high free stream turbulence. Due to their similar matrix they have, so far, been interpreted as "increases of the laminar heat transfer" (see [99]). They are long, highly turbulent boundary layer events with a reversal character. They are a result of an interaction between free stream turbulence, highly negative pressure gradients and, especially, an acceleration matrix with a down-stream variation. Their reliable prediction is presently the main problem in the design of cooled gas turbine blades. The complexity of this flow event is not recorded with sufficient accuracy in the numeric computation procedures used for turbulence models.

5.5.3.3 Correlation Equations for Calculating Turbulent Heat Transfer in Accelerated Flow

(124)

Because correlations are the simplest and quickest method to calculate heat transfer, there is a desire to use them in as many flow situations as possible. The numerous tests in this study provide the opportunity to examine and further develop correlation equations for turbulent heat transfer with respect to their use in highly accelerated flows with high external turbulence. My studies are based on the previously described heat transfer distributions with varying acceleration and high free stream turbulence, which were measured with a temperature ratio of $T_w/T_\infty = 0.64$. As stated in my analysis of reversal events, intensive wall cooling has no additional influence on boundary layer behavior (see Chapter 5.5.2, Illustration 5.36). Its presence only increases the absolute heat transfer, so that this additional effect can be considered separately.

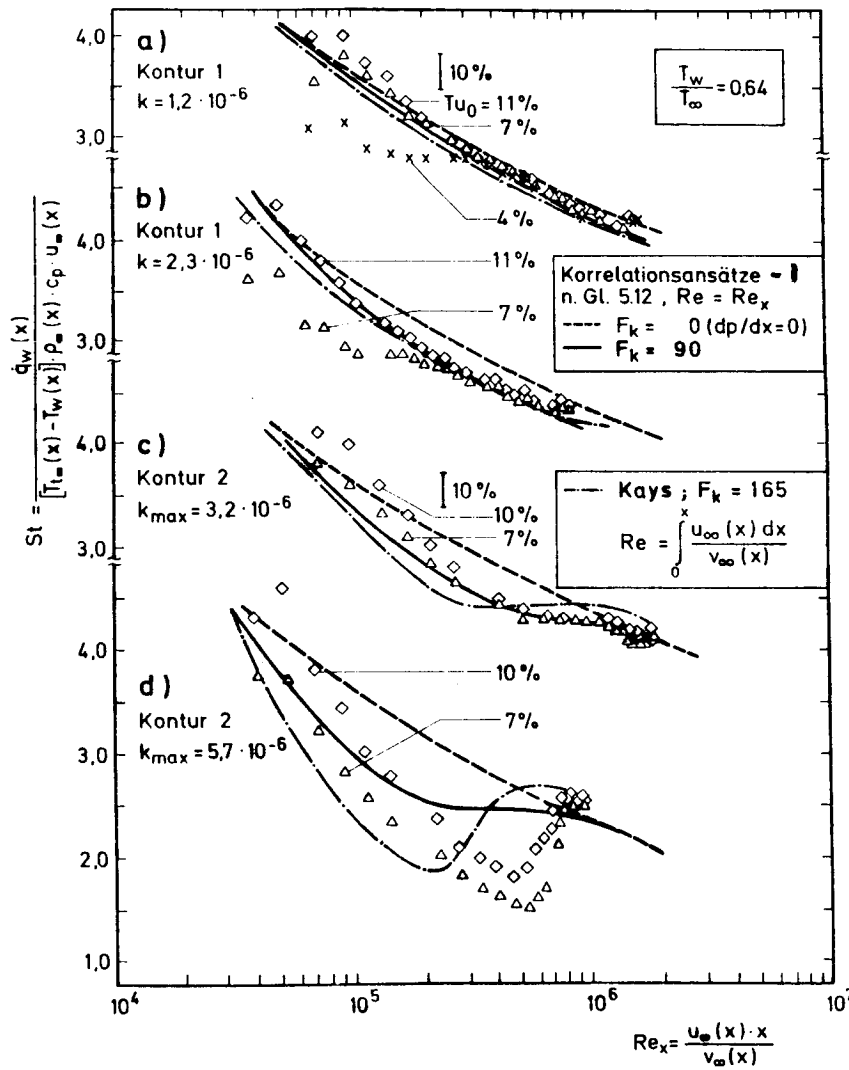
In Illustration 5.48, the measured heat transfer coefficients are again collated as a function of the local running length Reynolds number. Illustrations 5.48a and 5.48b provide comparison data for the tests conducted with contour 1 and acceleration values of up to $k = 2.3 \times 10^{-6}$. In the forward Reynolds number range, the Stanton numbers for $Tu_o = 4\%$ in Illustration 5.48a and for $Tu_o = 7\%$ in Illustration 5.48b represent portions of the reversal process. Illustrations 5.48c and 5.48d contain available comparison situations for medium and maximum acceleration intensities. They can be assigned to the tests with contour 2 ($k_{max} = 3.2 \times 10^{-6}$ and 5.7×10^{-6}). With these flows, acceleration of the boundary layer is replaced by a subsequent delay, starting with $Re_x \approx 3-5 \times 10^5$.

To correlate the turbulent heat transfer coefficients, I used a relationship by Kays (see [66], p. 248). It was originally deduced from Moretti's [112] data for almost isothermal boundary layers without external turbulence. It describes the local Stanton number

as a function of the Prandtl number Pr , the running length Reynolds number Re , and the local pressure gradient parameter $k(x)$. This correlation, expanded by the additional influence of wall cooling, is as follows:

$$St = 0,0295 \cdot Pr^{-0,4} \cdot Re^{-0,2} \cdot \left(1 - F_k \cdot \frac{k(x)}{St}\right) \cdot F_T \quad (5.12)$$

(125)



ORIGINAL PAGE IS OF POOR QUALITY

1 - correlation equations in acc. with eq. 5.12

Illustration 5.48: The Use of Correlations for the Calculation of Heat Transfer in Accelerated Flows

The value F_k , which occurs in equation (5.12), represents the effect of the pressure gradients. F_T represents the temperature decrease at the wall. F_T is assigned the mean value 1.08 for test comparisons because, according to the heat transfer distributions without acceleration (Illustrations 5.15 - 5.17), the increase of local Stanton numbers with $T_w/T_\infty = 0.64$ must be approximately 6-10%.

Kays [66] specifies the Reynolds number in equation 5.12 by an integral reference value

$$Re = \int_0^x \frac{u_\infty dx}{\nu_\infty}$$

and assigns the value 165 to the pressure gradient factor F_k . Illustration 5.48 shows the resulting matrix of the Stanton numbers for all test situations (hatched line). As demonstrated by the comparisons with tests, the heat transfer is calculated in a satisfactory manner for situations with constant acceleration (Illustrations 5.48a and b). In the higher accelerations with contour 2 of Illustration 5.48c and, especially in Illustration 5.48d, greater deviations from the test values can be observed. In accordance with the statements made in the previous chapter (see Illustration 5.47b), measurements in Illustration 5.47d do not represent flow events in the forward Reynolds number range, but flow events which are similar to reversal in the boundary layer. With

this comparison, Kays' relationship for turbulent boundary layers predicts heat transfer coefficients which are too low. It therefore becomes obvious that the correlation considers the attenuation effects on boundary layer turbulence with very high acceleration as too large. The reason for this is the influence of free stream turbulence, which was not considered. External turbulence counteracts this attenuation process which results in a delayed re-laminization initiation.

The observed inaccuracies and the fact that an integration to determine the Reynolds number according to Kays [66] requires great effort were the reasons I sought a development which eliminates the calculation of the reference Reynolds number, and which accurately describes the turbulent heat transfer as a direct function of the local running length Reynolds number. This was achieved by an adjustment of the pressure gradient factor F_k , with unchanged use of the formula context of equation (5.12). As shown by Illustrations 5.48a-c, the results obtained are in very good agreement with the test data by introducing the constant value $F_k = 90$. With this procedure and the use of the local running length Reynolds numbers

(127

$$Re = Re_x = \frac{u_\infty(x) \cdot x}{\nu_\infty(x)}$$

equation (5.12), in Illustrations 5.48a-c, provides an accurate matrix and a very realistic absolute value for the turbulent heat transfer (max. deviation 6-10%). The remaining increases in the forward Reynolds number range can be explained with post-transitional effects, which are a result of the high up-stream increases of the laminar heat transfer caused by acceleration (see Illustration 5.44a and b).

In contrast to the procedure used by Kays [66], which requires a greater effort, this expansion of the correlation also improved calculation results. Illustration 5.48c clearly shows that, in high acceleration, the influence of free stream turbulence considered by adjusting F_k and the use of local Reynolds numbers results in more accurate reproductions of the measured heat transfer coefficients. It is further pointed out that these measures resulted in a much better agreement with the test data for the transitional flow situation with highest (turbine-relevant) pressure gradients (Illustration 5.48d) in the forward acceleration range ($Re_x < 3 \times 10^5$).

In order to re-confirm the practicability of explicitly considering pressure gradient influence in correlations, Illustrations 5.48a-d shows the heat transfer coefficients (hatched lines), which were obtained with equation (5.12) by neglecting the pressure gradient terms ($F_k = 0$). All Stanton numbers calculated with this simplification are too high and their matrix is not accurately described. A satisfactory agreement with test data exists only with the very weakly accelerated boundary layer with $k = 1.2 \times 10^{-6}$ (Illustration 5.48a). This no longer applies for flows with higher velocity gradients. In this case, the correlation which considers the pressure gradient as an additional factor is clearly more favorable (Illustrations 5.48b-d).

With this systematic study of pressure gradient influences plus the (128
examination and further development of correlations for computing turbulent heat transfer in accelerated flows with high external turbulence, my analysis of experimental results (see [123], [124]) is concluded. Essential new information achieved on the influence of free stream turbulence, wall cooling and pressure gradients was based on thorough tests. In order to provide a good overview of this subject, all test data and the results obtained were thoroughly documented. This thoroughness fulfilled an important prerequisite for the examination and further development of complicated boundary layer calculation methods (integral and differential procedures).

My goal in the following chapters of this dissertation was to develop an integral procedure based on these experimental results, and to use it as an alternative to differential methods for an accurate, flexible computation of heat transfer in cooled gas turbine blades.

6. DEVELOPMENT OF AN INTEGRAL PROCEDURE TO COMPUTE TWO-
DIMENSIONAL BOUNDARY LAYERS WITH REVERSAL, HEAT TRANSFER,
PRESSURE GRADIENTS AND FREE STREAM TURBULENCE

(129)

6.1 Procedure Selection

The complexity of experimental flow events under the influence of free stream turbulence, wall cooling and pressure gradients requires highly flexible calculation procedures. These properties are contained in field methods, which provide a numerical solution for differential conservation equations in connection with a turbulence model (see [3]). This evidence has not yet been established for integral procedures. So far, these procedures failed due to the description of the long reversal events and due to the separate calculation of velocity and temperature boundary layers. According to previous studies (see Chapter 2.2) and my own determinations, these two properties are an important factor in a calculation program, which is to predict the blade heat transfer in extremely accelerated boundary layers.

In this dissertation I will show for the first time that the basic prerequisites for calculating transitional boundary layers in gas turbine blades can also be applied to integral procedures. I will also demonstrate that these integral procedures, just like differential procedures, are suitable for an accurate description of flows in blade boundary layers with high free stream turbulence, intense wall cooling and maximum pressure gradients.

The starting point for this calculation model are known conservation equations for impulse and kinetic energy used to determine the flow boundary layer. Two additional integral conservation equations were developed for the separate calculation of the temperature boundary layer and heat transfer. In analogy to the impulse and kinetic energy equations, they describe the enthalpy exchange in the boundary layer. In order to complete the equation system, I used a clearly arranged 1-equation turbulence model, which requires little

effort and which was tested on numerous occasions in connection with differential methods (see [4, 35, 47]). The model can be incorporated in the calculation algorithm, because it performs the integration of the balance of turbulence exchange events in the boundary layer. Turbulent shear stress distributions were computed with the aid of a mixing method hypothesis.

With integral procedures, formulations for the velocity and temperature profiles in the boundary layer must be specified for a (130 solution of the conservation equations. They form implicit definitive equations for wall tangential stress and the heat transfer at the wall. For this calculation, universal profile formulations were made for laminar, reversing and turbulent boundary layers. They can be used even in the most extreme acceleration situations found in turbines. When compared to field methods, the availability of these boundary layer matrices is the only flexibility restriction with these newly developed integral procedures.

The boundary layer in the reversal is modelled as a function of the boundary layer intermittance matrix. Profile formulations as well as the intensity of the boundary layer turbulence are determined by the respective value of the intermittance factor.

The description of the calculation procedure begins with the derivation of integral conservation equations for velocity and temperature. I will then introduce the profile formulations and the turbulence model. On this basis, I will model the boundary layer reversal.

6.2 Basic Equations

The theoretical description of boundary layers is based on the differential conservation equations for mass, impulse and energy. Using the prerequisite of a two-dimensional, stationary flow - which applies to blade circulation - we obtained the following parabolic differential equation system:

continuity equation:

$$\frac{\partial(\rho \cdot u)}{\partial x} + \frac{\partial(\rho \cdot v)}{\partial y} = 0 \quad (6.1)$$

impulse equation:

$$\rho \cdot u \cdot \frac{\partial u}{\partial x} + \rho \cdot v \cdot \frac{\partial u}{\partial y} = \frac{\partial \tau}{\partial y} - \frac{dp}{dx} \quad (6.2)$$

energy equation:

$$\rho u \cdot \frac{\partial h_0}{\partial x} + \rho \cdot v \cdot \frac{\partial h_0}{\partial y} = \frac{\partial}{\partial y} (\dot{q} - u \cdot \tau) \quad (6.3)$$

The variables in the conservation equations, like the velocities u and v , the fluid density ρ and the total enthalpy h_0 , represent chronological mean values. The diffusion terms on the right side of the balance equation are mainly determined by the tangential stress τ , the pressure gradient dp/dx (which is constant throughout the boundary layer) and the local heat flow distribution \dot{q} . (131)

The required integral conditions for flow and temperature boundary layers and the prerequisite parameters can be totally derived from these basic equations. The impulse and energy equations (equations 6.2 and 6.3) are multiplied by "weighted functions". They are then integrated through the wall distance and replaced by two common differential equations of the first degree. A large amount of literature (e.g. [20, 67]) is available for obtaining integral equations in this manner for the computation of the flow boundary layer. Referred to as impulse and kinetic energy equations, they are assigned to the "dissipation" integral procedure and are expressed as follows:

impulse equation:

$$\frac{d\delta_2}{dx} + \delta_2 \cdot (2 + H_{12} - Ma^2) \cdot \frac{1}{u_\delta} \cdot \frac{du_\delta}{dx} = \frac{\tau_w}{\rho_\delta \cdot u_\delta^2} = \frac{c_f}{2} \quad (6.4)$$

kinetic energy equation:

ORIGINAL COPY OF
OF POOR QUALITY

$$\frac{d\delta_3}{dx} + \delta_3 \cdot (3 + 2 \cdot H_{43} - Ma^2) \cdot \frac{1}{u_\delta} \cdot \frac{du_\delta}{dx} = \frac{2}{\rho_\delta u_\delta^3} \int_0^\delta \tau \cdot \frac{du}{dy} dy = c_D \quad (6.5)$$

The respective definitions for integral boundary layer values and form parameters are as follows:

$$\begin{aligned} \delta_1 &= \int_0^\delta \left(1 - \frac{\rho \cdot u}{\rho_\delta \cdot u_\delta}\right) dy ; & \delta_2 &= \int_0^\delta \frac{\rho \cdot u}{\rho_\delta \cdot u_\delta} \cdot \left(1 - \frac{u}{u_\delta}\right) dy \\ \delta_3 &= \int_0^\delta \frac{\rho \cdot u}{\rho_\delta \cdot u_\delta} \left[1 - \left(\frac{u}{u_\delta}\right)^2\right] dy ; & \delta_4 &= \int_0^\delta \frac{\rho \cdot u}{\rho_\delta \cdot u_\delta} \cdot \left(\frac{\rho_\delta}{\rho} - 1\right) dy \end{aligned} \quad (6.6)$$

$$H_{12} = \frac{\delta_1}{\delta_2} ; \quad H_{32} = \frac{\delta_3}{\delta_2} ; \quad H_{43} = \frac{\delta_4}{\delta_3}$$

The integral relationships required for describing the temperature boundary layer can be obtained with the basic equations in a similar manner. In accordance with a proposal made by Patankar and Spalding [123], the energy equation (6.3) is expanded with the weight functions $(h_\delta - h_{0\infty})^n$ ($n = 0; 1$). After eliminating the diagonal velocity v , it is partially integrated with equation (6.1) over the wall distance. This results in two enthalpy equations, which are in accordance with the flow equations (6.4) and (6.5): (132)

enthalpy equation 1:

$$\frac{d\delta_5}{dx} + \delta_5 \cdot \frac{1}{u_\delta} \cdot \frac{du_\delta}{dx} = \frac{\dot{q}_w}{\rho_\infty \cdot u_\delta (h_w - h_{0\infty})} = St \quad (6.7)$$

enthalpy equation 2:

$$\frac{d\delta_6}{dx} + \delta_6 \cdot \frac{1}{u_\delta} \cdot \frac{du_\delta}{dx} = 2 \cdot St + 2 \cdot c_{DH} \quad (6.8)$$

with

$$\delta_5 = \int_0^{\delta_t} \frac{\rho \cdot u}{\rho_\infty \cdot u_\delta} \left(\frac{h_0 - h_{0\infty}}{h_w - h_{0\infty}} \right) dy ; \quad c_{DH} = \int_0^{\delta_t} \frac{\dot{q}(\dot{q} - u \cdot \tau) \cdot \frac{\partial h_0}{\partial y}}{\rho_\infty u_\delta (h_w - h_{0\infty})^2} dy \quad (6.9)$$

$$\delta_6 = \int_0^{\delta_t} \frac{\rho \cdot u}{\rho_\infty \cdot u_\delta} \left(\frac{h_0 - h_{0\infty}}{h_w - h_{0\infty}} \right)^2 dy \quad H_{6,5} = \frac{\delta_6}{\delta_5}$$

The turbulent exchange events are only considered in the dissipation terms c_D and c_{DH} on the right side of the balance equations (6.5 and 6.8). In addition to the molecular transport, the tangential stress τ and the heat flow \dot{q} contain the transport components caused by the turbulent fluctuation movements. They are as follows:

$$\tau = \mu \cdot \frac{du}{dy} - \overline{\rho u'v'} = (\mu + \mu_t) \cdot \frac{du}{dy} \quad (6.10)$$

$$\dot{q} = \lambda \cdot \frac{dT}{dy} - \rho c_p \overline{T'v'} = (\lambda + \lambda_t) \cdot \frac{dT}{dy} \quad (6.11)$$

The turbulent components are expressed by the cross-correlation terms $-\overline{\rho u'v'}$ and $-\rho c_p \overline{T'v'}$. They occur as an additional unknown quantity of the equation system. In analogy to laminar transport, they are replaced by the introduction of a turbulent viscosity μ_t and a turbulent heat conductivity λ_t . A connection between the two values is made by determining the turbulent Prandtl number

$$Pr_t = \frac{\mu_t \cdot c_p}{\lambda_t} \quad (6.12)$$

which describes the relationship between the turbulent impulse and heat exchanges. When the turbulent Prandtl number is known - which can be replaced with $Pr_t \approx 0.9 = \text{const.}$ for all boundary layers flows - the determination of turbulent exchange events is reduced to the description of $\overline{u'v'}$ or the apparent viscosity μ_t . In our procedure, this is accomplished with the aid of a 1-equation turbulence model (see Chapter 6.4).

(133)

In addition, formulations for the velocity and temperature profiles are required for a solution of the differential equation system based on integral calculation. Velocity and temperature matrices are required for the calculation of the integral boundary layer values in equations (6.6) and (6.9) and for the determination of the dissipation integral c_D and c_{DH} . At the same time, the profile formulations provide the definitive equations for the friction coefficient c_f , which is required in equation (6.4), and the Stanton number St , which enters the integration equation (6.7).

6.3 Profile Formulations

6.3.1 Boundary Layer Profiles in Flows with Constant Material Values

Integral procedures are characterized by the fact that suitable profile formulations are required for the determination of velocity and temperature matrices. Similar to differential procedures with 'wall functions' (see [78]), known parameters enter the calculations with the profile formulations. In accordance with conservation equations (6.2) and (6.3), they must be completed in the following manner for the flow near the wall ($y = 0, u = v = 0$):

$$\left. \frac{\partial \tau}{\partial y} \right|_{y=0} = \frac{dp}{dx} \quad \text{or} \quad \left(\mu \cdot \frac{\partial^2 u}{\partial y^2} \right)_{y=0} = -\rho_\delta u_\delta \cdot \frac{du_\delta}{dx} \quad (6.13)$$

$$\left. \frac{\partial \dot{q}}{\partial y} \right|_{y=0} = 0 \quad \text{or} \quad \left(\lambda \cdot \frac{\partial^2 T}{\partial y^2} \right)_{y=0} = 0 \quad (6.14)$$

The observance of these 'wall conditions' is achieved by a square formulation for the velocity profile at the wall; for the temperature profile it is obtained by a linear matrix as follows:

$$u(y) = k_1 \times y + k_2 \times y^2 \quad (6.15)$$

$$T - T_w = k_3 \times y \quad (6.16)$$

Regardless whether the boundary layer is laminar, transitional or turbulent in character, this determines the viscous flow near the wall. In the similarity coordinates u^+ , T^+ and y^+ , which are useful for a general illustration of boundary layer profiles, the velocity and temperature matrices, which are described by equations (6.13) through (6.16) and the parameters

$$\tau_w = (\mu \cdot \frac{\partial u}{\partial y})_{y=0} \quad (6.17)$$

$$\dot{q}_w = (-\lambda \cdot \frac{\partial T}{\partial y})_{y=0} \quad (6.18)$$

are in accordance with the following:

$$u^+ = y^+ + k_2^* \cdot y^{+2} \quad (6.19)$$

$$T^+ = Pr \cdot y^+ \quad (6.20)$$

With the applicable definitions

$$u^+ = \frac{u}{u_\tau} ; \quad y^+ = \frac{y \cdot u_\tau}{\nu} ; \quad T^+ = \frac{(T - T_{st}) \cdot \rho \cdot u_\tau \cdot c_p}{\dot{q}_w} \quad (6.21)$$

$$k_2^* = -\frac{1}{2} \cdot \frac{\nu}{u_\tau^3} \cdot u_\delta \cdot \frac{du_\delta}{dx} \quad (6.22)$$

$$Pr = \frac{\mu \cdot c_p}{\lambda} ; \quad u_\tau = \sqrt{\tau_w / \rho} \quad (6.23)$$

the analysis of the boundary layer profiles is initially concentrated on the critical case of flows with constant material values.

Based on equations (6.19) and (6.20) for flows near the wall, analytical profile matrices were determined separately for laminar and turbulent flows which describe the total flow up to the edge of the boundary layer. By superimposing the laminar and turbulent profile formulations we are now able to model the boundary layer profiles for the laminar-turbulent reversal range.

6.3.1.1 Laminar Profiles

A modelling of the reversal and an inclusion of the acceleration intensities, which are representative for blade circulation, as proposed by Polhausen and Hartree (see [109]), were not possible with known profile formulations for laminar boundary layers. In the early development stages of the calculation program I determined that these matrices, which are based on simple polynomial formulations, are too inflexible. Therefore, they result in inappropriate overshoots of the boundary layer profiles, even in flows with relatively low acceleration. This overshoot behavior also occurred when these formulations were used for reversal modelling (see following chapters).

(135

In my newly developed version, the laminar boundary layer profiles, which can also be used as starting profiles, are in accordance with the schematic shown in Illustration 6.1. Temperature and velocity profiles were determined with identical formulas.

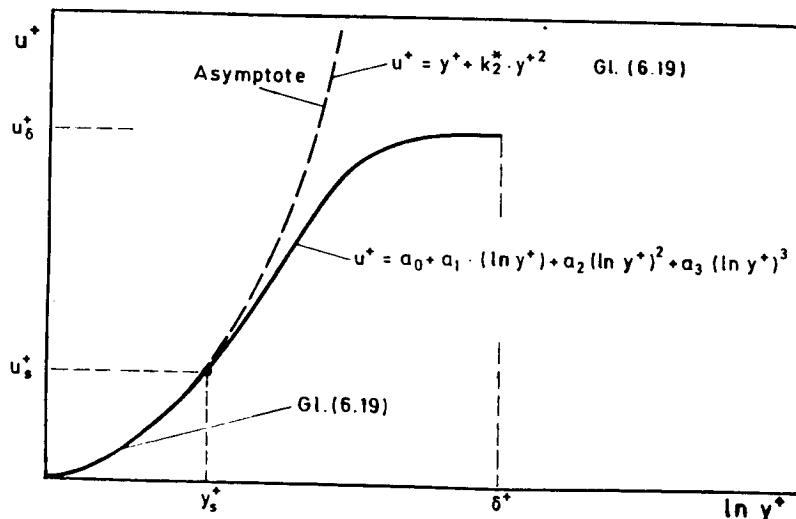


Illustration 6.1: The Laminar Profile Formulation

**ORIGINAL PAGE IS
OF POOR QUALITY**

In the section near the wall, the laminar velocity profiles are in agreement with the asymptotic matrix of equation (6.19). This was confirmed by my boundary layer tests (see Illustration 5.7). With a given wall distance y_s^+ , this matrix is replaced by a polynomial of the 3rd degree with logarithmic variables. The coefficients of the polynomial are determined by the locations and gradients near the validity limit for y_s^+ and at the edge of the boundary layer. The conditions for equation (6.19) are achieved at the $y^+ = y_s^+$ location. At the edge of the boundary layer, the condition

$$y^+ = \delta^+ : u^+ = u_0^+ ; \frac{du^+}{dy^+} = 0 \quad (6.24) \quad (136)$$

must be considered.

After solving the polynomial, the formulation for the entire laminar velocity profile is as follows:

$$u^+ = y^+ + k_2^* \cdot y^{+2} \quad (0 < y^+ < y_s^+) \quad (6.25)$$

$$\frac{u^+ - u_s^+}{u_0^+ - u_s^+} = K \cdot \eta + (3-2 \cdot K) \cdot \eta^2 + (K-2) \cdot \eta^3 \quad (y^+ > y_s^+)$$

with
$$K = \frac{(1+2 \cdot k_2^* \cdot y_s^+) \cdot \ln(\delta^+/y_s^+)}{(u_0^+ - u_s^+)} \cdot y_s^+ \quad (6.26)$$

and the dimensionless wall distance

$$\eta = \frac{\ln(y^+/y_s^+)}{\ln(\delta^+/y_s^+)} \quad (6.27)$$

With minor changes to the velocity profiles, which are mainly due to the differences in equations (6.19) and (6.20), the laminar temperature profile can be illustrated in a similar manner:

$$T^+ = Pr \cdot y^+ \quad (0 < y^+ < y_{st}^+) \quad (6.28)$$

$$\frac{T^+ - T_{st}^+}{T_{\delta_t}^+ - T_{st}^+} = K_t \cdot \eta_t + (3-2 \cdot K_t) \eta_t^2 + (K_t-2) \cdot \eta_t^3 \quad (y^+ > y_{st}^+)$$

with

$$K_t = \frac{Pr \cdot y_{st}^+ \cdot \ln(\delta_t^+ / y_{st}^+)}{(T_{\delta_t}^+ - T_{st}^+)} \quad (6.29)$$

and

$$n_t = \frac{\ln(y^+ / y_{st}^+)}{\ln(\delta_t^+ / y_{st}^+)} \quad (6.30)$$

The range limit y_s^+ (y_{st}^+) of the dual layer boundary layer profile determined in the above manner was, in comprehensive test calculations, determined for both unaccelerated and accelerated flows. To avoid an overlap of the profile in the outer range with the asymptote given in equation (6.19) or (6.20), the following distinction is made:

(137

$$\begin{aligned} y_s^+ &= \max \{ 11 ; y^+(u^+ = 0,25 \cdot u_0^+) \} \\ y_{st}^+ &= \max \{ 11 ; y^+(T^+ = 0,25 T_{\delta_t}^+) \} \end{aligned} \quad (6.31)$$

6.3.1.2 Turbulent Boundary Layer Profiles

The formulations for turbulent boundary layer profiles are based on the 3-layer model proposed by Walz and Neubert [126]. This model determines all three boundary layer area - laminar bottom layer, the area of the logarithmic wall theory, and the wake portion - cohesively and by including the wall relationship given by equation (6.19):

$$\begin{aligned} u^+ &= \left(\left(1 - \frac{1}{K} - C \cdot a \right) \cdot y^+ + K_2^* \cdot y^{+2} - C \right) \cdot e^{-a \cdot y^+} + \frac{1}{K} \cdot \ln(y^+ + 1) + \\ &+ C + \frac{P}{K} \cdot w(y/\delta) \end{aligned} \quad (6.32)$$

with $C = 5.1$; $K = 0.41$; $a = 0.3$.

C and κ form the constants of the logarithmic wall theory. In this profile formulation, the buffer layer constant "a" results in an even transition from the laminar bottom layer to the logarithmic range. Its value $a = 0.3$ was determined by Walz and Neubert with the aid of a test comparison. The follow-up function $w(y/\delta)$ is modelled according to Hinze

$$w(y/\delta) = \frac{1}{2} (1 - \cos(\pi \frac{y}{\delta})) \quad (6.33)$$

In equation (6.32) it is weighted with the applicable wake parameter P/κ . P/κ represents the increase of the velocity profile to the logarithmic wall theory at the edge of the boundary layer:

$$\frac{P}{\kappa} = u_{\delta}^+ - \left(\frac{1}{\kappa} \cdot \ln \delta^+ + C\right) \quad (6.34)$$

With the pressure gradient term $\kappa_2^* \times y^{+2}$, the profile formulation (equation 6.32) meets the complete wall connection theory (equation 6.19) and can therefore be used for accelerated flow. Based on a great variety of experimental studies (see Chapter 2.2), no change to the logarithmic wall theory is introduced if the calculation is made for flows with pressure gradients. The same applies to the temperature profiles, which is discussed in following chapters.

(138)

Because turbulent temperature profiles - like the velocity profile - are characterized by laminar bottom layers, the logarithmic wall theory and the wake area, equation 6.32 can be used for their description. By considering the flow conditions near the wall ($T^+ = Pr \times y^+$, equation 6.20), which are different from those in equation 6.19, the following formulation is established for the turbulent temperature profile:

$$T^+ = \left\{ \left(Pr - \frac{1}{\kappa_T} - C_t \cdot a \right) \cdot y^+ - C_t \right\} \cdot e^{-a \cdot y^+} + \frac{1}{\kappa_T} \cdot \ln(y^+ + 1) + C_T + \frac{1}{2} (1 - \cos(\pi \frac{y}{\delta_t})) \cdot \left[T_{\delta_t}^+ - \frac{1}{\kappa_T} \cdot \ln \delta_t^+ - C_t \right] \quad (6.35)$$

with $C_T = 3.8$; $\kappa_T = 1/Pr_t$; $Pr_t = 0.9$.

The constants of the logarithmic wall theory C_T and K_T , which are contained in equation 6.35, are determined independent of the respective cooling condition in flows with almost constant material values (cooling is introduced to the profile formation by transformation formulations). Experimental profile studies (see Chapter 5.5.1.2) have shown that, in this case, C_T has the value 3.8, as proposed by Sill [78] and Simonich and Bradshaw [54].

6.3.2 Boundary Layer Profiles in Flows with Changing Density

(139)

The formulations for temperature and velocity profiles were initially determined only for flows with almost constant material values. However, profile studies conducted by me and other authors showed that, with the aid of suitable profile transformations, these formulations can, in an unchanged form, also be applied to highly cooled boundary layer flows. This procedure will be described in the following paragraphs.

In order to perform profile transformations, the profile formulations introduced with the similarity coordinates $u^+ = f(y^+)$ and $T^+ = f(y^+)$ must be expressed in a more practical manner:

$$\frac{u}{u_\delta} = f_1\left(\frac{y}{\delta}\right); \quad \frac{T - T_w}{T_{\delta_t} - T_w} = f_2\left(\frac{y}{\delta_t}\right) \quad (6.36)$$

This can be achieved, as proposed by Walz [126], by forming the easily reconstructable interrelations for u_τ , y^+ and u^+

$$u_\tau = u_\delta \cdot \sqrt{c_f/2}; \quad u^+ = \frac{u}{u_\tau} = \frac{u}{u_\delta \cdot \sqrt{c_f/2}} \quad (6.37a)$$

$$y^+ = \frac{y \cdot u_\tau}{\nu} = \frac{y}{\delta} \cdot \frac{\delta}{\delta_2} \cdot Re_2 \cdot \sqrt{c_f/2} \quad (6.37b)$$

They are then inserted in the original profile formulations $u^+ = f(y^+)$ (equations 6.25 and 6.32). The laminar and turbulent formulations for the velocity profiles thus exhibit a structure which is implicitly dependent on c_f and Re_2

$$\frac{u}{u_\delta} = f\left(\frac{y}{\delta}, Re_2, c_f\right) \quad (6.38)$$

ORIGINAL PAGE IS
OF POOR QUALITY

and for which available transformation procedures can be directly used.

The transformation for the calculation of boundary layers in flows with changing density relates to the method described by Walz [126]. Within the profile context given by equation (6.38), c_f and Re_2 are replaced by material value correcting expressions. The Reynolds number Re_2 is corrected (with respect to temperature) with the free stream density and the wall viscosity in the following manner:

$$Re_2 = \frac{\rho_\delta \cdot u_\delta \cdot \delta_2}{\mu_w} \quad (6.39)$$

The actual tangential stress coefficient c_f is replaced by an incompressible reference value c_{fi} .

In accordance with van Driest (see Küster [128]), the c_f transformation for high free stream velocities is performed as follows: (140)

$$\frac{c_{fi}}{c_f} = A^2 \frac{T_w}{T_{\delta t}} [\arcsin \alpha + \arcsin \beta] \quad (6.40)$$

with

$$A = r \cdot \frac{\kappa' - 1}{2} Ma^2 \cdot \frac{T_{\delta t}}{T_w}; \quad E = \left(\frac{T_{\delta t}}{T_w} + r \cdot \frac{\kappa' - 1}{2} \cdot Ma^2 \cdot \frac{T_{\delta t}}{T_w} - 1 \right);$$

$$\kappa' = 1,4; \quad \alpha = \frac{2A^2 - B}{\sqrt{4A^2 + B^2}}; \quad \beta = \frac{B}{\sqrt{4A^2 + B^2}};$$

$$r = \text{Recovery-Faktor} = 0.88$$

In flows with non-constant material values and $Ma \rightarrow 0$ (in our case: $Ma < 0.3$) Küster's [128] simplified transformation is used for c_f :

$$\frac{c_{fi}}{c_f} = \frac{1}{4} \left(\sqrt{\frac{T_w}{T_{\delta t}}} + 1 \right)^2 \quad (6.41)$$

The transformation equations for c_f can also be used for laminar boundary layer flows, although these interrelations were only developed for turbulent boundary layers. The simplification is based on available literature (see Kays [64]), which states that cooling influences in laminar and turbulent boundary layers are generated in an approximately identical manner.

Similar to procedures used for the velocity profile, the inclusion of variable material values and the transformation of the temperature profile also occurs within the context described by equation (6.36). The relationship provided by equation (6.37a) for u_p is included in the development of this general temperature profile formulation in an unchanged manner. The wall distance coordinate y^+ is adjusted to the reference values of the enthalpy equation (equation 6.7). The impulse loss thickness δ_2 , which characterizes the flow boundary layer, is replaced by the enthalpy loss thickness δ_5 (equation 6.9). The boundary layer thickness δ is replaced with the thickness of the temperature boundary layer δ_t . This results in the following:

$$y^+ = \frac{y}{\delta_t} \cdot \frac{\delta_t}{\delta_5} \cdot Re_5 \cdot \sqrt{c_f/2} \quad (6.42)$$

The transformation of T^+ , which is required for the determination of the temperature profile in accordance with equation (6.36), will - by including the Stanton number St defined by equation (6.7), result in:

$$T^+ = \frac{T_w - T}{T_w - T_{\delta_t}} \cdot \frac{1}{St} \cdot \sqrt{c_f/2} \cdot \frac{T_w - T_{\delta_t}}{T_w - T_{0\delta_t}} \quad (6.43) \quad (141)$$

This transforms the profile formulations $T^+ = f(y^+)$ (equations 6.28 and 6.35) into

$$\frac{T - T_w}{T_{\delta_t} - T_w} = F\left(\frac{y}{\delta_t}; Re_5; c_f; St_x\right) \quad (6.44)$$

When considering variable material values, the transformation principle used for the velocity profile can be used. In the new profile illustration according to equation (6.44), Re_5 is formed with an average viscosity

$$Re_5 = \frac{\rho_\infty \cdot U_\delta \cdot \delta_5}{\mu_w} \quad (6.45)$$

The Stanton numbers and c_f values in reference to free stream density are replaced by the values St_i and c_{fi} , which were transformed with equations 6.40 or 6.41.

6.4 The Turbulence Model

A great number of turbulence models have been introduced for the determination of turbulent exchange events in boundary layers. Depending on the number of transport equations used for characteristic turbulence values, they are categorized into 0-equation, 1-equation, 2-equation and Reynolds stress models. The complexity and the general validity increase with the number of model equations. To find a good compromise between general validity, complexity, availability and user friendliness, I would like to use a 1-equation model developed by McDonald and Fish [5] and McDonald and Kreskovsky [49]. This model presents numerous expansion possibilities and its numeric solution is very simple. This type of model uses Prandtl's mixing method for the determination of the turbulent tangential stress distribution. The mixing path at the outer edge of the boundary layer is deduced from the integrated balance equation for turbulent, kinetic energy. This method has already been successfully used in the calculation of heat transfer in gas turbine blades (see [5]). In the following calculation procedure I will use the unchanged turbulence model for turbulent boundary layers. I will, however, introduce an expansion to the model for the calculation of the boundary layer reversal.

**ORIGINAL PAGE IS
OF POOR QUALITY**

The starting point for the turbulence model is the known differential transport equation for turbulent kinetic energy q . After a partial integration over the wall distance y , it is transformed into an integral condition for turbulence energy. According to McDonald et al [5, 49], it is as follows:

$$\frac{1}{2} \frac{d}{dx} \int_0^{\delta} \rho \cdot u \cdot q \, dy = \int_0^{\delta} \underbrace{-\rho \overline{u'v'}}_{\text{Prod.}} \cdot \frac{\partial u}{\partial y} \, dy - \int_0^{\delta} \underbrace{\rho \cdot \epsilon}_{\text{Diss.}} \cdot dy - \int_0^{\delta} \underbrace{\rho (\overline{u'^2 - v'^2})}_{\text{Norm.-Sp.-Prod.}} \cdot \frac{\partial u}{\partial x} \, dy + E \quad (6.46)$$

Konv. Entr.

with $q = \overline{u'^2} + \overline{v'^2} + \overline{w'^2}$

and $E = \frac{1}{2} q_{\delta} \cdot (\rho u \cdot \frac{d\delta}{dx} - \overline{\rho v})_{\delta}$; $(\overline{\rho v})_{\delta} = \rho_{\delta} u_{\delta} \cdot \frac{d\delta}{dx}$ (6.47)

The individual terms of equation (6.46) are, from left to right: convection, production, dissipation, normal stress production and 'entrainment' of turbulent kinetic energy. The entrainment portion E considers the turbulence energy ($q_{\delta} = 3 \times Tu^2 \times u_{\delta}^2$), which penetrates the boundary layer from the outside. It explicitly registered influences on free stream turbulence.

The connection between the kinetic turbulence energy q , which is contained in equation (6.46), and the additional turbulence components u' , v' , $\overline{u'v'}$, and ϵ is defined with additional model equations:

$$\begin{aligned} (q - f(\frac{y}{\delta}) \cdot q_{\delta}) \cdot a_1 &= -\overline{u'v'} \\ \overline{u'^2} &= a_2 \cdot q ; \quad \overline{v'^2} = a_3 \cdot q ; \quad f(\frac{y}{\delta}) = (1 - \cos(\pi \cdot \frac{y}{\delta}))/2 \\ \epsilon &= (-\overline{u'v'})^{3/2} / L \end{aligned} \quad (6.48)$$

With these formulations, the integral energy equation (equation 6.46) is transformed into a correlation which is only dependent on the shear stress $\overline{u'v'}(y/\delta)$. In turbulent boundary layers with high Reynolds numbers, the structural parameters a_1 , a_2 and a_3 have the values 0.15, 0.5 and 0.2 which were determined in experiments. In non-equilibrium boundary layers with low Reynolds numbers, a_1 experiences an additional Reynolds number correction, while a_2 and a_3 remain the same. This correction will be explained later.

The solution of the shear stress distribution $\overline{u'v'}(y/\delta)$ is continued (143) with a Prandtl mixing method equation.

$$-\overline{u'v'} = (\ell \cdot \frac{\partial u}{\partial y})^2 \quad (6.49)$$

The mixing path ℓ and the dissipation length L , which is required to determine the dissipation ϵ (equation 6.48), together with the wall distance are variable values. In fully turbulent flows, ℓ and L are modelled with the relationships

$$\frac{L}{\delta} = 0,1 \cdot \operatorname{tgh} \left(\frac{\kappa \cdot y}{0,1 \cdot \delta} \right) \cdot D \quad (6.50)$$

$$\frac{\ell}{\delta} = \frac{\ell_{\infty}}{\delta} \left\{ \operatorname{tgh} \left(\frac{\kappa \cdot y}{\ell_{\infty}} \right) + \left(1 - \operatorname{tgh} \left(\frac{\kappa \cdot \delta}{\ell_{\infty}} \right) \cdot f \left(\frac{y}{\delta} \right) \right\} \cdot D \quad (6.51)$$

is the von Karman constant ($\kappa = 0.41$) and ℓ_{∞} establishes the mixing path at the edge of the boundary layer.

The damping factor D considers the fact that turbulent exchange events disappear in the laminar bottom layer. The relationship, in this case, depends on the pressure gradient in the free flow. In this calculation, it is performed with the van Driest equation expanded by von Cebeci [129]:

$$D = 1 - e^{-y^+/A^+}; \quad A^+ = 26 \cdot [1 - 11,8 p^+] \quad (6.52)$$

$$p^+ = - \frac{v}{\rho \cdot u_T^3} \cdot \frac{dp}{dx}$$

With ℓ_{∞} , the distribution of the mixing path in accordance with equation (6.51) indicates a single-parameter context.

To calculate the free stream mixing path with the aid of turbulent kinetic energy equations is the immediate goal of this turbulence model. When ℓ_{∞} is known, the turbulent shear stress distribution required for the solution of the basic equation can be determined. The turbulent heat flow in the boundary layer can be determined with the relationship for the turbulent Prandtl number (equation 6.12). In order to determine the free stream mixing path, the turbulent kinetic energy (equation 6.46) is, with the additional relationships in equations (6.48) through (6.52), transformed to a common differential equation of the 1st degree for the unknown variable ℓ_{∞} . It can then be numerically integrated with very simple algorithms.

Reynolds Number Influences

(144)

In the above form, the turbulence model is suitable only for computing turbulent equilibrium boundary layers with high Reynolds numbers. Boundary layers with low Reynolds numbers, which are the main focus of this dissertation, are accompanied by additional viscosity influences which must be considered separately. McDonald and his colleagues [5, 49] specified this flow situation with Reynolds number dependent modifications of the structural parameter a_1 and the dissipation length L . Comparative calculations with the flat, unaccelerated turbulent plate boundary layer and a simplified analytical solution of the turbulent kinetic energy equation determined the following dependencies on the Reynolds number Re_2 (see [47]):

$$a_1 = a_0 \cdot (Re_2 / Re_{2,0}) \cdot [1 + 6,666 \cdot a_0 \cdot (Re_2 / Re_{2,0} - 1)] \quad (6.53)$$

$$L(y/\delta) = L_{\infty}(y/\delta) \cdot [1 - \exp(-1,63 \cdot \ln Re_2 + 9,7)] \quad (6.54)$$

ORIGINAL PAGE IS
OF POOR QUALITY

The applicable values 0.0115 and 100 are applied to the unknown values a_0 and $Re_{2,0}$. $L_{\infty}(y/\delta)$ is in accordance with the original context given by equation (6.50).

It can be seen in the above that, despite the relationships of equations (6.53) and (6.54), the turbulence model continues to be suitable only for conditions in the flat plate boundary layer without pressure gradient and heat transfer. Additional generalizations are required to enable a calculation of arbitrary, turbulent boundary layer flows. By making substitutions for Re_2 in the relationships (equations 6.53 and 6.54), McDonald et al [5, 49] introduces a more basic dependency on local boundary layer turbulence. The following turbulence Reynolds number was selected to describe boundary layer turbulence:

$$R_r = \frac{1}{\delta} \cdot \int_0^{\delta} \frac{v_t}{\nu} dy; \quad v_t = \lambda^2 \cdot \frac{\partial u}{\partial y} \quad (6.55) \quad (145)$$

To determine in what manner R_r must replace Re_2 in equations (6.53) and (6.54), McDonald and Fish [5] used experimental studies of turbulent boundary layers and their own comparative calculations with the turbulence model. The following definitive equation was determined as a result:

$$(6.56)$$

The range between $R_r = 1$ and $R_r = 40$ is bridged by a polynomial of the 3rd degree whose coefficients are obtained from the values given by equation (6.56) and derivations from applicable validity limits.

(NOTE: As a simplification to these boundary layer calculations, I have computed R_r with an analytical relationship (equation 6.59) developed by Forest [9])

6.5 Modelling the Boundary Layer Reversal

6.5.1 Determination of the Boundary Layer Intermittency

The transition from a laminar into a turbulent boundary layer matrix can be computed with a better agreement to actual conditions, if this transition is not treated as an abrupt event but as a location with finite length. To prove this in an integral procedure, we must define a transient function which describes the physical distribution of the intermittency factor in the reversal. The intermittency factor γ characterized the chronological fraction of turbulent flows in the transition range which alternates between laminar and turbulent flow. It has a zero value in laminar flow and the value one in fully turbulent boundary layer conditions. Intermediate values model the conditions in the reversal range. The intermittency factor γ is used to determine boundary layer formulations in the reversal and to specify the applicable boundary layer turbulence.

The matrix of the intermittency factor γ is determined by the model equations by Forest [9]. A simple differential equation applies for the reversal:

$$\frac{d\gamma}{dx} = \frac{\gamma e^{-\gamma}}{L_\gamma} \quad (6.57)$$

With γ_e , this retardation equation (6.57) is based on a presumed equilibrium intermittency. In a quasi-stationary reversal situation, the boundary layer flows toward this equilibrium intermittency. The actual delay is determined by the factor L_γ . According to Forest [9], L_γ depends on the boundary layer values Re_2 , δ_2 , and on the average effective viscosity $\bar{\nu}$ of the existing boundary layer flow. (146

$$L_\gamma = \frac{a \cdot Re_2 \cdot \delta_2}{(\bar{\nu}/\nu)} ; \quad a = 2,0 ; \quad (6.58)$$

\bar{v} is recorded with a semi-empirical correlation which considers the influences of pressure gradient and free stream turbulence.

$$\frac{\bar{v}}{v} = 1 + Re_2 \cdot (0,02 \cdot \gamma + 0,82 \cdot c_T \cdot Tu(x)) \quad (6.59)$$

with

$$c_T = \frac{0,75 - \bar{\beta}}{\bar{\beta} + 0,01}; \quad \bar{\beta} = \sqrt{0,0625 m^2 + \gamma^2}$$

$$(m = \text{effective Fohausen parameter}) \quad (6.60)$$

In this procedure, the equilibrium intermittency γ_e is identified with the intermittency behavior in unaccelerated flows, which is known from reversal tests. Referred to the standardized reversal coordinate $z = Re_2/Re_{2S}$, it has the matrix shown in Illustration 6.2 which is described in equation (6.61)

$$Re_{2S} = 163 + \exp(F(m) - \frac{F(m)}{6,91} \cdot \bar{Tu})$$

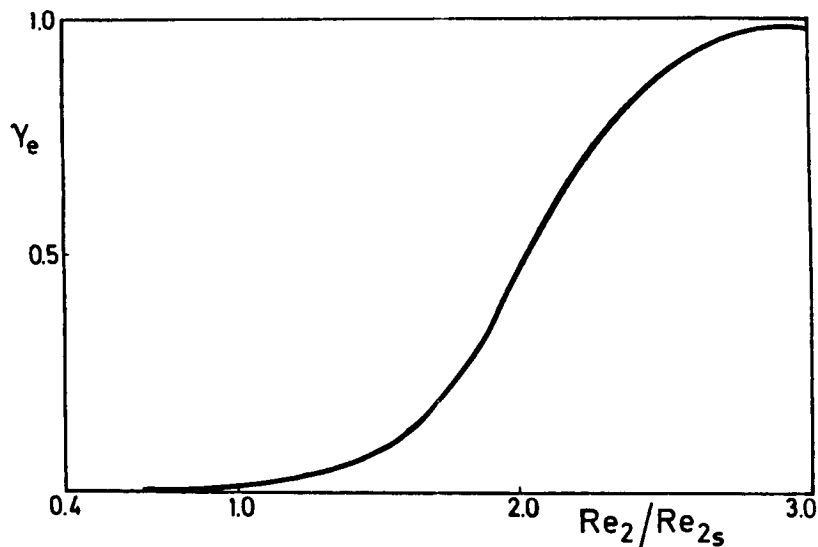


Illustration 6.2: Intermittency Matrix in the Reversal Area

$$\gamma_e = \frac{1}{1 + \exp(1-4,4 \cdot z)} ; \quad z = Re_2/Re_{2S} \quad (6.61) \quad (147)$$

Re_2 represents the impulse loss thickness Reynolds number at reversal initiation. With $z = 1$, the reversal begins with an initiation intermittency of approximately 1%. When the impulse loss thickness Reynolds number has tripled, it is regarded as completed with $z = 3$ (Illustration 6.2). This will guarantee a realistic, long reversal process.

To determine the reversal initiation (more accurately: the intermittency initiation), Forest [9] proposes the use of suitable correlation functions, which were determined on an experimental basis. In our case, I selected a relationship developed by Abu Ghannam and Shaw [45] for boundary layers with pressure gradient and external turbulence. This relationship demonstrates good agreement with tests performed for this dissertation (see Chapter 5.2.1, Illustration 5.2.1):

$$(6.62)$$

with

$$\begin{aligned} F(m) &= 6,91 + 12,75 m + 63,64 m^2 \quad \text{for } m < 0 \\ &= 6,91 + 2,48 m - 12,27 m^2 \quad \text{for } m > 0 \end{aligned}$$

with "m" in accordance with equation (6.60) and

$$\bar{T}_u = \frac{T_u(x) + T_u(x=0)}{2} + 2,7 \sqrt{\gamma} \quad [\%]$$

The turbulence intensity used for the determination of the reversal Reynolds numbers in equation (6.62) meets the criteria established by Abu Ghannam and Shaw [43] and the model hypothesis by Forest [9]. In order to record the attenuation behavior of the free stream turbulence (see Chapter 5.2), Abu Ghannam correlated the reversal initiation with average turbulence intensities between the running length x and the location of the boundary initiation. Forest also considered the influence of existing boundary layer intermittency. To consider the destabilizing effect in the reversal and after estimating the turbulence conditions in

the external boundary layer area, he modelled a supplement which is a function of $\int r$. According to this concept, the turbulence intensity Polhausen parameter (equation 6.60) is also included in the reversal condition (equation 6.62). The boundary layer intermittency and the Reynolds number for reversal initiation, which was determined with the correlation (equation 6.62), occur at locations with varying running length. The intermittency initiation, which is the basis for the reversal model is clearly ahead of the reversal Reynolds number obtained with equation (6.62) (see Chapter 5.5.2.1). To balance this fundamental difference in new calculation programs, comprehensive development computations were made for the adiabatic, flat and unaccelerated boundary layer by using various free stream data (free stream velocity, free stream turbulence). The required up-stream displacement of the intermittency initiation was determined in such a manner that the applicable increase of wall tangential stress occurred at a reversal location for Re_{2*} , which is described in equation (6.62). The result is summarized in a corrective function which is dependent on external turbulence. It provides the following relationship for the impulse loss thickness Reynolds number in the intermittency initiation (Re_{2S}) required for the calculation program:

(148

$$Re_{2S} = Re_{2S} (61.6.62) \cdot (1 - (0.05 \cdot \bar{T}_u + 0.1)) \quad (6.63)$$

Equations (6.47) through (6.63) provide all information required for determining the intermittency matrix during the laminar-turbulent boundary layer reversal. Intermittency has an influence on the turbulence model as well as on the determination of the reversal profiles for the velocity and temperature boundary layers.

If the calculation of transitional boundary layers is made for highly cooled surfaces, the impulse loss thickness Reynolds number Re_2 in equations (6.58) and (6.52) is determined with the free stream viscosity. This incorporates the important experimental determination that reversal events, even with maximum wall cooling, must be correlated with the Reynolds numbers which refer to free stream material values.

6.5.2 The Turbulence Model During Reversal

It is the function of the turbulence model to define turbulent transport events even in the reversal area. It is, in this case, also assumed that, during reversal, the turbulent mixing path ℓ continuously increases from zero to the value of a fully turbulent boundary layer. The dissipation length L increases in the same manner during the transition from the laminar to the turbulent flow. The increase of both values (ℓ, L) is an immediate function of the intermittency factor matrix. The required connection with γ is defined for the turbulent shear stress during reversal with an expanded mixing path equation:

(149)

$$-\overline{u'v'} = \gamma \cdot (\ell \cdot \frac{\partial u}{\partial y})^2 \quad (6.64)$$

This context represents an averaging of the turbulence events which, during reversal, occur only intermittently. In order to achieve the turbulent shear stress portion described in equation (6.64), the mixing path $\ell(y/\delta)$ described in Chapter 6.4 is replaced with $\int \gamma \times \ell(y/\delta)$. Because mixing path and dissipation length are subjected to an almost identical behavior in the boundary layer, $L(y/\delta)$ is also supplemented with $\int \gamma$. The remaining relationships of the turbulence model, including the Reynolds number corrections, are used unchanged for the calculation of the turbulence values during reversal.

6.5.3 Boundary Layer Profiles during Reversal

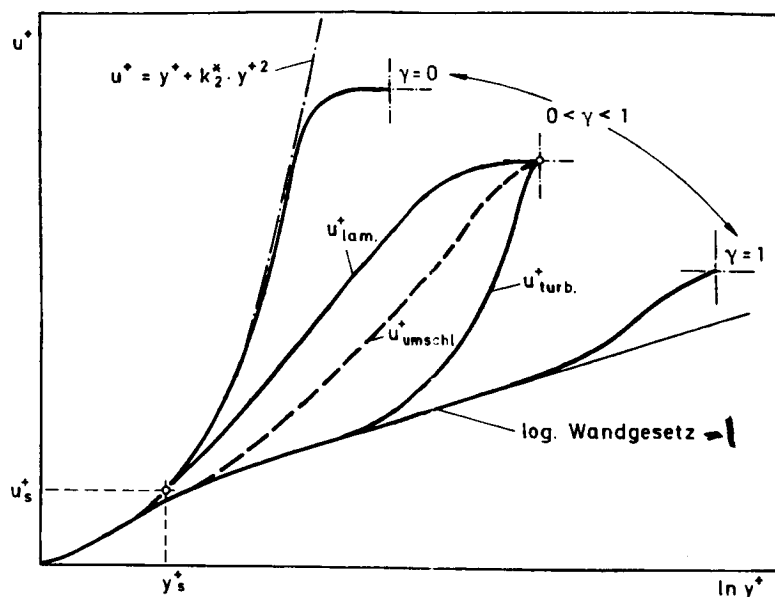
The laminar and turbulent flow event, which chronologically alternate by the value of the intermittency factor γ , are modelled by a superimposition of the laminar and turbulent profile formulations. This procedure of forming chronologically average reversal profiles was used in previous publications by Dhawan and Narashima [26] and Owen [25].

The superimposition of the laminar (equations 6.25 and 6.28) and turbulent (equations 6.31 and 6.34) profile formulations is determined by the intermittency factor γ according to the following formula:

$$\begin{aligned} u_{\text{umschl}}^+ &= u_{\text{lam}}^+ \cdot (1 - \gamma) + \gamma \cdot u_{\text{turb}}^+ \\ T_{\text{umschl}}^+ &= T_{\text{lam}}^+ \cdot (1 - \gamma) + \gamma \cdot T_{\text{turb}}^+ \end{aligned} \quad (6.65)$$

Illustration 6.3 is a sketch of the profile formation described in equation (6.35) in the reversal area. The laminar and turbulent partial profiles $u_{\text{lam}}^+(y^+)$, $u_{\text{turb}}^+(y^+)$, which are shown in the illustrations, always fulfill identical parameters near the wall and at the edge of the boundary layer. The dotted line represents the reversal profile formed for an arbitrary intermittency factor in accordance with equation (6.65).

When the reversal occurs ($0 < \gamma < 1$), the velocity profile approaches, with increasing intermittency, the known fully-turbulent form. An additional expansion of the range limit y_s^+ (or y_{st}^+), which also depends on the intermittency, was required to cause participation of the laminar profile component $u_{\text{lam}}^+(y^+)$ in this process.



1 - logarithmic wall theory

Illustration 6.3: Boundary Layer Profile during Reversal

Equation (6.31) was supplemented in such a manner that, at the end of the reversal process ($\gamma = 1$), that portion of the laminar partial profile which is near the wall and which is limited by y_s^+ (or y_{st}^+), is in accordance with the size of the laminar bottom layer of a turbulent boundary profile (limited by $y^+ = 6$).

$$\begin{aligned}
 y_s^+ &= y_{s \text{ lam}}^+ \cdot (1 - \gamma) + \gamma \cdot 6 \\
 y_{s_t}^+ &= y_{s_t \text{ lam}}^+ \cdot (1 - \gamma) + \gamma \cdot 6
 \end{aligned}
 \quad ; \quad y_{s \text{ lam}}^+, y_{s_t \text{ lam}}^+ \quad (6.66)$$

n.Gl. (6.31) \rightarrow

1 - in accordance with equation (6.31)

In initial calculations it was observed that, in special cases with reversal events far down-stream ($Tu \ll 1$) and very high u_{δ}^+ and y_{δ}^+ values, inaccuracies in the modelled reversal profile formation in the outer area of the boundary layer caused unrealistically high temperature and velocity gradients. In order to avoid this, the following limitations were introduced for the area $y/\delta > 0.5$:

$$y/\delta > 0,5 : \tau \leq \tau_w ; \dot{q} \leq \dot{q}_w ; \left. \frac{\partial u}{\partial y} \right|_w < \left. \frac{\partial u}{\partial y} \right|_w ; \left. \frac{\partial T}{\partial y} \right|_w < \left. \frac{\partial T}{\partial y} \right|_w$$

6.6 Solution Procedures

(151)

The solution of differential equations, which describe the problem, contains the numeric integration of the basic equations for flow and temperature boundary layers (equations 6.4, 6.5, 6.7, 6.8), the intermittency function (equation 6.67), and the determination of the integral balance (equation 6.46) for the turbulent kinetic energy. In connection with this, an evaluation of the profile equations for velocity and temperature matrices in the boundary layer must be made. This is done with the definitive equations for the Stanton number St and the friction coefficient c_f .

6.6.1 Evaluation of the Profile Equations

An evaluation of the profile equations is based on procedures used in integral equations. The thickness parameters δ_2 and δ_3 from the conservation equations of the flow boundary layer (equations 6.4 and 6.5) are used for the velocity profile. As profile form parameters Re_2 (in accordance with equation 6.39) and H_{32} (in accordance with equation 6.6) they have a direct influence on the solution process and represent conditions which must be met by the profile. By including these form parameters, an expanded equation (6.38) is achieved for the velocity matrix in the boundary layer:

$$\frac{u(x,y)}{u_{\delta}(x)} = f\left(\frac{y}{\delta(x)}, c_f(x), Re_2(x), H_{32}(x)\right) \quad (6.67)$$

c_f (for cooled boundary layers replaced by the transformation value c_{fi} , see Chapter 6.3.2) and the boundary layer thickness $\delta(x)$ are established as implicit values due to the profile evaluation. This process, which occurs in stages, is as follows: δ is determined with a starting value for c_f , which is obtained from the solution of the preceding calculation stage. The boundary layer thickness δ is adjusted in such a manner that, after adding the profile with an integration, impulse loss thickness δ_2 is in agreement with the setpoint value from the impulse equation. In the second stage of the profile adjustment an examination is made as to whether the form parameter H_{32} of the velocity profile, which has just been determined, is in agreement with the setpoint value in the boundary layer equations. When this is not the case, c_f is adjusted, which is followed by another determination of the boundary layer thickness δ and another examination of H_{32} . This procedure is repeated until c_f and $\delta(x)$ converge in a solution.

The temperature profile is determined in accordance with the above procedure. Therefore, I will only show the most important differences to the velocity profile. The temperature profile has the solution structure: (152

$$\frac{T - T_w}{T_{\delta_t} - T_w} = F\left(\frac{y}{\delta_t(x)}, Re_5(x), St, H_{65}(x)\right) \quad (6.68)$$

It is the definitive equation for the temperature boundary layer thickness $\delta_t(x)$ and the Stanton number St . Re_5 (equation 6.45) and H_{65} (equation 6.9) represent the form parameters of the temperature profile from the enthalpy equations.

6.6.2 Integrating the Differential Equation

The calculation program performs a successive integration of the available differential equation system which consists of impulse and energy equations (equations 6.4 and 6.5) for the computation of the flow boundary layer, the two enthalpy equations (equations 6.7 and 6.8) to determine the heat transfer and the temperature boundary layer, the intermittency functions (equation 6.57), and the turbulent kinetic energy equation (equation 6.47) to determine boundary layer turbulence. All basic equations are common differential equations of the 1st degree which can be integrated in a simple manner with the standard differential method. The forward direction is determined by the respective size of the impulse loss thickness. For a solution of rapid local parameter changes (pressure gradient, free stream turbulence, etc.)

$$\Delta x = 0.2 \times \delta_2(x) \quad (6.69)$$

was selected for all equations. The integration of impulse and energy equations occurs in connection with the evaluation of the velocity profile. The same applies to the enthalpy equations and the determination of the temperature profile. The differential equations are solved in an implicit manner to guarantee numeric stability.

6.7 Testing the Calculation Program with the Aid of Experimental Results

(153)

This chapter describes testing of the integral procedure with experimental data and other tests obtained from literature. The procedure test is performed in stages, starting with an elementary analysis of the flat, unaccelerated plate boundary layer and ending with the flow with maximum pressure gradients and intense wall cooling.

6.7.1 Boundary Layer without Pressure Gradient

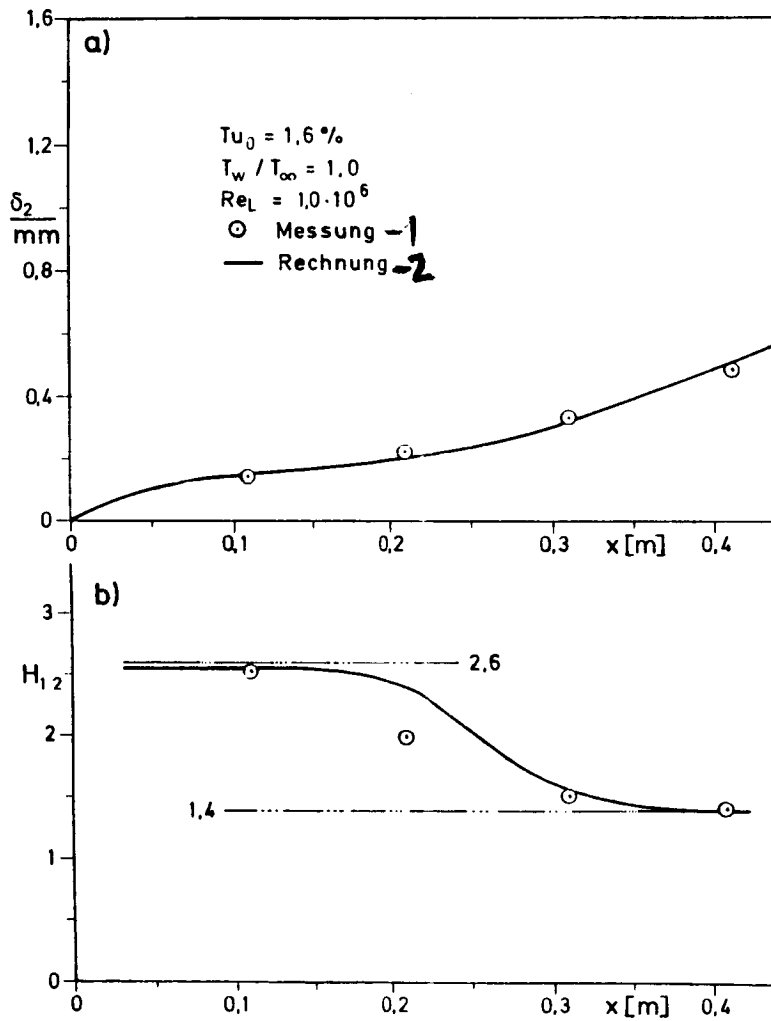
6.7.1.1 The Laminar-Turbulent Boundary Layer Reversal with Low Free Stream Turbulence Intensity

The comparison between calculated and actual test results begins with the elementary case of a flat, unaccelerated, adiabatic boundary layer with low free stream turbulence ($Tu_o = 1.6\%$, $u_o = 40$ m/s, $Re_L = 1.0 \times 10^6$). Similar comparative data were provided by Arnal [15] and Aby Ghannam [45]. The flow situation in our tests, where the reversal occurs throughout large plate areas, serves for an evaluation of the selected reversal model in the calculation program. Comprehensive boundary layer and transition tests on this subject (see Chapter 5.3.1) indicate a three-dimensional reversal process which starts in the center of the tunnel and expands downstream (including in diagonal direction). The Reynolds numbers at reversal initiation measured in the center of the tunnel is in agreement with data previously determined by other authors (see [45]).

Illustrations 6.4a and 6.4b show a comparison between test and calculation for the boundary layer values δ_2 and H_{12} . In this case, the calculation was started with an impulse loss thickness Reynolds number of $Re_2 = 140$. The respective distance of the starting point from the leading edge of the plate was determined with the known analytical Blasius relationship (equation 5.8). At 20 mm it is thus very close to the boundary layer origination point. The tangential stress coefficient c_f and the respective boundary layer thickness δ (see profile equations, Chapter 6.3.1), which are required to determine the laminar starting profile, were obtained with Thwaites' [130] procedure and the given impulse loss thickness Reynolds number.

In the entire flow are, the calculation is in good agreement with the test data. The reversal, which is initiated by boundary layer turbulence, starts - as in the test - at a distance of 150 - 200 mm from the boundary layer initiation. It results in an impulse loss thickness increase, which is modelled by the calculation with excellent agreement.

(154



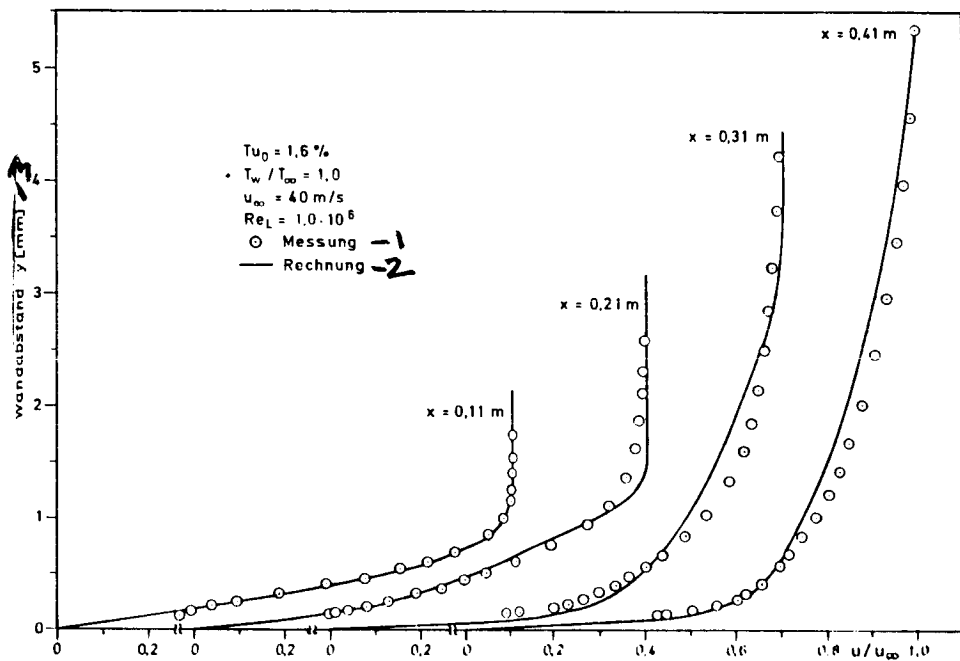
1 - test; 2 - calculation

Illustration 6.4: Impulse Loss Thickness Matrix $\delta_2(x)$ and Form Parameter $H_{12}(x)$ in a Transitional Boundary Layer

C-3

The behavior of the form parameter H_{12} is shown in Illustration 6.4b for the same flow situation. According to Blasius' theory (see e.g. [108]) there is an asymptotic value of 2.6 for unaccelerated laminar boundary layers. This value is reproduced both in the test and in the calculation. The calculation shows noticeable deviations from the test only in surface 2 ($x = 0.21$ m). Experiment and model calculation are in good agreement again at reversal termination ($x > 0.3$ m).

(155)



- 1 - test; 2 - calculation;
 3 - wall distance

Illustration 6.5: Velocity Profiles in the Reversal Area - Isothermal Flow

Illustration 6.5 is another depiction of this test situation. It provides more details with the aid of velocity profiles in the 4 measurement surfaces with $x = 0.11; 0.21; 0.31$ and 0.41 m. The laminar profile in test surface 1 and the reversal profile in test surface 2 are in excellent agreement with the calculation program. There are slight deviations with $x = 0.31$ m. The physical reversal process starts earlier in the calculation and its profile is not as full. The agreement is better in the subsequent test surface ($x = 0.41$ m). It is obvious that there are turbulent boundary layer matrices in the test as well as in the calculation. In addition, the calculated boundary layer thickness increase is in good agreement with observed data.

6.7.1.2 Boundary Layers with Varying Free Stream Turbulence

156

The most significant influence of external turbulence is that the laminar-turbulent boundary layer reversal occurs at an earlier point. The reasons for this is heat transfer rates which are considerably higher. In addition, heat transfer and tangential stress coefficients are slightly increased in turbulent boundary layers (see Chapter 5.5.2).

Illustration 6.6 is a comparison of calculation and test where the turbulence intensity at the beginning of the plate experiences a step-by-step increase from 2.3% to 8.7%. The external velocity in this example is 55 m/s. In contrast to the above described experiment, a free stream temperature of 470 K was realized and the test plate was cooled in such a manner that there was a constant temperature ratio of $T_w/T_\infty = 0.64$. This value represents the conditions in highly convectively cooled gas turbine blades.

The calculation was started with $x = 20$ mm, immediately behind the uncooled leading edge of the plate which had a length of 15 mm. As in all test situations, the applicable starting Reynolds number Re_2 was determined with the Blasius relationship (equation 5.8). The initial velocity profile was established in accordance with the previous example. A Stanton number St_{x_0} and a temperature boundary layer thickness δ_t was given for the initial temperature profile. The context for this procedure is based on analytical equations for flows with varying velocity and temperature boundary layer initiations by Kays [64] and Jischa [68]. It is as follows:

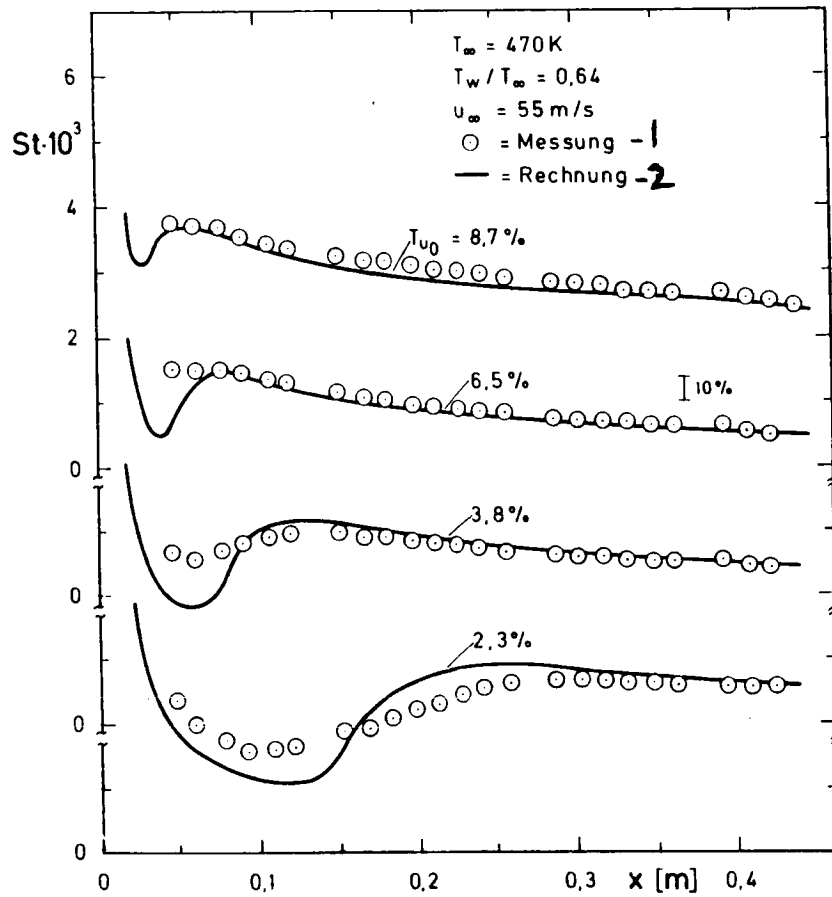
$$St_{x_0} = 0,332 \cdot Pr^{-2/3} Re_{x_0}^{-0,5} [1 - (\frac{\xi}{x_0})^{0,75}]^{-1/3} \quad (6.70)$$

$$\left. \frac{\delta_t}{\delta} \right|_{x=x_0} = \left[\frac{13}{14} \cdot \frac{1}{Pr} \cdot (1 - (\frac{\xi}{x_0})^{3/4}) \right]^{-1/3}$$

(ξ = uncooled starting length)

(x_0 = starting point for the calculation)

The model calculation provides a good description of the advance of the reversal as a function of turbulence intensity. The reversal length is also in good agreement with the test. With maximum turbulence intensity ($Tu_0 = 8.7\%$), the Stanton numbers in the reversal increase starting with an impulse loss thickness Reynolds number of $Re_2 = 135$. The early reversal thus starts below the limiting Reynolds number (indifference Reynolds number) for reversal initiation, which is known from linear stability theory and which - according to available literature (see [22, 45]) - has a value of $Re_2 \approx 160$. This early reversal is caused by the Reynolds number correction for the intermittency initiation, which was introduced with equation (6.63). It is an important contributor to a good reproduction of the test data. Test and calculation are in very good agreement in all cases in the turbulent range.

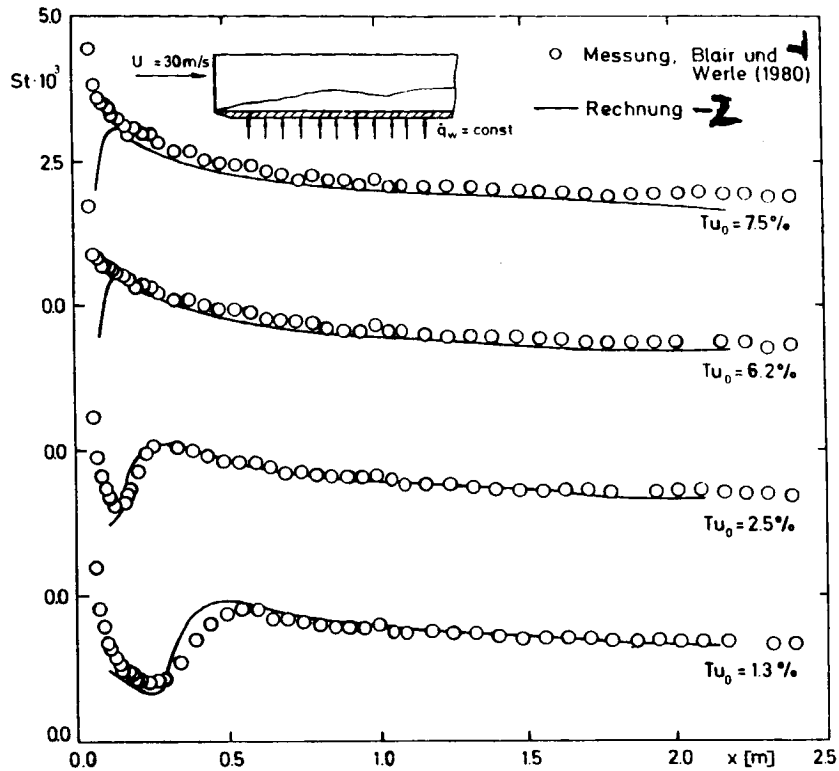


1 - test; 2 - calculation

Illustration 6.6: Stanton Number Matrices in Transitional Boundary Layers with Variable Free Stream Turbulence (Cooled Wall, $dp/dx = 0$)

Tests which, with the aid of heat transfer distributions, show the influence of free stream turbulence on the reversal (even with isothermal conditions) were recently conducted by Blair and Werle [37] on a slightly heated plate with constant heat flow ($\dot{q}_w(x) = \text{const.}$). Illustration 6.7 compares the data with model calculations and shows that a good agreement was achieved. With high turbulence intensities of 6.2% and 7.5%, the laminar-turbulent reversal already occurs within the unheated leading edge of the plate, which was attached for design reasons. It was not immediately available to the calculation, because the procedure for both uncooled and unheated starting lengths is designed for the flow immediately behind this plate. Even in the above cases with high free stream turbulence, the calculation procedure was started in a laminar manner. This is the reason why, in the illustrations of the calculation results, reversal events are still shown. However, the good agreement with the data for low free stream turbulence confirms that the integral procedure provides an accurate reversal description.

(158



- 1 - tests, Blair and Werle (1980)
- 2 - calculation

Illustration 6.7: Stanton Number Matrices on the Flat, Unaccelerated Plate with Varying Free Stream Turbulence and a Slightly Heated Wall (Tests by Blair and Werle [37])

Illustration 6.8 shows the significance of external turbulence for the boundary layer parameters tangential stress, impulse loss thickness and form parameter for various turbulence intensities. In these tests, wall and free stream temperatures had the same level (no heat transfer, flow condition 2 in Table 5.1). The comparison

(160

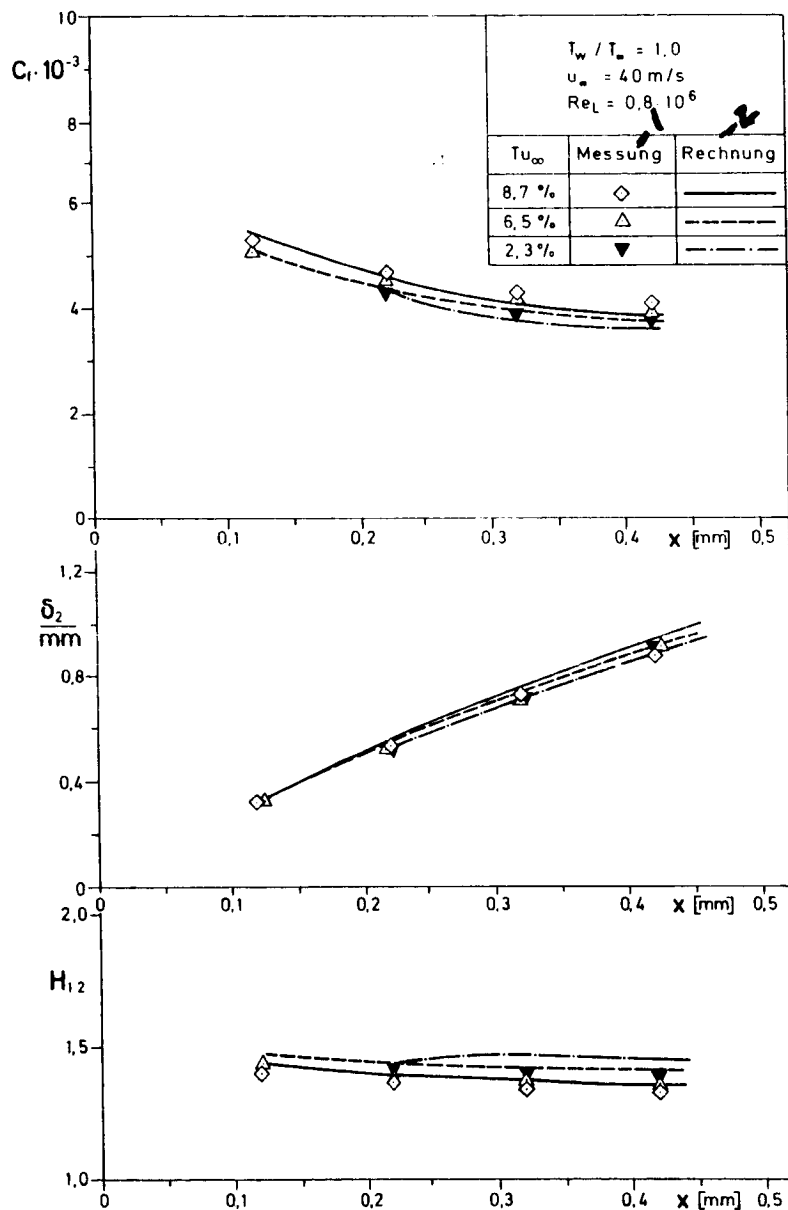
between test and calculation refers only to turbulent boundary layer flows. Because reversal behavior was still present in test surface 1 ($x = 0.12$ m) with a minimum free stream velocity of ($Tu_0 = 2.3\%$), the re-calculation was begun at the subsequent test location (with $x = 0.22$ m). In all cases, the program was initiated in a turbulent area; the values for Re_2 and H_{32} were derived from the tests. An adjustment of the profile equation at this point determined the additional start values for c_f and H_{12} . A distribution proposed by Voges ([131], see [4]), which also records the influence of external turbulence, was selected as a starting profile for the boundary layer turbulence. This given profile was used to solve the integral turbulence equation (equation 6.46) and to determine the mixing path distribution at the starting location.

Illustration 6.8a shows the measured and calculated c_f matrices. The effect of tangential stress increase induced by free stream turbulence is also present in the calculation. The deviation from the test data is only minor (maximum deviation approx. 6%). The applicable impulse loss thicknesses are re-calculated in Illustration 6.8b. A special situation occurs in this test: an increasing free stream turbulence results in a deformation of the boundary layer profiles without a noticeable change of the local impulse loss thickness (Illustration 6.8, see Illustration 5.12, Chapter 5.3.2). The calculation describes a general situation where increasing turbulence results in an increase of the impulse loss thickness (Illustration 6.8b). However, as shown by Illustration 6.8b, the resulting differences are only minor.

A mirror-image trend of the tangential stress coefficient occurs in the form parameters H_{12} (Illustration 6.8c). Increasing external turbulence generates fuller boundary layer profiles which result in a decrease of the form parameters. This behavior is accurately reproduced by the calculation procedure. When calculating with minimum free stream turbulence ($Tu_0 = 2.3\%$), a build-up process is observed during which the form parameter increases slightly.

The deformation of the turbulent boundary layer profiles generated by external turbulence is examined in Illustration 6.9 for the same flow conditions. The velocity profiles determined in test surface 4 ($x = 0.42$ m) are applied in a semi-logarithmic manner, and a comparison is made with applicable model calculations.

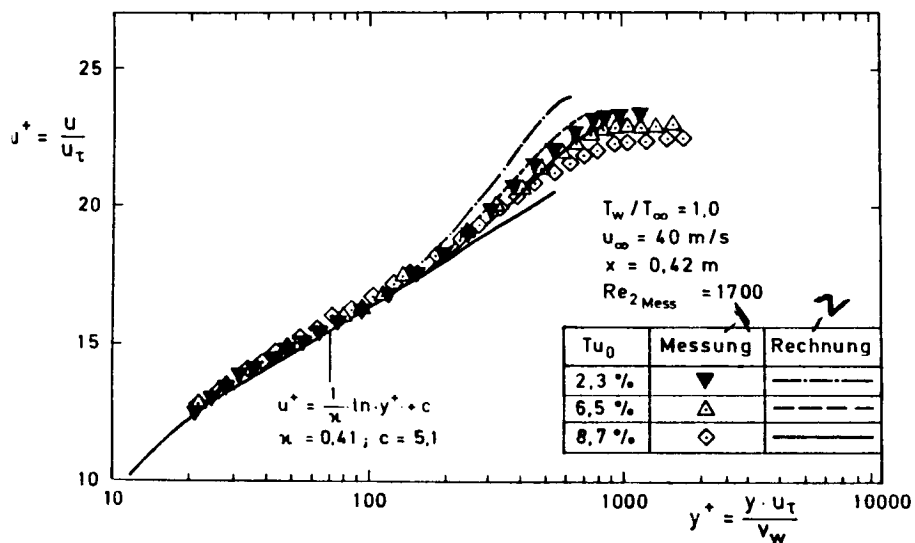
(160)



1 - test; 2 - calculation

Illustration 6.8: Friction Coefficients, Impulse Loss Thicknesses and Form Parameters in Turbulent Boundary Layers with Varying Free Stream Turbulence ($dp/dx = 0$, Uncooled Wall)

The so-called wake portion, i.e. the deviation from the logarithmic wall theory in the external boundary layer zone, decreases with increased free stream turbulence, while the validity of the wall theory remains unchanged. Both effects are recorded by the integral procedure in good agreement with the test data.



1 - test; 2 - calculation

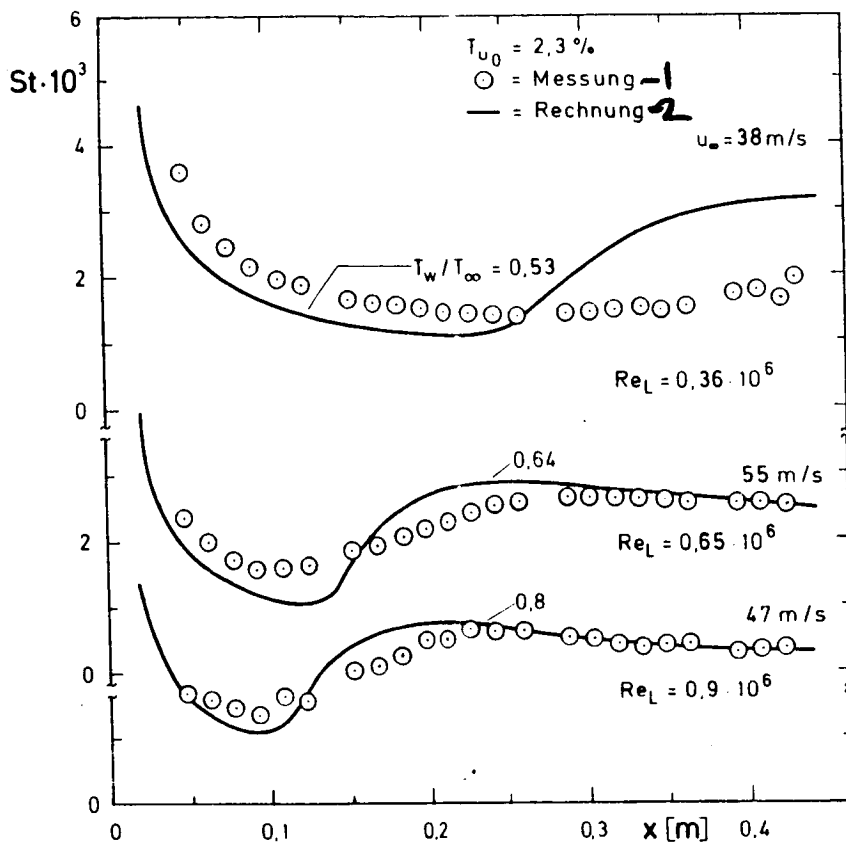
Illustration 6.9: Dimensionless Turbulent Velocity Profiles during Varying Free Stream Turbulence

6.7.1.3 Transitional Boundary Layers with Wall Cooling

According to experimental findings, wall cooling results in an increase of heat transfer and wall tangential stress. At the same time, there are changes in the velocity and temperature matrices within the boundary layer which can be attributed to fuller profiles. Contrary to the rules of linear stability theory, I did not, in my tests, discover a stabilization and delay of the reversal due to wall cooling, when free stream turbulence was continuously present (see Chapter 5.52).

Illustration 6.10 is an example of three test series conducted with varying temperature conditions T_w/T_∞ and the applicable calculations for the relatively low turbulence intensity of 2.3%.

(162)



1 - test; 2 - calculation

Illustration 6.10: Heat Transfer and Boundary Layer Development with Varying Wall Cooling and Low Free Stream Turbulence ($dp/dx = 0$)

The flow velocity was variable in the tests, so that a variation of the Reynolds number is an additional factor. In the case of maximum wall cooling ($T_w/T_\infty = 0.53$) and minimum flow velocity ($u_\infty = 38$ m/s), a laminar flow over wide areas of the plate occurs in the tests. Starting with $x = 0.2$ m, this flow, with slowly increasing Stanton numbers, is replaced by a reversal. This type of reversal behavior is reflected in the calculations; however, the transition to turbulent flow is more rapid than in the experiment. There are also differences between test data and calculations in the laminar

boundary layer section. The discrepancy is caused by calculated heat transfer coefficients, which are too low. This is caused by the applied material value transformation for the determination of velocity and temperature profiles during wall cooling; it is insufficient in this case. This was to be expected, because the tests showed a higher increase of the laminar heat transfer with wall cooling than is known from literature, and because it is predicted by the material value transformations implemented in the calculation program (see Chapter 5.5.1). The differences between test and calculation data in the laminar boundary layer area are a function of the intensity of the wall cooling. This is confirmed by the lesser discrepancies during reduced wall cooling, which is identical to an increased temperature ratio T_w/T_∞ .

In Illustration 6.10, the increase of external velocity from 38 to 55 m/s and the reduction of wall cooling from the value $T_w/T_\infty = 0.53$ (which is hardly possible under actual conditions) to $T_w/T_\infty = 0.64$, which is a realistic condition in turbines, shows a much earlier boundary layer reversal. This is confirmed by the model with respect to reversal initiation as well as to the length of the reversal. There is very good agreement in the turbulent zone.

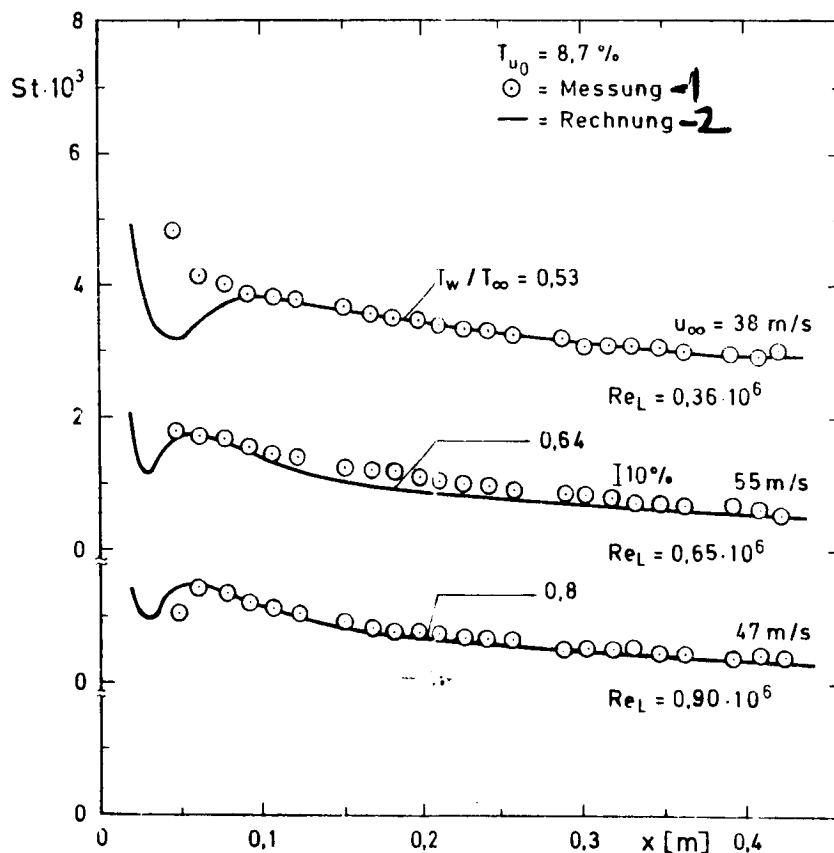
In comparison to the above test, a further reduction of wall cooling to $T_w/T_\infty = 0.8$ and external velocity (from 55 to 47 m/s) - as shown in the lower half of the illustration - causes location and length of the laminar-turbulent reversal to remain almost unchanged. This is verified by the calculation. In this case, the accuracy of the calculation is especially good in all boundary layer areas.

Illustration 6.11 compares tests with a turbulence intensity of 8.7%, which is a typical condition in turbines, to their respective calculations. Due to the high turbulence, the reversal - in all temperature conditions - occurs very close to the leading edge of the plate. This is also shown in calculations. Identical results for the distribution of heat transfer in turbulent boundary layer zones are achieved by both the test and the calculation. The

influence of wall cooling in turbulent boundary layers is thus verified by applied profile transformations in a very accurate manner.

The tangential stress coefficients for the heat transfer coefficients during high free stream turbulence and variable wall cooling, as described in Illustration 6.11, and for an additional adiabatic situation (flow conditions 1.1, 3, 4 from Table 5.1) are shown in Illustration 6.12. The decreasing Reynolds number is a contributing factor to the increase of c_f -values with increasing wall cooling. The calculated matrices are in agreement with the test results. In all cases, variations are less than 10%.

(164

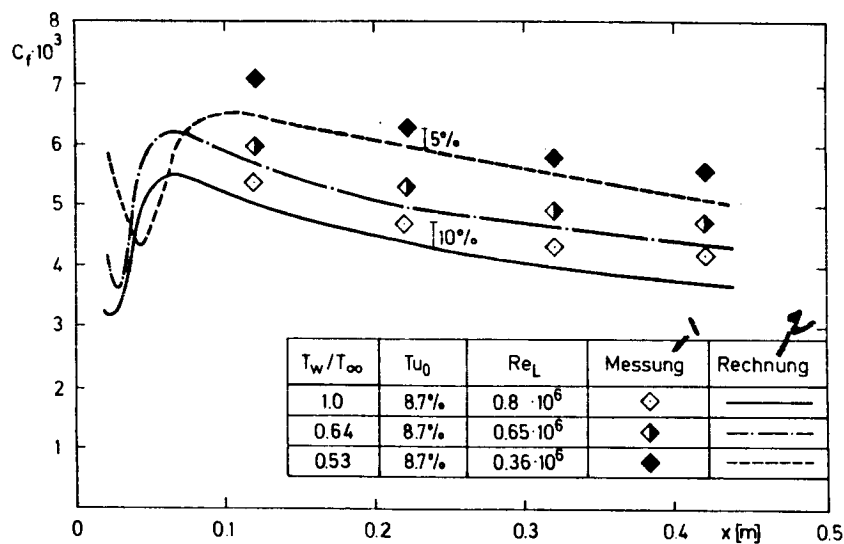


1 - test; 2 - calculation

Illustration 6.11: Heat Transfer and Boundary Layer Development with Varying Wall Cooling and High Free Stream Turbulence ($dp/dx = 0$)

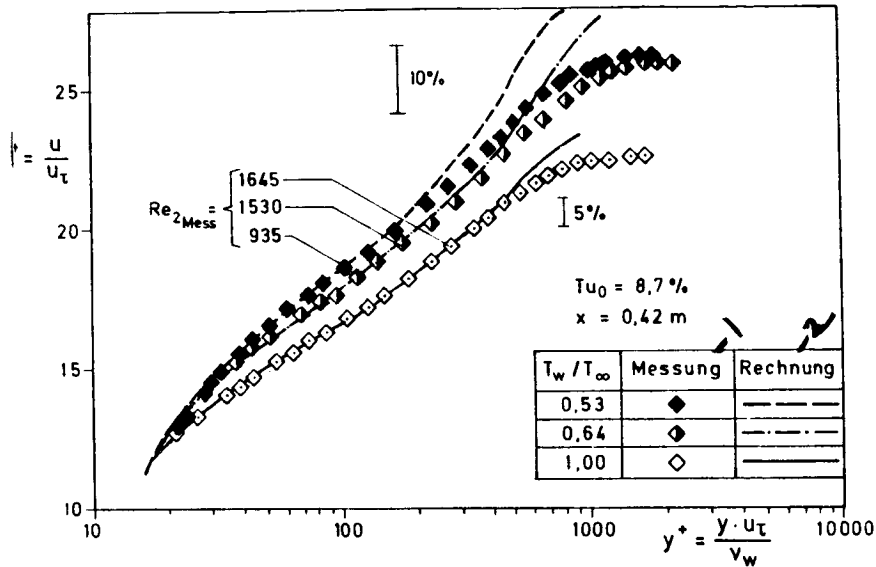
The velocity and temperature profiles shown in Illustrations 6.13 and 6.14 must be assigned to the c_f -values in test surface 4 ($x = 0.42$ m). Illustration 6.13 shows the influence of wall cooling on the logarithmic wall theory. Due to varying density and viscosity as a function of the wall distance, the area of the wall theory obtains greater y^+ - and u^+ - values if, as shown in Illustration 6.13, these coordinates are derived from material data at the wall. This event is simulated by the calculation program in an almost perfect manner, which is proof of the practicality of applied profile transformations.

(165



1 - test; 2 - calculation

Illustration 6.12: Resistance Coefficients in Unaccelerated Flows with Varying Wall Cooling



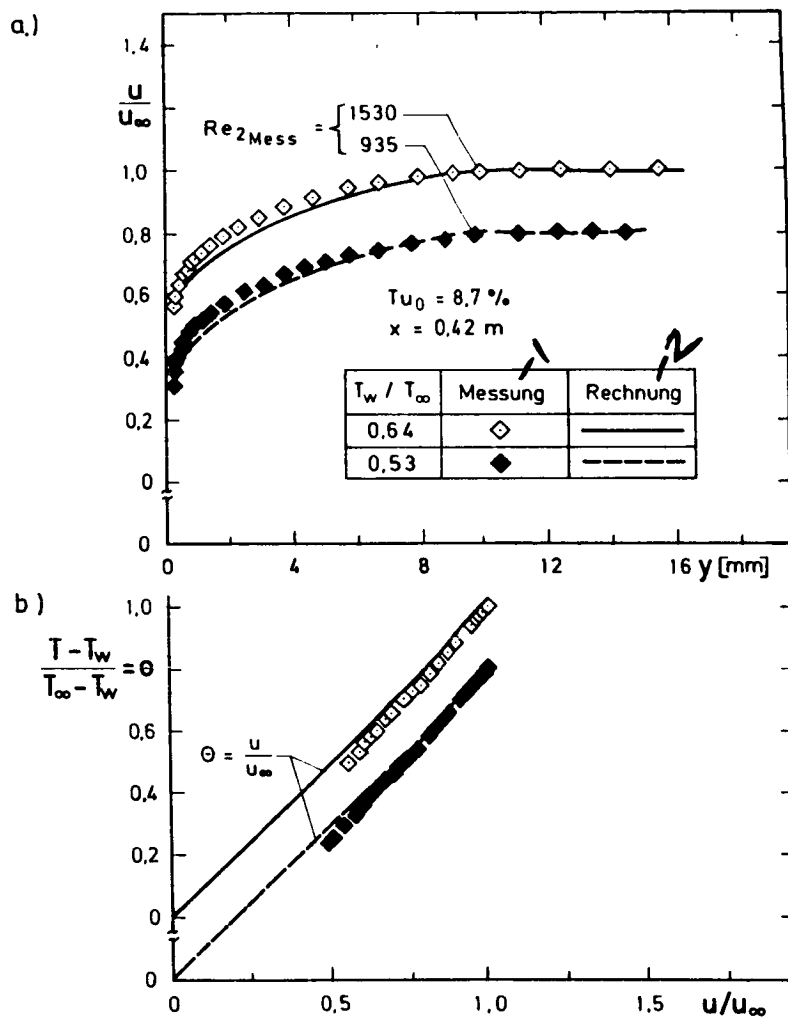
1 - test; 2 - calculation

Illustration 6.13: Dimensionless Turbulent Velocity Profiles with and without Wall Cooling

The only differences (max. 10 %) exist in the wake area. This flow area is mainly determined by the material data at the edge of the boundary layer. This is not considered in the material value determination of the entire boundary layer, which was introduced by the transformation in the profile equations. Because of this, greater deviations are shown on the edges of the boundary layer. Another factor, which contributes to an over-emphasis of the wake area, are the friction coefficients c_f , which are calculated too low by up to 10% (see Illustration 6.12, $x = 0.42$ m). Because of this, excessive edge values u_δ^+ are used for calculating the profile matrix (see profile equations, Chapter 6.3). This applies even in situations without wall cooling ($T_w / T_\infty = 0.42$ m). (166)

The two velocity matrices for cooled situations are shown again in Illustration 6.14a, where the wall distance was not standardized. Despite the deviations in the boundary layer's external area observed in Illustration 6.13, which is a very sensitive semi-logarithmic illustration, turbulent profiles are in good agreement with the tests.

The respective temperature matrices are shown in Illustration 6.14b in a dimensionless form and as a function of velocity. The calculated matrices are in agreement with a linear distribution which, with an incompressible flow ($T_w/T_\infty \rightarrow 1.0$, $Ma \rightarrow 0$) and a Prandtl number of 1, forms an asymptote. The measured deviation from this ideal temperature theory is not substantiated by the integral procedure with given profile equations. However, as shown by the applicable Stanton numbers in Illustration 6.11, this imperfection does not have an appreciable negative affect on the quality of calculated heat transfer.



1 - test; 2 - calculation

Illustration 6.14: Velocity and Temperature Profiles with High Wall Cooling

6.7.2 Flows with Pressure Gradients

In my experiment, I studied boundary layers under the influence of two different pressure gradient matrices, which simulate the circulation on the pressure and vacuum sides of a turbine blade. The various pressure gradient matrices were superimposed with variations of the Reynolds number, free stream turbulence and wall cooling. In the following paragraphs, integral procedures will be used to re-calculate the characteristic flow situations.

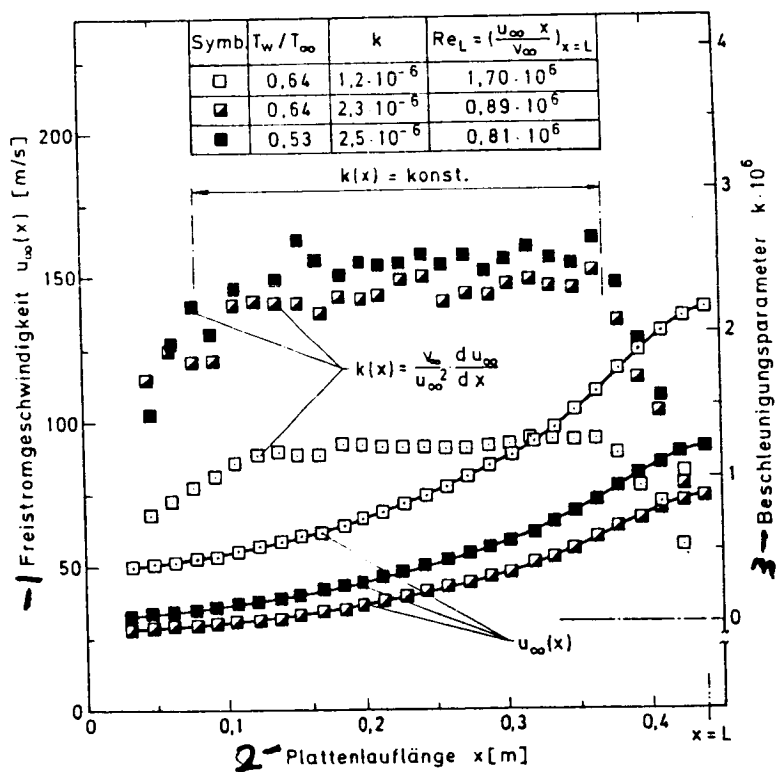
6.7.2.1 Comparative Calculations for Constant Free Stream Acceleration

Illustration 6.15 provides a summary of the test situations with almost constant free stream acceleration ($k(x) = \text{const.}$). It shows distributions obtained with contour 1 of the free stream velocity $u_\infty(x)$ and the acceleration parameter $k(x)$ for flow conditions with varying wall cooling ($T_w/T_\infty = 0.64$ and 0.53), the acceleration intensity ($k = 1.2 \times 10^{-6}$; 2.3×10^{-6} and 2.5×10^{-6}) and the Reynolds number of the plate's running length which, in Illustration 6.15, was determined at the flowoff conditions at the plate end. Additional information on these flows can be found in Table 5.1 (flow conditions 6, 7, 8). As in all other re-calculations, the turbulence intensity matrix in the free flow is given by the test data (see Chapter 5.2)

The measured Stanton numbers for $Re = 1.7 \times 10^6$ are, for various turbulence intensities, compared to model calculations in Illustration 6.16. In all cases, the calculation starts with $x = 0.02$ with an initial Reynolds number of $Re_2 = 112$. Using the Blasius relationship for laminar boundary layers without pressure gradients (equation 5.8), initial Reynolds numbers were also approximated in accelerated flow conditions. The best agreement is shown in Illustration 6.16 for the test situation with maximum free stream turbulence, $Tu_0 = 11\%$. Despite acceleration ($k = 1.2 \times 10^{-6}$)

the turbulence causes the boundary layer reversal to occur very early, which is simulated by the calculation. There is also a very good agreement between test and calculation data in the turbulent boundary layer section. The calculation predicts a short laminar boundary layer matrix with an inlet turbulence of 4%, while the test already shows a reversal flow at that location (see Illustration 5.46a). The differences between test and calculation are, as usual, minor in the following boundary layer area. In tests with a turbulence intensity of only 2.3%, the reversal to turbulent flow occurs very slowly and seems to be completed at the plate end. The reason for this is the superimposed acceleration.

(169



- 1 - free stream velocity;
- 2 - running length of the plate;
- 3 - acceleration parameters

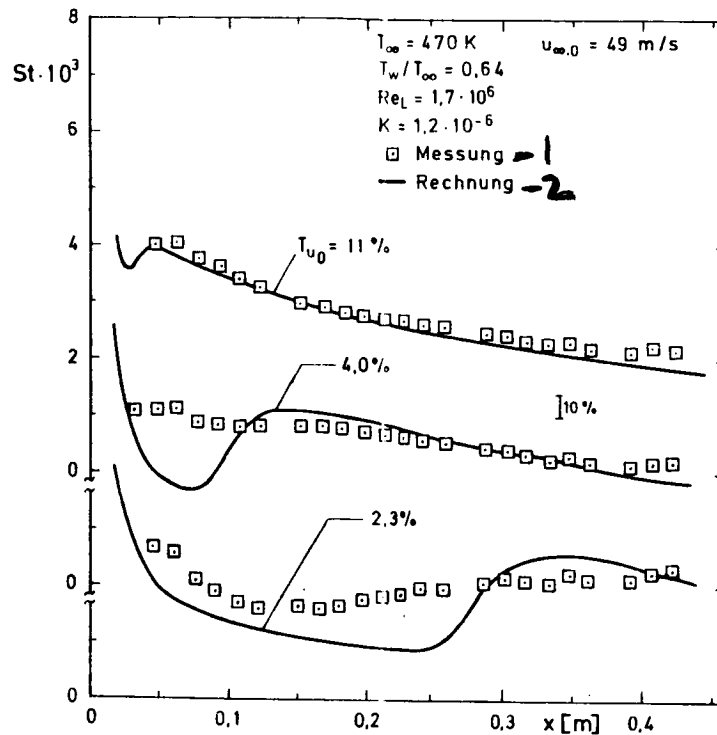
Illustration 6.15: Velocity and Acceleration Parameter Matrices of Re-Calculated Test Cases with Contour 1 (Contour on the 'Pressure Side')

In this case, the calculation predicts a reversal initiation further down-stream, which is followed by a relatively fast reversal process. This is the reason for deviations between test and calculation results in the area between $x = 0.15$ m and 0.26 m.

Illustration 6.17 shows analogous tests with higher acceleration (or smaller Reynolds numbers, see Illustration 5.46b) with $k=2.3 \times 10^{-6}$. The more intense acceleration causes a stronger attenuation of the turbulence movement in the boundary layer. Because of this, there is no reversal with minimum external turbulence intensity. The calculation is in excellent agreement with this behavior. With a free stream turbulence of 4%, a balance is shown in the test between the destabilizing effect of external turbulence and the stabilizing influence of free stream acceleration, which results in constant Stanton numbers throughout large areas of the plate. In contrast to this, the calculation model indicates a discrete reversal process. This causes deviations from the measured Stanton numbers of up to 15%.

(170

Turbulent boundary layer flows are again present throughout the entire test area with maximum free stream turbulence, $Tu_0 = 11\%$. This boundary layer behavior is described by the integral procedure with good accuracy.

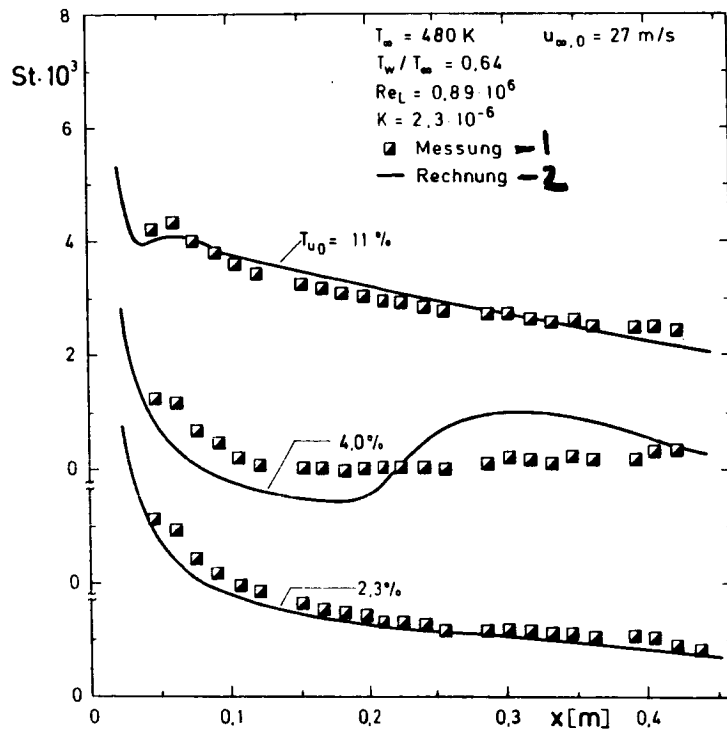


1 - test; 2 - calculation

Illustration 6.16: Stanton Number Matrix in Accelerated Flows
(Contour on the 'Pressure Side', high Reynolds Number)

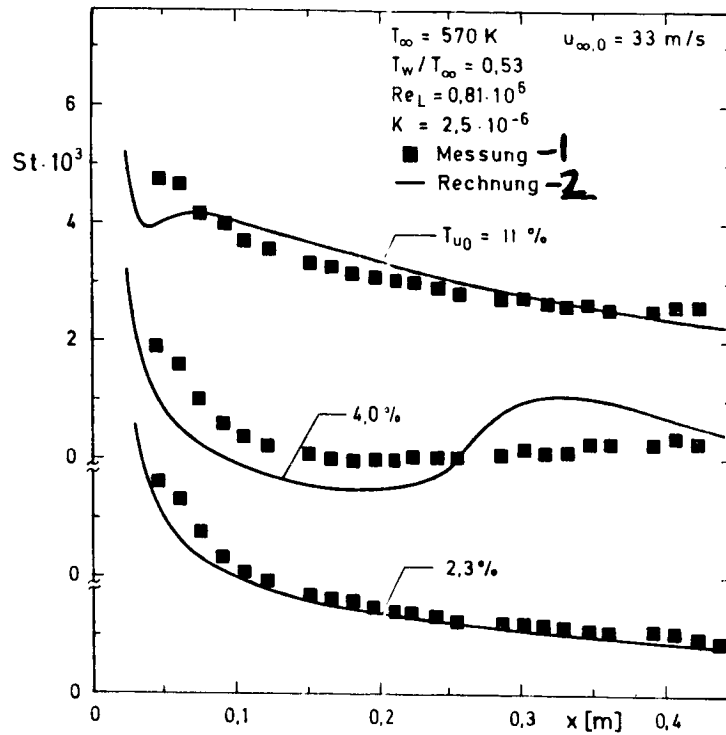
A situation similar to Illustration 6.17, with identical flow turbulence intensities is shown in Illustration 6.18. The Reynolds number - and therefore the acceleration intensity $k(x)$ matrix - is, compared to the above described situation, almost identical (see Illustration 6.15). The only difference is the increased cooling ($T_w/T_\infty = 0.53$ versus 0.64). With this flow parameter constellation there is no boundary layer or reversal behavior change compared to the test with lower wall cooling ($T_w/T_\infty = 0.64$; Illustration 6.17). This phenomenon was discussed in detail in Chapter 5.5.2 in the analysis of test results. The reason for it is that the wall cooling does not result in any noticeable boundary layer stabilization. The calculation is in accordance with this reversal

theory. All other comparative calculations show the same reversal behavior as with low cooling intensity ($T_w/T_\infty = 0.64$; Illustration 6.17). The best agreement between test and calculation is again with minimum and maximum free stream turbulence ($Tu_0 = 2.3$ and 11%), while with medium flow turbulence of $Tu_0 = 4.0\%$, the above weaknesses of the reversal calculation can again be observed. (172)



1 - test; 2 - calculation

Illustration 6.17: Stanton Number Matrix in Accelerated Flows (Contour on the 'Pressure Side', Low Reynolds Number)



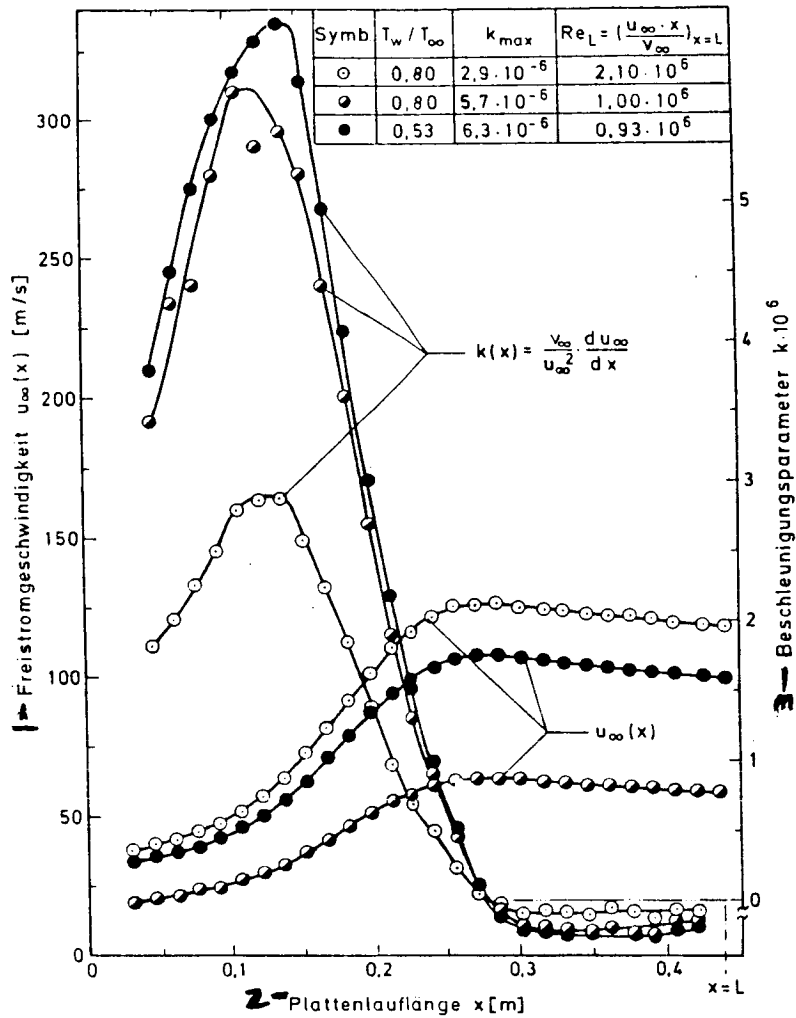
1 - test; 2 - calculation

Illustration 6.18: Stanton Number Matrix in Accelerated Flows with High Wall Cooling (Contour 1, Low Reynolds Number)

6.7.2.2 Comparative Calculations for Flows Accelerated on the Vacuum Side

The distribution of the external velocity and the acceleration parameters $k(x)$ of this example are summarized in Illustration 6.19. Again, we must distinguish between three situations: a test with a high Reynolds number ($Re_L = 2.1 \times 10^6$) and a temperature ratio of $T_w/T_\infty = 0.8$; another test with $T_w/T_\infty = 0.8$ but reduced Reynolds number ($Re_L = 1.0 \times 10^6$); and an experiment with the lowest Reynolds number $Re_L = 0.93 \times 10^6$ and intense wall cooling of $T_w/T_\infty = 0.53$ (see Table 5.1, test numbers 9, 12, 13).

(173)

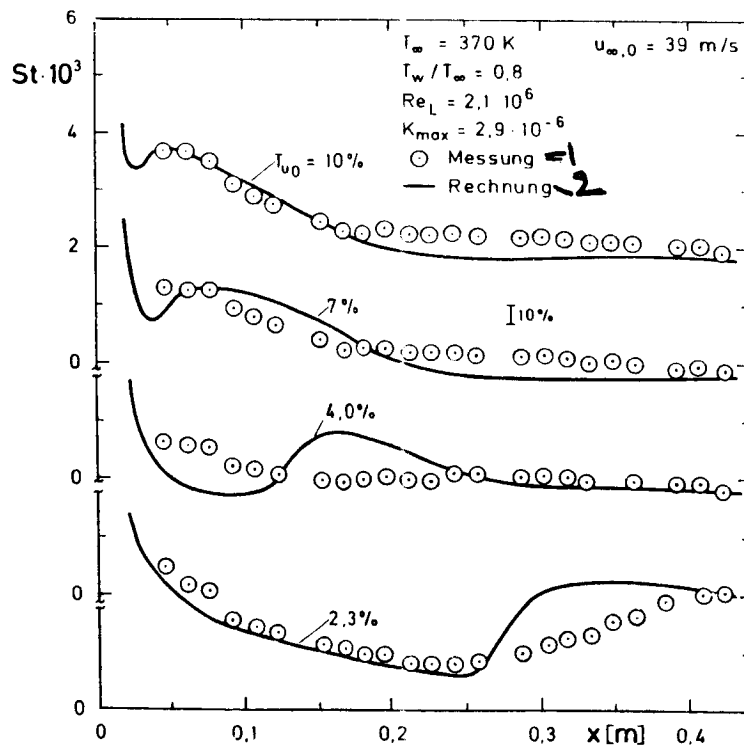


- 1 - free stream velocity
- 2 - running length of the plate
- 3 - acceleration parameter

Illustration 6.19: Velocity and Acceleration Parameter Matrices of Re-Calculated Test Cases with Contour 2 ('Vacuum Side')

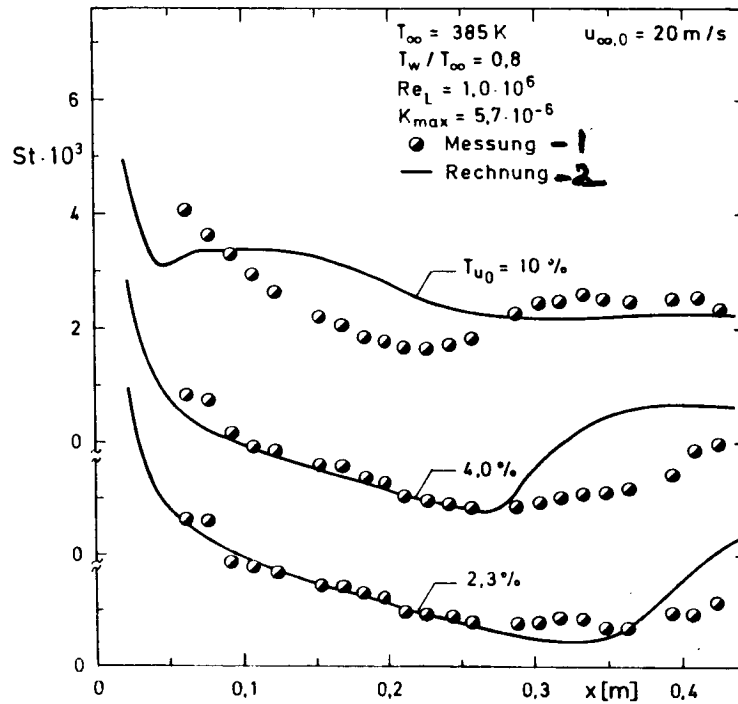
In the last two cases, the relaminization criteria of $k \approx 3 \times 10^{-6}$ is clearly exceeded by the acceleration intensities $k_{\max} = 5.7 \times 10^{-6}$ and $k_{\max} = 6.3 \times 10^{-6}$. Such intensive acceleration conditions are very typical for actual gas turbine blade circulation. They place highest demands on the calculation program.

Illustration 6.20 compares model calculations with high Reynolds numbers to tests where the flow turbulence intensity of 2.3% was increased to 10%. The alternating effects of pressure gradients with transitional events are described in an accurate manner. The reversal initiation is accurately shown with minimum turbulence intensity, $Tu_0 = 2.3\%$, while the following reversal process occurs more rapidly in the test. With 4.0% flow turbulence, differences exist only in the forward plate section ($x < 0.2$ m). Again, they can be attributed to the fact that the test shows reversal behavior of the boundary layer starting with the beginning of the plate, while the laminar calculation shows the reversal at a later point, after a distinct laminar initiation.



1 - test; 2 - calculation

Illustration 6.20: Stanton Number Matrix in Highly Accelerated Flows (Contour on the 'Vacuum Side' High Reynolds Number)



1 - test; 2 - calculation

Illustration 6.21: Stanton Number Matrix with Highly Accelerated Flow (Contour on the 'Vacuum Side', Low Reynolds Number)

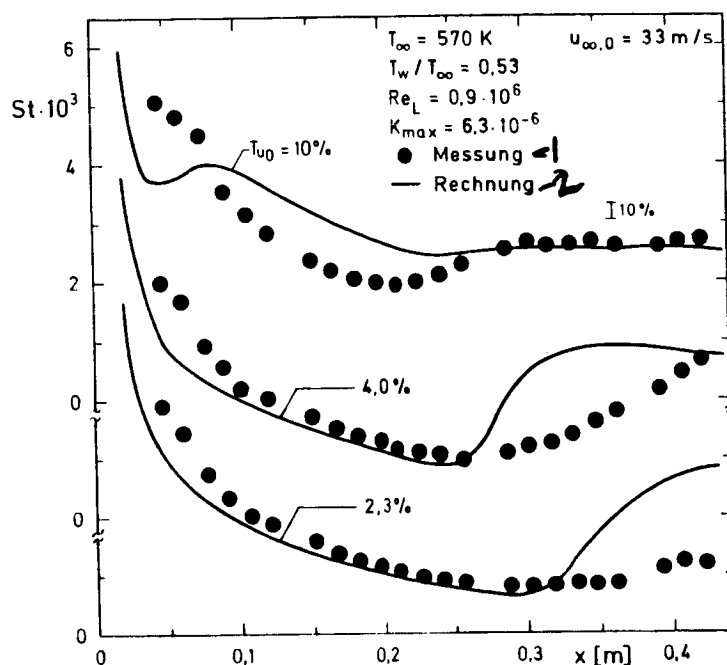
In the cases with maximum flow turbulence ($Tu_0 = 7\%$ and 10%), there is satisfactory agreement with the test. However, compared to previous cases with and without constant acceleration, there are certain inaccuracies in the turbulent flow areas. There are maximum deviations of 10-15%.

In cases of maximum acceleration with $k_{\max} = 5.7 \times 10^{-6}$, Illustration 6.21, even more distinct effects of the pressure gradient can be observed. With the lowest turbulence intensity of 2.3%, the turbulence in the accelerated flow area is attenuated so much that, even in the delayed area ($x > 0.26$ m), the reversal is only gradual. The reversal initiation, which is located near the end of the plate, is accurately reproduced by the calculation model. However, the reversal to the turbulent condition occurs somewhat earlier in the calculation. A similar behavior is observed with a higher turbulence intensity of 4.0%. The test with the highest free stream turbulence, $Tu_0 = 10\%$, represents the very complicated flow situation where, starting with the beginning of the plate, there is a quasi-stable laminar-turbulent intermediate condition during the entire acceleration phase. In contrast to the laminar situation, the heat transfer is, in this case, higher by 100 percent or more. This boundary layer behavior was discussed and analyzed in detail in Chapter 5.6 and Illustration 5.47b. Due to a lack of accurate initiation profiles (this starting location was not permissible for profile tests), the applicable calculation was begun in a laminar manner, i.e. contrary to the experimental result. The same applies to all other cases with low free stream turbulence in Illustration 6.21. The laminar boundary layer initiation of the calculation is followed by a discrete reversal area, which is completed after approximately 100 mm of plate running length and which, down-stream of this location, results in heat transfer coefficients which are exclusively turbulent. The discrepancy between test and calculation is up to 50% in the accelerated flow section. However, a careful adjustment of the calculation (6.57), which describes the intermittency matrix, to the given flow behavior, will result in better agreement. Because no general criteria could be found for the reproduction of these complex boundary layer events (this requires comprehensive boundary layer tests), I did not perform such an expansion of the calculation program. It should be noted, however, that the connection between turbulence model and intermittency function, which was used in the calculation procedure, is the best method for carrying out such a procedure.

(176

The spirit of the comparison described in Illustration 6.21 can be applied to Illustration 6.22. In Illustration 6.22, the calculation program is examined for an identical Reynolds number, and thus the same acceleration conditions, but with far more intensive wall cooling ($T_w/T_\infty = 0.53$ versus $T_w/T_\infty = 0.8$). As expected, this final example is in agreement with the test. In addition, the calculation shows the same boundary layer behavior as in the previous situation with low wall cooling (Illustration 6.21). The boundary layer behavior which, as shown by the calculation, confirms again that a modelling of the reversal with wall cooling and external turbulence is only performed correctly when, as in our program, the reversal Reynolds number, which causes the laminar-turbulent boundary layer transition, is applied to the free stream viscosity and not to a viscosity computed from a reference temperature.

(177



1 - test; 2 - calculation

Illustration 6.22: Heat Transfer Coefficients in Highly Accelerated and Highly Cooled Boundary Layer Flow (Contour 2)

This chapter described the calculation of transitional boundary layers, both with and without pressure gradients with varying free stream turbulence and varying wall cooling. The examples introduced above showed that the influences of these parameters are accurately recorded by the newly developed integral procedure. The best agreement between test and calculation is always in turbulent boundary layer sections. There are differences in the prediction of the reversal length, if the flow has pressure gradients (acceleration) and low turbulence intensities. In this case, a more careful adjustment of the reversal model should result in better agreement. In some cases with pressure gradient and increased flow turbulence, differences occurred with heat transfer coefficients at the beginning of the plate. They can, on the one hand, be attributed to the more rapid reversal behavior in the calculation model, and, on the other hand, to different initiation conditions. An initial laminar boundary layer was assumed in the calculation, while reversal conditions were already present in the tests. A more exact starting condition for the calculation was not possible, because the flow in this area was not accessible. Pertinent information on this subject is not available in literature. With similar flow situations, the calculation of cooled blade boundary layers presents identical starting value problems. Therefore, it should be the goal of further studies to analyze the velocity and turbulence structure in initial boundary layers, which are influenced by these external turbulences and pressure gradients.

(178

The remaining inaccuracies of the calculation program signify the present level of numeric boundary layer calculation. They should not be attributed to the selection of the calculation method - integral or differential procedures - but to the unreliability of present turbulence models. Even highly developed $k-\epsilon$ turbulence models, which were incorporated in differential procedures, are unable to give a better description of long reversal processes. This was clearly demonstrated by parallel calculations for the test situations in this chapter, i.e. the Lam-Bremhorst- $k-\epsilon$ turbulence model, which requires a great deal more effort (see [4, 110]). With an almost identical quality of the results in laminar and turbulent

boundary layer sections, the reversal length was predicted even more accurately with the simple integral procedure and its turbulence model.

7. SUMMARY

(179)

This dissertation discussed the influences of free stream turbulence, wall cooling and pressure gradients on the heat transfer and the boundary layer development in cooled surfaces. In order to determine the significance which is to be attributed to these parameters, individually or when superimposed, comprehensive experimental and theoretical studies were conducted with transitional boundary layers. The reasons for this were a lack of basic knowledge and insufficient data on heat transfer and boundary layer behavior in cooled gas turbine blades.

The experiments, which consisted of an analysis of local heat transfer and a study of applicable boundary layer profiles, were performed in an even boundary layer tunnel. Free stream turbulence intensities varied between 1.6 and 11 %. In order to determine the influence of pressure gradients, accelerated flows were generated. Expressed by the acceleration parameter k , they exist in the blade circulation of gas turbines with:

$$k = \frac{v_w}{u_\infty^2} \cdot \frac{du_\infty}{dx} = 1,2 - 6,3 \cdot 10^{-6}$$

To simulate realistic turbine conditions, a step-by-step increase of the free stream temperature was performed, which resulted in the temperature ratios $T_w/T_\infty = 1.0; 0.8; 0.64; \text{ and } 0.53$.

The test results confirm and supplement effects as they are known from previous studies. These studies were conducted with mostly low free stream turbulence, low free stream acceleration and without consideration to wall cooling. Based on this and by including turbine-like flow conditions, additional problems were solved which are important for heat transfer and boundary layer

development in cooled gas turbine blades. This includes the following: the influence of wall cooling on the laminar-turbulent reversal process; the significance of wall cooling in turbulent boundary layers with free stream turbulence; and boundary layer behavior in flows with very intensive acceleration and high external turbulence.

The tests show that, in boundary layers with free stream turbulence, even the most intensive wall cooling will not result in a change of reversal behavior. Consequently, the influence of external turbulence dominates over the effect of wall cooling, which stabilizes the boundary layer.

Heat transfer and boundary layer tests further revealed that, in turbulent boundary layers, the effects of free stream turbulence are not dependent on the wall cooling. The deformation of boundary layer profiles caused by external turbulence and the resulting increase of wall tangential stress and heat transfer are identical with events at the uncooled wall.

Without changing the effects of free stream turbulence, the wall cooling results in a deformation of the boundary layer profiles and an increase of the heat transfer. The test with maximum cooling in laminar boundary layers resulted in a heat transfer increase of up to 20%. Under the same conditions, local heat transfer coefficients increase by only about 10-12% in the area of the turbulent boundary layer.

A study of the influences of negative pressure gradients revealed that, in a combination of high free stream turbulence and high free stream acceleration - which is typical for gas turbine blades - there are flow situations where, over large areas, the boundary layer obtains an almost stable laminar-turbulent intermediate condition. In contrast to laminar flow, these conditions result in drastic increases in the heat transfer (up to 100%). A closer analysis of this event showed that the occurrence of stable laminar-turbulent intermediate conditions is a function of high free stream

(180

intensities, intensive pressure gradients and the acceleration path along the wall. Because of its complexity and the present level of available information, this boundary layer flow cannot be accurately described and characterized. Further boundary layer studies are therefore recommended.

In order to reconstruct experimental results in a theoretical manner, a numerical calculation procedure was developed which is based on an expanded integral method. As with differential procedures, this new procedure conducts a separate calculation of flow and temperature boundary layers. This eliminates the use of analogy equations for the determination of heat transfer, which is common practice with integral procedures. The velocity and temperature distributions in the boundary layer are established with suitable profile equations. These boundary layer matrices are the only flexibility limitation as compared to field methods. A single equation turbulence model, which was further developed in this dissertation, was used - in connection with a mixing path equation - to describe the turbulent exchange events in the boundary layer. The results of the numeric calculation are in good agreement with experimental data. Re-calculations show that the influences of free stream turbulence, wall cooling and pressure gradients are accurately represented. The goal of assigning the efficiency of field methods to integral procedures, which are required for an accurate prediction of the heat transfer in cooled gas turbine blades, was thereby achieved.

(181)

The best agreement between calculation and test is in flows with high external turbulence. Reversal initiation and reversal length are very accurately described in most cases. This is mainly due to the expanded reversal model. There are deviations in the calculation of the reversal length with accelerated flow and a low free stream turbulence. Under these flow conditions, the reversal process is faster than in the test. An improvement of the agreement between calculation and test requires additional fine-tuning of reversal and turbulence modelling.

In summary, it can be stated that the above studies resulted in discoveries on the influence of free stream turbulence, pressure gradients and wall cooling, which were unknown before and which expand our understanding of heat transfer and boundary layer behavior on cooled surfaces, especially on cooled gas turbine blades. Newly developed calculation procedures provide theoretical support for experimental findings. The results can be used in the design of cooled gas turbine blades.

B. REFERENCES

(182)

- [1] Rudey, R.a., Graham, R.w.: A Review of NASA Combuster and Turbine Heat Transfer Research, ASME Paper 84-GT-113, presented at ASME GT. Conf. 1984, Amsterdam
- [2] Hennecke, D.K.: Heat Transfer Problems in Aero-Engines. Paper presented at XIV ICHMT Symposium on "Heat and Mass Transfer in Rotating Machinery", 30 Aug - 3 Sept 1982, Dubrovnik, Yugoslavia
- [3] Nealy, D.A., Mihelc, M.S., Gladden, H.J.: Measurement of Heat Transfer Distribution Over the Surface of Highly Loaded Turbine Nozzle Guide Vanes. ASME Paper No. 83-GT-53, presented at ASME Gas-Turbine Conference, Phoenix, Arizona, March 1983
- [4] Scheurer, H.: Entwicklung eines Verfahrens zur Berechnung zwei-dimensionaler Grenzschichten an Gasturbinenschaufeln (Development of a Procedure of Calculating Two-Dimensional Boundary Layers on Gas Turbine Blades) Diss. Inst. f. Fluid Mechanics, Univ. Karlsruhe, 1983
- [5] McDonald, H., Fish, R.W.: Practical Calculations of Transitional Boundary Layers, Int. J. Heat Mass Transfer, Vol. 16, 1973, pp. 1729-1744
- [6] Herring, H.J., Mellor, G.L.: A Computer Program to Calculate Laminar and Turbulent Boundary Layer Development. NASA CR 1564 Mar. 1970
- [7] Cebeci, T., Smith, A.M.O.: Analysis of Turbulent Boundary Layers. Academic Press, New York, 1974
- [10] Brown, A., Martin, B.W.: Heat Transfer to Turbine Blades with special Reference to the Effects of Mainstream Turbulence. ASME Papers No. 79-GT-26, Mar. 1979
- [11] McNally, W.D.: FORTRAN - Program for Calculating Compressible Laminar and Turbulent Boundary Layers in Arbitrary Pressure Gradients. NASA TN D-5681, 1970.
- [12] Nealy, D.H.: Some Effects of Variable Surface Temperature on Heat Transfer to a Partially Porous Flat Plate. ASME Journal of Engineering for Power, Oct. 1973, pp. 317-325.
- [13] Gauntner, D.J., Sucec, I.: Method for Calculating Convective Heat Transfer Coefficients over Turbine Vane Surfaces. NASA TP-1134, 1978
- [14] Hennecke, D.K.: A Calculation for the External Heat Transfer to Turbine Blades. AGARD-AG-164, 1972, pp. 265 - 276.

- [15] Arnal, D., Julien, J.C., Michel, R.: Analyse Experimentale et Calcule de l'Apparition et du Developpement de la Transition de la Couche limite (Experimental and Calculation Analysis of the Appearance and Development of Transitional Boundary Layers). AGARD-CP-224, 1977, pp 13-1 - 13-18
- [16] Schubauer, G.B., Skramstad, H.K.: Laminar-Boundary-Layer Oscillations and Transition on a Flat Plate. NACA-Report No. 909, 1943 (183)
- [14] Schubauer, G.B., Klebanoff, P.S.: Contributions on the Mechanics of Boundary-Layer Transition. NACA Report 1289, 1955
- [18] Klebanoff, P.S., Tidstrom, K.D., Sargent, L.M.: The Three-Dimensional Nature of Boundary-Layer Instability. J. Fluid Mech., Vol. 12, 1961, pp.1-34
- [19] Tani, I.: Boundary-Layer Transition. Ann. Rev. Fluid Mech. Vol. 1, 1969, pp. 169-196
- [20] Morkovin, M.V.: Instability, Transition to Turbulence and Predictability. AGARD-AG-236, 1978
- [21] Reshotko, E.: Boundary-Layer Stability and Transition. Ann. Rev. Fluid Mech., Vol 8, 1976, pp. 311 - 349
- [22] Schlichting, H.: Grenzschichttheorie (Boundary Layer Theory), 8th ed., 1982, G. Braun Publishing House, Karlsruhe
- [23] Eppler, R., Fasel, H.: Laminar-Turbulent Transition. Springer Publishing House, Berlin, 1980
- [24] Ghon, H.: Literaturstudie zum laminar-turbulenten Umschlag in ebenen, zweidimensionalen Wandgrenzschichten (Literature Study of the Laminar-Turbulent Reversal in Flat, Two-Dimensional Wall Boundary Layers). Thesis Nr. 154, 1980, Inst. for Fluid Mechanics, Prof. Dr. S. Witting, Engineer, Univ. Karlsruhe, Sponsor: G. Scheuerer, Engineer
- [25] Owen, F.K.: Transition Experiments on a Flat Plate at Subsonic and Supersonic Speeds. AIAA Journal, 1970 Vol. 8 No. 3, pp. 518 - 523
- [26] Dhawan, S., Narashima, R.: Some Properties of Boundary Layer Flow during the Transition from Laminar to Turbulent Motion. J. Fluid Mech., Vol. 3, 1958, pp. 418 - 436
- [27] Gad-El-Hak, M., Backwelder, R.F., Riley, J.J.: On the Growth of Turbulent Regions in Laminar Boundary Layers. J. Fluid Mach., 1981, Vol. 110, pp. 73 - 95
- [28] William, W.W.: Survey and new Measurements of Turbulent Structure near the Wall. The Phys. of Fluids, 1977 Pt. 2, pp. S9 - S21

- [29] Brown, G.L., Thomas, A.S.W.: Large Structure in a Turbulent Boundary Layer. The Phys. of Fluids, 1977, No. 10, Pt 2, pp. S243 - S252
- [30] Bradshaw, P.: Turbulence. Springer Publishing House, 1976
- [31] White, B.R.: Low-Reynolds-Number Turbulent Boundary Layers. Trans. ASME, 1981, Vol 103, pp. 624 - 630
- [32] Murlis, N.J., Tsai, H., Bradshaw, P.: The Structure of Turbulent Boundary Layers at Low Reynolds Numbers. J. Fluid Mech., 1982, Vol 122, pp. 13 - 56
- [33] Murlis, B.J.: The Structure of a Turbulent Boundary at Low Reynolds Number. Ph.-D.-Thesis, June 1975, Department of Aeronautics, Imperial College of Science and Technology, University of London (184)
- [34] Head, M.R., Bandyopadhyay, P.: Slow Visualization of Turbulent Boundary Layer Structure. AGARD-CP-271, 1979, pp. 25-1-11
- [35] Junkhan, G.H., Serovy, G.K.: Effects of Free-Stream Turbulence and Pressure Gradient on Flat-Plate Boundary Layer Velocity Profiles and on Heat Transfer. Trans. ASME Journal of Heat Transf., May 1967
- [36] Blair, M.F., Werle, M.J.: The Influence of Free-Stream Turbulence on the Zero Pressure Gradient Fully Turbulent Boundary Layer. United Technologies Research Center, East Hartford, CT, Rept. No. R80-914388-17, 1981
- [37] Blair, M.F., Werle, M.J.: Combined Influence of Free-Stream Turbulence and Favorable Pressure Gradients on Boundary Layer Transition and Heat Transfer. United Technologies Research Center, East Hartford, CT, Rept.No. R81-914388-17, 1981
- [38] Blair, M.F.: Influence of Free-Stream Turbulence on Boundary Layer Transition in Favorable Pressure Gradients. ASME-Paper 82-GT-4, published at ASME Gas Turbine Conference, London, Apr. 1982
- [39] Blair, M.F.: Influence of Free-Stream Turbulence on Turbulent Boundary Layer Heat Transfer and mean Profile Development. Trans ASME, Journal of Heat Transf. Vol 105, Febr. 1983, Part 1 and 2
- [40] Kestin, J., Maeder, P.F., Wang, H.E.: Influence of Turbulence on the Transfer of Heat from Plates with and without a Pressure Gradient. Int. J. Heat Transfer, Vol 3, pp. 133-154, Pergamon Press 1961

- [41] Büyüktür, H.R., Kestin J., Maeder P.F.: Influence of Combined Pressure Gradient and Turbulence on the Transfer of Heat from a Plate. Int J. Heat Mass Transfer, Vol. 7, pp. 1175-1186, Pergamon Press 1964
- [42] V.Driest, F.R., Blumer, C.B.: Boundary Layer Transition: Freestream Turbulence and Pressure Gradient Effects. AIAA J. Vol. 1, No. 6, June 1963, pp. 1303-1306
- [43] Hall, D.J., Gibbings, J.C.: Influence of Stream Turbulence and Pressure Gradient upon Boundary Layer Transition. J. Mech. Eng. Science, Vol 14, No. 2, 1972, pp. 134-146
- [44] Cosigny, H., Chan, C., Richards, B.E.: The Effect of Pressure Gradient and External Turbulence on Heat Transfer to a Cold Flat Plate. Report ART-7902 HC-CKC-BER/NT, 1979, von Karman Institute, Rhode Saint Genese, Belgium
- [45] Abu-Ghannam, B.J., Shaw, R.: Natural Transition of Boundary Layers -The Effects of Turbulence, Pressure Gradient and Flow History. T.N., Turbomachinery Section, Department of Mechanical Engineering, University of Liverpool, Apr. 1979 (185)
- Abu-Ghannam, B.J.: Boundary Layer Transition in Relation to Turbo Machinery Blades. Univ. of Liverpool, Liverpool, 1979
- [46] Kline, S.J., Lisin, A.V., Waitman, B.A.: Preliminary Experimental Investigations of Effect of Free-Stream Turbulence on Turbulent Boundary Layer Growth. NASA TN D-368 Mar 1960
- [47] Charnay, G., Comte-Bellot, G., Mathieu, J.: Development of a Turbulent Boundary Layer on a Flat Plate in an External Turbulent Flow. AGARD-CP-93, 1972, pp. 27.1-10
- [48] Huffman, G.D., Zimmermann, D.R., Bennet, W.A.: The Effect of Free-Stream Turbulence Level on a Turbulent Boundary Layer. AGARD-CP-164, 1972, pp. 91-115
- [49] McDonald, H., Kreskovsky, J.P.: Effect of Free Stream Turbulence on the Turbulent Boundary Layer. Int. J. Heat Mass Transfer, Vol. 17, pp. 705-716, Pergamon Press 1974
- [50] Evans, R.L.: Free Stream Turbulence Effects on the Turbulent Boundary Layer. Aeronautical Research Council, C.P. No. 1282, Cambridge University, 1974
- [51] Green, J.E.: On the Influence of Free Stream Turbulence on a Turbulent Boundary Layer, as it relates to Wind Tunnel Testing at Subsonic Speeds. AGARD Report 602, 1973

- [52] Robertson, J.M., Holt, C.F.: Stream Turbulence Effects on Turbulent Boundary Layers. J.Hydraulics Div., Proc. ASCE, Vol. 98, HY6, 1972
- [53] Bradshaw, P.: Effects of Free-Stream Turbulence on Turbulent Shear Layers. Imperial College Aero Report 74-10, and ARC 35648, 1974
- [54] Simonich, J.C., Bradshaw, P.: Effect of Free-Stream Turbulence on Heat Transfer through a Turbulent Boundary Layer. Trans ASME, J. Heat Transfer, Vol. 100, 1978, pp. 671-677
- [55] Bradshaw, P.: Effect of Free-Stream Turbulence on Boundary Layers. Proc. AFOSR-HTTM-STANFORD, Conf. 1980, Vol. 1, pp. 86-90, Dep. Mech. Eng., Stanford, California
- [56] Hancock, P.E.: Effect of Free-Stream Turbulence on Turbulent Boundary Layers. PhD Thesis, Imperial College, London 1980
- [57] Pedisius, A.A., Kazimekas, P.-V.A., Slanciankas, A.A.: Heat Transfer from a Plate to a High Turbulence Air Flow. Heat Transfer - Soviet Research, Vol. 11, 1979, pp. 125-134
- [58] Meier, H.U., Kreplin, H.P.: Influence of Free-Stream Turbulence on Boundary Layer Development. AIAA Journal, Vol. 18, 1980, pp. 11-15
- [59] Hancock, P.E., Bradshaw, P.: The Effect of Free Stream Turbulence on Turbulent Boundary Layers. J. Fluids Eng., Vol. 105, 1983, pp. 284-289
- [60] Raghunathan, S., McAdam, R.J.W.: Freestream Turbulence Effects on Attached Subsonic Turbulent Boundary Layers. AIAA Journal, Vol. 21, No. 4, 1983, pp. 503-08
- [61] Edwards, A., Furber, M.N.: The Influence of Free Stream Turbulence on Heat Transfer by Convection from an Isolated Region of a Plane Surface in Parallel Air Flow. Proc. Inst. Mech. E170, pp. 941, 1956
- [62] Sugawara, S., Sato, T.: Heat Transfer on the Surface of a Flat Plate in Forced Convection. Mem. Fac. Engng, Kyoto, Vol. 14, pp. 21, 1952
- [63] Reynolds, W.C., Kays, W.M., Kline, S.J.: Heat Transfer in the Incompressible Boundary Layer with Constant Wall Temperature. Stanford Univ. Report, NACA Contr. Naw 6494, 1957
- [64] Kays, W.M.: Convective Heat and Mass Transfer. McGraw-Hill Publishing House, 1st ed., 1966

(186

- [65] Wehle, F., Brandt, F.: Einfluß der Temperaturabhängigkeit der Stoffwerte auf den Wärmeübergang an der laminar überströmten ebenen Platte (Influence of Temperature Dependency of Material Values on the Heat Transfer at a Flat Plate with Laminar Flow). Wärme- und Stoffübertragung, 16, 1982, pp. 129-136
- [66] Back, L.H.: Acceleration and Cooling Effects in Laminar Boundary Layers - Subsonic, Transonic and Supersonic Speeds. AIAA-Journal, Vol. 8, No. 4, pp. 794-802, 1970
- [67] Back, L.H., Cuffel, R.F., Massier, P.F.: Laminar, Transition, and Turbulent Boundary Layer Heat Transfer Measurements with Wall Cooling in Turbulent Air Flow through a Tube. Trans ASME Journal of Heat Transfer, 1969, pp. 477-487
- [68] Jischa, M.: Konvektiver Impulse-, Wärme- und Stoffaustausch (Convective Impulse, Heat and Material Exchanges). Vieweg Publishing House, 1982
- [69] Watson, R.D.: Wall Cooling Effects on Hypersonic Transitional/Turbulent Boundary Layers at High Reynolds Numbers. AIAA Journal Vol. 15, No. 10, 1977, pp. 1455-1461
- [70] Fischer, M.C.: Influence of Moderate Wall Cooling on Cone Transition at $M = 13.7$ in Helium. Journal of Spacecraft and Rockets, Vol. 10, 1973, pp. 282-283
- [71] White, F.M.: Viscous Fluid Flow. McGraw-Hill Publishing House, New York, 1974
- [72] Spalding, D.B., Chi, S.W.: The Drag of a Compressible Turbulent Boundary Layer on a Smooth Flat Plate with and without Heat Transfer. Journal of Fluid Mechanics, Vol. 18, Part 1, 1964, pp. 117-143
- [73] Gran, R.L., Lewis, J.E., Kubota, T.: The Effect of Wall Cooling on a Compressible Turbulent Boundary Layer. J. Fluid Mech. 1974, Vol. 66, Pt, 3, pp. 507-528
- [74] Lee, R.E., Yanta, W.J.: Velocity Profile, Skin Friction Balance and Heat Transfer Measurements of the Turbulent Boundary Layer at Mach 5 and Zero Pressure Gradient. Naval Ordnance Lab. TR-69-106, 1969 (187)
- [75] Chi, S.W., Spalding, D.B.: Influence of Temperature Ratio on Heat Transfer to a Flat Plate Through a Turbulent Boundary Layer in Air. AIChE, Proc. 3rd Int. Heat Transf. Conf. Vol. 2, 1966, pp. 41-49
- [76] Back, L.H., Cuffel R.F., Massier, P.F.: Effect of Wall Cooling on the Mean Structure of a Turbulent Boundary Layer in Low speed Gas Flow. Int. J. Heat Mass Transfer, Vol. 13, pp. 1029-1047, 1970

- [77] Fernholz, M.: Der Einfluß des Wärmeübergangs auf das Geschwindigkeitsprofil und die Wandreibung in turbulenten Wandgrenzschichten (The Influence of Heat Transfer on the Velocity Profile and Wall Friction in Turbulent Wall Boundary Layers). DFVLR research report FB 72-26, 1972, pp. 135-140
- [78] Still, K.M.: Wärme- und Stoffübertragung in turbulenten Strömungsgrenzschichten längs verdunsteter welliger Wasserfilme (Heat and Material Transfer in Turbulent Flow Boundary Layers of Evaporated, Rippled Water Films). Dissertation 1982, Inst. f. Fluid Mech., Univ. Karlsruhe
- [79] Eriksen, S., Wittig, S., Rüd, K.P.: Optical Measurements of the Transport Properties in a Highly Cooled Turbulent Boundary Layer at Low Reynolds Number. Proc. 4th Turbulent Shear Flow Conference 1983, Karlsruhe, W.G.
- [80] Erikson, S., Wittig, S., Dullenkopf, K.: The Application of LDA and LDF Anemometry to the Study of Boundary Layer Transport Properties under Gas Turbine Conditions. Proceedings of Int. Symposium on Application of Laser-Doppler Anemometry to Fluid Mechanics, Lisbon, July 1984
- [81] Reynolds, W.C., Kays, W.M., Kline S.J.: Heat Transfer in the Turbulent Incompressible Boundary Layer (I.Constant Wall Temperature). NASA-Memo 12-1-58 W
- [82] Kelnhöfer, W.J.: Wall Temperature and Prandtl Number Effects on Turbulent Boundary Layer Thickness and Shape Factors for Subsonic Compressible Gas Flow over a Flat Plate. Journal Eng. for Power, 1969, pp. 281-284
- [83] Rotte, J.C.: Die turbulente Grenzschicht an einer stark geheizten ebenen Platte bei Unterschallströmung (The Turbulent Boundary Layer on a Strongly Heated Flat Plate during Subsonic Flow). Wärme- und Stoffübertragung 7, 1974, pp. 133-144
- [84] Cheng, R.K., Ng, T.T.: Some Aspects on Strongly Heated Turbulent Boundary Layer Flow. Phys. Fluids, Vol. 25 (8), 1982, pp. 1333-1341
- [85] Rotta, J.C.: über den Einfluß der Mach'schen Zahl und des Wärmeüberganges auf das Wandgesetz turbulenter Strömung (On the Influence of the Mach Number and Heat Transfer on the Wall Theory of Turbulent Flows). Zeitschrift der Flugwiss. 7, 1959, Vol. 9, pp. 264-274
- [86] Kays, W.M., Moffat, R.J.: The Behaviour of Transpired Turbulent Boundary Layers. Excerpt from: Studies in Convection. Ed. B.E. Launder, Academic Press, 1975

- [87] Perry, A.E.: Turbulent Boundary Layer in Decreasing Adverse Pressure Gradient. J. Fluid Mech., 1966, Vol. 26, Part 3, pp. 481-506
- [88] Samuel, A.E., Joubert, P.N.: A Boundary Layer Developing in an Increasingly Adverse Pressure Gradient. J. Fluid Mech., 1974, Vol. 66, Part 3, pp. 481-505
- [89] Hatton: A.P., Eustace, V.A.: Heat Transfer through the Incompressible Turbulent Boundary Layer with Accelerating and Decelerating Flows. AICHE 1966, Proc. 3rd Int. Heat Transfer Conf., pp. 34-30
- [90] Boldman, D.R., Schmidt, J.F., Fortini, A.: Turbulence, Heat Transfer and Boundary Layer Measurements in a Conical Nozzle with a Controlled Inlet Velocity Profile. NASA TN D-3221, 1966
- [91] Cebeci, T., Smith, A.M.O.: Analysis of Turbulent Boundary Layers. Academic Press, New York
- [92] Lewis, J.E., Gran, R.L., Kubota, T: An Experiment on the Adiabatic Compressible Turbulent Boundary Layer in Adverse and Favourable Pressure Gradients. J. Fluid Mech. 1972, Vol. 51, Part 4, pp. 657-672
- [93] Clauser, F.H.: The Turbulent Boundary Layer. Advances in Applied Mechanics IV, Academic Press, New York, 1956
- [94] Rotta, J.: Turbulent Boundary Layer in Incompressible Flow. Progr. Aeron. Sci., Vol. 2, 1962, pp. 1-219
- [95] Townsend, A.A.: Equilibrium Layers and Wall Turbulence. J. Fluid Mech., Vol. 11, 1961
- [96] Szablewski, W.: Turbulente Grenzschichten in Ablösenähe (Turbulent Boundary Layers Close to Separation). ZAMM 49, Vol. 4, 1969, pp. 215-225
- [97] Coles, D.: The Law of the Wake in the Turbulent Boundary Layer. J. Fluid Mech., Vol. 1, 1956, pp. 191-226
- [98] McDonald, H.: The Effect of Pressure Gradient on the Law of the Wall in Turbulent Flow. J. Fluid Mech., 1969, Vol. 35, Part 2, pp. 311-336
- [99] Krisnamoorthy, V.: Effect of Turbulence on Heat Transfer in a Laminar and Turbulent Boundary Layer over a Gas Turbine Blade. ASME Paper No. 82-GT-146, presented at ASME Gas Turbine Conference, London, Apr. 1982
- [100] Rose, W.G.: Interaction of Grid Turbulence with a Uniform Mean Shear. J. of Fluid Mechanics. Vol. 44, part 4, 1970



- [101] Baines, W.D., Peterson, E.G.: An Investigation of Flow through Screens. Transaction of the ASME, Paper No. 50-A-23, 1951
- [102] Taylor, R.E.: High Temperature, High Pressure, 11. 1969
- [103] Dubbel: Taschenbuch für den Maschinenbau (Mechanical Engineering Handbook). 13th Ed., Springer Publishing House Berlin, Vol. 1, pp. 874, 1974
- [104] McMillan, F.A.: Experiments on Pitot-Tubes in Shear Flow. Gt. Brit. ARC Rep. and Mem. 3028, London, 1957 (189)
- [105] Quarmby, A., Das, H.: Displacement Effects on Pitot-Tubes with Rectangular Mouth. The Aeronautical Quarterly, May 1969
- [106] Patel, V.C.: Calibration of Preston-Tube and Limitations on its Use in Pressure Gradients. J. of Fluid Mech., Vol. 23, Part 1, pp. 285-208
- [107] Holmes, W.E., Luxton, R.E.: Measurement of Turbulent Skin-Friction by a Preston Tube in the Presence of Heat Transfer. J. of Mech. Enmg. Science, Vol. 9, No. 3, 1967
- [108] Coles, D.: The Turbulent Boundary Layer in a Compressible Fluid. The Physics of Fluid, Vol. 7, No. 9, 1964
- [109] Walz, A.: Strömungs- und Temperaturgrenzschichten (Flow and Temperature Boundary Layers). G. Braun Publishing House, Karlsruhe, pp. 40 ff, 1966
- [110] Witig, S., Rodi, W., Rüd, K., Eriksen, S., Scheurer, H. and Schulz, A.: Experimentelle und theoretische Untersuchungen zur Bestimmung von Wärmeübergangszahlen an gekühlten Gas-turbinenschaufeln (Experimental and Theoretical Studies on the Determination of Heat Transfer Coefficients on Cooled Gas Turbine Blades). Final report of FVV project 241: 'Gas Turbine Blade Coolin'. Forschungsberichte Verbrennungskraftmaschinen, Vol. 326, 1983, FVV Frankfurt/Main
- [111] Eriksen, S., Wittig, S., Schulz, A., Hassa, C.: Laser-Doppler und Laser-Zwei-Focus Messungen in laminaren und turbulenten Wandgrenzschichten (Laser-Doppler and Laser-Dual-Focus Tests in Laminar and Turbulent Wall Boundary Layers). VDI report, No. 487, "Fluid Mechanics '83", VDI Publishing House 1983, pp. 181-189
- [112] TSI: Instruction Manual for Counter Model 1990
- [113] Stevenson, W.H., Thompson, H.D., Bremmer, R., Roesler, T.: Laser velocimeter Measurements in Turbulent and Mixing Flows. Technical Rep. AFAPL-TR-79-1009, Part II. School of Mech. Eng., Purdue University, Indiana, USA

- [114] Degussa: AEROSIL: Herstellung, Eigenschaften und Anwendung (AEROSIL: Production, Properties and Application). Firm Degussa, Frankfurt, 3rd edition (new version) 1978
- [115] Coles, D.E.: The Turbulent Boundary Layer in a Compressible Fluid. RAND Report, R-403-Pr
- [116] Levy, S.: Effect of Large Temperature Changes (Including Viscous Heating) upon Laminar Boundary Layers with Variable Free-Stream Velocity. Journal of Aeronautical Sciences, Vol. 21, No. 7, July 1954, pp. 459-474
- [117] Hislop, G.S.: The Transition of a Laminar Boundary Layer in a Wind Tunnel. Ph. D. Thesis, Cambridge University (1940)
- [118] Brown, B., Burton, R.C.: The Effects of Free-Stream Turbulence and Velocity Distribution on Heat Transfer to Curved Surfaces. ASME Pap. No. 77-GT-48 (1977)
- [119] Martin, B.W., Brown, A., Garrett, S.E.: Heat Transfer to a PVD Rotor Blade at High-Subsonic Passage Throat Mach Number. Proceedings of the Institution of Mech. Eng., Vol. 192, No. 12 (1978) (190)
- [120] Wells, C.S.: Effect of Free-Stream Turbulence on Boundary Layer Transition. Am. Inst. Aero. Astr. Jour. 5 (1967)
- [121] Taylor, J.R.: Temperature and Heat Flux Distributions in Incompressible Turbulent Equilibrium Boundary Layers. Int. J. Heat Mass Transfer, 15 (1972), pp. 2473-2488
- [122] Moretti, P.A.: PhD Dissertation, Department of Mechanical Engineering, Stanford University, Stanford, Calif. 1965
- [123] Rüd, K.P., Sill, K.H., Wittig, S.: Einfluß der Freistromturbulenz auf den Wärmeübergang an stark gekühlten Oberflächen (Influence of Free Stream Turbulence on the Heat Transfer on Highly Cooled Surfaces). VDI Reports, No. 487, Fluid Mechanics 83, VDI Publishing House, 1983, pp. 171-180
- [124] Rüd, K.P., Wittig, S.: Free-Stream Turbulence and Pressure Gradient effects on Heat Transfer and Boundary Layer Development on Highly Cooled Surfaces. Journal of Engineering for Gas Turbines and Power, Vol. 107, Jan. 1985, pp. 54-59
- [125] Patankar, S.V., Spalding, B.D.: A Calculation Procedure for Heat Transfer by Forced Convection through Two-Dimensional Uniform-Property Turbulent Boundary Layers on Smooth Impermeable Walls. Proc. 3rd Heat Transf. Conf., Vol. 2, AICHE, 1966
- [126] Neubert, W., Walz, A.: Beitrag zur Berechnung zweidimensionaler kompressibler Grenzschichten mit Integralbedingungen (On the Calculation of Two-Dimensional Compressible Boundary Layers with Integral Conditions). Special publication for the 60th birthday of Prof. E. Truckenbrodt, Engineer, Department for Fluid Mechanics, Munich, 1977

- [127] Hinze, J.O.: Turbulence. McGraw-Hill Book Comp., New York, 2nd Ed. 1975
- [128] Küster, H.J.: Ein Integralverfahren zur Berechnung zweidimensionaler turbulenter Grenzschichten mit Druckgradient und Wärmeübergang auf der Basis einer Kompressibilitätstransformation (An Integral Procedure for the Calculation of Two-Dimensional Turbulent Boundary Layers with Pressure Gradient and Heat Transfer based on a Compressibility Transformation). Diss. Technical University Berlin, 1972
- [129] Cebeci, T.: Behavior of Turbulent Flow near a Porous Wall with Pressure Gradient. AIAA-Journal, 1970, Vol. 8, pp. 2152-2156
- [130] Thwaites, P.: An Approximate Calculation of Laminar Boundary Layers. Aeron. Quarterly, Vol. 7, 1949, pp. 245-280
- [131] Vodes, R.: Entwicklung eines anwendungsnahen Berechnungsverfahrens für die Strömungs- und Temperaturgrenzschicht (Development of a Practical Calculation Procedure for Flow and Temperature Boundary Layers). Technical University Munich, Institute for Fluid Mechanics, Rep.-Nr. 79/11, 1979

CURRICULUM VITAE

(191

 Born in 
 Father: Helmut Rüd, master blacksmith
 Mother: Elsa Rüd

1960 - 1965 Waldshut Elementary School

1965 - 1973 Hochrein High School, Waldshut
 Graduation in modern languages

1973 - 1979 General Mechanical Engineering
 University of Karlsruhe

1975 - 1979 Scientific Assistant at various institutes
 of the mechanical engineering faculty

4 July 1979 Graduation (Diplom)

September 1979 - August 1985 Scientist at the Institute of Fluid Mechanics,
 University of Karlsruhe

since July 1983 Group Leader of the research group
 "gas turbine blade cooling" at the same
 institute

since July 1984 Member, special research project 167
 "Highly Stressed Combustion Chambers"

STANDARD TITLE PAGE

1. Report No. NASA TM-88524	2. Government Accession No.	3. Recipient's Catalog No.	
4. Title and Subtitle TRANSITIONAL BOUNDARY LAYERS UNDER THE INFLUENCE OF HIGH FREE STREAM TURBULENCE INTENSIVE WALL COOLING AND HIGH PRESSURE GRADIENTS IN HOT GAS CIRCULATION		5. Report Date February 1987	6. Performing Organization Code
7. Author(s) Klaus Rued		8. Performing Organization Report No.	10. Work Unit No.
9. Performing Organization Name and Address SCITRAN Box 5456 Santa Barbara, CA 93108		11. Contract or Grant No. NASw-4004	13. Type of Report and Period Covered Translation
12. Sponsoring Agency Name and Address National Aeronautics and Space Administration Washington, D.C. 20546		14. Sponsoring Agency Code	
15. Supplementary Notes Translation of: "Transitionale Grenzschichten unter dem Einfluss hoher Freistromturbulenz, intensiver Woxnudkuehlung und starken Druckgradienten in Heissgasstroemungen," thesis submitted at University Karlsruhe, 1985, pp. 1-191			
16. Abstract This book discusses the requirements for fundamental experimental studies of the influence of free stream turbulence, pressure gradients and wall cooling. Under turbine-like free stream conditions, comprehensive tests of transitional boundary layers with laminar, reversing and turbulent flow increments were performed to decouple the effects of the parameters and to determine the effects during mutual interaction.			
ORIGINAL PAGE IS OF POOR QUALITY			
17. Key Words (Selected by Author(s)) TURBULENCE BOUNDARY LAYERS BOUNDARY LAYER INTERACTION FREE STREAM PRESSURE GRADIENTS WALL COOLING HOT GAS CIRCULATION		18. Distribution Statement Unclassified and Unlimited This report is available to the public without restriction.	
19. Security Classif. (of this report) Unclassified	20. Security Classif. (of this page) Unclassified	21. No. of Pages 226	22. Price

(NASA-TM-88524) TRANSITIONAL BOUNDARY LAYERS UNDER THE INFLUENCE OF HIGH FREE STREAM TURBULENCE, INTENSIVE WALL COOLING AND HIGH PRESSURE GRADIENTS IN HOT GAS CIRCULATION Ph.D. (National Aeronautics and

N87-16983

Unclas
43862